

POLITECNICO DI TORINO  
FIRST SCHOOL OF ENGINEERING – *DEPARTMENT OF MECHANICAL AND  
AEROSPACE ENGINEERING*

DOCTORATE SCHOOL  
PhD in Biomedical Engineering – XXVII Cycle



PhD Dissertation

***Chitosan based biomaterials:  
soft tissue engineering applications***

**Supervisor**

Prof. Gianluca Ciardelli

**PhD Candidate**

Francesca Ruini

S189229

**February 2015**



## **Table of contents**

Acknowledgments.....	xi
Short <i>Curriculum Vitae</i> .....	xiii
List of Publications.....	xiv
Abstract.....	xvi
Executive summary.....	xviii
List of Abbreviations.....	xxiv
Introduction to the Thesis Format.....	xxviii

### **Section I**

#### **Chitosan as a biomaterial**

##### **Chapter 1**

##### **Chitosan based biomaterials: state of the art and future perspective in soft tissue engineering regeneration and repair**

1.1 Introduction.....	3
1.2 Chitosan structure.....	4
1.3 Structure-property relationship.....	5
1.4 Biological properties of chitosan.....	6
1.5 Application of chitosan based biomaterials.....	7
1.5.1 Soft Tissue engineering.....	7
1.5.1.1 Chitosan in cartilage tissue engineering.....	8
1.5.1.2 Chitosan in liver tissue engineering.....	10
1.5.1.3 Chitosan in nerve tissue engineering.....	12
1.5.1.4 Chitosan in vascular application.....	14
1.5.2 Wound dressing.....	15
1.5.3 Drug delivery.....	17
1.6 Thesis goal.....	21
References.....	24

**Section II**  
**Effects of non cytotoxic crosslinkers on CS flat membranes**

**Chapter 2**

**Chitosan membranes for tissue engineering: comparison of different crosslinkers**

Abstract.....	38
2.1 Introduction.....	38
2.2 Experimental.....	40
2.2.1 Materials.....	40
2.2.2 Methods.....	40
2.2.3 Sample characterization.....	41
2.2.3.1 Fourier transform infrared-attenuated total reflectance spectroscopy (FTIR-ATR).....	41
2.2.3.2 Surface wettability.....	41
2.2.3.3 Swelling and dissolution test.....	41
2.2.3.4 Morphological characterization and element distribution.....	42
2.2.3.5 Thermogravimetric analysis (TGA).....	42
2.2.3.6 Differential scanning calorimetry (DSC).....	42
2.2.3.7 Mechanical properties.....	42
2.2.3.8 Statistics.....	43
2.3 Results and discussion.....	43
2.3.1 Membrane preparation.....	43
2.3.2 Fourier transform infrared-attenuated total reflectance spectroscopy (FTIR-ATR).....	44
2.3.3 Surface wettability.....	45
2.3.4 Swelling and dissolution test.....	46
2.3.5 Morphological characterization and element distribution.....	49
2.3.6 Thermogravimetric analysis (TGA).....	50
2.3.7 Differential scanning calorimetry (DSC).....	52
2.3.8 Mechanical properties.....	53
2.4 Conclusion.....	54
References.....	56

**Section III**  
**Chitosan for peripheral nerve regeneration**

**Chapter 3**  
**Peripheral nerve tissue engineering: state of the art**

3.1 Introduction.....	61
3.2 Biology of the peripheral nerve and injuries .....	61
3.2.1 Central and peripheral nervous systems.....	61
3.2.2 Nervous tissue cell types.....	62
3.2.3 Structure of the nerve.....	64
3.2.4 Nerve injuries classification.....	65
3.2.5 Peripheral nerve regeneration after injuries.....	67
3.2.6 Surgical approaches.....	69
3.2.7 Tissue engineering in peripheral nerve injury.....	70
3.2.7.1 Biomaterials in nerve regeneration.....	72
3.2.7.1.1 Synthetic biomaterials used for NGCs.....	72
3.2.7.1.2 Natural polymers for NGCs.....	74
3.2.7.2 The structure of a neural scaffold.....	79
3.2.7.3 Cellular therapy: support cells.....	82
3.2.7.4 Biomolecular therapy.....	83
References.....	86

**Chapter 4**  
**Chitosan crosslinked flat membranes for peripheral nerve regeneration**

Abstract.....	93
4.1 Introduction.....	94
4.2 Experimental.....	95
4.2.1 Materials.....	95
4.2.2 Methods.....	95
4.2.3 Sample characterization.....	95
4.2.3.1 Evaluation of CS based membranes permeability.....	95
4.2.3.2 <i>In vitro</i> cell tests on CS based samples.....	96
4.2.3.2.1 Cytotoxicity study on CS/GPTMS_DSP and CS/DSP.....	96
4.2.3.2.2 Cell adhesion on CS/GPTMS_DSP samples.....	97
4.2.3.2.3 Proliferation assay on CS/GPTMS_DSP samples.....	97
4.2.3.2.4 Real Time Reverse-Transcriptase-Polymerase-Chain-Reaction (Real Time RT-PCR) analysis on CS/GPTMS_DSP.....	97

4.2.3.2.5 Neurite outgrowth assay on CS/GPTMS_DSP.....	99
4.2.3.3 <i>In vivo</i> tests on CS/GPTMS_DSP and CS/DSP.....	99
4.2.3.3.1 <i>In vivo</i> qualitative analysis on: biocompatibility, rolling up and suturability.....	99
4.2.3.3.2 Animals and surgery.....	100
4.2.3.3.3 Postoperative assessment of functional recovery.....	101
4.2.3.3.4 Resin embedding and electron microscopy.....	101
4.2.3.3.5 Design-based quantitative morphology of nerve fibre regeneration.....	102
4.2.3.3.6 Immunohistochemistry and confocal laser microscopy.....	102
4.2.3.4 Statistics.....	103
4.3 Results and discussion.....	103
4.3.1 Evaluation of CS based membranes permeability.....	103
4.3.2 <i>In vitro</i> cell tests on CS based samples.....	104
4.3.2.1 Cytotoxicity study on CS/GPTMS_DSP and CS/DSP.....	104
4.3.2.2 Cell adhesion on CS/GPTMS_DSP samples.....	105
4.3.2.3 Proliferation assay on CS/GPTMS_DSP samples.....	106
4.3.2.4 Real Time Reverse-Transcriptase-Polymerase-Chain-Reaction (Real Time RT-PCR) analysis on CS/GPTMS_DSP.....	107
4.3.2.5 Neurite outgrowth assay on CS/GPTMS_DSP.....	109
4.3.3 <i>In vivo</i> tests on CS/GPTMS_DSP and CS/DSP.....	110
4.3.3.1 Postoperative assessment of functional recovery.....	110
4.3.3.2 Light and transmission electron microscope analysis.....	111
4.3.3.3 Design-based quantitative morphology of nerve fibre regeneration.....	113
4.3.3.4 Immunohistochemistry and confocal laser microscopy.....	113
4.4 Conclusion.....	114
References.....	116

## Chapter 5

### Bi-layer CS membranes for nerve tissue engineering

Abstract.....	118
5.1 Introduction.....	118
5.2 Experimental.....	119
5.2.1 Materials.....	119
5.2.2 Methods.....	119
5.2.3 Sample characterization.....	120
5.2.3.1 Fourier transform infrared-attenuated total reflectance spectroscopy (FTIR-ATR).....	120
5.2.3.2 Surface wettability.....	120
5.2.3.3 Mechanical properties.....	120

5.2.3.4 Swelling and dissolution tests.....	120
5.2.3.5 Permeability of bi-layer CS based membranes.....	121
5.2.3.6 Preliminary <i>in vivo</i> tests.....	121
5.2.3.6.1 Animals and surgery.....	121
5.2.3.6.2 Resin embedding and electron microscopy.....	122
5.2.3.6.3 Immunohistochemistry and confocal laser microscopy.....	123
5.2.3.7 Statistics.....	123
5.3 Results and discussion.....	123
5.3.1 Fourier transform infrared-attenuated total reflectance spectroscopy (FTIR-ATR).....	123
5.3.2 Surface wettability.....	124
5.3.3 Mechanical properties.....	125
5.3.4 Swelling and dissolution tests.....	126
5.3.5 Permeability of bi-layer CS based membranes.....	128
5.3.6 Preliminary <i>in vivo</i> tests.....	128
5.3.6.1 Light and transmission electron microscope analysis.....	129
5.3.6.2 Immunohistochemistry and confocal laser microscopy.....	130
5.4 Conclusion.....	131
References.....	132

## Chapter 6

### CS electrospun nanofibres for nerve tissue engineering

Abstract.....	133
6.1 Introduction.....	133
6.2 Experimental.....	135
6.2.1 Materials.....	135
6.2.2 Electrospun membrane preparation.....	135
6.2.2.1 Preparation of solutions for electrospinning.....	135
6.2.2.2 Electrospinning of CS nanofibres.....	135
6.2.3 Membrane preparation and optimization of solution and process parameters.....	135
6.2.3.1 Solution parameters and viscosity tests.....	135
6.2.3.2 Process parameters.....	136
6.2.3.3 Fibres morphology and element distribution.....	136
6.2.4 Electrospun membranes characterization.....	136
6.2.4.1 Fourier transform infrared-attenuated total reflectance spectroscopy (FTIR-ATR).....	136
6.2.4.2 Thermogravimetric analysis (TGA).....	136
6.2.4.3 Mechanical properties.....	136

6.2.4.4 Fibres dissolution.....	137
6.2.5 Statistical analysis.....	137
6.3 Results and discussion.....	137
6.3.1 Optimization of the electrospinning parameters.....	137
6.3.1.1 Solution viscosity and its effect on electrospun nanofibres.....	137
6.3.1.2 Process parameters.....	139
6.3.2 Characterization of CS based nanofibres.....	139
6.3.2.1 Fibres morphology and element distribution.....	139
6.3.2.2 Fourier transform infrared-attenuated total reflectance spectroscopy (FTIR-ATR).....	140
6.3.2.3 Thermogravimetric analysis (TGA).....	141
6.3.2.4 Mechanical properties.....	142
6.3.2.5 Fibres dissolution.....	143
6.4 Conclusion.....	145
References.....	146

## Section IV

### Chitosan for wound dressing

#### Chapter 7

#### Wound healing dressing: state of the art

7.1 Introduction.....	150
7.2 Structure and function of the skin.....	150
7.3 Wounds and wound healing process.....	152
7.4 Factors which impair wound healing chronic wounds.....	155
7.5 Wound dressing.....	156
7.5.1 Classification of wound dressings.....	156
7.5.1.1 Traditional dressings.....	157
7.5.1.2 Modern dressings.....	157
7.5.1.2.1 Hydrocolloids.....	158
7.5.1.2.2 Alginates.....	158
7.5.1.2.3 Synthetic hydrogels.....	159
7.5.1.2.4 Semi- permeable adhesive films.....	159
7.5.1.2.5 Foam dressings.....	160
7.5.1.2.6 Tissue engineered skin substitutes.....	160
7.5.1.2.6.1 Biocompatible polymers for wound dressings.....	162
7.5.1.2.6.1.1 Natural polymers for wounds healing.....	163
7.5.1.2.6.1.2 Synthetic polymers for wound healing.....	165

7.6 Medicated dressings for wound delivery.....	168
7.6.1 Antimicrobials.....	168
7.6.2 Growth factors.....	169
7.6.3 Supplements.....	170
References.....	172

## Chapter 8

### Porous CS based membranes with improved antimicrobial properties for the treatment of chelonian shell injuries

Abstract.....	181
8.1 Introduction.....	181
8.2 Experimental.....	184
8.2.1 Materials.....	184
8.2.2 Methods.....	184
8.2.3 Sample characterization.....	184
8.2.3.1 Morphological characterization and element distribution.....	184
8.2.3.2 Thermogravimetric analysis (TGA).....	185
8.2.3.3 Mechanical properties.....	185
8.2.3.3.1 Tensile test.....	185
8.2.3.3.2 Compressive test.....	185
8.2.3.4 Water uptake and dissolution test.....	186
8.2.3.5 Drug release evaluation.....	186
8.2.3.6 Antibacterial tests.....	186
8.2.3.7 Preliminary <i>in vivo</i> tests.....	187
8.2.3.8 Statistics.....	187
8.3 Results and discussion.....	187
8.3.1 Morphological characterization and element distribution.....	187
8.3.2 Thermogravimetric analysis (TGA).....	191
8.3.3 Mechanical properties.....	193
8.3.3.1 Tensile test.....	193
8.3.3.2 Compressive test.....	195
8.3.4 Water uptake and dissolution tests.....	196
8.3.5 Drug release evaluation.....	199
8.3.6 Antibacterial tests.....	200
8.3.7 Preliminary <i>in vivo</i> test.....	201
8.4 Conclusion.....	202
References.....	203

**Section V**  
**Conclusions**

**Chapter 9**

**Final discussion and conclusions**

9.1 General discussion.....	208
9.2 Conclusion and future work.....	213
References.....	215

## Acknowledgments

Nei tre anni di dottorato ho avuto l'opportunità di sviluppare nuove competenze e di lavorare con persone provenienti da diversi gruppi di ricerca sia del Politecnico di Torino che di altri istituti nazionali ed europei.

Un ringraziamento particolare va al mio relatore, il Prof. Gianluca Ciardelli, non solo per il suo supporto scientifico e i suoi insegnamenti ma, anche per essersi dimostrato sempre molto disponibile. Ringrazio inoltre la mia tutor, Chiara, per avermi guidato e sopportato in questo lungo percorso. E' stata una degna maestra!

Nel periodo di dottorato ho avuto la possibilità di svolgere parte del lavoro sperimentale presso il Dipartimento di Biologia Animale e dell'Uomo dell'Università di Torino, presso il gruppo di ricerca della Prof.ssa Isabelle Perroteau che mi ha permesso di approfondire nozioni di biologia cellulare con particolare riferimento alle interazioni biomateriali/tessuti. Ringrazio le Prof. ssa Perroteau e i suoi collaboratori per l'aiuto e per avermi accolto con grande disponibilità.

Inoltre, durante questi anni ho collaborato con l'Istituto per le Neuroscienze Cavalieri Ottolenghi (NICO) e il Dipartimento di Scienze Cliniche e Biologiche dell'Università di Torino. Ringrazio il Prof. Stefano Geuna, il Dott. Pieluigi Tos, Stefania Raimondo e Giulia Ronchi per aver svolto le prove preliminari *in vivo*.

La parte della tesi relativa alla realizzazione delle nanofibre tramite electrospinning è stata svolta in collaborazione con Nanostructured Interfaces and Surfaces (NIS) Centre of Excellence del Dipartimento di Chimica dell'Università di Torino. Ringrazio il Prof. Marco Zanetti e la Prof. ssa Pierangiola Bracco per la disponibilità dimostratami e per l'aiuto nella realizzazione delle nanofibre. La parte della tesi inerente allo sviluppo di membrane porose finalizzata al trattamento delle ferite del carapace delle tartarughe è stata condotta in collaborazione con il Dipartimento di Scienze Veterinarie, Università di Torino. Ringrazio la Prof.ssa Patrizia Nebbia per aver svolto i test antibatterici e il Dott. Nicola Di Girolamo per i test *in vivo*.

In queste tre anni ho avuto modo di conoscere persone gentili e disponibili ma, soprattutto cari amici. Un ringraziamento particolare va a Tiziana (in arte Tisssssssssssiana) che mi ha aiutato sotto molteplici aspetti e mi ha rallegrato con le sue uscite alternative; Chiara, la mia fantastica tutor dal ciuffo ribelle, e Irene, che pur chiamandomi "la Ruini", ha saputo alleggerire le giornate con le sue uscite.

Un grazie infinito a tutto il gruppo di ricerca con cui in questi anni ho avuto l'opportunità di lavorare: Valeria, Diego (il mio fornitore di articoli in cambio di dolci), Giuseppe (Gioseffino), Giuseppe (Seffo), Mara, Francesco (Penny), Diana, Antonella, Clara, Marina, Giulia, Monica, Susanna, Emilia, Umberto, Silvia e Tianrhan.

Un Ringraziamento particolare a mia mamma e mio babbo per avermi sempre sostenuto in tutto e per tutto! A mia sorella Martina perché è la persona che più mi conosce.

Ultimo ma, non ultimo il mio pensiero è rivolto a Marco (chiamato dal gruppo Marcobaldo) che è sempre al mio fianco...

## **Short Curriculum Vitae**

Francesca Ruini was born in 1986 in Biella (BI), Italy. She received a BS degree (October 2008) and a MS degree (December 2011) in Biomedical Engineering from Politecnico di Torino. During her MS degree thesis, she focused on the development of internal fillers based on blends of natural polymers for the loading and the release of growth factors able to promote the nerve regeneration after injuries (within the project: “Moving again! New approaches arising from molecular neuroscience for the treatment of movement impairment (MOVAG)” -Compagnia San Paolo).

In 2012 she was qualified to practice the profession of Industrial Engineer. From January 2012 to December 2014 she was a PhD student in Biomedical Engineering at the Mechanical and Aerospace Engineering, Politecnico di Torino, where she worked on the development of bioartificial constructs for repairing peripheral nerves. Her research activity is part of BICONERVE (“Biomimetic constructs for nerve regeneration”) Regional project, which is aimed at the development of innovative multicomponent devices (membranes) for guided peripheral nerve regeneration.

As a PhD student of Industrial Bioengineering group, she has been involved for scientific research in BIODRESS (“Biopolymer based dressings for efficient wound management”) MANUNET ERA-NET project and for the application of biodegradable membranes in the veterinary field (collaboration with the Department of Veterinary Sciences, Università di Torino)

Francesca Ruini has hands-on experience in Scanning electron microscopy (SEM), energy-dispersive spectroscopy (EDS), contact angle measurements, mechanical testing, Differential scanning calorimetry (DSC), Thermogravimetric analysis (TGA), Fourier Transform Infrared Spectroscopy (FTIR), and UV-Vis spectroscopy. She also matured experience in Enzyme-Linked ImmunoSorbent Assay (ELISA) and in vitro biological tests during her MS degree thesis.

Up today, as a results of her research work, she is the author of 3 articles (1 published, 2 submitted) and 6 abstracts in national/international conference proceedings.

## List of Publications

### **International Journals with referee**

1. Tonda-Turo C., Gnavi S., Ruini F., Gambarotta G., Gioffredi E., Chiono V., Perroteau I, and Ciardelli G. "Development and characterization of novel agar and gelatin injectable hydrogel as filler for peripheral nerve guidance channels". Journal of Tissue Engineering and Regenerative Medicine. 2014. DOI:10.1002/term.1902.

### **SUBMITTED**

1. **Ruini F.**, Tonda-Turo C., Chiono V. and Ciardelli G. Chitosan membranes for tissue engineering: comparison of different crosslinkers. International Journal of Biological Macromolecules.
2. Salgarella A., Giudetti G., Ricotti L., Camboni D., Puleo G. L., **Ruini F.**, Tonda-Turo C., Chiono V., Ciardelli G., Micera S., Menciasci A., Calogero M. O."A bio-hybrid mechanotransduction system based on ciliate cells". Microelectronic Engineering. Special issue "Micro/Nano Biotechnologies & Systems 2014.

### **Communications in National/International Conferences**

1. Nebbia P., Argentati M., Tonda Turo C. **Ruini F.**, Ciardelli G, Di Girolamo N., Bert E., Robino P. In vitro antimicrobial activity of chitosan-silver and chitosan-gentamicin membranes on Staphylococcus aureus and Escherichia coli.
2. Tonda-Turo C., **Ruini F.**, Gnavi S., Di Blasio L., Primo L., Chiono V., Perroteau I., Ciardelli G Naturally-derived hydrogels as a tool for growth factors release in peripheral nerve tissue engineering. XXV Congresso Nazionale Società Italiana di Microchirurgia. Bologna (Italy), November 8, 2013.
3. **Ruini F.**, Tonda Turo C., Gnavi S., Di Blasio L., Primo L., Chiono V., Perroteau I., Ciardelli G. Hydrogels as a tool for growth factors release in peripheral nerve tissue engineering. 25th European Conference on Biomaterials, Madrid (Spain), September 8-12, 2013 (oral presentation).
4. Tonda-Turo C., **Ruini F.**, Gnavi S., Di Blasio L., Primo L., Chiono V., Perroteau I., Ciardelli G Hydrogels based on natural polymers for growth factors release in peripheral nerve tissue engineering. Congresso Società Italiana Biomateriali Baveno (Italy) June 3-5, 2013.

5. Tonda-Turo C., **Ruini F.**, Gnavi S., Di Blasio L., Primo L., Chiono V., Perroteau I., Ciardelli G. Naturally derived hydrogels for growth factors release in peripheral nerve tissue engineering. 3<sup>rd</sup> Termis World Congress, “ Tissue Engineering and Regenerative Medicine”. Vienna (Austria), September 5-8, 2012
6. Gnavi S., Tonda-Turo C., **Ruini F.**, Di Blasio L., Primo L., Ciardelli G., Geuna S. & Perroteau I. Hydrogel as a tool for gradual release of Growth Factors in Peripheral Nerve Tissue Engineering. 8<sup>th</sup> FENS forum of Neuroscience. Barcelona (Spain), July 14-18, 2012.
7. Chiono V., Carmagnola I., Ferreira A. M., Nardo T., Gentile P., Tonda-Turo C., **Ruini F.**, Abrigo M., Boccafoschi F., Ciardelli G. Layer-by-layer as a tool to tailor the surface properties of biomedical devices. GNB Congress 2012, Rome (Italy), June 26-29, 2012.

## Abstract

In recent years, considerable attention has been given to **chitosan** (CS)-based biomaterials and their applications in the field of soft tissue engineering (TE). CS is a glycosaminoglycan derived from chitin, the primary structural polymer in crustacean exoskeletons. CS is biocompatible, biodegradable, easily formed into various structures (i.e. sponges, nanofibers and films) under mild processing conditions and can be chemically modified through graft copolymerization and crosslinking. However, the rapid degradation of CS and its low mechanical strength are concerns that may limit its use in clinical applications.

In the first part of the thesis, **different non cytotoxic crosslinkers** were used aiming at improving the structural properties of CS. Genipin (GP),  $\gamma$ -glycidoxypropyltrimethoxysilane (GPTMS), dibasic sodium phosphate (DSP) were selected as biocompatible CS crosslinkers as reported in literature. After a preliminary physico-chemical and mechanical characterization, the proper crosslinking compounds were selected for the development of different typologies of CS scaffolds for both human and veterinary applications.

**CS- based scaffolds were developed as nerve guidance channels (NGCs) and internal fillers fabrication to promote peripheral nerve regeneration in humans.** Two CS based hollow NGCs were prepared and tested *in vitro* and *in vivo* (coded as CS flat membrane and bi-layer CS membrane) and a CS based nanostructured internal filler was optimized and characterized *in vitro*.

- i. **CS flat membranes** were prepared by solvent casting. According to the results obtained in the first part of the thesis, DSP alone (CS/DSP) or in association with the GPTMS (CS/GPTMS\_DSP) were used as crosslinkers. CS crosslinked membranes showed permeation to nutrients and did not exert any cytotoxic effect on RT4-D6P2T. The higher mechanical stability of CS/GPTMS\_DSP under wet state allowed to confirm the RT4-D6P2T attachment and proliferation as well as the neurite outgrowth of dorsal root ganglia (DRG) on CS substrates. Before *in vivo* implantation in rats, CS/GPTMS\_DSP and CS/DSP membranes were easily rolled up to form a NGC. Then, membranes were used to bridge median nerve defects in rats. After 12 week post-operative CS/GPTMS\_DSP tubes were found to be detached from the distal suturing site and functional recovery did not occurred. On the other hand, crushed nerve encircled with CS/DSP membranes, allowed nerve fibre regeneration and functional recovery, showing similar results to autografts.
- ii. **Bi-layer CS membranes** were developed using a two-step coating technique. CS/DSP and CS/GPTMS\_DSP flat membranes were combined to produce scaffold structures with good biocompatibility in the inner layer (CS/DSP) and with the desired mechanical strength imparted by the outer (CS/GPTMS\_DSP, GPTMS 25% wt./wt.). Gradual water

uptake and permeation to small molecules was observed compared to single layers. From *in vivo* tests, median nerves treated with bi-layer tubes displayed regenerated and aligned fibres at the injury site.

- iii. **CS crosslinked electrospun nanofibres** were fabricated by electrospinning solutions containing CS, polyethylene oxide (PEO), and dimethylsulphoxide (DMSO). PEO and DMSO were introduced to allow the spinnability of CS solutions at high polymer concentration with controllable fiber size and increase fiber yields by relaxing CS chain entanglement. Optimization of the process and solution parameters allowed to obtain CS nanofibres with size of  $128\pm 17$  nm. To increase CS stability in aqueous media, DSP was used as crosslinker. After DSP crosslinking fibre size decreased to  $109\pm 17$  nm while an increase in the mechanical strength (E, from  $63\pm 10$  MPa to  $113\pm 8$  MPa) was observed compared to uncrosslinked nanofibrous matrices.

**In the third part of the thesis, CS porous membranes with improved antimicrobial properties were prepared for veterinary application.** The developed scaffolds were fabricated by freeze-drying to promote the wound healing process and to reduce the bacterial proliferation in chelonian shell injury site. Different ratios of silver nanoparticles (AgNPs, 5%, 10% and 15% wt. /wt.) and gentamicin sulphate (GS, 3.5 mg/ml) were loaded into the CS/GPTMS\_DSP membranes to impart the proper antibacterial properties and to favor drug release avoiding the risk of systemic toxicity. After a preliminary *in vitro* characterization, CS/GPTMS\_DSP loaded with AgNPs at a concentration of 10% wt./wt (CS/GPTMS\_DSP\_AgNP10) was selected as ideal candidate for this application field. GS release profile from CS/GPTMS\_DSP\_GS evidenced high burst release of the antibiotics in the first day (about 70%). Finally, GS and AgNPs (10 % wt./wt.) effect on bacterial inhibition was evaluated and confirmed against Gram<sup>+</sup> and Gram<sup>-</sup>.

The results reported in this thesis work demonstrate that CS is a promising candidate for applications in human and veterinary soft TE. Mechanical and physico-chemical properties of CS scaffolds can be tuned by using different crosslinking methods. By the *in vitro* characterization, GPTMS and DSP were selected as ideal compounds to the development of scaffolds for peripheral nerve regeneration (in human) and wound healing (in animals). Four different morphologies (3 for peripheral nerve regeneration and 1 for wound healing application) were obtained by varying the fabrication methods and the final composition. All membranes were found to satisfy the requirements for the application of interest. CS based membranes developed for peripheral nerve regeneration were found to be biocompatible, and successful functional recovery was observed in case of CS/DSP and bi-layer membranes. Porous membranes with improved antimicrobial properties were prepared to enhance wound healing in chelonians and were found to be effective against a broad spectrum of bacteria following the release of two different investigated antimicrobial agents (AgNPs and GS).

## Executive Summary

Repair and regeneration of tissues and organs using biomaterials, cells and/or growth factors is the ultimate goal of tissue engineers. One of the main challenges in tissue regeneration is to closely mimic the structures and properties of native tissues. In this context, in recent years, considerable attention has been given to chitosan based materials and their applications in the field of soft tissue engineering. **Chitosan** (CS) is a natural polymer from renewable resources, obtained from shell of shellfish that exhibits outstanding properties such as a marked biocompatibility, biodegradability and antibacterial activity. Due to these promising biological features and its easy chemical modification and processability into 2D and 3D scaffolds (i.e. gel, films, nanofibers, sponges, nanoparticles), CS has been investigated for wound dressing, drug delivery system and soft tissue engineering among which cartilage, liver, peripheral nerve and vascular field applications [1]. CS matrices present few drawbacks that limit their use in clinical applications such as low mechanical strength and low structural integrity under physiological condition. The improvement of CS properties can be achieved by modifying CS with different crosslinking agents (i.e. glutaraldehyde,  $\gamma$ -glycidoxypropyltrimethoxysilane, tripolyphosphate, genipin) [2-5] or by combining the natural polymer to synthetic ones (i.e. poly( $\epsilon$ -capolactone), poly(vinyl alcohol), polyethylenoxide) [6, 7]. Blending with synthetic polymers can introduce a residue of solvents and other compounds/impurities that can damage the natural polymers and consequently affect cell growth and proliferation. For this reason, **in the first part of the thesis, CS was crosslinked using different ionic and covalent compounds** with the aim to provide the basis for the selection of a crosslinking strategy able to impart the required properties to CS membranes in the design of a biomaterial. CS crosslinked flat membranes were prepared via solvent casting following the addition of different crosslinking agents: genipin (GP),  $\gamma$ -glycidoxypropyltrimethoxysilane (GPTMS), dibasic sodium phosphate (DSP) and a combination of GPTMS and DSP (GPTMS\_DSP). The three crosslinkers were selected since literature data reported interesting biological properties using these agents compared to others (epoxy compounds, aldehydes and carbodiimides). Although many works reported the use of crosslinked CS membranes, a complete characterization and comparison of CS membranes crosslinked with different biocompatible agents is still lacking.

A chemico-physical and mechanical characterization of CS crosslinked samples (CS/GP, CS/GPTMS, CS/DSP and CS/GPTMS\_DSP) was performed. CS membranes showed that the presence of GP or GPTMS did not affect the surface wettability but improved the mechanical resistance and the stability of CS samples in aqueous environment. On the contrary, DSP addition contributed to increase the hydrophilicity, the water uptake and the flexibility of CS. The simultaneous use of GPTMS and DSP allowed to combine the

features obtained both from GPTMS and DSP crosslinkers. From the obtained results, the proper crosslinking agents were selected for the development of different typologies of CS scaffolds for both human and veterinary applications in soft tissue engineering (Fig. 1). **In the second part of the thesis**, biocompatible and biodegradable innovative devices based on **CS** were developed **to promote peripheral nerve regeneration in humans**. Peripheral nerve regeneration is a challenging scientific field with relevant clinical and socioeconomic implications, since nerve injuries may lead to a lifelong function impairment and pain that may seriously compromise the quality of life. Transected peripheral nerve fibres are able to regenerate reaching functional recovery when an appropriate microenvironment is provided. Unfortunately, severe trauma often cause abundant substance loss and inherent regeneration is not possible; therefore, alternative surgical techniques should be used to bridge the proximal and distal stumps. Modern bioengineering and TE approaches are currently focused on the development of devices that provide an appropriate microenvironment to support and enhance the regeneration process [8]. Nerve guidance channels (NGCs) are a promising growth permissive substrate having nanostructured topography, haptotactic cues (ECM proteins), chemotactic cues (neurotrophic factors) that support Schwann cells or stem cells. Advances in engineered NGCs are directed to mimic the properties of natural tissues using multifunctional materials and/or conduits that can solve the limitations associated with traditional surgical approaches (short gap length, lay regeneration time, possible neuroma formation). Among the various biomaterials investigated, CS seems to be an ideal candidate for nerve regeneration due to its similarity in the molecular structure to GAGs and its neuroprotective properties.

For this purpose, three different **CS crosslinked membranes** were developed to favor Schwann cells adhesion and proliferation as well as nerve functional recovery. Different morphologies were obtained by varying the fabrication methods and the final composition. Two alternative for CS based hollow nerve guide channels were developed and tested *in vitro* and *in vivo* (coded as CS flat membrane and bi-layer CS membrane) while a CS based nanostructured internal filler was optimized and characterized *in vitro*.

**CS flat membranes** were prepared using DSP alone (CS/DSP) or in association with the GPTMS (CS/GPTMS\_DSP) as crosslinkers. The constituent ratio of crosslinking agents and CS was selected in the first part of the thesis to obtain a composite material having both proper mechanical properties and good biocompatibility. CS/DSP and CS/GPTMS\_DSP flat membranes were produced by solvent casting and they could be easily enwrapped to form a NGC in wet state (Fig. 1A). The developed membranes allowed nutrient permeation and were found not to exert any cytotoxic effect on RT4-D6P2T. The higher mechanical stability of CS/GPTMS\_DSP under physiological condition allowed to evaluate and confirmed the RT4-D6P2T adhesion, proliferation and function on the biomaterial. Moreover, CS/GPTMS\_DSP showed to direct RT4-D6P2T attachment resulting in characteristic cell morphology typical of SCs, and to support the neurite outgrowth of dorsal root ganglia (DRG) cultured on this substrate. The easily manipulation and

suturability of both the developed conduits allowed to perform *in vivo* tests. Membranes were used for bridge implantation across 10-mm long median nerve defects in rats, and the outcome of peripheral nerve repair at 12 weeks post-implantation was evaluated by a combination of electrophysiological assessment, immunohistochemical and histological investigation. During *in vivo* tests CS/GPTMS\_DSP tubes were detached from the distal suturing site and functional recovery did not occurred as confirmed by confocal laser microscopy which displayed poor axonal regeneration and irregular orientation. On the other hand, crushed nerve encircled with CS/DSP membranes, allowed nerve fibre regeneration and functional recovery, with effects approaching those elicited by nerve autografts, which are generally considered as the gold standard for treating large peripheral nerve defects.

**Bi-layer CS membranes** were developed by combining two kinds of CS flat membranes. They were crosslinked with different agents to produce scaffold structures with good biocompatibility in the inner layer and with the desired mechanical strength (following the addition of GPTMS) imparted by the outer one. In detail, CS/DSP and CS/GPTMS\_DSP were selected for the realization of the internal and external layer, respectively. The amount of GPTMS was lowered from 50 wt.% to 25wt.% to allow the rolling up, suturability of bi-layer membranes and to reduce the risk of distal detachment (Fig. 1B). The developed membranes were prepared by a two-step coating technique method, which allowed to control the wall thickness and to achieve a tight connection between the two distinct layers. The single layers interacted during the double layer fabrication process as confirmed physico-chemical analysis. The preliminary characterization of the developed membranes showed an increase in the surface wettability of the inner layer ( $41^{\circ}\pm 9^{\circ}$ ) and improved mechanical properties compared to CS/DSP, associated to the presence of GPTMS in the external layer. Bi-layer samples also exhibited slower swelling rate and permeation to model molecules (Stokes radius around 14 Å) compared to single layer inferring that the developed scaffold may be suitable for slow release of GFs and drug delivery application. Finally, preliminary *in vivo* tests were carried out on the bi-layer fat membranes for bridge implantation across 10-mm long median nerve defects in rats. After 12 weeks post-operative, nerves treated with bi-layer tubes displayed regenerated and aligned fibers at the injury site through light and transmission electron microscopy and observation as well as immunohistochemistry analysis (Fig. 2).

**CS crosslinked electrospun nanofibres** mimicking the complex biological structures of the natural extracellular matrix (ECM) were prepared from acetic acid solutions. CS nanofibres were fabricated by electrospinning solutions containing CS, polyethylene oxide (PEO), and dimethylsulphoxide (DMSO). PEO is a biocompatible synthetic polymer and was used to allow the spinnability of CS solutions at high polymer concentration with controllable fiber size; DMSO was introduced into the CS/PEO solution as a co-solvent to improve processing conditions and increase fiber yields by relaxing CS chain

entanglement. Optimization of the process and solution parameters allowed to obtain CS nanofibres with size around 130 nm. To increase CS stability in aqueous media, DSP was used as crosslinker (Fig. 1C). DSP crosslinking did not modify the nanofibre matrix morphology but decreased fibre size from  $128\pm 17$  nm to and  $109\pm 17$  nm, respectively. The presence of DSP increased the mechanical strength (E, from  $63\pm 10$  MPa to  $113\pm 8$  MPa) and the structural integrity of CS crosslinked nanofibres compared to uncrosslinked nanofibrous matrices.

**In the third part of the thesis, the possibility to apply CS as biomaterial for antibacterial membranes for veterinary application was investigated.** CS membranes were fabricated with the aim to promote wound healing in chelonians by reducing the bacterial proliferation at the wound site.

Skin TE is an emerging field in veterinary application: the development of biodegradable membranes apart from their fundamental protective functions could be conducive in wound regeneration, and would be able to shorten the healing process of the epidermis and skin of animals. Moreover, application of dressing materials based on natural products with improved antimicrobial properties could stimulate the healing processes. Consequently the damaged skin will be regenerated, limiting the systemic use of antibiotics. Antibiotic side-effects often result in wrong action or even damage to the patient's kidney and liver, and decrease of the bacterial proliferation at the wound site. In this thesis work, **CS porous membranes with improved antimicrobial properties** were fabricated by freeze-drying to promote the wound healing process and reduce the bacterial proliferation in injured chelonian shells. To increase CS mechanical properties and biocompatibility, GPTMS and DSP crosslinkers were added to the CS solution (CS/GPTMS\_DSP). The constituent ratio of crosslinking agents and CS was selected according to the results of the first part of the thesis. Different ratios of silver nanoparticles (AgNPs, 5%, 10% and 15% wt./wt. respect to the total amount of CS) and gentamicin sulphate (GS, 3.5 mg/ml dosage selected according to the conventional veterinary treatment for chelonian carapace healing) were incorporated into the CS matrices to impart the proper antibacterial properties and guarantee drug controlled release in time and in space avoiding the risk of systemic toxicity. Mechanical characterization performed on samples showed that the incorporation of AgNPs or GS enhanced the stiffness of CS/GPTMS\_DSP samples. Moreover, a strict correlation was observed between the Young modulus and the amount of AgNPs incorporated into the membranes: E increased as the AgNPs concentration shifted from 5% wt. to 15 wt.%. The high swelling degree was observed for all samples loaded with the antimicrobial agent reaching final values of about 1200-1300 % and 950% for AgNPs and GS loaded membranes, after 24 hours of incubation in physiological solution, respectively. The incorporation of the antimicrobial agents into CS/GPTMS\_DSP affected the surface morphologies of porous membranes: pore occlusion on the surface of CS based membranes containing AgNPs was detected, by increasing the amount of AgNPs. For this reason, CS/GPTMS\_DSP loaded with AgNPs at a concentration of 10% wt./wt

(CS/GPTMS\_DSP\_AgNP10) was selected as the ideal candidate for this application. GS release profile from CS/GPTMS\_DSP loaded with the antibiotics evidenced a high burst release of the antibiotics in the first 24 hours (about 70% with respect to the GS loaded into the membranes), followed by a gradual release at a decreasing rate over time. Finally, the effect of GS and AgNPs (10 % wt./wt., optimized concentration) on bacterial inhibition was evaluated. The presence of either AgNPs or GS improved the antimicrobial activity of CS based porous membranes. GS loaded samples were highly efficient against *E. coli*, *S. aureus* and *E. fecalis* strains while CS/GPTMS\_DSP\_AgNP10 increased the inhibitory effect against *P. aeruginosa* and *P. mirabilis* bacteria compared to control and GS loaded samples (Fig. 3).

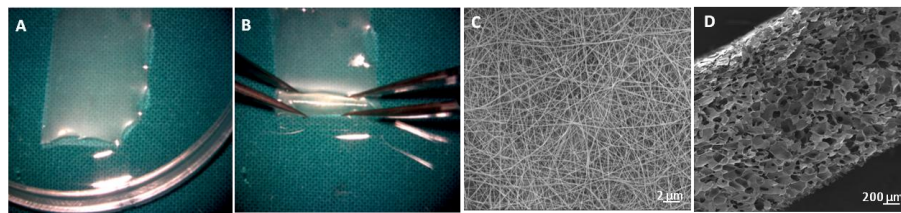


**Fig. 1** Different morphologies of CS based scaffolds for peripheral nerve regeneration (A, B, C) and wound healing (D). Image of CS/DSP (A) and bi-layer membranes (B) before *in vivo* implantation; B) SEM image of CS crosslinked nanofibres; D) SEM image of the fracture section of CS/GPTMS\_DSP porous membranes loaded with GS.

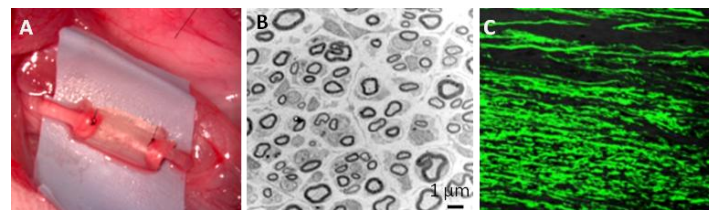


**Fig. 2.** Peripheral nerve regeneration using bi-layer membranes after 12 weeks post-operative. A) Bi-layer membrane after implantation. B) Electron microscope images of regenerated nerves and C) neurofilament staining on longitudinal sections confirmed peripheral nerve regeneration by the formation of aligned and oriented fibres from the proximal to the distal stump.

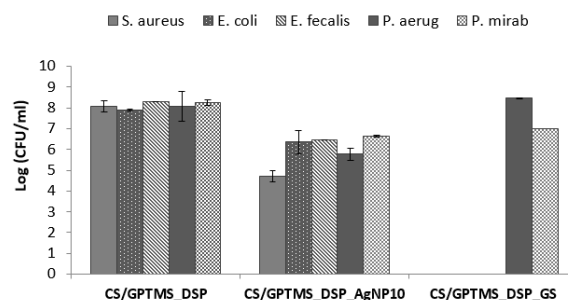


**Fig. 3.** Kinetics of growth inhibition of *S. Aureus*, *E. Coli*, *E. Fecalis*, *P. aeruginosa* and *P. mirabilis* in presence CS/GPTMS\_DSP, CS/GPTMS\_DSP\_GS and CS/GPTMS\_DSP\_AgNP10. AgNPs or GS loaded into CS porous membranes increased the antibacterial activity against five different bacteria strains.

## References

1. Khor, E. and L.Y. Lim, Implantable applications of chitin and chitosan. *Biomaterials*, 2003. **24**(13): p. 2339-49.
2. Singh, A., et al., External stimuli response on a novel chitosan hydrogel crosslinked with formaldehyde. *Bulletin of Materials Science*, 2006. **29**(3): p. 233-238.
3. Beppu, M.M., et al., Crosslinking of chitosan membranes using glutaraldehyde: Effect on ion permeability and water absorption. *Journal of Membrane Science*, 2007. **301**(1-2): p. 126-130.
4. Deng, Y., et al., Preparation and characterization of hyaluronan/chitosan scaffold crosslinked by 1-ethyl-3-(3-dimethylaminopropyl) carbodiimide. *Polymer International*, 2007. **56**(6): p. 738-745.
5. Muzzarelli, R.A.A., Genipin-crosslinked chitosan hydrogels as biomedical and pharmaceutical aids. *Carbohydrate Polymers*, 2009. **77**(1): p. 1-9.
6. Chuang, W.Y., et al., Properties of the poly(vinyl alcohol)/chitosan blend and its effect on the culture of fibroblast in vitro. *Biomaterials*, 1999. **20**(16): p. 1479-1487.
7. Chang, H.H., et al., A novel chitosan-gammaPGA polyelectrolyte complex hydrogel promotes early new bone formation in the alveolar socket following tooth extraction. *PLoS One*, 2014. **9**(3): p. e92362.
8. Jkema-Paassen, J., et al., Transection of peripheral nerves, bridging strategies and effect evaluation. *Biomaterials*, 2004. **25**(9): p. 1583-92.

## List of Abbreviations

### A

**Ag:** silver

**AgNP:** silver nanoparticle

### B

**BAL:** biohybrid artificial liver

**BAX:** cell lymphoma 2 (Bcl2)-associated X protein

**Bcl2:** B cell lymphoma 2

**BDNF:** brain derived neurotrophic factor

**BMSC:** bone marrow stem cell

### C

**CFU:** colony-forming units

**CMDBS:** carboxymethyl benzylamide sulfonate dextran

**CMC:** carboxymethylcellulose

**CNS:** central nervous system

**CS:** chitosan

**CS/DSP:** dibasic sodium phosphate crosslinked CS

**CS/GP:** genipin crosslinked CS

**CS/GPTMS:**  $\gamma$ -glycidoxypropyltrimethoxysilane (GPTMS) crosslinked CS

**CS/GPTMS\_DSP:** GPTMS and DSP crosslinked CS

**CS/GPTMS25\_DSP:** GPTMS (25% w/w) and DSP crosslinked CS

**CS/GPTMS\_DSP\_AgNP:** AgNP loaded CS/GPTMS\_DSP

**CS/GPTMS\_DSP\_GS:** gentamicin sulphate loaded CS/GPTMS\_DSP

**CS M.G:** chitosan medical grade

### D

**DD:** deacetylation degree

**dNTP:** deoxynucleotide triphosphate

**DIV:** days *in vitro*

**DMEM:** Dulbecco's modified Eagle's medium

**DMSO:** dimethyl sulfoxide

**DRG:** dorsal root ganglia

**DSC:** differential scanning calorimetry

**DSP:** dibasic sodium phosphate

**DTG:** derivative of TGA

## E

**E:** Young's modulus

**E\*:** collapse modulus

**ECM:** extracellular matrix

**EDC:** 1-ethyl-3-(3-dimethylaminopropyl)carbodiimide

**EDS:** energy dispersive X-ray spectrometry

**EGF:** epidermal growth factor

## F

**FBS:** fetal bovine serum

**FD-4:** FITC-labeled dextran of 4400 Da

**FD-10:** FITC-labeled dextran of 10000 Da

**FD-20:** FITC-labeled dextran of 20000 Da

**FDA:** food and drug administration

**FGF:** fibroblast growth factor

**FTIR-ATR:** Fourier transform infrared-attenuated total reflectance spectroscopy

## G

**GAG:** glycosaminoglycan

**GDNF:** glial cell line-derived neurotrophic factor

**GF:** growth factor

**GL:** gelatin

**GM-CSF:** granulocyte-macrophage colony-stimulating factor

**GP:** genipin

**GPTMS:**  $\gamma$ -glycidoxypropyltrimethoxysilane

**GS:** gentamicin sulphate

## H

**HA:** hyaluronic acid

## I

**IGF-1:** insulin-like growth factor-1

## L

**LN:** laminin

## M

**MC:** microbial cellulose

**MMT:** montmorillonite

**mTor:** mammalian target of rapamycin

**M<sub>w</sub>:** molecular weight

## **N**

**NF-H:** neurofilament-H  
**NGC:** nerve guidance channel  
**NGF:** nerve growth factor  
**NHS:** N-hydroxysuccinimide  
**NT-3:** neurotrophin -3

## **O**

**OLT:** orthotopic liver transplantation

## **P**

**PAF:** paraformaldehyde solution  
**PBS:** phosphate buffer saline  
**PCL:** poly( $\epsilon$ -caprolactone)  
**PCLF–Ppy:** polycaprolactone fumarate–polypyrrole  
**PDGF:** platelet derived growth factor  
**PEG:** poly(ethylene glycol)  
**PEO:** poly(ethylene oxide)  
**PGA:** polyglycolic acid  
**PHBHHx:** poly(hydroxybutyrate-co-hydroxyhexanoate)  
**PLGA:** poly(L-lactic-co-glycolic acid)  
**PLLA:** poly(L-lactic acid)  
**PMN:** polymorphonuclear leukocytes  
**PNI:** peripheral nerve injury  
**PNS:** peripheral nervous system  
**Poly(DLLA-CL):** poly(DL-lactic-co- $\epsilon$ -caprolactone)  
**Poly(TMC-CL):** poly(trimethylenecarbonate-co- $\epsilon$ -caprolactone)  
**Ppy:** polypyrrole  
**PRP:** platelet-rich-plasma  
**PVA:** polyvinyl alcohol  
**PVP:** polyvinylpyrrolidone

## **R**

**RT-PCR:** Reverse-Transcriptase-Polymerase-Chain-Reaction

## **S**

**SC:** Schwann cell  
**SEM:** scanning electron microscopy analysis  
**SF:** silk fibroin  
**SFM:** serum-free medium  
**SOD:** superoxide dismutase

## **T**

**TBP:** TATA-binding protein

**TE:** tissue engineering

**TGA:** thermogravimetric analysis

**TGF- $\beta$ :** transforming growth factor- $\beta$

**TGF- $\beta$ 1:** transforming growth factor- $\beta$ 1

**TNF- $\alpha$ :** tumour necrosis factor- $\alpha$

**TPP:** tripolyphosphate

**TSA:** tryptone soy agar

**TSB:** tryptone soy broth

## **U**

**UBC:** ubiquitin gene C

**UV:** ultraviolet

## **V**

**VAC:** vacuum assisted closure

**VEGF:** vascular endothelial growth factor

**$\sigma^*$ :** collapse strength

**$\epsilon^*$ :** collapse strain

## Introduction to the Thesis Format

This thesis is divided into **V sections**, containing globally 9 chapters (5 of them describing the experimental work performed): the content of each section is summarized below.

**Section I** (Chapter 1) gives an overview of the current state of the art of chitosan-based materials focusing on their application in soft tissue engineering, wound dressing and drug delivery. The section finishes with the definition of thesis goals.

**Section II** (Chapter 2) describes the preparation and characterization of chitosan flat membranes using different crosslinking agents that are applied to improve chitosan mechanical strength and stability under physiological conditions. Chitosan films are obtained by solvent casting of the polymer solution crosslinked using genipin,  $\gamma$ -glycidoxypropyltrimethoxysilane, dibasic sodium phosphate and a combination of  $\gamma$ -glycidoxypropyltrimethoxysilane and dibasic sodium phosphate. The possibility to tailor the final properties of CS scaffolds through crosslinking is a key strategy to apply CS in different biomedical and tissue engineering applications optimizing the materials features to the biological and surgical requirements.

**Section III** presents an overview of the current state of the art on peripheral nerve tissue engineering, focusing on all the scientific and technological aspects, which have been demonstrated to be crucial for a successful approach within this field, as well as some brief insights on future trends (Chapter 3). Section III is also focused on the preparation and characterization of flat membranes (Chapter 4), bi-layer membranes (Chapter 5) and nanofibrous structures (Chapter 6) that can be applied as artificial conduits or internal fillers for peripheral nerve repair after injuries. In Chapter 4, chitosan flat membranes are prepared by solvent casting of a chitosan solution crosslinked with dibasic sodium phosphate and a combination of  $\gamma$ -glycidoxypropyltrimethoxysilane and dibasic sodium phosphate. The flat membranes show permeability to nutrients and suitable biological properties, both *in vitro* and *in vivo*, for their use in clinical application. Chapter 5 describes the fabrication of bi-layer membranes by solvent casting with the aim to produce scaffold structures with good biocompatibility in the inner layer and with the desired mechanical strength protruded by the outer. The multi-component membranes show a tight connection between the two layers, permeability to nutrients and promote peripheral nerve regeneration. In Chapter 6 crosslinked chitosan nanofibres are prepared by electrospinning to be used as internal filler to favor Schwann cells adhesion and proliferation.

**Section IV** describes the current state of the art on wound healing and skin tissue engineering, focusing the attention on advanced wound management dressings, their key advantages and shortcomings, which have been demonstrated to be crucial for a successful approach within this field (Chapter 7). Within this section, the preparation and characterization of chitosan porous membranes with improved antimicrobial properties for the treatment of chelonian shell injuries is described (Chapter 8). Porous membranes loaded with silver nanoparticles and gentamicin sulphate are prepared via freeze-drying technique with the aim to promote wound healing and to reduce the bacterial proliferation in chelonians after carapace lesions. The membranes loaded with gentamicin or silver nanoparticles show good bactericidal activity against both of *Gram*<sup>+</sup> and *Gram*<sup>-</sup> bacteria. Preliminary *in vivo* tests are carried out on *Testudo Hermannii* for both the two typologies of membranes.

Finally, **Section V** (Chapter 9) presents the main achievements of the work against the scope of the present thesis drawing general conclusions and indications for future work.

## **Section I**

# **Chitosan as a biomaterial**



# Chapter 1

## Chitosan based biomaterials: state of the art and future perspective in soft tissue engineering regeneration and repair

### 1.1 Introduction

Tissue engineering (TE) is a multidisciplinary field that combines fundamental principles from materials engineering and molecular biology in efforts to solve critical medical problems, as tissue loss and organ failure. It involves the fundamental understanding of structure–function relationships in normal and pathological tissues and the development of biological substitutes that promote tissue repair and/or functional restoration.

In this regenerative approach, the biomaterial scaffolds provide not only temporary three dimensional frameworks to form the designed tissues, but essentially acts as an artificial extracellular matrix to support cell growth and proliferation. In this regard, considerable attention has been given to chitosan (CS), because of its unique biological properties including biocompatibility, biodegradability to harmless products, nontoxicity, physiological antibacterial, haemostatic, antitumoral and anticholesteremic properties [1-6]. Furthermore, due to the cationic nature of CS molecules and the abundant functional amine and hydroxyl groups on the molecular chain, CS has been selected as a promising biomaterial for carrying proteins and other active molecules through physical or chemical means [7]. These properties, find several biomedical applications in soft tissue engineering [8-10], wound healing [11-13] and as excipients for drug delivery [14-18].

CS can be easily processed into gels [15, 19, 20], membranes [21, 22], nanofibers [16, 23-27], nanoparticles [7, 17, 28-30], scaffolds [11, 31-33] and sponges [18, 34-36].

The first part of chapter 1 discusses the chemical and physical properties of CS, including the structure and extraction method, and structure-property relationship. Then, a second part of chapter 1 reviews the biological properties of CS that are fundamental properties for the applicability of CS as potential biomaterial for fabrication of biomedical devices. In the last part, the attention is focused on the use of CS based biomaterials and system for soft tissue engineering, wound dressing and drug delivery applications.

## 1.2 Chitosan: structure

CS derives from chitin that is the second most abundant natural biopolymer commonly found in shells of marine crustaceans and cell walls of fungi. CS is a linear, semi-crystalline polysaccharide composed of (1→4)-2-acetamido-2-deoxy-β-D-glucan (N-acetyl D-glucosamine) and (1→4)-2-amino-2-deoxy-β-D-glucan (D-glucosamine) units [37]. It is obtained by partial deacetylation of chitin in the solid state under alkaline conditions (concentrated NaOH) or by enzymatic hydrolysis in the presence of particular enzymes, among of chitin deacetylase [38]. Because of the semicrystalline morphology of chitin, CS occurs as a copolymer of N-acetylglucosamine and N-glucosamine structural units randomly or block distributed throughout the biopolymer chain. Generally, CS has three types of reactive functional groups, an amino group (C2 position) as well as both primary and secondary hydroxyl groups (C3 and C6 positions) which allow CS modification such as graft copolymerization for the production of scaffolds for different TE applications. The structure of chitin and CS are showed in Fig. 1.1. The two most important structural parameters that affect the properties of CS are the deacetylation degree (DD) and molecular weight ( $M_w$ ). The  $M_w$  of CS is dependent on the initial source material (shrimp, crab, fungi, etc.) and can decrease during deacetylation processes [39, 40]. The DD of CS is calculated as the ratio of D-glucosamine to the sum of D-glucosamine and N-acetyl D-glucosamine and gives indication of the number of amino groups along the chains. To be named “chitosan”, the deacetylated chitin should contain at least 60% of D-glucosamine residues [41] (which corresponds to a DD of 60). The deacetylation process of CS is based on processing of the native polymer with alkali: increasing time and temperature the highest DD (>90%) materials can be obtained [40, 42]. CS  $M_w$  can range from 300 to over 1000 kDa with a DD from 30% to 95%. However, commercially available CS has an average  $M_w$  ranging from 3.8 to 20 kDa and a DD from 66 to 95%. CS is semi-crystalline and the degree of crystallinity is a function of the DD. Crystallinity is maximal for both chitin (i.e. 0% deacetylated) and fully deacetylated (i.e. 100%) CS. The DD governs important physical-chemical properties of the CS polymer such as solubility and conformation, being critical for the effectiveness of various technological applications. The CS solubilization occurs in diluted acidic aqueous solutions (pH <6) by protonation of the  $-NH_2$  function on the C2 position of the D -glucosamine repeat unit, leading to the repulsion between positively charged macromolecular chains, allowing water molecules to diffuse into the macromolecular chains and conferring the cationic nature to the polymer [43]. Organic acids such as acetic, lactic, and formic acid and inorganic acid such as hydrochloric acid are generally used to dissolve CS. Due to its polycationic nature, CS possesses the ability to process scaffolds into various forms, such as gels [9, 15, 19], films [44-46] and fibers [23, 25, 26] and can form ionic complexes with a wide variety of natural or synthetic anionic species, such as metal ions [47-49], proteins [50, 51], DNA [52, 53] and some negatively charged synthetic polymers as poly(acrylic acid) [54, 55].

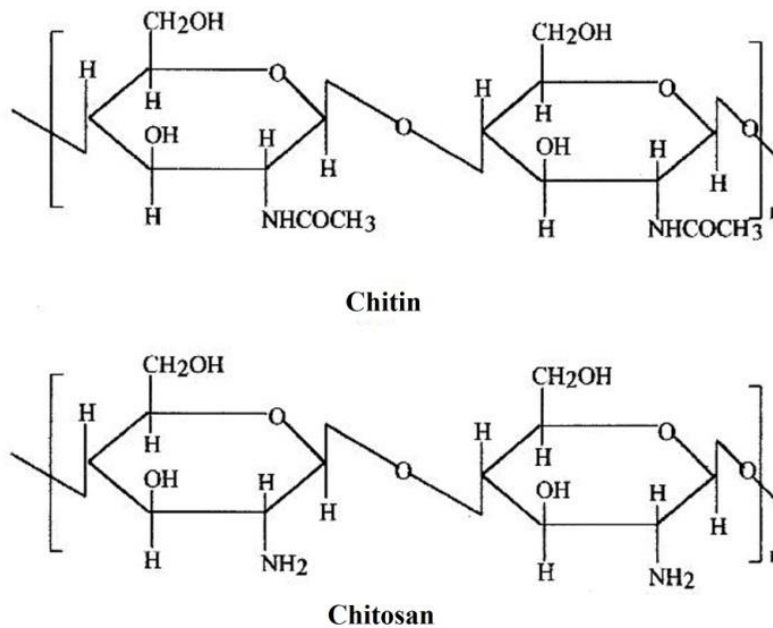


Fig. 1.1. Chemical structure of chitin and CS.

### 1.3 Structure-property relationship

The physical and biological properties of CS are largely dependent on two main structural parameters:  $M_w$  and DD, among a few others. As discussed in paragraph 1.2, crystallinity depends on the DD and a maximum value of crystallinity is obtained for fully deacetylated CS (i.e., 100% deacetylated) because of higher chemical regularity and more flexible polymer chains. Crystallinity, DD and  $M_w$  affect CS solubility. Crystallinity and DD are responsible for the hydration of the polymer, which determines the accessibility with respect to internal sites of the polymer and is directly related to the kinetics of hydration and adsorption behavior. In addition, the solubility of CS in acidic solution (pH below 6) increases with the decrease of the  $M_w$  [56].

DD and  $M_w$  control CS degradability and affected the mechanical properties. The *in vitro* degradation rate has been shown to decrease with an increasing DD (if DD is greater than 50%, i.e., in the “chitosan” range) while an opposite trend has been observed for CS with DDs lower than 50% [57] (“chitin” range). CSs of higher  $M_w$  have been shown to degrade more slowly than those having lower  $M_w$ s [58]. Ratajska et al. have investigated the biodegradation process of three CS samples characterized by similar values of DD (DD = 82-87%) but strongly differentiated  $M_w$  values (ranging from 97 to 473 kD) in an aqueous medium. The results obtained indicate that the shortest time of biodegradation was observed in the CS sample with the lowest  $M_w$  [59]. CS with higher  $M_w$  and higher DD possessed a lower affinity for the enzyme and a slower degradation rate.

As regard the mechanical properties, several studies investigated the relationship between the mechanical properties of CS films and CS  $M_w$  and DD. In general, higher  $M_w$ , and as a consequence higher crystallinity, improves the mechanical properties as evidenced by the enhanced tensile strength [60-62]. During the film formation, CS forms

hydrogen bonds between hydroxyl groups and amino groups in CS film which increase with the increasing amount of amino and hydroxyl groups, due to the increase in concentration of CS [63]. Increase in DD also has a positive effect on the tensile strength of CS films [40], because of higher DD in the CS range (when DD > 50%) resulted in higher crystallinity.

Viscosity and swelling degree are also associated to  $M_w$ , DD and crystallinity. The viscosity of CS increases with an increase in  $M_w$ , DD and crystallinity and decreases when temperature increased. Viscosity also influences the enzymatic degradation: low DD and viscosity tend to degrade CS more rapidly [64].

CS with a lower  $M_w$  has been found to have a low crystallinity and higher swelling index and permeability [62, 65, 66]. Moreover, by lowering the charge density CS's binding capacity for anionic compounds decreases [62].

Due to the fact that the physicochemical properties are greatly influenced by CS structural parameters, controlling  $M_w$  and DD could be a useful tool to design finely tuned CS-based devices for biomedical applications.

#### **1.4 Biological properties of chitosan**

CS offers unique opportunities to the development of many different applications because of its remarkable biological properties: biocompatibility, low toxicity, biodegradability to harmless products, antibacterial activity, mucoadhesive and its affinity to anionic components. In this regard, CS have been used in food [67], pharmaceutical [68], textile [69, 70], water treatment [71, 72] and biomedical industries. The biological properties make also CS a promising candidate for the purpose of drug delivery for a host of drug moieties (antiinflammatories, peptides etc.) [2, 28].

The elucidation of the biological properties will lead to a better understanding of CS medical and pharmaceutical interest.

1. Biocompatibility and toxicity depend on the preparation method and on the DD (biocompatibility increases with DD increase). Several studies have been performed *in vitro* to evaluate the biocompatibility of CS using a variety of cell types such as fibroblasts [73-75], osteoblasts [74, 76], chondrocytes [76], keratinocytes [73-75, 77], neural cells [74, 78, 79], and hepatocytes [6, 80, 81]. Results have shown that CS is nontoxic and can support these types of cells to adhere and proliferate, which suggests that CS is compatible with these cell types.
2. Biodegradability: CS has been shown to be degraded *in vivo* by enzymes such as lysozymes [82] and chitinases [83], to N-glucosamine oligosaccharide, which is endogenous to human body. This oligosaccharide can be incorporated in metabolic pathways or be further excreted [84]. As the  $M_w$  decreases, the absorption of CS by intestine increases [85]. The degradation rate is also inversely related to the degree of crystallinity which is controlled mainly by the DD [86]. Structural parameters ( $M_w$ , DD and crystallinity) could be used to finely tune the degradation rate for biomedical applications.

3. Antimicrobial activity: numerous studies have demonstrated broad-spectrum antimicrobial activities of CS against *Gram*<sup>+</sup> (i.e. *Staphylococcus aureus*) and *Gram*<sup>-</sup> (i.e. *Escherichia coli*) bacteria [87, 88]. This biological property of CS relied on numerous intrinsic and extrinsic factors, such as pH, microorganism species, presence or absence of metal cations and  $M_w$ . The exact mechanisms of the antimicrobial activities of CS are not clear; however, two modes have been proposed as an explanation to this property. The first one is attributable to the polycationic nature of CS: the amino groups present in the polymeric chain of CS interact with the negative charges from the residues of macromolecules (lipopolysaccharides and proteins) in the membranes of bacterial cells leading to altered membrane permeability which interfere with the nutrient exchange between the exterior and interior of the cell [89]. In this model the  $NH^{3+}$  groups can also compete with  $Ca^{2+}$  for the electronegative sites on the surface, compromising its integrity and causing cellular death. The second mechanism proposes that CS acts as a chelating agent that selectively binds trace metals and thus inhibits the production of toxins and microbial growth [90]. Finally, CS of low  $M_w$  has been shown to be capable of entering the cell's nucleus itself, interacting with the DNA and affecting the synthesis of proteins and inhibiting the action of various enzymes [91].
4. Mucoadhesion: CS can be explained by the presence of negatively charged residues (sialic acid) in the mucin – the glycoprotein that composes the mucus. In acidic medium, CS amino groups are positively charged and can thus interact with the mucin. This mucoadhesion is directly related to the DD of CS: actually, if CS DD increases, the number of positive charges also increases, which leads to improved mucoadhesive properties [92].
5. Affinity to biological anionic components: CS can be complexed with negatively charged because of the cationic primary amino groups of CS. This property makes CS a good candidate in the field of gene [93, 94] and drug [17, 28, 29, 44] delivery systems. Also, the mucoadhesive property of CS potentially permits a sustained interaction between the macromolecule being “delivered” and the membrane epithelia, promoting more efficient uptake [44, 95] and the ability to open intercellular tight junctions, facilitating its transport into the cells [96].

CS also exerts a haemostatic [97, 98], hypocholesterolemic [99, 100] and hipolipidemic activity [101] and immunity-enhancing [102] and antitumor effects [103] which may be attributed to its cationic nature.

## **1.5 Application of CS based biomaterials**

### **1.5.1 Soft Tissue engineering**

TE is a multidisciplinary field based on the application of biological, chemical, and engineering principles to the repair, restoration, or regeneration of living tissues by using biomaterials, cells, and factors alone or in combination [104]. Scaffold-based TE is one of the most well studied approaches to regenerate different types of tissues, which involves

seeding cells together with signaling molecules on a biodegradable matrix, culturing them *in vitro* and implanting them into *in vivo* defects. In this context, biomaterials, usually in the form of porous scaffolds, play multiple significant roles to provide structural maintenance of the defect shape, act as a delivery vehicle for bioactive molecules and cells and serve as temporary ECM for cell adhesion, proliferation, differentiation, and maturation. The bioinspired cell–scaffold interface must necessarily meet a variety of demanding and coupled requirements, such as biocompatibility and biodegradability of the materials, physico-chemical and mechanical properties and morphological characteristics, all at different length scales.

After some advances and relatively successful clinical applications for hard tissues over the past decade [105], much of the effort is now being directed at soft tissue reconstruction. Engineering two-dimensional (2D) soft tissues (i.e. cornea [106] and skin [5]), and complex three-dimensional (3D) tissues (i.e. cardiac, muscular and neural) is a far more challenging task.

Among different biomaterials, CS is an ideal candidate in soft TE applications since its combined promising biological features (controllable biodegradability, biocompatibility and antimicrobial activity) with easy processability into 2D or 3D scaffolds. CS has been widely applied as bulk materials for TE scaffold fabrication showing good biocompatibility with a variety of cell types such as osteoblasts [74, 76], chondrocytes [76], fibroblasts [73-75], neural [74, 78, 79], and endothelial cells [73-75, 77] and has the potential to be applied in cartilage, liver, nerve, skin and blood vessels applications.

#### **1.5.1.1 Chitosan in cartilage tissue engineering**

Articular cartilage damage is among the most encountered musculoskeletal diseases, eventually leading to total joint replacement if not treated properly. The articular cartilage consisting of hyaline cartilage tissue has very little capacity for spontaneous healing because of the avascular nature of the tissue.

Due to the limited potential for self-repair of the articular cartilage, surgical operations have been used by orthopedics including allograft osteochondral transplantation [107], autologous chondrocyte transplantation [108], allogeneic juvenile cartilage transplantation (DeNovo NT<sup>®</sup>) [109], mosaicplasty [110], and microfracture technique [111]. However, no current procedures for cartilage repair have successfully regenerated long-lasting hyaline cartilage tissue to replace a cartilaginous lesion. To solve this limitation, TE provides a new method for cartilage repair by culturing isolated chondrocytes on a variety of scaffolds. To structurally mimic the environments of the cartilage tissue, the fundamental structure of a scaffold should be a 3D system with adequate mechanical strength considering the articular cartilage mobility. Both synthetic [112] and natural [113-115] scaffolding materials have been used for cell delivery in cartilage regeneration. Synthetic polymers present many drawbacks: i) the creation and accumulation of acidic by-products; ii) low biocompatibility; and iii) a possible *in vivo* inflammatory foreign body reactions [78]. In contrast, natural materials often have high

levels of biocompatibility and biofunctional motives. Such biomaterials including collagen [116], cellulose [117], CS [76, 118], fibrin [119] and silk [120] maintain a differentiated cell phenotype and allow rapid cell expansion. However, they are not mechanically stable enough and the rate of their biodegradation is practically high [121]. To enhance mechanical stability specific components including natural or synthetic materials are generally used to fabricate composite structures which can offer biological cues to promote tissue-specific interactions, while providing desired mechanical properties. Among the natural polymers, CS can be easily molded in various forms (i.e. bulk porous scaffolds, films, hydrogels and beads) and it has a superior biocompatibility because of its structural similarity with glycosaminoglycans (GAGs), naturally present in the extracellular matrix of cartilage [122, 123]. Lahiji et al., have demonstrated that chondrocytes grown on CS film exhibit a spherical morphology and express type II collagen and aggrecan [76, 118]. Zhang et al. performed a series of studies using adipose-derived stem cells loaded on a polyelectrolyte complex scaffold based on poly(L-glutamic acid) and CS to repair full thickness articular cartilage defects. Poly(L-glutamic acid) was conjugated with CS through electrostatic interaction to develop a porous scaffold by a phase separation method. The scaffolds with a pore size of 150–200  $\mu\text{m}$  and a porosity of about 93% provided a favorable environment for the maintenance of adipose-derived stem cells proliferation, migration and chondrogenic differentiation achieving a successful hyaline cartilage regeneration over a period of 12 weeks [124].

CS hydrogels holds great potential as an artificial ECM to regenerate hyaline cartilage since they can be delivered to the defect site in a minimally invasive manner and have shown to be able to maintain the round phenotype of chondrocytes. Remya et al. developed a hydrogel based on CS and hyaluronic acid derivative and cultured chondrocytes encapsulated into the gel over a period of one month. CS hyaluronic acid hydrogel were found to mimic the GAG-rich ECM and to preserve the typical round morphology of chondrocytes throughout the course of the investigation period. Moreover, the developed hydrogels were found to allow the retention of anionic GAGs, proteoglycans and other negatively charged species secreted by the active chondrocytes that further increases the ECM concentration around the cells [125]. The formation of ionic complexes of CS with the negatively charged GAGs has regarded further important property in cartilage TE. This ion complexing mechanism can be used to immobilize chondroitin sulfates with hydrogel materials which mimic the GAG-rich ECM of their articulation because CS has a protective effect against GAGs hydrolysis by their specific enzymes [126].

In addition to the CS properties mentioned above, signaling molecules such as GFs and small peptide sequences and plasmid DNA encoding specific GFs can be incorporated into CS scaffolds for cartilage TE. DNA complexation with CS has been shown to protect plasmids from degradation by nucleases and also facilitates cellular transfection by poorly understood interactions with cell membranes [127]. The release of specific GFs in a controlled fashion has been shown to promote the ingrowth and biosynthetic ability of

chondrocytes. Lee et al. developed a three-dimensional collagen/chitosan/glycosaminoglycan (GAG) scaffold in combination with transforming growth factor-beta1 (TGF- $\beta$ 1)-loaded CS microspheres. TGF- $\beta$ 1 was loaded into CS microspheres using an emulsion-crosslinking method. Then chondrocytes were seeded in the scaffold and incubated in vitro for 3 weeks. This scaffold exhibited controlled release of TGF- $\beta$ 1 and promoted cartilage regeneration [128].

Recently, the treatment of cartilage defects by combining CS based scaffold and autologous whole blood have been shown to promote hyaline repair cartilage because of CS thrombogenic activity could improve the stabilization of the clot formed in the lesion [129, 130].

TE approach with more expanded understanding of articular cartilage and associated pathologies may provide the chitosan-based material that supports chondrogenesis, which can improve the quality of neocartilage produced and the integration with the host tissue as well as the long-term outcomes of cartilage repair in clinical settings.

#### **1.5.1.2 Chitosan in liver tissue engineering**

It is widely accepted that of the currently available therapeutic options, orthotopic liver transplantation (OLT) seems to be the best solution for patients suffering from severe liver dysfunction or terminal liver failure. However, the insufficient donor organs for OLT worldwide, the high cost and the requirement for life-long immunosuppressive drugs have urgently increased the requirement for new therapies for acute and chronic liver disease [131]. Various non biological approaches, such as hemodialysis, hemoperfusion, and plasmapheresis, have limited success because of insufficient replacement of the synthetic and metabolic functions of the liver in these systems [132, 133]. On the other hand, extracorporeal biological treatment, including whole-liver perfusion, liver-slice perfusion, and cross-hemodialysis, have shown some beneficial results, but they are difficult to implement in a clinical setting [134]. For these reasons, many researchers have developed various extracorporeal biohybrid artificial liver (BAL) systems which consist of functional liver cells supported by an artificial cell culture material. In particular, it incorporates hepatocytes into a bioreactor in which the cells are immobilized, cultured, and induced to perform the hepatic functions by processing the blood or plasma of liver-failure patients. The BAL devices for liver TE require a suitable ECM for hepatocyte culture because hepatocytes are anchorage-dependent cells and are highly sensitive to the ECM milieu for the maintenance of their viability and differentiated functions [135]. Hepatocytes *in vivo* survive in a three-dimensional system that is formed by various kinds of ECM components of human liver such as collagen and GAG, which provide mechanical integrity to the liver tissues and harbor several bioactive signals and molecules for cells [136]. Porous scaffolds with large surface-to-volume ratio are relevant to hepatocytes attachment.

Among the natural polymer, CS is a promising biomaterial in liver TE due to the similarity of its structure to GAGs which are component of the liver ECM. CS membranes would

allow the organization of hepatocytes into a three-dimensional architecture, providing mechanical integrity and a space for the diffusion of nutrients and metabolites to and from the cells [137]. Verma et al. showed that unmodified CS can be used as a synthetic matrix to induce the aggregation of human hepatocyte cell line, HepG2, into three dimensional spheroids with appropriate liver tissue-specific functions like albumin secretion and urea synthesis [138]. Moreover, the presence of both the reactive amino and hydroxyl groups in CS allow to chemically modify and physically manipulate the scaffolds into different pore structures [41]. Li et al. showed that the micro-structure of porous scaffolds provided large surface area for cells to adhere and facilitate nutrient and oxygen transportation [139, 140]. Another strategy in liver TE concerned with developing CS based scaffolds modified with galactose moieties as a specific adhesive ligand to the asialoglycoprotein receptor (ASGPR) expressed on the surface of hepatocytes [141, 142]. Park et al. demonstrated galactosylated CS as a new synthetic ECM for hepatocyte attachment through the specific interaction between ASGPR on hepatocytes and galactose ligands of galactosylated CS [142]. Seo et al. developed a highly porous sponge composed of alginate and galactosylated CS as a synthetic ECM for hepatocytes. The presence of galactose ligands facilitated hepatocyte aggregation in the developed scaffold resulting in the maintenance of high cell activity by the intercellular adhesion molecules in the 3D culture system [143]. Furthermore, Fan et al. suggested a potential ability to improve primary hepatocytes bioactivity and liver specific functions on galactosylated CS/hyaluronic acid (HA) sponges by co-culturing both primary hepatocytes and endothelial cells on the hybrid scaffold - thus closely mimicking the dominant cell populations in the intact liver. The binding of the galactose ligand to ASGPR induced liver-targeted transfer of glycoproteins while HA provided anchorage sites for endothelial cells through the cell surface receptor, CD44. As a result, the contact of hepatocytes with endothelial cells appeared to stimulate higher hepatic-specific gene expression and urea production as compared to that achieved in the monoculture system of hepatocytes [144]. The nanotopography of the galactosylated CS based scaffold has also been shown to influence liver specific functions. Feng et al. developed a nanofibrous scaffold based on galactosylated CS and found that the nanofibrous matrix enhanced the maintainance of the albumin secretion and urea synthesis of hepatocytes but did not show much effect on cell attachment. Moreover, the balancing action between galactose ligands and nanotopography induced the formation of flat hepatocyte aggregates which were mechanically stable than spheroidal aggregates on GC films [145].

Although matrices composed of CS can provide an appropriate environment for the regeneration of liver cells, the low mechanical strength and the poor blood biocompatibility of the natural polymer have limited their use in liver TE. Considering that liver is a highly vascular inter-organ that must provide hepatocytes with sufficient oxygen and nutrients, thrombus formation can lead to occlusion and decreased membrane efficiency. Therefore, technologists have proposed a new method to fabricate a BAL with new composition in order to prevent the thrombus formation. Wang et al., developed an

ammonia-treated collagen–CS–heparin matrix for an implantable BAL and found that the presence of heparin into the ammonia- treated collagen–CS matrices could improve the blood biocompatibility respect collagene/CS based scaffolds and did not affect the porosity, the mechanical strength and the stability in an enzyme solution [146].

### **1.5.1.3 Chitosan in nerve tissue engineering**

The regeneration of traumatized peripheral nerve has been attempted in many different ways, which have in common the goal of directing the regenerating nerve fibres into the proper endoneurial tubes. To repair peripheral nerve injuries with neural gaps (more than 20 mm), the current standard treatment uses conventional autologous nerve graft to bridge the neural gap and facilitate nerve regeneration and reconnection. However, due to the intrinsic limitations of autografts, recent advancements in nerve regeneration have involved the application of TE principles based on the regulation of cell behavior and tissue progression through the development of an engineered nerve grafts that mimics the natural ECM and can support three-dimensional cell cultures. Successful nerve regeneration requires TE scaffolds not only for mechanical support of growing neuritis and impediment of ingrowths of fibrous scar tissues, but also to send biological signals to guide the axonal growth cone to the distal stump. Among the various biomaterials that have been investigated, scaffolds made of CS based materials have drawn much attention [147]. CS has been studied as a candidate material for nerve regeneration due to its neuroprotective properties [148] in addition to the already mentioned properties of, biodegradability, biocompatibility and antibacterial activity. Recent *in vitro* studies revealed the suitability of CS membranes as substrate for survival and orientation of Schwann cell (SC) [78] as well as survival and differentiation of neuronal cells [57]. In addition, CS tubes alone or in combination with other biomaterials such as polyglycolic acid (PGA), collagen, alginate can efficiently bridge peripheral nerve defects [149-152]. Chew et al. showed that CS aligned nanofibrous tubes supported the adhesion, migration and proliferation of SCs, providing a similar guide for regenerating axons to Büngner bands in the nervous system [153]. However, CS matrices have been shown to have low mechanical strength under physiological conditions and to be unable to maintain a predefined shape for transplantation, which has limited their use as nerve guidance conduits in clinical applications. The improvement of their mechanical properties can be achieved by modifying CS with different crosslinking agents (i.e. glutaraldehyde,  $\gamma$ -glycidoxypropyltrimethoxysilane, tripolyphosphate, genipin) [33, 154, 155] or by combining CS to synthetic ones [23, 156]. Furthermore, to enhance functional outcomes of peripheral nerve regeneration yielded by nerve conduits alone, biochemical cues, such as support cells, GFs and peptides, are usually incorporated into CS based nerve conduit. Recently, CS based, nerve growth factor (NGF)-loaded nerve conduits have been prepared with the aim of CS nerve cell affinity. 8 mg of NGF were first immobilized onto CS in solution (20 ml) by means of genipin, a crosslinking agent of natural origin, followed by fabrication of nerve conduits through a technique of injection molding (Fig. 1.2A and B).

Genipin was selected to exert both to crosslink CS for polymer modification and concurrently to immobilize NGF onto modified CS. The NGF loaded CS conduits were non-cytotoxic to primary cultured SCs and showed *in vitro* neuro-affinity to PC12 cells in terms of keeping the activity of NGF within nerve conduits, i.e., the ability to stimulate neuronal differentiation of PC12 cells. More intriguingly, the continuous release profile of NGF from NGF loaded CS crosslinked nerve conduits, within a 60-days, consisted of an initial burst that was controlled by concentration gradient-driven diffusion, followed by a zero-order release due to the degradation of CS (Fig. 1.2C) [155].

Few studies reported the blending of CS with a peptide to enhance nerve cell attachment. Mingyu et al. showed an improved attachment, differentiation and growth on the CS/poly(L-lysine) composite materials when compared to cells cultured on CS membranes. The improved nerve cell affinity on the CS/poly(L-lysine) composite materials had been attributed to the increased hydrophilicity by the abundant hydroxyl group and the positive surface charge of CS [157]. Hsu et al., fabricated a laminin (LN)-modified CS multi-walled nerve conduit combined with bone marrow stem cell (BMSC) to enhance axonal regeneration. The *in vitro* and *in vivo* approaches were used to analyze the complex interactions between CS scaffold, cells and cell regulatory molecules and to evaluate long-term biosafety and efficiency for clinical application. LN-CS multi-walled conduit embedded with stem cells supported the regeneration of functional connections between two ends of a severed sciatic nerve. This study also demonstrates the capacity of stem cell therapy to prevent the inflammatory responses caused by CS, resulting in long-term maintenance of the regenerative capacity and to enhance the long-term restoration of motor functions [158]. CS support nerve cell adhesion and neurite outgrowth, making this material potential candidates for scaffolds in neural TE.

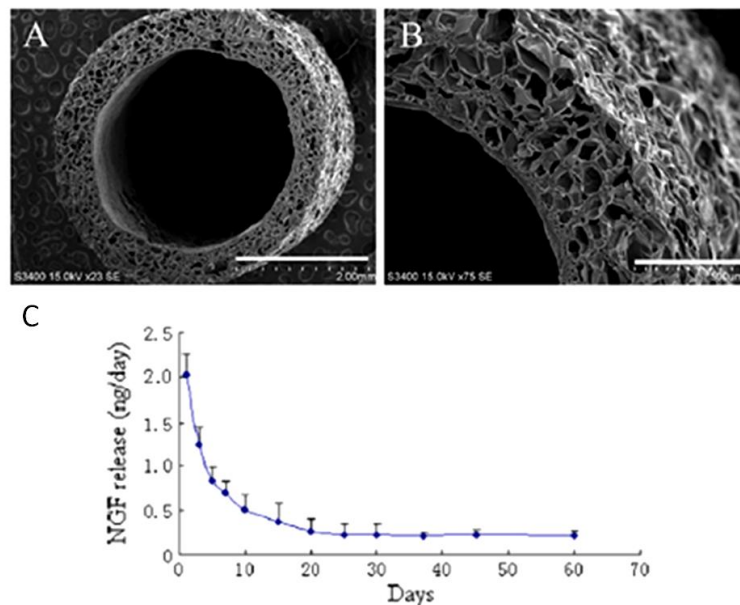


**Fig. 1.2.** SEM images of CS nerve conduits [155]. Side view of the conduit (A), cross-section view of conduit (B), (C) Daily in vitro release of NGF from the CS based nerve conduit to PBS (pH 7.4) at 37°C. Copyright © 2007 Elsevier, © 2005 & 2008 Wiley.

#### 1.5.1.4 Chitosan in vascular tissue engineering

Nowadays, vascular diseases are the largest causes of mortality in the industrialized society. Despite progresses in prevention and treatment, an increasing aging population, the global spread of smoking, and the growing epidemics of obesity and diabetes ensure a rising the incidence of cardiovascular diseases in the next decades. Reconstructive surgery using autologous vessel grafts, particularly small diameter vein or artery (<4 mm), is the conventional therapeutic approach for substitution of diseased vessels or for generation of bypass to improve blood supply downstream of stenosed vessels. Conversely, its disadvantages including the secondary site injure and the potential coexistent diseases of autologous vessel limited its use and, in some circumstances, the application of artificial grafts is necessary. Although some artificial vascular grafts have achieved success in clinical application, products with small diameters (<4 mm) are rarely commercialized, owing to their high failure rate. The transplantation of small-diameter artificial vascular grafts is often ascribed to the poor blood compatibility of artificial vascular grafts, which leads to the adhesion of platelets and plasma protein, and subsequent aggregation and thrombus formation [159, 160]. In this context, TE at the vascular level aims to generate biological substitutes of arterial and vein conduits with functional characteristics of native vessels, combining cellular components with biodegradable scaffolds. The scaffolds made of different materials, such as synthetic polymers, natural materials, and decellularized xenogenous tissues, have been utilized in blood vessel TE. CS has been widely investigated in this field due to its structure similar to GAGs, which are the components of the ECM. However, one disadvantage of CS is its poor hemocompatibility, because the cationic profile causes the unnecessary adhesion of negatively charged platelets, which limits its application in vascular TE. However, the cationic nature of CS can be exploited for pH-dependent electrostatic interactions with anionic GAGs distributed widely throughout the body and other negatively charged species. GAG-based materials hold promise because of their growth inhibitory effects on vascular smooth muscle cells and their anticoagulant activity. For example, CS has been complexed with heparin in order to control heparin release, thereby enhancing the anti-thrombogenic property and attracting an protecting many heparin binding GFs, such as bFGF [161], VEGF [162], and PDGF [163]. Chupa et al. incorporated GAG into porous CS scaffolds with the aim to overcome both incomplete endothelialization and smooth muscle cell hyperplasia, which are two main problems contributing to the failure of existing small-diameter vascular grafts [164]. Madihally et al. fabricated a family of CS scaffolds, including heparin modified porous tubes, which had the potential for application in blood vessel TE [41]. More recently, a hybrid small-diameter vascular graft was developed from synthetic polymer poly( $\epsilon$ -caprolactone) (PCL) and natural polymer CS by the co-electrospinning technique (Fig. 1.3A, B). Heparin was immobilized on the grafts through ionic bonding between heparin and CS fibers. Heparin functionalization was found to improve the hemocompatibility of the PCL/CS vascular grafts, by the reduction of platelet adhesion (Fig 1.3C, D), and moderately to inhibit the proliferation of vascular smooth muscle cells,

a main factor for neointimal hyperplasia [165]. In another study, nanocoatings of CS and HA were deposited onto arteries through a layer-by-layer technique coating significantly reduced the adhesion of blood platelets, thus demonstrating a restored patency of the denuded arteries [166]. The complex of CS and anionic GAG is supposed to be a promising approach for the development of artificial vascular graft due to the anticoagulant activity and the inhibitory effects on vascular smooth muscle cells.

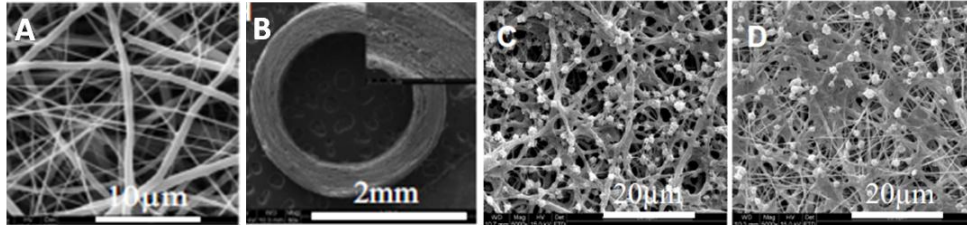


**Fig. 1.3:** SEM images of CS nerve conduits of electrospun PCL/CS hybrid mats [165]. (A), PCL/CS fiber hybrid mats (B) cross section of tri-layered PCL/CS hybrid tubular grafts (insert shows the enlargement), platelets adhering on the surface of PCL/CS hybrid mats (C) before and (D) after heparin functionalization. Copyright © 2007 Elsevier, © 2005 & 2008 Wiley.

### 1.5.2 Wound dressing

Wound healing can be problematic in several clinical settings because of massive tissue injury (burns), wound healing deficiencies (chronic wounds), or congenital conditions and diseases. The healing of a skin wound is a complicated course, including a wide range of cellular, molecular, physiological, and biological processes. The skin plays an important role in homeostasis and the prevention of invasion by microorganisms. Immediate coverage with a wound dressing is generally necessary after the skin is damaged with the attempt to rapidly produce a construct that offers the complete regeneration of functional skin by fulfilling its many normal functions: barrier formation; pigmentary defence against UV irradiation; thermoregulation; and mechanical and aesthetic functions [167]. In past decades, many biological skin substitutes such as xenograft, allografts, and autografts have been employed for wound healing. However, due to the antigenicity or the limitation of donor sites, the skin substitutes cannot accomplish the purpose of the skin recovery. In this context, engineered skin substitutes have been developed to address the medical need for wound coverage and tissue repair. An ideal engineered wound dressing should be elastic and biocompatible and it should protect the wound from bacterial infection. Moreover, current strategies are focused on the acceleration of the wound repair at molecular and systemic levels. Efforts have been focused on the use of biologically derived materials such as, chitins and its derivatives, which are capable of accelerating the healing process. CS has been found to promote tissue granulation and accelerate wound healing through the recruitment of inflammatory cells such as polymorphonuclear leukocytes (PMN) and macrophages to the wound site [168]. Moreover, CS has many other useful and advantageous biological properties in the application as a wound dressing, such as biocompatibility, biodegradability, hemostatic

activity and anti-infectious activity [169-171]. CS and its derivative have been found to evoke a minimal foreign body reaction, with little or no fibrous encapsulation. It observed the typical course of healing with formation of normal granulation tissue, often with accelerated angiogenesis. Okamoto et al. reported that CS influenced all stages of wound repair in experimental animal models [172]. In the inflammatory phase, CS has unique hemostatic properties that are independent of the normal clotting cascades. *In vivo* this polymer can also stimulate the proliferation of fibroblasts and modulate the migration behavior of neutrophils and macrophages modifying subsequent repair processes such as fibroplasias and reepithelialization. Due to the ease of processability of this natural polymer, CS based skin substitutes can be fabricated in the form of non-wovens, nanofibrils, composites, films, scaffolds and sponges to mimic the stratified microstructure of skin tissue and to provide a temporary ECM for cell infiltration and vascularization. Various forms of wound dressing based on CS and its derivatives are actually commercially available (Table 1.1).

Freeze-drying CS solutions has been frequently used to fabricate CS-based scaffolds for skin regeneration, which typically exhibit pore sizes of 100-200  $\mu\text{m}$  and pore volume of more than 90% [173]. Asymmetric CS based scaffolds have also been prepared by a controlled freezing-lyophilization process or by applying an additional dense layer of biomaterials on top of the CS substitutes, producing a bilayer structure to mimic the native skin structure [174]. For example, Mi et al. prepared asymmetric CS membrane with skin surface layer supported on a macroporous sponge-like sublayer through immerse-precipitation phase-inversion method [175]. Ma et al. fabricated CS bilayer scaffold via the formation of a dense film by the casting method and a porous sponger layer lyophilized with porogens at  $-28^{\circ}\text{C}$  [176]. Recently, the use of polymeric nanofibres has attracted considerable interest due to high surface area to volume ratio, high porosity, pore size distribution and morphology. Chen et al. reported that electrospun CS/collagen/polyethylene oxide nanofibrous membrane crosslinked by glutaraldehyde vapor is beneficial in wound healing application. They indicated non-cytotoxicity for these nanofibres regarding 3T3 fibroblast growth and *in vitro* biocompatibility [177]. Naseri et al., developed electrospun CS/polyethylene oxide-based randomly oriented fiber mats reinforced with 50 wt% of chitin nanocrystals and crosslinked using genipin. The crosslinked nanocomposite fiber mats enriched with chitin nanocrystals improved the moisture stability of the electrospun mats and facilitated water-mediated crosslinking processes. Moreover, the addition of chitin nanocrystals had a positive impact on the mechanical properties of the fibrous mats showing a tensile strength of 64.9 MPa and modulus of 10.2 GPa and allowing the membranes to maintain their flexibility. Developed mats were also compatible toward adipose derived stem cells after 7 days and can be considered as a potential candidate for wound dressing application [178]. CS based skin substitutes, having hydrogel-forming properties have been also considered to be advantageous in their application as a wound dressing material because of their high water content and biocompatibility. A hydrogel sheet composed of a blended powder of

alginate, chitin/CS and fuciodan (ACF-HS) has been developed as a functional skin scaffolds with the aim to create in vivo a moist environment with exudates environment for rapid wound healing [179]. Full thickness skin defects were made on the backs of rats. After a pretreatment of mitomycin solution, ACF-HS was applied to the healing-impaired wounds. Histological examination demonstrated significantly advanced granulation tissue and capillary formation in the skin damage treated with ACF-HS on day 7, as compared to those left untreated. Furthermore, antibiotic-loaded CS-based scaffolds have been used to treat severe skin injuries. For example, artificial skin substitutes made of CS membrane or porous scaffolds could be used to release antibacterial agents such as nanotitanium dioxide [180] or silver (Ag), in the form of metallic nanoparticles [181] or sulfadiazine cream [13], and exhibit good antimicrobial properties. Lee et al. designed a novel wound dressing by obtaining electrospun CS nanofibres containing various ratios of silver nanoparticles (AgNPs) (AgNPs contents=0, 4, 2, 1.3, and 0.7 wt. %) with the aim to investigate its antibacterial efficacy in a zone of inhibition antibacterial test system. AgNPs were synthesized directly by chemical reduction within the CS solution. In antibacterial testing, the pure CS nanofibres were observed to not substantially inhibit bacterial growth. But CS/AgNPs nanofibers displayed a high degree of effectiveness against Gram<sup>-</sup> *Pseudomonas aeruginosa* and Gram<sup>+</sup> Methicillin-resistant *Staphylococcus aureus*. Additionally, the quantity of AgNPs was increased in the fibres and consequently antibacterial properties were enhanced against both microorganisms [182]. In addition, CS-based scaffold can be functionalized to carry GFs able to accelerate skin wound healing. For example, Mizuno et al. reported that CS was a good wound healing material and incorporation of that to basic fibroblast growth factor (BFGF) accelerated the rate of healing.

**Table 1.1** Commercially available CS and its derivatives based wound dressing materials

Material	Trade name	Manufacturer
Chitosan and its derivatives	Tegasorb®	3M
	Tegaderm®	3M
	HemCon Bandage TM	HemCon
	Chitodine®	IMS
	Trauma DEX®	Medafor

### 1.5.3 Drug delivery

Apart from applications soft TE and wound dressing, CS has been applied for drug delivery system fabrication. Thanks to its unique feature of being positively charged in physiological condition, CS is especially advantageous in forming stable complex with negative compounds, which makes CS a good candidate for drug encapsulation and controlled release [183]. CS has also showed the ability to adhere to the mucosal surface and it is capable of penetrating the tight junctions between epithelial cells [96]. In addition, CS and its derivatives can be processed under mild conditions, avoiding GFs and

drug inactivation due to otherwise harsh processing conditions, and it can be fabricated into different forms and shapes to incorporate bioactive molecules for various *in vivo* applications. To date CS and its derivatives have been applied as carriers for drugs [184, 185], peptides [186] or genes [187-189] delivery. Particularly, CS has been used in the preparation of mucoadhesive formulations [190, 191], improving the dissolution rate of the poorly soluble drugs [192], drug targeting [193, 194] and enhancement of peptide absorption [195].

Presently, a variety of CS-based drug delivery materials in the forms of gels [196], tablets [197], beads [198, 199], films [200] and particles [201, 202] have been developed and studied. Different types of CS-based drug delivery systems are summarized in Table 1.2. For example, Azab et al. developed a CS-based hydrogel cross-linked with glutaraldehyde and loaded with <sup>131</sup>I-norcholesterol radioisotope for cancer therapy. CS hydrogels were tested in a breast cancer xenograft mouse model showing a reduction in the progression rate of the tumor, and preventing 69% of tumor recurrence and metastatic spread. Importantly, little or no systemic distribution of the radioisotope after hydrogel implantation was observed [203]. In another study, Senel et al. designed CS gels (at 1 or 2% concentration) or film forms for local delivery of chlorhexidine gluconate, an antifungal agent, to the oral cavity. Due to bioadhesive property and high viscosity of the selected natural polymer, CS drug delivery systems were found to remain in the oral cavity and release the drug for a long period of time, thus enhancing the clinical effect. Release of the chlorhexidine gluconate from gel (2% concentration) and film was maintained for 3 hours and a higher antifungal agent release was observed from gels compared to film [204].

Among the different typologies of drug delivery system, CS based microspheres/nanoparticles are widely studied for controlled release of drugs, antibiotics, proteins, peptide drugs anti-inflammatory, steroids, antidiabetic, diuretics, amino acid and vaccines. Emulsion, chemical or ionic gelation [205], coacervation/precipitation [206, 207] and spray-drying [208] have been used for CS- based drug delivery system fabrication; these techniques were selected since they reduce the risk of drug, peptide and gene denaturation. Method selection depends upon factors such as particle size requirement, thermal and chemical stability of the active drug molecule, reproducibility of the release kinetic profiles, stability of the final product and residual toxicity associated with the final product. Pan *et al.* prepared insulin-loaded CS nanoparticles by ionotropic gelation of CS with tripolyphosphate (TPP) anions. The positively charged, stable CS nanoparticles showed particle size in the range of 250-400 nm. Insulin association was up to 80%. *In vitro* release experiments indicated initial burst release which is pH-sensitive. CS nanoparticles enhanced the intestinal absorption of insulin to a greater extent than the aqueous solution of CS *in vivo*. After administration of 21 iu/kg insulin in the CS nanoparticles, hypoglycemia was prolonged over 15 hours. The average pharmacological bioavailability relative to subcutaneous injection of insulin solution was up to 14.9 [209]. Preparations of CS nanoparticles loaded with plasmid DNA encoding surface protein of

Hepatitis B virus using the complex coacervation technique have been reported [207]. The attempt of this work was to provide plasmid DNA carrier system for nasal mucosal immunization against hepatitis B. The loading efficiency, the transfection efficacy and the ability of CS nanoparticles to protect DNA against nuclease digestion were demonstrated. Huang *et al.* prepared CS microspheres by the spray-drying method using type-A gelatin and ethylene oxide–propylene oxide block copolymer as modifiers. Shape, size and surface morphology of the microspheres were significantly influenced by the concentration of gelatin. Betamethasone disodium phosphate-loaded microspheres demonstrated a good drug stability (less 1% hydrolysis product), high entrapment efficiency (95%) and positive surface charge (37.5 mV) [210].

Self-assembly technique is a feasible and cost effective strategy to prepare CS drug carriers. The self assembly process of CS is similar to many other biological molecules (DNA, RNA and proteins) that occur in water phase normal conditions. This process leads to the formation of polyelectrolyte-complexes by electrostatic interaction, which is optically homogeneous, stable nano-dispersion at colloidal level. Self-assembled nanostructures display excellent properties such as protein encapsulation efficiency and prolonged drug release process [211]. Moreover, through self-assembly CS-based micelles have gained attention owing to their ability to solubilize many poorly water-soluble drug [211]. Therefore, various CS derivatives have been prepared via modifications to enhance CS solubility in aqueous solution as well as to provide a hydrophobic portion for the core and a hydrophilic portion for the shell by micelle formation [212-214]. Many studies have reported that CS based self-assembled nanostructures significantly improved the delivery efficiency of therapeutic proteins [215], genes [216] and small molecules [217, 218]. For example, CS self-assembly nanostructures have shown to significantly enhance insulin delivery [215, 219]. Mukhopadhyay *et al.* prepared CS/insulin nanoparticles by self-assembly method and showed self assembled nanoparticles were 200–550 nm in size with almost 85% insulin encapsulation efficiency. Additionally, the *in vivo* oral administration of nanoparticles in diabetic mice indicated significant intestinal absorption of insulin, reducing the blood glucose level within 4 hours in comparison with subcutaneous injections [220]. In another study, Bisht *et al.* reported an easy method to encapsulate doxorubicin-dextran in CS self assembly nanoparticles for cancer therapy. Thanks to the conjunction with dextran and the enclosure in CS nanoparticles, the cardiotoxicity of doxorubicin was alleviated in normal heart cells [221].

**Table 1.2.** CS based drug delivery systems prepared by different methods for various kinds of drugs

Type of system	Method of preparation	Drug
Tablets	matrix	diclofenac sodium, pentoxyphylline, salicylic acid, theophylline
Microspheres/ Microparticles	coating	propranolol HCl
	emulsion cross-linking	theophylline, cisplatin, pentazocine, phenobarbitone, theophylline, insulin, 5-fluorouracil, diclofenac sodium, griseofulvin, aspirin, diphtheria toxoid, pamidronate, suberoylbisphosphonate, mitoxantrone, progesterone
	coacervation/precipitation	prednisolone, interleukin-2, propranolol-HCl
	spray-drying	cimetidine, famotidine, nizatidine, vitamin D-2, diclofenac sodium, ketoprofen, metoclopramide-HCl, bovine serum albumin, ampicillin, cetylpyridinium chloride, oxytetracycline, betamethasone felodipine
Nanoparticles	ionic gelation	gadopentetic acid
	emulsion-droplet coalescence	
	coacervation/precipitation	DNA, doxorubicin
Beads	ionic gelation	nsulin, ricin, bovine serum albumin, cyclosporin A
	reverse micellar method coacervation/precipitation	doxorubicin adriamycin, nifedipine, bovine serum albumin, salbutamol sulfate, lidocaine-HCl, riboflavin
Films	Solution casting	sosorbide dinitrate, chlorhexidine gluconate, trypsin, granulocyte-macrophage colony-stimulating factor, acyclovir, riboflavine, testosterone, progesterone, beta-oestradiol
Gel	Crosslinking	chlorpheniramine maleate, aspirin, theophylline, caffeine, lidocaine-HCl, hydrocortisone acetate, 5-fluorouracil

## 1.6 Thesis goal

The main purpose of this work is the development of **chitosan (CS) based membranes for human and veterinary soft tissue regeneration and repair.** In this work, different typologies of CS scaffolds are prepared varying the **chemical composition** by using different crosslinking mechanisms and the **membrane structure** through different fabrication techniques.

CS has been selected as a candidate material for the development of bioartificial constructs in the field of soft TE because of its attractive properties in terms of biocompatibility, biodegradability, non-antigenicity, antibacterial activity and low cost [222]. Moreover, CS matrices of various forms such as films [75] porous scaffolds [223], hydrogels [15], nanofibers [224-226] can be easily fabricated. However, the main limitations of CS for TE applications are its inadequate mechanical strength and low stability in biological environment. The improvement of CS properties can be achieved by modifying CS with ionic or covalent crosslinking agents (i.e. glutaraldehyde,  $\gamma$ -glycidoxypropyltrimethoxysilane, tripolyphosphate, genipin) [227-230].

In the first part of this thesis, **CS based compact films** are **crosslinked using different compounds** with the aim to provide the basis for the selection of a crosslinking strategy able to impart the required properties to CS membranes in the design of a biomaterial.

Three non cytotoxic compounds, genipin (GP),  $\gamma$ -glycidoxypropyltrimethoxysilane (GPTMS), dibasic sodium phosphate (DSP), widely used as CS crosslinking agents, have been selected. GP is a biocompatible crosslinking agent, and it is less-toxic than traditional chemical agents, such as formaldehyde, glutaraldehyde and epoxy compounds [227, 228]. GPTMS is a silane coupling selected for its oxygen permeability [231], biocompatibility and biodegradability [229]. DSP is a non-toxic polyanion which can interact with CS via electrostatic forces to form ionic crosslinked membrane [230]. The effect of crosslinking on CS based biomaterials and scaffolds performances in terms of physico-chemical, thermal and mechanical properties, as well as degradation and water stability is described in the first part of this thesis.

The aim of the second part of the thesis is the development of different **CS based membranes for peripheral nerve TE in human applications.** Membranes chemical composition is selected in order to i) provide suitable mechanical and physico-chemical properties (ii), favour wrapping and suturing at the implant site, (iii) avoid the risk of compression of the regenerating nerve and (iv) ensure the supply of oxygen and nutrients. Different CS based scaffold morphologies are obtained by varying the fabrication methods. Two alternatives for CS based hollow nerve guide channels (coded as CS flat membrane and bi-layer CS membrane) and a CS based nanostructured as internal filler are prepared.

- **CS flat membranes** crosslinked with DSP alone (CS/DSP) or in association with the GPTMS (CS/GPTMS\_DSP) are fabricated with a solvent casting technique. The constituent ratio of crosslinking agents and CS are selected in the first part of this

thesis to obtain a composite material having both proper mechanical properties and good biocompatibility. At first, permeability study on the crosslinked flat samples is necessary to ensure the diffusion of nutrients through the CS/DSP and CS/GPTMS\_DSP flat films. Then, the cellular response of glial-like cells, the rolling up and the suturability are evaluated on CS/GPTMS\_DSP and CS/DSP flat membranes. *In vivo* tests are carried out on both the two types of nerve scaffolds for bridge implantation across 10-mm long median nerve defects in rats, and the outcome of peripheral nerve repair at 12 weeks post-implantation is investigated.

- **Bi-layer CS membranes** are prepared by a two-step coating technique. By this method, two kinds of CS flat membranes crosslinked with different compounds (optimized in the first part of the thesis) are combined to produce scaffold structures with good biocompatibility in the inner layer and with the desired mechanical strength protruded by the outer one. In detail, CS/DSP is selected as inner layer due to its biocompatibility and its capability to promote peripheral nerve functional recovery (results confirmed by *in vivo* test performed on CS flat membranes), while CS/GPTMS\_DSP (GPTMS 25 % wt./wt.) is used for the realization of the outer layer. GPTMS addition increases mechanical strength and water stability of samples. The amount of GPTMS is optimized to allow the rolling up, suturability of bi-layer membranes and to reduce the risk of distal detachment. The two steps coating technique allows to control the wall thickness and to achieve a tight connection between the two layers. The initial studies are focused on a general physico-chemical, mechanical, dissolution and water uptake analysis of the CS bi-layered membranes. Permeability to nutrients using model molecules is evaluated and confirmed. Preliminary *in vivo* analysis of peripheral nerve recovery is carried out by rolling the developed membranes to form hollow conduits used to bridge 10 mm median nerve defects in rats.
- **Chitosan electrospun nanofibres** are obtained starting from a 0.5 M acetic acid solution and using the electrospinning equipment. A first part of this work is focused on the optimization of the processing parameters to obtain CS based nanofibres from CS acetic acid solutions. Polyethylene oxide (PEO) and dimethylsulphoxide (DMSO) are added to the CS solution: PEO is a biocompatible synthetic polymer used to allow the spinnability of CS solutions at high polymer concentration with controllable fiber size; DMSO is introduced into the CS/PEO solution as a cosolvent to improve processing conditions and increase fiber yields by relaxing CS chain entanglement [226]. Process parameters are selected to prepare nanofibres in the range of 100-200 nm that have been reported to be advantageous for glial cell adhesion and proliferation as compared to fibres with 700 nm dimensions [232]. The use of DSP (the constituent ratio has been selected in the first part of this thesis) as a crosslinker of the nanofibres allows to neutralize CS/PEO\_DMSO solution and does not influence the nanofibre structure. After preliminary morphological, physico-chemical and mechanical characterisation of DSP crosslinked CS based nanofibres (CS/PEO\_DMSO\_DSP), the

structural integrity of nanofibres in physiological solution is examined under physiological conditions.

The aim of the third part of this thesis is the development of **CS based porous membranes for the treatment of wound injuries in veterinary applications**. Due to the similarity of animal wound healing process with humans, skin TE seems to be a promising alternative approach to treat wound injuries compared to conventional treatments adopted by veterinarians. The developed membranes should: i) absorb exudates and toxic components from the wound surface; ii) maintain a high humidity at the wound/dressing interface in order to avoid desiccation and to promote re-epithelialization and cellular migration; iii) protect the wound from bacterial penetration; iv) allow gaseous exchange, necessary for the introduction of oxygen to the wound site as well as the elimination of carbon dioxide and v) be biodegradable, avoiding to periodically remove the device causing trauma to the wound.

CS has been selected for the current study because of its widely use in wound management both in humans and animals: CS stimulates the migration of PMNs and macrophages [233], explicating an anti-inflammatory effect and is a hemostatic effect [234-238].

The goal of this part of the thesis is the design of **CS porous membranes with improved antimicrobial properties** able to promote the wound healing process and to reduce the bacterial proliferation in chelonian shell injury site. On the basis of the results obtained in the first part of the thesis, CS membranes are crosslinked with GPTMS and DSP and are fabricated by freeze-drying. Silver nanoparticles (AgNPs) and gentamicin sulphate (GS) are incorporated into the CS matrices to impart the proper antibacterial properties and to guarantee drug controlled release in time and in space avoiding the risk of systemic toxicity. Three different concentrations for the incorporation of AgNPs (5%, 10% and 15% wt./wt) are investigated while GS dosage is selected according to the conventional veterinary treatment for chelonian carapace healing. After a preliminary analysis on morphological, mechanical and water absorption properties, AgNPs with intermediate concentration is selected as ideal candidate. GS release analysis from CS porous membranes loaded with the antibiotics is evaluated. Antibacterial efficacy against Gram<sup>+</sup> and Gram<sup>-</sup> bacteria is investigated. Finally preliminary *in vivo* tests on Testudo Hermannii are conducted.

This thesis work addresses the research activities of: BICONERVE (“Biomimetic constructs for nerve regeneration”) financed Regional project, and a collaboration with the Department of Veterinary Sciences, Università di Torino and the “Clinica per animali esotici” in Roma.

## References

1. Solov'eva, T., et al., Marine Compounds with Therapeutic Potential in Gram-Negative Sepsis. *Marine Drugs*, 2013. **11**(6): p. 2216-2229.
2. Illum, L., Chitosan and its use as a pharmaceutical excipient. *Pharmaceutical Research*, 1998. **15**(9): p. 1326-1331.
3. Thomas, V., M. Bajpai, and S.K. Bajpai, In Situ Formation of Silver Nanoparticles within Chitosan-attached Cotton Fabric for Antibacterial Property. *Journal of Industrial Textiles*, 2011. **40**(3): p. 229-245.
4. Kim, K.W., et al., Antimicrobial activity of native chitosan, degraded chitosan, and O-carboxymethylated chitosan. *Journal of Food Protection*, 2003. **66**(8): p. 1495-1498.
5. Busilacchi, A., et al., Chitosan stabilizes platelet growth factors and modulates stem cell differentiation toward tissue regeneration. *Carbohydrate Polymers*, 2013. **98**(1): p. 665-676.
6. Seo, W.G., et al., Synergistic cooperation between water-soluble chitosan oligomers and interferon-gamma for induction of nitric oxide synthesis and tumoricidal activity in murine peritoneal macrophages. *Cancer Letters*, 2000. **159**(2): p. 189-195.
7. Agnihotri, S.A., N.N. Mallikarjuna, and T.M. Aminabhavi, Recent advances on chitosan-based micro- and nanoparticles in drug delivery. *Journal of Controlled Release*, 2004. **100**(1): p. 5-28.
8. Ji, C.D. and J. Shi, Thermal-crosslinked porous chitosan scaffolds for soft tissue engineering applications. *Materials Science & Engineering C-Materials for Biological Applications*, 2013. **33**(7): p. 3780-3785.
9. Valmikinathan, C.M., et al., Photocrosslinkable chitosan based hydrogels for neural tissue engineering. *Soft Matter*, 2012. **8**(6): p. 1964-1976.
10. Vrana, N.E., et al., Characterization of poly(vinyl alcohol)/chitosan hydrogels as vascular tissue engineering scaffolds. *Macromolecular Symposia*, 2008. **269**: p. 106-110.
11. Madhumathi, K., et al., Development of novel chitin/nanosilver composite scaffolds for wound dressing applications. *Journal of Materials Science-Materials in Medicine*, 2010. **21**(2): p. 807-813.
12. Dai, M., et al., Chitosan-Alginate Sponge: Preparation and Application in Curcumin Delivery for Dermal Wound Healing in Rat. *Journal of Biomedicine and Biotechnology*, 2009.
13. Mi, F.L., et al., Control of wound infections using a bilayer chitosan wound dressing with sustainable antibiotic delivery. *Journal of Biomedical Materials Research*, 2002. **59**(3): p. 438-449.
14. Jayakumar, R., R.L. Reis, and J.F. Mano, Synthesis and characterization of pH-sensitive thiol-containing chitosan beads for controlled drug delivery applications. *Drug Delivery*, 2007. **14**(1): p. 9-17.
15. Bhattarai, N., J. Gunn, and M.Q. Zhang, Chitosan-based hydrogels for controlled, localized drug delivery. *Advanced Drug Delivery Reviews*, 2010. **62**(1): p. 83-99.
16. Li, W., et al., Preparation, Characterization, and Property of Chitosan/Polyethylene Oxide Electrospun Nanofibrous Membrane for Controlled Drug Release. *Integrated Ferroelectrics*, 2014. **151**(1): p. 164-178.
17. Unsoy, G., et al., Synthesis of Doxorubicin loaded magnetic chitosan nanoparticles for pH responsive targeted drug delivery. *European Journal of Pharmaceutical Sciences*, 2014. **62**: p. 243-250.
18. Lai, H.L., A. Abu'Khalil, and D.Q.M. Craig, The preparation and characterisation of drug-loaded alginate and chitosan sponges. *International Journal of Pharmaceutics*, 2003. **251**(1-2): p. 175-181.
19. Moura, M.J., et al., In Situ Forming Chitosan Hydrogels Prepared via Ionic/Covalent Co-Cross-Linking. *Biomacromolecules*, 2011. **12**(9): p. 3275-3284.

20. Aziz, M.A., et al., Antimicrobial Properties of a Chitosan Dextran-Based Hydrogel for Surgical Use. *Antimicrobial Agents and Chemotherapy*, 2012. **56**(1): p. 280-287.
21. Lieder, R., et al., Solution casting of chitosan membranes for in vitro evaluation of bioactivity. *Biological Procedures Online*, 2013. **15**.
22. Pandis, C., et al., Chitosan-silica hybrid porous membranes. *Materials Science & Engineering C-Materials for Biological Applications*, 2014. **42**: p. 553-561.
23. Cooper, A., et al., Aligned chitosan-based nanofibers for enhanced myogenesis. *Journal of Materials Chemistry*, 2010. **20**(40): p. 8904-8911.
24. Tsai, R.Y., et al., Electrospun chitosan-gelatin-polyvinyl alcohol hybrid nanofibrous mats: Production and characterization. *Journal of the Taiwan Institute of Chemical Engineers*, 2014. **45**(4): p. 1975-1981.
25. Wang, N., et al., Electrospun nanofibrous chitosan membranes modified with polyethyleneimine for formaldehyde detection. *Carbohydrate Polymers*, 2014. **108**: p. 192-199.
26. Jayakumar, R., et al., Novel chitin and chitosan nanofibers in biomedical applications. *Biotechnology Advances*, 2010. **28**(1): p. 142-150.
27. Shalumon, K.T., et al., Single step electrospinning of chitosan/poly(caprolactone) nanofibers using formic acid/acetone solvent mixture. *Carbohydrate Polymers*, 2010. **80**(2): p. 413-419.
28. Jain, A., et al., Docetaxel loaded chitosan nanoparticles: Formulation, characterization and cytotoxicity studies. *International Journal of Biological Macromolecules*, 2014. **69**: p. 546-553.
29. Dev, A., et al., Preparation of poly(lactic acid)/chitosan nanoparticles for anti-HIV drug delivery applications. *Carbohydrate Polymers*, 2010. **80**(3): p. 833-838.
30. Jayakumar, R., et al., Chitosan conjugated DNA nanoparticles in gene therapy. *Carbohydrate Polymers*, 2010. **79**(1): p. 1-8.
31. Baldino, L., et al., Chitosan scaffolds formation by a supercritical freeze extraction process. *Journal of Supercritical Fluids*, 2014. **90**: p. 27-34.
32. Lin, C.Y., L.T. Li, and W.T. Su, Three dimensional chitosan scaffolds influence the extra cellular matrix expression in Schwann cells. *Materials Science & Engineering C-Materials for Biological Applications*, 2014. **42**: p. 474-478.
33. Li, G.C., et al., Effect of silanization on chitosan porous scaffolds for peripheral nerve regeneration. *Carbohydrate Polymers*, 2014. **101**: p. 718-726.
34. Anisha, B.S., et al., Chitosan-hyaluronic acid/nano silver composite sponges for drug resistant bacteria infected diabetic wounds. *International Journal of Biological Macromolecules*, 2013. **62**: p. 310-320.
35. Ding, C.M., et al., Perfusion seeding of collagen-chitosan sponges for dermal tissue engineering. *Process Biochemistry*, 2008. **43**(3): p. 287-296.
36. Rossi, S., et al., "Sponge-like" dressings based on biopolymers for the delivery of platelet lysate to skin chronic wounds. *International Journal of Pharmaceutics*, 2013. **440**(2): p. 207-215.
37. Rinaudo, M., Chitin and chitosan: Properties and applications. *Progress in Polymer Science*, 2006. **31**(7): p. 603-632.
38. Venkatesan, J. and S.K. Kim, Chitosan Composites for Bone Tissue Engineering-An Overview. *Marine Drugs*, 2010. **8**(8): p. 2252-2266.
39. Prashanth, K.V.H., F.S. Kittur, and R.N. Tharanathan, Solid state structure of chitosan prepared under different N-deacetylating conditions. *Carbohydrate Polymers*, 2002. **50**(1): p. 27-33.
40. Cao, W.L., et al., Effects of the degree of deacetylation on the physicochemical properties and Schwann cell affinity of chitosan films. *Journal of Biomaterials Applications*, 2005. **20**(2): p. 157-177.

41. Madihally, S.V. and H.W.T. Matthew, Porous chitosan scaffolds for tissue engineering. *Biomaterials*, 1999. **20**(12): p. 1133-1142.
42. Tsaih, M.L. and R.H. Chen, The effect of reaction time and temperature during heterogenous alkali deacetylation on degree of deacetylation and molecular weight of resulting chitosan. *Journal of Applied Polymer Science*, 2003. **88**(13): p. 2917-2923.
43. Wang, W.P., et al., A new green technology for direct production of low molecular weight chitosan. *Carbohydrate Polymers*, 2008. **74**(1): p. 127-132.
44. Hermans, K., et al., Development and characterization of mucoadhesive chitosan films for ophthalmic delivery of cyclosporine A. *International Journal of Pharmaceutics*, 2014. **472**(1-2): p. 10-19.
45. Inta, O., R. Yoksan, and J. Limtrakul, Hydrophobically modified chitosan: A bio-based material for antimicrobial active film. *Materials Science & Engineering C-Materials for Biological Applications*, 2014. **42**: p. 569-577.
46. Jridi, M., et al., Physical, structural, antioxidant and antimicrobial properties of gelatin-chitosan composite edible films. *International Journal of Biological Macromolecules*, 2014. **67**: p. 373-379.
47. Shankar, P., et al., Comparative studies on the removal of heavy metals ions onto cross linked chitosan-g-acrylonitrile copolymer. *International Journal of Biological Macromolecules*, 2014. **67**: p. 180-188.
48. Ferrero, F., C. Tonetti, and M. Periolatto, Adsorption of chromate and cupric ions onto chitosan-coated cotton gauze. *Carbohydrate Polymers*, 2014. **110**: p. 367-373.
49. Kandile, N.G. and A.S. Nasr, Environment friendly modified chitosan hydrogels as a matrix for adsorption of metal ions, synthesis and characterization. *Carbohydrate Polymers*, 2009. **78**(4): p. 753-759.
50. Campina, J.M., et al., Studies on the interactions between bovine beta-lactoglobulin and chitosan at the solid-liquid interface. *Electrochimica Acta*, 2010. **55**(28): p. 8779-8790.
51. Zhang, Y.N., Y. Yang, and T.Y. Guo, Genipin-crosslinked hydrophobical chitosan microspheres and their interactions with bovine serum albumin. *Carbohydrate Polymers*, 2011. **83**(4): p. 2016-2021.
52. Li, X.W., et al., Sustained expression in mammalian cells with DNA complexed with chitosan nanoparticles. *Biochimica Et Biophysica Acta-Gene Structure and Expression*, 2003. **1630**(1): p. 7-18.
53. Liu, W.G., et al., An investigation on the physicochemical properties of chitosan/DNA polyelectrolyte complexes. *Biomaterials*, 2005. **26**(15): p. 2705-2711.
54. Pavinatto, F.J., L. Caseli, and O.N. Oliveira, Chitosan in Nanostructured Thin Films. *Biomacromolecules*, 2010. **11**(8): p. 1897-1908.
55. Kim, T.H., et al., Chemical modification of chitosan as a gene carrier in vitro and in vivo. *Progress in Polymer Science*, 2007. **32**(7): p. 726-753.
56. Sashiwa, H. and S.I. Aiba, Chemically modified chitin and chitosan as biomaterials. *Progress in Polymer Science*, 2004. **29**(9): p. 887-908.
57. Freier, T., et al., Controlling cell adhesion and degradation of chitosan films by N-acetylation. *Biomaterials*, 2005. **26**(29): p. 5872-5878.
58. Zhang, H. and S.H. Neau, In vitro degradation of chitosan by a commercial enzyme preparation: effect of molecular weight and degree of deacetylation. *Biomaterials*, 2001. **22**(12): p. 1653-1658.
59. Ratajska, M., et al., Studies on the biodegradation of chitosan in an aqueous medium. *Fibres & Textiles in Eastern Europe*, 2003. **11**(3): p. 75-79.
60. Park, S.Y., K.S. Marsh, and J.W. Rhim, Characteristics of different molecular weight chitosan films affected by the type of organic solvents. *Journal of Food Science*, 2002. **67**(1): p. 194-197.

61. Miyata, T., T. Iwamoto, and T. Uragami, Characteristics of Permeation and Separation for Propanol Isomers through Poly(Vinyl Alcohol) Membranes Containing Cyclodextrin. *Journal of Applied Polymer Science*, 1994. **51**(12): p. 2007-2014.
62. Trung, T.S., et al., Functional characteristics of shrimp chitosan and its membranes as affected by the degree of deacetylation. *Bioresource Technology*, 2006. **97**(4): p. 659-663.
63. Uragami, T., et al., Structure of Chemically-Modified Chitosan Membranes and Their Characteristics of Permeation and Separation of Aqueous-Ethanol Solutions. *Journal of Membrane Science*, 1994. **88**(2-3): p. 243-251.
64. Kyoko Kofuji, C.-J.Q., Masumi Nishimura, Ikumi Sugiyama, Yoshifumi Murata, Susumu Kawashima, Relationship between physicochemical characteristics and functional properties of chitosan. 2005. **41**(11).
65. Chen, R.H. and H.D. Hwa, Effect of molecular weight of chitosan with the same degree of deacetylation on the thermal, mechanical, and permeability properties of the prepared membrane. *Carbohydrate Polymers*, 1996. **29**(4): p. 353-358.
66. Chen, X.G., et al., Molecular affinity and permeability of different molecular weight chitosan membranes. *Journal of Agricultural and Food Chemistry*, 2002. **50**(21): p. 5915-5918.
67. Agullo, E., et al., Present and future role of chitin and chitosan in food. *Macromolecular Bioscience*, 2003. **3**(10): p. 521-530.
68. Baldrick, P., The safety of chitosan as a pharmaceutical excipient. *Regulatory Toxicology and Pharmacology*, 2010. **56**(3): p. 290-299.
69. Lim, S.H. and S.M. Hudson, Application of a fiber-reactive chitosan derivative to cotton fabric as an antimicrobial textile finish. *Carbohydrate Polymers*, 2004. **56**(2): p. 227-234.
70. El-Tahlawy, K.F., et al., The antimicrobial activity of cotton fabrics treated with different crosslinking agents and chitosan. *Carbohydrate Polymers*, 2005. **60**(4): p. 421-430.
71. Yamada, K., et al., Water purification through bioconversion of phenol compounds by tyrosinase and chemical adsorption by chitosan beads. *Biotechnology Progress*, 2005. **21**(3): p. 823-829.
72. Zeng, D., J. Wu, and J.F. Kennedy, Application of a chitosan flocculant to water treatment. *Carbohydrate Polymers*, 2008. **71**(1): p. 135-139.
73. Neamnark, A., et al., In vitro biocompatibility of electrospun hexanoyl chitosan fibrous scaffolds towards human keratinocytes and fibroblasts. *European Polymer Journal*, 2008. **44**(7): p. 2060-2067.
74. Sangsanoh, P., et al., In vitro biocompatibility of electrospun and solvent-cast chitosan substrata towards Schwann, osteoblast, keratinocyte and fibroblast cells. *European Polymer Journal*, 2010. **46**(3): p. 428-440.
75. Chatelet, C., O. Damour, and A. Domard, Influence of the degree of acetylation on some biological properties of chitosan films. *Biomaterials*, 2001. **22**(3): p. 261-268.
76. Lahiji, A., et al., Chitosan supports the expression of extracellular matrix proteins in human osteoblasts and chondrocytes. *Journal of Biomedical Materials Research*, 2000. **51**(4): p. 586-595.
77. Lim, C.K., et al., In vitro biocompatibility of chitosan porous skin regenerating templates (PSRTs) using primary human skin keratinocytes. *Toxicology in Vitro*, 2010. **24**(3): p. 721-727.
78. Yuan, Y., et al., The interaction of Schwann cells with chitosan membranes and fibers in vitro. *Biomaterials*, 2004. **25**(18): p. 4273-4278.
79. Amado, S., et al., Use of hybrid chitosan membranes and N1E-115 cells for promoting nerve regeneration in an axonotmesis rat model. *Biomaterials*, 2008. **29**(33): p. 4409-4419.
80. Kawase, M., et al., Application of glutaraldehyde-crosslinked chitosan as a scaffold for hepatocyte attachment. *Biological & Pharmaceutical Bulletin*, 1997. **20**(6): p. 708-710.

81. Chu, X.H., et al., In vitro evaluation of a multi-layer radial-flow bioreactor based on galactosylated chitosan nanofiber scaffolds. *Biomaterials*, 2009. **30**(27): p. 4533-4538.
82. Kean, T. and M. Thanou, Chitin and Chitosan: Sources, Production and Medical Applications. *Renewable Resources for Functional Polymers and Biomaterials*, 2011(1): p. 292-318.
83. Funkhouser, J.D. and N.N. Aronson, Chitinase family GH18: evolutionary insights from the genomic history of a diverse protein family. *Bmc Evolutionary Biology*, 2007. **7**.
84. Pangburn, S.H., P.V. Trescony, and J. Heller, Lysozyme Degradation of Partially Deacetylated Chitin, Its Films and Hydrogels. *Biomaterials*, 1982. **3**(2): p. 105-108.
85. Zeng, L.T., et al., Absorption and distribution of chitosan in mice after oral administration. *Carbohydrate Polymers*, 2008. **71**(3): p. 435-440.
86. Yang, Y.M., et al., The controlling biodegradation of chitosan fibers by N-acetylation in vitro and in vivo. *Journal of Materials Science-Materials in Medicine*, 2007. **18**(11): p. 2117-2121.
87. No, H.K., et al., Antibacterial activity of chitosans and chitosan oligomers with different molecular weights. *International Journal of Food Microbiology*, 2002. **74**(1-2): p. 65-72.
88. Zheng, L.Y. and J.A.F. Zhu, Study on antimicrobial activity of chitosan with different molecular weights. *Carbohydrate Polymers*, 2003. **54**(4): p. 527-530.
89. Liu, H., et al., Chitosan kills bacteria through cell membrane damage. *International Journal of Food Microbiology*, 2004. **95**(2): p. 147-155.
90. Cuero, R.G., G. Osuji, and A. Washington, N-Carboxymethylchitosan Inhibition of Aflatoxin Production - Role of Zinc. *Biotechnology Letters*, 1991. **13**(6): p. 441-444.
91. Rabea, E.I., et al., Chitosan as antimicrobial agent: Applications and mode of action. *Biomacromolecules*, 2003. **4**(6): p. 1457-1465.
92. He, P., S.S. Davis, and L. Illum, In vitro evaluation of the mucoadhesive properties of chitosan microspheres. *International Journal of Pharmaceutics*, 1998. **166**(1): p. 75-88.
93. Lavertu, M., et al., High efficiency gene transfer using chitosan/DNA nanoparticles with specific combinations of molecular weight and degree of deacetylation. *Biomaterials*, 2006. **27**(27): p. 4815-4824.
94. Saranya, N., et al., Chitosan and its derivatives for gene delivery. *International Journal of Biological Macromolecules*, 2011. **48**(2): p. 234-238.
95. Hejazi, R. and M. Amiji, Chitosan-based gastrointestinal delivery systems. *Journal of Controlled Release*, 2003. **89**(2): p. 151-165.
96. Illum, L., et al., Chitosan as a novel nasal delivery system for vaccines. *Advanced Drug Delivery Reviews*, 2001. **51**(1-3): p. 81-96.
97. Yang, J., et al., Effect of chitosan molecular weight and deacetylation degree on Hemostasis. *Journal of Biomedical Materials Research Part B-Applied Biomaterials*, 2008. **84B**(1): p. 131-137.
98. Whang, H.S., et al., Hemostatic agents derived from chitin and chitosan. *Journal of Macromolecular Science-Polymer Reviews*, 2005. **C45**(4): p. 309-323.
99. Sugano, M., et al., A Novel Use of Chitosan as a Hypocholesterolemic Agent in Rats. *American Journal of Clinical Nutrition*, 1980. **33**(4): p. 787-793.
100. Moon, M.S., H.S. Lee, and Y. Kim, Hypocholesterolemic effects of chitosan in rats fed with high cholesterol diet. *Faseb Journal*, 2006. **20**(5): p. A1017-A1017.
101. Zhang, W., et al., The hypolipidemic activity of chitosan nanopowder prepared by ultrafine milling. *Carbohydrate Polymers*, 2013. **95**(1): p. 487-491.
102. Smith, A., M. Perelman, and M. Hinchcliffe, Chitosan: a promising safe and immune-enhancing adjuvant for intranasal vaccines. *Hum Vaccin Immunother*, 2014. **10**(3): p. 797-807.
103. Qin, C.Q., et al., Enzymic preparation of water-soluble chitosan and their antitumor activity. *International Journal of Biological Macromolecules*, 2002. **31**(1-3): p. 111-117.

104. Laurencin, C.T., et al., Tissue engineering: Orthopedic applications. *Annual Review of Biomedical Engineering*, 1999. **1**: p. 19-46.
105. Amini, A.R., C.T. Laurencin, and S.P. Nukavarapu, Bone tissue engineering: recent advances and challenges. *Crit Rev Biomed Eng*, 2012. **40**(5): p. 363-408.
106. Nishida, K., et al., Corneal reconstruction with tissue-engineered cell sheets composed of autologous oral mucosal epithelium. *New England Journal of Medicine*, 2004. **351**(12): p. 1187-1196.
107. Bugbee, W.D. and F.R. Convery, Osteochondral allograft transplantation. *Clinics in Sports Medicine*, 1999. **18**(1): p. 67-+.
108. Minas, T. and L. Peterson, Autologous chondrocyte transplantation. *Operative Techniques in Sports Medicine*, 2000. **8**(2): p. 144-157.
109. Adkisson, H.D., et al., The Potential of Human Allogeneic Juvenile Chondrocytes for Restoration of Articular Cartilage. *American Journal of Sports Medicine*, 2010. **38**(7): p. 1324-1333.
110. Hangody, L., et al., Mosaicplasty for the treatment of articular cartilage defects: Application in clinical practice. *Orthopedics*, 1998. **21**(7): p. 751-756.
111. Blevins, F.T., et al., Treatment of articular cartilage defects in athletes: An analysis of functional outcome and lesion appearance. *Orthopedics*, 1998. **21**(7): p. 761-768.
112. Li, W.J., et al., Biological response of chondrocytes cultured in three-dimensional nanofibrous poly(epsilon-caprolactone) scaffolds. *Journal of Biomedical Materials Research Part A*, 2003. **67A**(4): p. 1105-1114.
113. Lee, C.R., A.J. Grodzinsky, and M. Spector, The effects of cross-linking of collagen-glycosaminoglycan scaffolds on compressive stiffness, chondrocyte-mediated contraction, proliferation and biosynthesis. *Biomaterials*, 2001. **22**(23): p. 3145-3154.
114. Wang, Y.Z., et al., Cartilage tissue engineering with silk scaffolds and human articular chondrocytes. *Biomaterials*, 2006. **27**(25): p. 4434-4442.
115. Yoo, H.S., et al., Hyaluronic acid modified biodegradable scaffolds for cartilage tissue engineering. *Biomaterials*, 2005. **26**(14): p. 1925-1933.
116. Aigner, T. and J. Stove, Collagens - major component of the physiological cartilage matrix, major target of cartilage degeneration, major tool in cartilage repair. *Advanced Drug Delivery Reviews*, 2003. **55**(12): p. 1569-1593.
117. Svensson, A., et al., Bacterial cellulose as a potential scaffold for tissue engineering of cartilage. *Biomaterials*, 2005. **26**(4): p. 419-431.
118. Nettles, D.L., S.H. Elder, and J.A. Gilbert, Potential use of chitosan as a cell scaffold material for cartilage tissue engineering. *Tissue Engineering*, 2002. **8**(6): p. 1009-1016.
119. Eyrych, D., et al., In vitro and in vivo cartilage engineering using a combination of chondrocyte-seeded long-term stable fibrin gels and polycaprolactone-based polyurethane scaffolds. *Tissue Engineering*, 2007. **13**(9): p. 2207-2218.
120. Baek, H.S., et al., Enhanced chondrogenic responses of articular chondrocytes onto porous silk fibroin scaffolds treated with microwave-induced argon plasma. *Surface & Coatings Technology*, 2008. **202**(22-23): p. 5794-5797.
121. Tan, H.P., et al., Gelatin/chitosan/hyaluronan scaffold integrated with PLGA microspheres for cartilage tissue engineering. *Acta Biomaterialia*, 2009. **5**(1): p. 328-337.
122. Amler, M.H. and R.Z. Legeros, Hard Tissue Replacement (Htr) Polymer as an Implant Material. *Journal of Biomedical Materials Research*, 1990. **24**(8): p. 1079-1089.
123. VandeVord, P.J., et al., Evaluation of the biocompatibility of a chitosan scaffold in mice. *Journal of Biomedical Materials Research*, 2002. **59**(3): p. 585-590.
124. Zhang, K.X., et al., Repair of an articular cartilage defect using adipose-derived stem cells loaded on a polyelectrolyte complex scaffold based on poly(L-glutamic acid) and chitosan. *Acta Biomaterialia*, 2013. **9**(7): p. 7276-7288.

125. Remya, N.S. and P.D. Nair, Engineering cartilage tissue interfaces using a natural glycosaminoglycan hydrogel matrix--an in vitro study. *Mater Sci Eng C Mater Biol Appl*, 2013. **33**(2): p. 575-82.
126. Sechriest, V.F., et al., GAG-augmented polysaccharide hydrogel: a novel biocompatible and biodegradable material to support chondrogenesis. *Journal of Biomedical Materials Research*, 2000. **49**(4): p. 534-41.
127. Leong, K.W., et al., DNA-polycation nanospheres as non-viral gene delivery vehicles. *Journal of Controlled Release*, 1998. **53**(1-3): p. 183-93.
128. Lee, J.E., et al., Effects of a chitosan scaffold containing TGF-beta1 encapsulated chitosan microspheres on in vitro chondrocyte culture. *Artif Organs*, 2004. **28**(9): p. 829-39.
129. Chevrier, A., et al., Chitosan-glycerol phosphate/blood implants increase cell recruitment, transient vascularization and subchondral bone remodeling in drilled cartilage defects. *Osteoarthritis Cartilage*, 2007. **15**(3): p. 316-27.
130. Hoemann, C.D., et al., Chitosan-glycerol phosphate/blood implants elicit hyaline cartilage repair integrated with porous subchondral bone in microdrilled rabbit defects. *Osteoarthritis Cartilage*, 2007. **15**(1): p. 78-89.
131. Khanna, A., et al., Liver transplantation for metabolic liver diseases. *Surg Clin North Am*, 1999. **79**(1): p. 153-62, ix.
132. Knell, A.J. and D.C. Dukes, Dialysis procedures in acute liver coma. *Lancet*, 1976. **2**(7982): p. 402-3.
133. Opolon, P., High-permeability membrane hemodialysis and hemofiltration in acute hepatic coma: experimental and clinical results. *Artif Organs*, 1979. **3**(4): p. 354-60.
134. Naruse, K., et al., Development of a new extracorporeal whole-liver perfusion system. *J Artif Organs*, 2003. **6**(3): p. 211-7.
135. LeCluyse, E.L., P.L. Bullock, and A. Parkinson, Strategies for restoration and maintenance of normal hepatic structure and function in long-term cultures of rat hepatocytes. *Advanced Drug Delivery Reviews*, 1996. **22**(1-2): p. 133-186.
136. Reid, L.M., Stem cell biology, hormone/matrix synergies and liver differentiation. *Curr Opin Cell Biol*, 1990. **2**(1): p. 121-30.
137. De Bartolo, L., et al., Novel membranes and surface modification able to activate specific cellular responses. *Biomol Eng*, 2007. **24**(1): p. 23-6.
138. Verma, P., et al., Formation and characterization of three dimensional human hepatocyte cell line spheroids on chitosan matrix for in vitro tissue engineering applications. *In Vitro Cellular & Developmental Biology-Animal*, 2007. **43**(10): p. 328-337.
139. Li, J., et al., Culture of primary rat hepatocytes within porous chitosan scaffolds. *Journal of Biomedical Materials Research Part A*, 2003. **67**(3): p. 938-43.
140. Li, J.L., et al., Culture of hepatocytes on fructose-modified chitosan scaffolds. *Biomaterials*, 2003. **24**(13): p. 2317-2322.
141. Cho, C.S., et al., Galactose-carrying polymers as extracellular matrices for liver tissue engineering. *Biomaterials*, 2006. **27**(4): p. 576-85.
142. Park, I.K., et al., Galactosylated chitosan as a synthetic extracellular matrix for hepatocytes attachment. *Biomaterials*, 2003. **24**(13): p. 2331-7.
143. Seo, S.J., et al., Alginate/galactosylated chitosan/heparin scaffold as a new synthetic extracellular matrix for hepatocytes. *Tissue Engineering*, 2006. **12**(1): p. 33-44.
144. Fan, J., et al., Preparation and characterization of chitosan/galactosylated hyaluronic acid scaffolds for primary hepatocytes culture. *J Mater Sci Mater Med*, 2010. **21**(1): p. 319-27.
145. Feng, Z.Q., et al., Electrospun Chitosan Nanofibers for Hepatocyte Culture. *Journal of Biomedical Nanotechnology*, 2010. **6**(6): p. 658-666.
146. Wang, X.H., et al., Preparation and characterization of a collagen/chitosan/heparin matrix for an implantable bioartificial liver. *Journal of Biomaterials Science-Polymer Edition*, 2005. **16**(9): p. 1063-1080.

147. Freier, T., et al., Chitin-based tubes for tissue engineering in the nervous system. *Biomaterials*, 2005. **26**(22): p. 4624-32.
148. Pangestuti, R. and S.K. Kim, Neuroprotective properties of chitosan and its derivatives. *Marine Drugs*, 2010. **8**(7): p. 2117-28.
149. Haastert-Talini, K., et al., Chitosan tubes of varying degrees of acetylation for bridging peripheral nerve defects. *Biomaterials*, 2013. **34**(38): p. 9886-904.
150. Patel, M., et al., Collagen-chitosan nerve guides for peripheral nerve repair: a histomorphometric study. *Journal of Biomaterials Applications*, 2008. **23**(2): p. 101-21.
151. Ao, Q., et al., The regeneration of transected sciatic nerves of adult rats using chitosan nerve conduits seeded with bone marrow stromal cell-derived Schwann cells. *Biomaterials*, 2011. **32**(3): p. 787-96.
152. Fan, W., et al., Repairing a 35-mm-long median nerve defect with a chitosan/PGA artificial nerve graft in the human: a case study. *Microsurgery*, 2008. **28**(4): p. 238-42.
153. Chew, S.Y., et al., The effect of the alignment of electrospun fibrous scaffolds on Schwann cell maturation. *Biomaterials*, 2008. **29**(6): p. 653-61.
154. Lu, G., et al., Controlling the degradation of covalently cross-linked carboxymethyl chitosan utilizing bimodal molecular weight distribution. *Journal of Biomaterials Applications*, 2009. **23**(5): p. 435-51.
155. Yang, Y., et al., Nerve conduits based on immobilization of nerve growth factor onto modified chitosan by using genipin as a crosslinking agent. *Eur J Pharm Biopharm*, 2011. **79**(3): p. 519-25.
156. Zhang, L., et al., Degradation and compatibility behaviors of poly(glycolic acid) grafted chitosan. *Mater Sci Eng C Mater Biol Appl*, 2013. **33**(5): p. 2626-31.
157. Mingyu, C., et al., Surface modification and characterization of chitosan film blended with poly-L-lysine. *Journal of Biomaterials Applications*, 2004. **19**(1): p. 59-75.
158. Hsu, S.H., et al., New nerve regeneration strategy combining laminin-coated chitosan conduits and stem cell therapy. *Acta Biomaterialia*, 2013. **9**(5): p. 6606-15.
159. Zheng, W., et al., Endothelialization and patency of RGD-functionalized vascular grafts in a rabbit carotid artery model. *Biomaterials*, 2012. **33**(10): p. 2880-91.
160. Chung, S., et al., Bioresorbable elastomeric vascular tissue engineering scaffolds via melt spinning and electrospinning. *Acta Biomaterialia*, 2010. **6**(6): p. 1958-67.
161. Fujita, M., et al., Vascularization in vivo caused by the controlled release of fibroblast growth factor-2 from an injectable chitosan/non-anticoagulant heparin hydrogel. *Biomaterials*, 2004. **25**(4): p. 699-706.
162. Huang, M., et al., Polyelectrolyte complexes stabilize and controllably release vascular endothelial growth factor. *Biomacromolecules*, 2007. **8**(5): p. 1607-14.
163. Park, Y.J., et al., Platelet derived growth factor releasing chitosan sponge for periodontal bone regeneration. *Biomaterials*, 2000. **21**(2): p. 153-9.
164. Chupa, J.M., et al., Vascular cell responses to polysaccharide materials: in vitro and in vivo evaluations. *Biomaterials*, 2000. **21**(22): p. 2315-22.
165. Yao, Y., et al., Effect of sustained heparin release from PCL/chitosan hybrid small-diameter vascular grafts on anti-thrombogenic property and endothelialization. *Acta Biomaterialia*, 2014. **10**(6): p. 2739-49.
166. Groth, T. and A. Lendlein, Layer-by-layer deposition of polyelectrolytes--a versatile tool for the in vivo repair of blood vessels. *Angew Chem Int Ed Engl*, 2004. **43**(8): p. 926-8.
167. Metcalfe, A.D. and M.W. Ferguson, Bioengineering skin using mechanisms of regeneration and repair. *Biomaterials*, 2007. **28**(34): p. 5100-13.
168. Takei, T., et al., Synthesis of a chitosan derivative soluble at neutral pH and gellable by freeze-thawing, and its application in wound care. *Acta Biomaterialia*, 2012. **8**(2): p. 686-93.
169. Fukasawa, M., et al., The hemostatic effect of deacetylated chitin membrane on peritoneal injury in rabbit model. *Surg Today*, 1992. **22**(4): p. 333-8.

170. Cho, Y.W., et al., Water-soluble chitin as a wound healing accelerator. *Biomaterials*, 1999. **20**(22): p. 2139-45.
171. Ong, S.Y., et al., Development of a chitosan-based wound dressing with improved hemostatic and antimicrobial properties. *Biomaterials*, 2008. **29**(32): p. 4323-32.
172. Okamoto, Y., et al., Evaluation of chitin and chitosan on open wound healing in dogs. *J Vet Med Sci*, 1995. **57**(5): p. 851-4.
173. Ma, L., et al., Collagen/chitosan porous scaffolds with improved biostability for skin tissue engineering. *Biomaterials*, 2003. **24**(26): p. 4833-41.
174. Han, C.M., et al., Application of collagen-chitosan/fibrin glue asymmetric scaffolds in skin tissue engineering. *J Zhejiang Univ Sci B*, 2010. **11**(7): p. 524-30.
175. Mi, F.L., et al., Fabrication and characterization of a sponge-like asymmetric chitosan membrane as a wound dressing. *Biomaterials*, 2001. **22**(2): p. 165-73.
176. Ma, J., et al., A preliminary in vitro study on the fabrication and tissue engineering applications of a novel chitosan bilayer material as a scaffold of human neonatal dermal fibroblasts. *Biomaterials*, 2001. **22**(4): p. 331-6.
177. Chen, Z.G., et al., Electrospun collagen-chitosan nanofiber: a biomimetic extracellular matrix for endothelial cell and smooth muscle cell. *Acta Biomaterialia*, 2010. **6**(2): p. 372-82.
178. Naseri, N., et al., Electrospun chitosan-based nanocomposite mats reinforced with chitin nanocrystals for wound dressing. *Carbohydr Polym*, 2014. **109**: p. 7-15.
179. Murakami, K., et al., Hydrogel blends of chitin/chitosan, fucoidan and alginate as healing-impaired wound dressings. *Biomaterials*, 2010. **31**(1): p. 83-90.
180. Peng, C.C., et al., Composite nano-titanium oxide-chitosan artificial skin exhibits strong wound-healing effect-an approach with anti-inflammatory and bactericidal kinetics. *Macromolecular Bioscience*, 2008. **8**(4): p. 316-27.
181. Luo, C., et al., The role of poly(ethylene glycol) in the formation of silver nanoparticles. *J Colloid Interface Sci*, 2005. **288**(2): p. 444-8.
182. Lee, S.J., et al., Electrospun chitosan nanofibers with controlled levels of silver nanoparticles. Preparation, characterization and antibacterial activity. *Carbohydr Polym*, 2014. **111**: p. 530-7.
183. Bernkop-Schnurch, A. and S. Dunnhaupt, Chitosan-based drug delivery systems. *Eur J Pharm Biopharm*, 2012. **81**(3): p. 463-9.
184. Ruel-Gariepy, E., et al., A thermosensitive chitosan-based hydrogel for the local delivery of paclitaxel. *Eur J Pharm Biopharm*, 2004. **57**(1): p. 53-63.
185. Wang, Q., et al., Chitosan/polyethylene glycol blend fibers and their properties for drug controlled release. *Journal of Biomedical Materials Research Part A*, 2008. **85**(4): p. 881-7.
186. Kim, J.H., et al., Antitumor efficacy of cisplatin-loaded glycol chitosan nanoparticles in tumor-bearing mice. *Journal of Controlled Release*, 2008. **127**(1): p. 41-9.
187. Buyuktimkin, B., et al., Vaccine-like controlled-release delivery of an immunomodulating peptide to treat experimental autoimmune encephalomyelitis. *Mol Pharm*, 2012. **9**(4): p. 979-85.
188. Kim, Y.H., et al., Structural characteristics of size-controlled self-aggregates of deoxycholic acid-modified chitosan and their application as a DNA delivery carrier. *Bioconjug Chem*, 2001. **12**(6): p. 932-8.
189. Roy, K., et al., Oral gene delivery with chitosan-DNA nanoparticles generates immunologic protection in a murine model of peanut allergy. *Nat Med*, 1999. **5**(4): p. 387-91.
190. Aspden, T.J., et al., Chitosan as a nasal delivery system: the effect of chitosan solutions on in vitro and in vivo mucociliary transport rates in human turbinates and volunteers. *J Pharm Sci*, 1997. **86**(4): p. 509-13.

191. Martinac, A., et al., Development and bioadhesive properties of chitosan-ethylcellulose microspheres for nasal delivery. *International Journal of Pharmaceutics*, 2005. **291**(1-2): p. 69-77.
192. Desai, K.G. and H.J. Park, Preparation of cross-linked chitosan microspheres by spray drying: effect of cross-linking agent on the properties of spray dried microspheres. *J Microencapsul*, 2005. **22**(4): p. 377-95.
193. Kunjachan, S., et al., Chitosan-based macrophage-mediated drug targeting for the treatment of experimental visceral leishmaniasis. *J Microencapsul*, 2011. **28**(4): p. 301-10.
194. Park, J.H., et al., Targeted delivery of low molecular drugs using chitosan and its derivatives. *Adv Drug Deliv Rev*, 2010. **62**(1): p. 28-41.
195. Portero, A., C. Remunan-Lopez, and H.M. Nielsen, The potential of chitosan in enhancing peptide and protein absorption across the TR146 cell culture model-an in vitro model of the buccal epithelium. *Pharm Res*, 2002. **19**(2): p. 169-74.
196. Tsai, C.J., et al., Chitosan hydrogel as a base for transdermal delivery of berberine and its evaluation in rat skin. *Biological & Pharmaceutical Bulletin*, 1999. **22**(4): p. 397-401.
197. Huanbutta, K., et al., Impact of salt form and molecular weight of chitosan on swelling and drug release from chitosan matrix tablets. *Carbohydr Polym*, 2013. **97**(1): p. 26-33.
198. Xu, Y., et al., Preparation of dual crosslinked alginate-chitosan blend gel beads and in vitro controlled release in oral site-specific drug delivery system. *International Journal of Pharmaceutics*, 2007. **336**(2): p. 329-37.
199. Gupta, K.C. and M.N. Ravi Kumar, Drug release behavior of beads and microgranules of chitosan. *Biomaterials*, 2000. **21**(11): p. 1115-9.
200. Pavaloiu, R.D., et al., Composite films of poly(vinyl alcohol)-chitosan-bacterial cellulose for drug controlled release. *International Journal of Biological Macromolecules*, 2014. **68**: p. 117-24.
201. Ko, J.A., et al., Preparation and characterization of chitosan microparticles intended for controlled drug delivery. *International Journal of Pharmaceutics*, 2002. **249**(1-2): p. 165-74.
202. Hassan, E.E., R.C. Parish, and J.M. Gallo, Optimized formulation of magnetic chitosan microspheres containing the anticancer agent, oxantrazole. *Pharm Res*, 1992. **9**(3): p. 390-7.
203. Azab, A.K., et al., Biocompatibility evaluation of crosslinked chitosan hydrogels after subcutaneous and intraperitoneal implantation in the rat. *Journal of Biomedical Materials Research Part A*, 2007. **83**(2): p. 414-22.
204. Senel, S., et al., Enhancing effect of chitosan on peptide drug delivery across buccal mucosa. *Biomaterials*, 2000. **21**(20): p. 2067-71.
205. Baumgart, P., et al., Intracellular calcium during beta-adrenoreceptor blockade in essential hypertension. *Am J Nephrol*, 1986. **6 Suppl 1**: p. 66-8.
206. Grenha, A., B. Seijo, and C. Remunan-Lopez, Microencapsulated chitosan nanoparticles for lung protein delivery. *European Journal of Pharmaceutical Sciences*, 2005. **25**(4-5): p. 427-37.
207. Khatri, K., et al., Plasmid DNA loaded chitosan nanoparticles for nasal mucosal immunization against hepatitis B. *International Journal of Pharmaceutics*, 2008. **354**(1-2): p. 235-41.
208. Yang, M., et al., Characterisation of salmon calcitonin in spray-dried powder for inhalation. Effect of chitosan. *International Journal of Pharmaceutics*, 2007. **331**(2): p. 176-81.
209. Pan, Y., et al., Bioadhesive polysaccharide in protein delivery system: chitosan nanoparticles improve the intestinal absorption of insulin in vivo. *International Journal of Pharmaceutics*, 2002. **249**(1-2): p. 139-47.

210. Huang, Y., M. Yeh, and C. Chiang, Formulation factors in preparing BTM-chitosan microspheres by spray drying method. *International Journal of Pharmaceutics*, 2002. **242**(1-2): p. 239-42.
211. Gong, J., et al., Polymeric micelles drug delivery system in oncology. *Journal of Controlled Release*, 2012. **159**(3): p. 312-23.
212. Ryan, S.M., et al., Advances in PEGylation of important biotech molecules: delivery aspects. *Expert Opin Drug Deliv*, 2008. **5**(4): p. 371-83.
213. El-Sherbiny, I.M. and H.D. Smyth, Poly(ethylene glycol)-carboxymethyl chitosan-based pH-responsive hydrogels: photo-induced synthesis, characterization, swelling, and in vitro evaluation as potential drug carriers. *Carbohydr Res*, 2010. **345**(14): p. 2004-12.
214. Kato, Y., H. Onishi, and Y. Machida, N-succinyl-chitosan as a drug carrier: water-insoluble and water-soluble conjugates. *Biomaterials*, 2004. **25**(5): p. 907-15.
215. Mao, S., et al., Self-assembled polyelectrolyte nanocomplexes between chitosan derivatives and insulin. *J Pharm Sci*, 2006. **95**(5): p. 1035-48.
216. Mao, S., W. Sun, and T. Kissel, Chitosan-based formulations for delivery of DNA and siRNA. *Adv Drug Deliv Rev*, 2010. **62**(1): p. 12-27.
217. Mitra, S., et al., Tumour targeted delivery of encapsulated dextran-doxorubicin conjugate using chitosan nanoparticles as carrier. *Journal of Controlled Release*, 2001. **74**(1-3): p. 317-323.
218. Tian, Q., et al., Self-assembly and liver targeting of sulfated chitosan nanoparticles functionalized with glycyrrhetic acid. *Nanomedicine*, 2012. **8**(6): p. 870-9.
219. Yin, L., et al., Drug permeability and mucoadhesion properties of thiolated trimethyl chitosan nanoparticles in oral insulin delivery. *Biomaterials*, 2009. **30**(29): p. 5691-700.
220. Mukhopadhyay, P., et al., pH-sensitive chitosan/alginate core-shell nanoparticles for efficient and safe oral insulin delivery. *International Journal of Biological Macromolecules*, 2015. **72**: p. 640-8.
221. Bisht, S. and A. Maitra, Dextran-doxorubicin/chitosan nanoparticles for solid tumor therapy. *Wiley Interdiscip Rev Nanomed Nanobiotechnol*, 2009. **1**(4): p. 415-25.
222. Dash, M., et al., Chitosan-A versatile semi-synthetic polymer in biomedical applications. *Progress in Polymer Science*, 2011. **36**(8): p. 981-1014.
223. Breyner, N.M., et al., Effect of a Three-Dimensional Chitosan Porous Scaffold on the Differentiation of Mesenchymal Stem Cells into Chondrocytes. *Cells Tissues Organs*, 2010. **191**(2): p. 119-128.
224. Subramanian, A., et al., Preparation and evaluation of the electrospun chitosan/PEO fibers for potential applications in cartilage tissue engineering. *Journal of Biomaterials Science-Polymer Edition*, 2005. **16**(7): p. 861-873.
225. Zhang, Y.Z., et al., Electrospun biomimetic nanocomposite nanofibers of hydroxyapatite/chitosan for bone tissue engineering. *Biomaterials*, 2008. **29**(32): p. 4314-4322.
226. Bhattarai, N., et al., Electrospun chitosan-based nanofibers and their cellular compatibility. *Biomaterials*, 2005. **26**(31): p. 6176-6184.
227. Muzzarelli, R.A.A., Genipin-crosslinked chitosan hydrogels as biomedical and pharmaceutical aids. *Carbohydrate Polymers*, 2009. **77**(1): p. 1-9.
228. Sung, H.W., et al., In vitro evaluation of cytotoxicity of a naturally occurring cross-linking reagent for biological tissue fixation. *Journal of Biomaterials Science-Polymer Edition*, 1999. **10**(1): p. 63-78.
229. Tian, D., P. Dubois, and R. Jerome, Biodegradable and biocompatible inorganic-organic hybrid materials .1. Synthesis and characterization. *Journal of Polymer Science Part a-Polymer Chemistry*, 1997. **35**(11): p. 2295-2309.
230. Berger, J., et al., Structure and interactions in covalently and ionically crosslinked chitosan hydrogels for biomedical applications. *European Journal of Pharmaceutics and Biopharmaceutics*, 2004. **57**(1): p. 19-34.

231. Suzuki, T. and Y. Yamada, Effect of end group modification on gas transport properties of 6FDA-TAPOB hyperbranched polyimide-silica hybrid membranes. *High Performance Polymers*, 2007. **19**(5-6): p. 553-564.
232. Christopherson, G.T., H. Song, and H.Q. Mao, The influence of fiber diameter of electrospun substrates on neural stem cell differentiation and proliferation. *Biomaterials*, 2009. **30**(4): p. 556-64.
233. Rickard, K.A., et al., Role of nutrition support in the management of children with cancer. *Prog Clin Biol Res*, 1983. **132D**: p. 179-92.
234. Ghishan, F.K., The role of nutrition in the overall management of pediatric patients. *Pediatr Ann*, 1999. **28**(2): p. 98-9.
235. Cope, F.O., The role of nutrition in AIDS management completes rite of passage. *J Int Assoc Physicians AIDS Care*, 1995. **1**(6): p. 26-9.
236. Ren, J., J. Li, and F. Liu, [Role of energy metabolism in nutrition management of critically ill patients]. *Zhonghua Yi Xue Za Zhi*, 1995. **75**(6): p. 346-8, 382-3.
237. Pelletier, D.L. and R. Shrimpton, The role of information in the planning, management and evaluation of community nutrition programmes. *Health Policy Plan*, 1994. **9**(2): p. 171-84.
238. Cerra, F.B., The role of nutrition in the management of metabolic stress. *Crit Care Clin*, 1986. **2**(4): p. 807-19.

## **Section II**

# **Chitosan: effects of non cytotoxic crosslinkers**



# Chapter 2

## Chitosan membranes for tissue engineering: comparison of different crosslinkers

### Abstract

Chitosan (CS), a derivative of the naturally occurring biopolymer chitin, is an attractive material for biomedical applications because of its biocompatibility, biodegradability and immunological, antibacterial and wound-healing properties. However, the physical and mechanical stability of CS based materials are strongly influenced by the crosslinking method. In this work, the effect of the three crosslinking agents genipin (GP),  $\gamma$ -glycidoxypropyltrimethoxysilane (GPTMS), dibasic sodium phosphate (DSP) and a combination of GPTMS and DSP (GPTMS\_DSP) on CS physicochemical, thermal, morphological, mechanical properties, swelling and degradation behavior at physiological condition was investigated. The possibility to tailor the final properties of CS scaffolds through crosslinking is a key strategy to apply CS in different biomedical and tissue engineering applications. The obtained results reveal that the optimization of the crosslinking mechanism provide CS membrane properties required in different biomedical applications.

### 2.1 Introduction

Tissue engineering (TE) provides a novel way to assist and accelerate the regeneration and repairing of defective and damaged tissues based on the natural healing potential of humans. A major goal of TE is the design of biomaterial-based scaffolds containing cells and signaling molecules, as transplantable constructs, to enable the recovery of physiological functions in the host alternatively to conventional surgical techniques. In this context, biomaterial composition and processing technologies play a pivotal role in the field of TE. Among the various biomaterials, polysaccharides have recently gained interest as materials for scaffold fabrication, since their carbohydrate moieties interact

with or are integral component of several matrix glycoproteins and cell adhesion molecules [1]. Chitosan (CS), a copolymer of glucosamine and N-acetyl-glucosamine, is obtained by alkaline deacetylation of chitin, which is the main component of the exoskeleton of crustaceans, such as shrimps [2]. CS has attracted considerable interests for biomedical applications due to its attractive properties in terms of biocompatibility, biodegradability, non-antigenicity, antibacterial activity and low cost [3]. Moreover, CS offers several advantages that make it particularly enticing for TE applications: CS can be easily molded into matrices of various forms such as films [4], porous scaffolds [5], hydrogels [6], nanofibers [7-9] and drug carriers [10]. As a result of the protonation of free amino groups under acidic conditions ( $\text{pH} < 6$ ), CS exhibits a pH-dependent cationic nature and has the ability to interact with anionic components (glycosaminoglycans and proteins) [11, 12].

For most medical application, CS has been crosslinked in order to improve its mechanical strength and its structural integrity under physiological conditions. Commonly used chemical crosslinkers in literature include epoxy compounds [13], aldehydes (formaldehyde, glyceraldehyde and glutaraldehyde) [14, 15] and carbodiimides [16, 17]. They all exhibit a certain degree of cytotoxicity and may therefore impair biocompatibility of CS scaffolds. For this reason, increasing interest has been recently gained by less cytotoxic crosslinking agents such as enzymes [18] or naturally derived crosslinking agents, having a lower toxicity [19-22]. The effect of crosslinking strongly influences the *in vivo* performance of the scaffolds in terms of mechanical properties, degradation, water stability and cellular response. An analysis and comparison of different CS crosslinkers is however not currently available and is the aim of this study. Three compounds, widely used as CS crosslinkers, were selected. Genipin (GP), a natural cross-linker, is an aglucone of geniposide extracted from *Gardenia jasminoides* and obtained from geniposide via enzymatic hydrolysis. GP is 10,000 times less toxic than glutaraldehyde [20, 23] although its crosslinking mechanism is similar to other synthetic chemical crosslinking agents. Glycidoxypropyltrimethoxysilane (GPTMS) is a silane coupling agent, which has epoxy and methoxysilane groups. The epoxy groups react with the amino groups of CS molecules while the methoxysilane groups are hydrolyzed and form silanol groups [24]. GPTMS has been largely used to crosslink CS films and membranes for different TE applications [25, 26]. Introduction of silica into the biomaterials has been shown to increase its oxygen permeability [27], biocompatibility, biodegradability [28] and to improve the flexibility of the CS based samples [25]. Dibasic sodium phosphate (DSP) is a non-toxic polyanion which can interact with CS via electrostatic forces to form ionic crosslinked membrane [29]. A novel *in situ* forming CS formulation has been recently developed via coupled ionic and covalent co-cross-linking [30]. The addition of DSP (as ionic crosslinker) neutralizes CS based samples avoiding the need of a rinsing step in sodium hydroxide solution. By combining DSP with GP, porous scaffolds were also fabricated by chemical cross-linking showing higher mechanical and chemical properties compared to those obtained using the single crosslinkers [30].

Despite the numerous reports on the potential applications of CS scaffolds as biomaterials in clinics and pharmaceutical field, reports that compare the effect of different crosslinkers on the physicochemical, thermal and mechanical properties are still lacking. For this reason, this work compares the effects of various crosslinking methods (through covalent or ionic bonding) on the physicochemical, thermal and mechanical properties of CS flat membranes. The crosslinking agents used included GP, GPTMS, dibasic sodium phosphate (DSP), and a combination of GPTMS and DSP. The GP, GPTMS and DSP amounts were selected on the basis of data from literature analysing the use of different crosslinking agents [19, 25, 30].

## **2.2 Experimental**

### **2.2.1 Materials**

CS (medium molecular weight, 75%-85% deacetylation degree), GPTMS and DSP were supplied from Sigma Aldrich. GP was purchased from Challenge Bioproducts Ltd. Taiwan. All solvents used were of analytical grade and used without further purification.

### **2.2.2 Methods**

CS was dissolved in acetic acid solution 0.5 M at room temperature by continuous stirring to obtain a 2.5 % (w/v) solution. The crosslinked membranes were prepared according to the following procedures:

- I. GP-crosslinked samples (CS/GP) were obtained by adding GP (2.5% w/w) to the CS solution. The resulting solution was kept under moderate stirring until a green-bluish gel started to form as suggested by visual inspection and by the viscosity increase of the mixture.
- II. GPTMS-crosslinked samples (CS/GPTMS) were prepared by adding GPTMS (75% w/w) to CS solution. The amount of GPTMS was selected according to literature [25] in order both to obtain the maximum crosslinking degree of CS chains and to increase the mechanical properties. The resulting solution was kept under stirring at room temperature for 1 hour.
- III. DSP-crosslinked samples (CS/DSP) were obtained by adding DSP 1M (one drop per second) to the CS solution with a concentration of 7.5 % v/v with respect to the natural polymer solution volume. The mixed solution was kept under stirring at room temperature for about 10 minutes.
- IV. GPTMS\_DSP-crosslinked samples (CS/GPTMS\_DSP) were obtained adding GPTMS (50% w/w) to the CS solution. The resulting CS/GPTMS solution was kept under stirring for 1 hour, followed by the dropwise addition (one drop per second) of DSP 1M (concentration 7.5 % v/v) and maintained under moderate stirring for 10 minutes.

Then, 10 ml of each solution (CS/GP , CS/ GPTMS, CS/DSP and CS/GPTMS) was poured into 6 cm Petri dishes and air-dried for 48 h to obtain flat membranes. All crosslinked

dried samples were dipped into demineralised water for 10 minutes and then the water pH values were measured to evaluate the presence of acidic residues. Uncrosslinked CS flat membranes were prepared as control following the procedures described above without adding any crosslinker. Acid pH were obtained for CS, CS/GP, CS/GPTMS films. Consequently, CS, CS/GP, CS/GPTMS samples were neutralized by rinsing in a 0.1M NaOH solution followed by 5 washing in distilled water to obtain physiological pH.

### **2.2.3 Sample characterization**

#### **2.2.3.1 Fourier transform infrared-attenuated total reflectance spectroscopy (FTIR-ATR)**

The FTIR-ATR spectra of CS, CS/GP, CS/GPTMS, CS/DSP, CS/GPTMS\_DSP samples were recorded at room temperature in a Perkin Elmer Spectrometer in the range 2000-600  $\text{cm}^{-1}$  at a resolution of 4  $\text{cm}^{-1}$ .

#### **2.2.3.2 Surface wettability**

The static contact angle of CS, CS/GP, CS/GPTMS, CS/DSP and CS/GPTMS\_DSP films were measured at room temperature using a KSV instrument equipped with a CAM 200 software for data acquisition. Sessile drop method was applied, using a 5  $\mu\text{L}$  double distilled water droplet. For each angle reported, at least five measurements on different surface locations were measured and results were expressed as average value  $\pm$  standard deviation.

#### **2.2.3.3 Swelling and dissolution test**

The swelling and dissolution behavior of the uncrosslinked and crosslinked CS samples were evaluated by immersing the samples in PBS (pH 7.4) at 37°C. The swelling degree was measured after 1, 3, 6, 9 and 24 hours while the dissolution degree was evaluated after 1, 3, 5, 7, 14, 28 and 56 days. The swelling percentage was calculated as:

$$\Delta W_s (\%) = (W_s - W_0) / W_0 * 100$$

where  $W_0$  and  $W_s$  are the sample weights before and after swelling respectively. The dissolution percentage was calculated as:

$$\Delta W_d (\%) = (W_0 - W_d) / W_0 * 100$$

where  $W_d$  is the dried sample weight after dissolution. The solution pH was measured at the same time intervals during the swelling and the dissolution tests, and its stable value at around 7 (physiological pH) was verified. For each experimental time, three samples were measured and the results were expressed as averages value  $\pm$  standard deviation.

#### **2.2.3.4 Morphological characterization and element distribution**

The external surface morphology of CS, CS/GPTMS, CS/DSP and CS/GPTMS\_DSP flat membranes was observed by scanning electron microscopy (SEM LEO – 1430, Zeiss). Using an energy dispersive spectrometer (EDS), qualitative compositional analysis was performed and punctual elemental composition of materials with high spatial resolution was accomplished. Samples were sputter coated with gold in a undervacuum chamber prior to SEM-EDS examination.

#### **2.2.3.5 Thermogravimetric analysis (TGA)**

Thermal degradation was measured using a TA INSTRUMENT Q500 equipment. The experiments were performed with a 10-15 mg sample in aluminum pans under a dynamic nitrogen atmosphere between 40°C and 800 C. The experiments were run at a scanning rate of 10°C/min and obtained results were analyzed using TA Universal Analysis software.

#### **2.2.3.6 Differential scanning calorimetry (DSC)**

DSC was performed on CS based membranes using a TA INSTRUMENT DSC Q20. Accurately weighted (6-10 mg) samples were placed into aluminum cups and sealed. A small hole was done at the top of the cup in order to allow the release of water. An empty cup was used as reference. The samples were detected in the first heating scan run in the temperature range of 30–200 °C. The experiments were run at a scanning rate of 10°C/min. Water evaporation temperature ( $T_{we}$ ) and enthalpy ( $\Delta H_{we}$ ) were calculated as the temperature of the maximum value of the endotherm and the peak area, respectively. For CS/GP, CS/GPTMS, CS/DSP and CS/GPTMS\_DSP samples, the enthalpy values were normalized based on the contents of uncrosslinked CS.

#### **2.2.3.7 Mechanical properties**

The tensile mechanical properties were performed on dry and wet flat membranes using MTS QTest/10 device equipped with load cells of 50N and of 10N, respectively. Rectangular strips of 30 mm x 10 mm size were cut from each films and strained to break at a constant crosshead speed of 2 mm/min. Using the associated software Test Works, break stress and strain were determined. The elastic modulus was calculated from the slope of the linear portion of the stress–strain curve. To measure the thickness of the films, digital calibrator was used. Prior to tensile testing in wet state, samples were immersed in phosphate buffered saline (PBS, pH 7.4) for 10 min at 25°C. Four specimens for each kind of material were tested. The results were expressed as average values  $\pm$  standard deviation.

### 2.2.3.8 Statistics

Experiments were repeated three times and results expressed as an mean  $\pm$  standard deviation. Statistical significance was calculated using analysis of variance (ANOVA). A comparison between two means was analyzed using Tukey's test with statistical significance level set at  $p < 0.05$ .

## 2.3 Results and discussion

### 2.3.1 Membrane preparation

Crosslinked CS membranes were obtained from casting the CS acetic acid aqueous solution containing GP, GPTMS, DSP or a combination of GPTMS and DSP respectively. In all processes, in situ crosslinking and sample preparation were performed with the conventional fabrication technique in order to provide a convenient way of preparing crosslinked CS membranes. Fig. 2.1 schematizes the different crosslinking mechanisms. The GP reaction is influence by the pH value. In acetic acid solution (acidic condition), a nucleophilic attack by the amino groups of CS on the olefinic carbon atom at C-3 occurs, followed by opening the dihydropyran ring and attachment of the secondary amino group on the newly formed aldehyde group while the short chains of condensed GP act as crosslinking bridges. The dark-blue coloration that appears in the samples exposed to air is associated with the oxygen radical induced polymerization of GP as well as its reaction with amino groups (Fig. 2.1A). GPTMS reacts with the amino groups of CS chains through its oxirane ring. Meanwhile the hydration of the trimethoxy groups of GPTMS moiety forms silantriol pendent through acid-catalyzed reaction. Dehydration reaction among the silantriol groups occurs during the drying process and forms inter-chain linkages between CS chains [20] (Fig. 2.1B). DSP is a sodium salt of phosphoric acid able to increase the pH value of CS solution to around neutrality ( $pH \approx 7$ ). DSP is negatively charged in solution and thus may interact with CS via electrostatic forces to form ionic crosslinked membrane (Fig. 2.1C). The combination of GPTMS and DSP exploit both the chemical and ionic co-crosslinking mechanism (Fig. 2.1D).

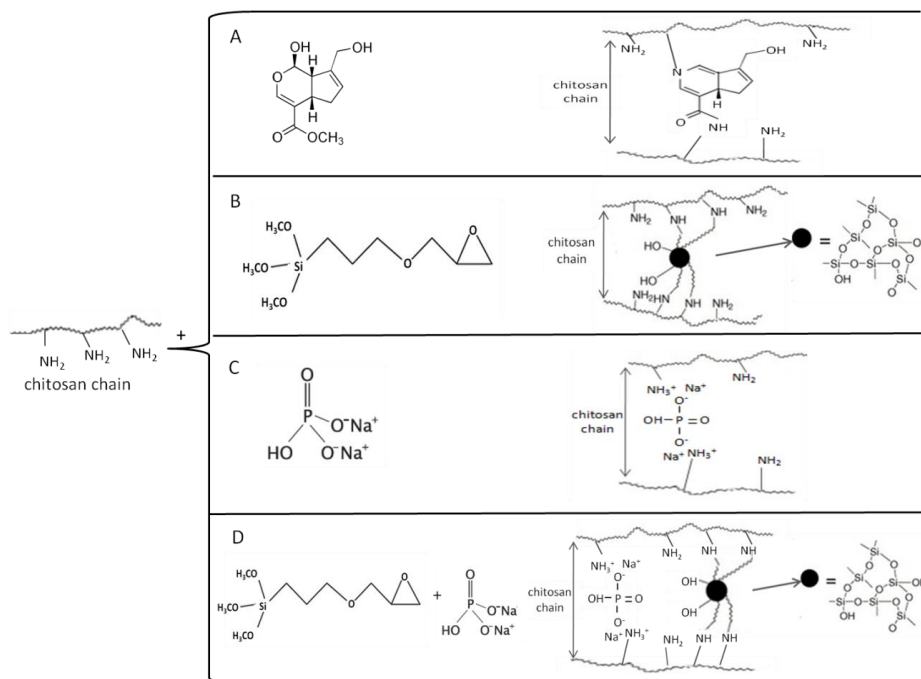


**Fig. 2.1.** Chemical structure of CS crosslinked with: GP (A), GPTMS (B), DSP (C) and a combination of GPTMS and DSP (D).

### 2.3.2 Fourier transform infrared-attenuated total reflectance spectroscopy (FTIR-ATR)

In Fig. 2.2, the FTIR-ATR spectra of CS, CS/GP, CS/GPTMS, CS/DSP and CS/GPTMS\_DSP are reported. The five spectra showed the typical adsorption bands of CS: peaks at  $1151\text{ cm}^{-1}$  (C-O-C stretching) and at  $1019\text{ cm}^{-1}$  (C-O stretching) were associated to vibrational modes typical of the saccharide structure of CS [31]; absorption bands at  $1637\text{ cm}^{-1}$  and  $1542\text{ cm}^{-1}$  resulted from axial stretching of C=O in amide group (amide I band) and  $\text{NH}_2$  bending vibration of amino groups and N-H bending of amide groups, respectively; the vibration modes at  $1414\text{ cm}^{-1}$  and at  $1319\text{ cm}^{-1}$  were assigned to O-H bending (originating from CS deacetylation) and C-H bending vibrations [31]. No significant differences were detected between the CS and CS/GP spectra, as also described by Mi et al. [32]. The introduction of silane groups by GPTMS crosslinker (CS/GPTMS samples), caused the appearance of new bands at  $920\text{ cm}^{-1}$ , at  $1020\text{ cm}^{-1}$  and  $1150\text{ cm}^{-1}$  in FTIR spectra, associated with the stretching of Si-OH bonds and Si-O-Si vibrations, respectively [25, 26]. In addition, the peak at  $1000\text{--}1100\text{ cm}^{-1}$  broadened and increased its intensity owing to the absorption from Si-O-C stretching bonds [33]. As regard the CS/DSP FTIR spectra, new peaks were detected at  $1150\text{ cm}^{-1}$  and  $1000\text{ cm}^{-1}$  which could be attributed to the  $\text{PO}_3$  out-of-phase stretching. Bands at  $989\text{ cm}^{-1}$  and  $943\text{ cm}^{-1}$  were associated with  $\text{PO}_3$  in-phase-stretching. The detected peaks at  $861\text{ cm}^{-1}$  and at  $814\text{ cm}^{-1}$  were associated with P-OH stretching and P-O-P asymmetric stretching vibration respectively [34]. The FTIR spectra of CS/GPTMS\_DSP hybrid sample showed the typical adsorption bands of both the ionic and covalent crosslinkers: bands at  $1200\text{ cm}^{-1}$ , due to the Si-O-Si bonds, confirmed the crosslinking of CS by GPTMS; peaks at  $1150\text{ cm}^{-1}$  and  $1000\text{ cm}^{-1}$  ( $\text{PO}_3$  out-of-phase stretching),  $861\text{ cm}^{-1}$

(P-OH stretching) and  $814\text{ cm}^{-1}$  (P-O-P) asymmetric groups evidenced the presence of DSP. The absorption band at  $1720\text{ cm}^{-1}$  was observed in CS/GPTMS, CS/DSP and CS/GPTMS\_DSP spectra and could be attributed to the stretching vibration of C=O groups, probably due to acetic acid residuals [35].

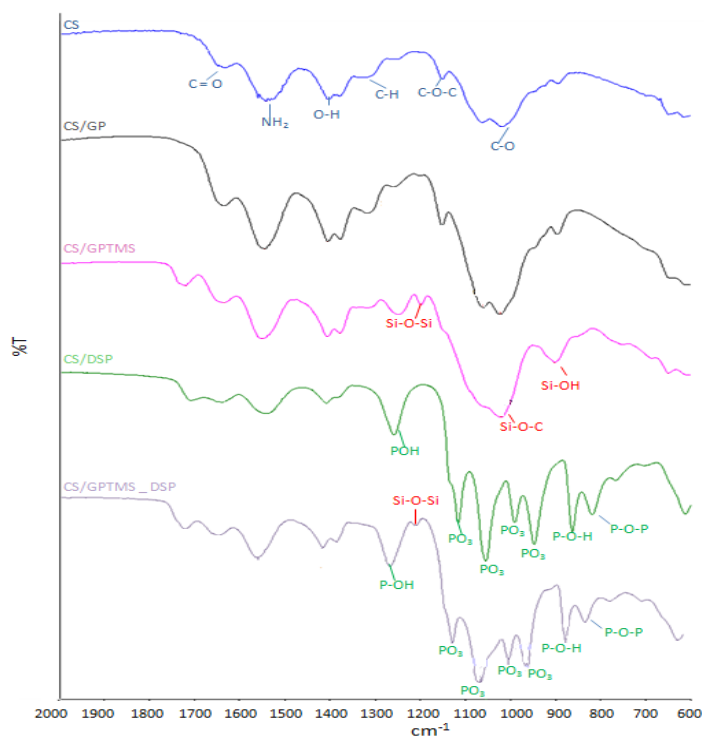


**Fig. 2.2.** FTIR-ATR spectra of CS, CS/GP, CS/GPTMS, CS/DSP and CS/GPTMS-DSP films.

### 2.3.3 Surface wettability

The static water contact angles of both crosslinked and uncrosslinked CS flat membranes are reported in Fig. 2.3. Uncrosslinked CS samples displayed a slightly hydrophilic behavior with a contact angle in the  $83^{\circ}$ – $88^{\circ}$  range. Crosslinking with GP or GPTMS did not change the surface wettability significantly ( $85.1^{\circ} \pm 0.9^{\circ}$  for CS/GP and  $85.8^{\circ} \pm 1.0^{\circ}$  for CS/GPTMS). On the other hand, CS/DSP based samples presented a significant higher hydrophilicity respect to the CS, CS/GP and CS/GPTMS samples. The enhanced hydrophilicity caused by the addition of DSP is attributed to the presence of hydrophilic phosphate groups in DSP. Water contact angles of CS/DSP and CS/GPTMS\_DSP film samples were not significantly different ( $66.0^{\circ} \pm 9.7^{\circ}$  for CS/DSP and  $57.7^{\circ} \pm 9.2^{\circ}$  for CS/GPTMS\_DSP). The presence of DSP is expected to effort *in vitro* and *in vivo* cells response since cell adhesion, which depends on various parameters, is known to be maximised on surfaces with an intermediate wettability (with  $50$ – $70^{\circ}$  water contact angle) [36, 37].

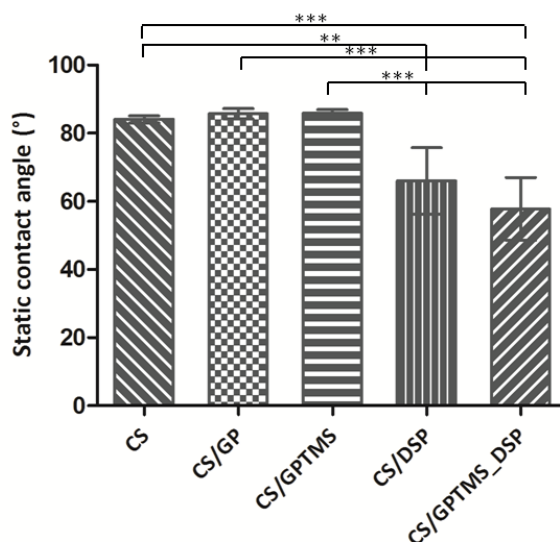


**Fig. 2.3.** Static water contact angle of CS, CS/GP, CS/GPTMS, CS/DSP and CS/GPTMS\_DSP film samples. Histograms reported the average values and the standard deviations. \*\*p < 0.001 and \*\*\*p < 0.0001.

#### 2.3.4 Swelling and dissolution tests

The swelling and dissolution of CS network greatly depend on the internal structural parameters of the swelling network such as the amounts of constituent polymers present, crosslink density of the membrane, presence of hydrophilic and/or hydrophobic functional groups, etc. Fig. 2.4A reports the swelling degrees of CS, CS/GP, CS/GPTMS, CS/DSP and CS/GPTMS\_DSP samples, respectively. A comparison of the swelling percentage of CS crosslinked samples reveals that the water uptake of uncrosslinked samples is significantly higher than for all CS crosslinked specimens at each time point (\*\*p < 0.0001). CS is a hydrophilic, cationic polymer, which causes CS flat membranes to have a higher water uptake respect to ionic and covalent crosslinked samples: CS/GP, CS/DSP, CS/GPTMS and CS/GPTMS\_DSP contain less free  $\text{NH}_3^+$  moieties and decrease the ability of CS to form hydrogen bonds with water molecules. Moreover, the presence of GPTMS causes a maximum reduction in the swelling degree of CS associated to the formation of a well-organized polymer structure [25]. In detail, CS and CS/DSP films increased considerably their weight immediately after 1 h of immersion in PBS solution showing a significantly higher degree of water uptake of  $1366 \pm 189\%$  and  $532 \pm 25\%$ , respectively (\*\*p < 0.0001). By contrast, the swelling degree of CS/GPTMS and CS/GPTMS\_DSP reached values of  $7 \pm 4\%$  and  $29 \pm 12\%$  respectively, after 1 h incubation in PBS. Both films achieved equilibrium swelling degree after immersion for 3 h and the maximum degree of water uptake was about  $30 \pm 2\%$  for CS/GPTMS and  $48 \pm 2\%$  for CS/GPTMS\_DSP after 24 h. No significant differences were observed between CS/GPTMS and CS/GPTMS\_DSP samples at each time step. The presence of many Si-OH and Si-O-Si groups, which depends on the degree of polymerization of GPTMS has been shown to influence water uptake: an increase in the GPTMS content contributes to an increase in

number of hydrophilic silicate units, and reduces as a consequence CS water uptake [25]. An increase of swelling degree was observed by adding DSP to CS/GPTMS and could be attributed to the presence of hydrophilic phosphate groups in DSP. This behaviour is confirmed for CS/DSP samples where a higher water uptake is observed. An intermediate behavior was observed for CS/GP specimens reaching a stable value swelling degree of  $280\pm 30\%$  after 1 h of immersion in PBS. CS/GP crosslinked films showed low swelling ratio as compared to uncrosslinked CS that could be due to the formation of molecular linkages (heterocyclic amino linkage) by GP.

Dissolution tests were performed on crosslinked CS films, with the aim to study their stability in aqueous environment. The degradation profiles of crosslinked CS samples after 56 days of immersion in PBS are presented in Fig 2.4B. The stability of the CS based samples in PBS solution increased when GPTMS and GP were used as crosslinking agents. Analyzing the weight loss degree, CS/GPTMS\_DSP and CS/DSP membranes presented a significant dissolution after 1 day immersion in PBS reaching values of 38% and 44%, respectively. CS/GPTMS and CS/GP films showed lower weight loss respect to CS/DSP and CS/GPTMS\_DSP specimens, with 15% and 18% degradation respectively after 1 day and reached a final value of about 35% and 21% after 56 days incubation in PBS. Compared to the CS/DSP and CS/GPTMS\_DSP samples that lost the 67% and 50% of the initial weight after 8 weeks, chemical crosslinking by the addition of GPTMS or GP agents enhanced the stability in aqueous media. CS/GP samples reached a stable value of weight loss after 1 day in immersion in PBS solution. On the contrary, the presence of DSP as ionic crosslinking increased the weight loss 1 day after immersion in PBS and was associated to the release of salts into the PBS solution.

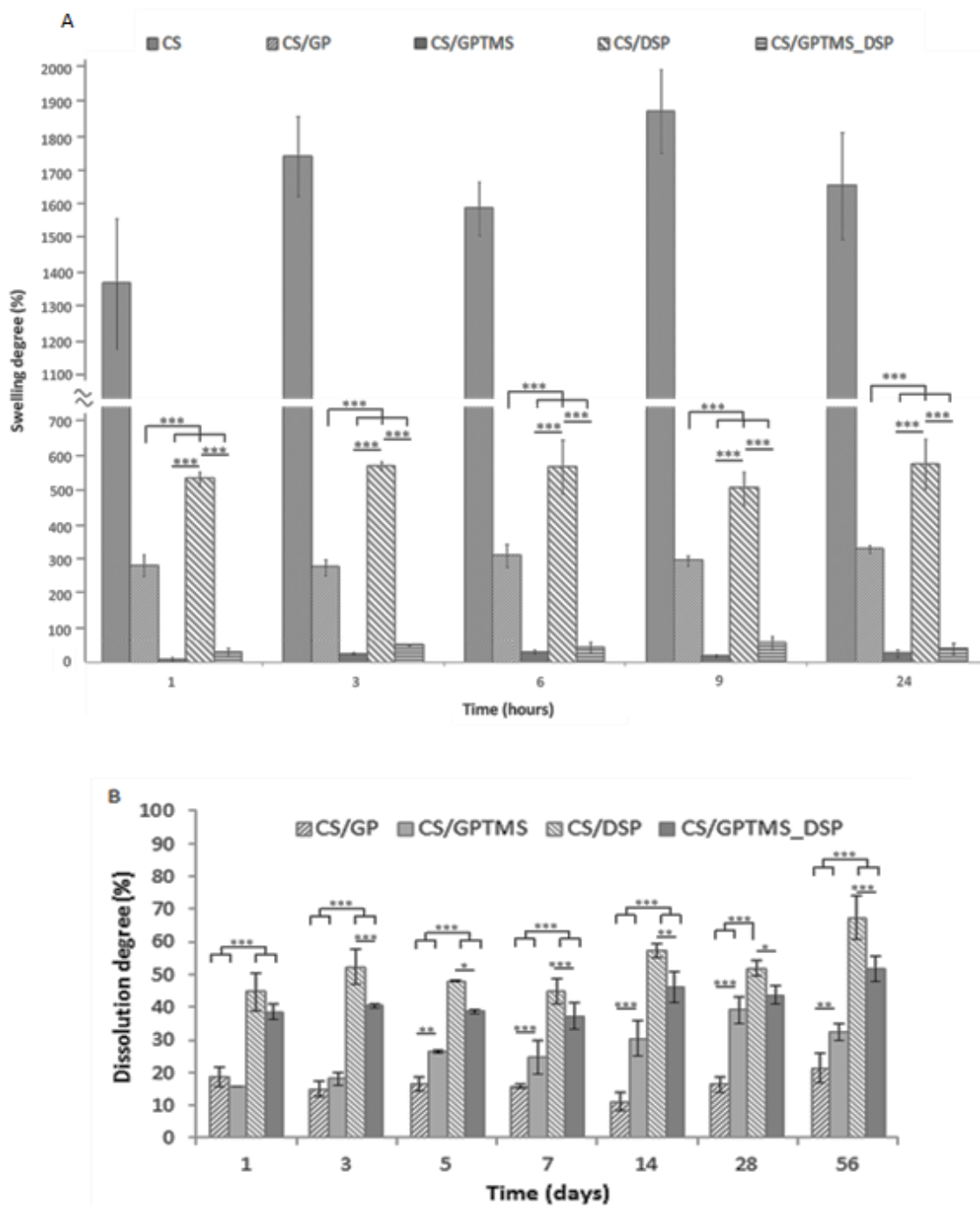


**Fig. 2.4.** Swelling (A) and dissolution (B) degrees for CS/GP, CS/GPTMS, CS/DSP and CS/GPTMS\_DSP films. Measurements were carried out in PBS at pH 7.4, at 37 °C. Column heights correspond to the mean values. Bars indicate standard deviations (n = 3). \*p < 0.05, \*\*p < 0.001 and \*\*\*p < 0.0001.

### 2.3.5 Morphological characterization and chemical composition

SEM-EDS analysis was performed on the surfaces of films to evaluate the effect of the different crosslinking methods on sample morphology and chemical composition. EDS elemental mapping is a powerful method to identify the elemental composition in distinct region of a material [38, 39]. No phase separation between CS and crosslinking agents was observed (data not shown). Fig. 2.5 reports the EDS element-mapping on the surface for CS/GP, CS/GPTMS, CS/DSP and CS/GPTMS\_DSP films. EDS spectra of crosslinked samples (insert in Fig. 2.5 A, B, C, D) showed the characteristic elements of CS: carbon (C) and oxygen (O) and also the peak relative to silicon (Si) for CS/GPTMS and to sodium (Na) and phosphate (P) for CS/DSP, respectively; moreover, characteristic peaks corresponding to Si, Na and P elements were found on the CS/GPTMS\_DSP films and were associated both to the presence of both the ionic and covalent crosslinkers (insert in Fig. 2.5). No compositional differences were found between CS and CS/GP samples (data not shown). The green and the red spots corresponding to silicon (Si) and phosphorus (P) elements (Fig. 2.5) were found homogeneously distributed in the CS/GPTMS and CS/DSP samples, respectively while both spots were observed to be uniformly dispersed in CS/GPTMS\_DSP films. The EDS mapping results suggested uniform CS crosslinking for all the analysed compositions.

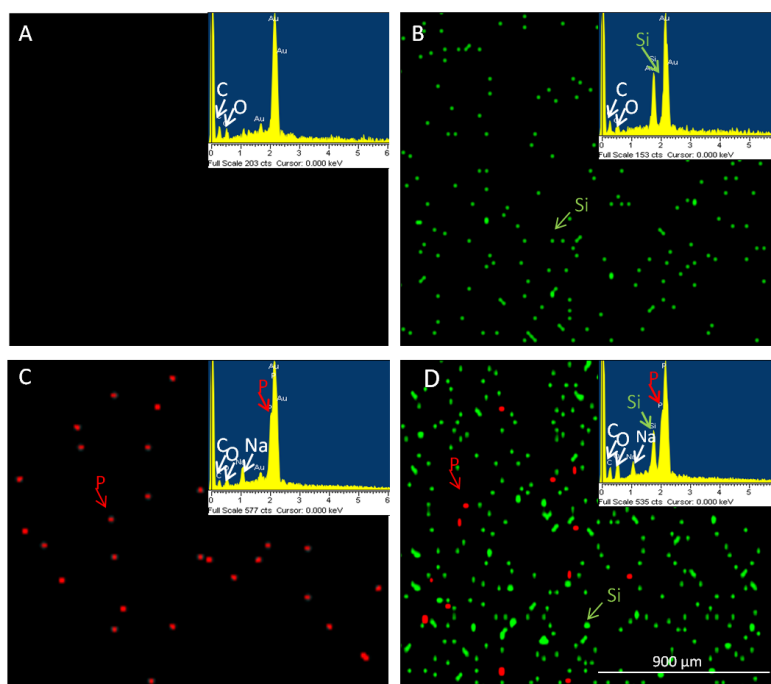


**Fig. 2.5.** EDS spectra of compact films: surface of (A) CS/GP, (B) CS/GPTMS, (C) CS/DSP and CS/GPTMS\_DSP.

### 2.3.6 Thermogravimetric analysis (TGA)

The decomposition profile of CS, CS/GP, CS/GPTMS, CS/DSP and CS/GPTMS\_DSP membranes was evaluated by TGA analysis in a temperature range from 40°C to 800 °C. The derivative of TGA curves (DTG), as shown in Fig. 2.6, revealed two separate degradation phenomena both for crosslinked and uncrosslinked CS samples: the first decomposition step started from 50°C and continued to above 150 °C and was related to the water evaporation; the second weight loss was observed in the 180-400 °C temperature range and was attributed to the decomposition of CS main chains. Pure CS showed a first thermal degradation at around 103 °C and a second stage, associated to the thermal and oxidative decomposition of CS and to the vaporization and elimination of volatile products, starting at 181 °C and reaching a maximum at 265 °C with a total weight loss of 35% [40]. In CS/GP samples, the second degradation step started at about 190 °C and degradation was completed at 497 °C. The temperature of the maximum degradation rate was measured at 264 °C. No relevant differences in the weight loss associated to this second step were observed for CS/GP samples respect to pure CS. According to literature [41], the obtained result confirmed that GP addition had no influence on thermal stability of CS membranes. CS/GPTMS hybrids exhibited improved thermal stability respect to pure CS and CS/GP film samples. The initial weight loss of CS/GPTMS samples was attributed to water evaporation. The second degradation step resulted from the thermal degradation of the crosslinked material. The temperature of maximum rate of degradation was shifted to a higher value respect to CS and CS/GPTMS (281 °C) and associated with a weight loss of 27%. A new weight loss was observed in a temperature range between 330 °C and 550 °C. Such changes might indicate the hybridization between the organic and inorganic parts, as suggested by a previous study [42]. The weight loss at 281 °C might be due to the cleavage of relatively unstable parts of the polymeric compound and the structural reorganization of the polysiloxane, while the third weight loss stage might correspond to the complete decomposition of the backbone of the polymeric matrix. In CS/DSP samples the first degradation step was observed at around 80 °C and the corresponding weight loss was higher than CS, CS/GP and CS/GPTMS due to superior hydrophilicity of CS/DSP. Polymer pyrolysis was detected in the 250-500 °C range temperature with the maximum rate of degradation at 271 °C. During the degradation step, weight loss was also associated to DSP reactions: at higher temperatures than 210°C, DSP starts to condense forming disodium pyrophosphate and above 300 °C metaphosphates form, leading to an additional weight loss [43] (31%). For CS/GPTMS\_DSP the first degradation stage started at about 100 °C and the second stage showed a rapid weight at about 273 °C due to degradation of CS. Complete degradation occurred at 550 °C confirming an increase of the thermal stability of CS films caused by the hybridization between the organic and inorganic parts of CS/GPTMS\_DSP samples. The total weight loss of the crosslinked and uncrosslinked CS samples at about 550 °C was in a range between 50% and 58%. The remaining solid residue is mostly due to the formation of inorganic compounds containing C, N and O. Similar multi-degradation

behavior of CS film was reported in the literature [44, 45]. Table 2.1 collects the maximum degradation rate temperature ( $T_d$ ) of CS based samples and the corresponding weight losses. The  $T_d$  values of CS and CS/GP films were similar, while for the other crosslinked samples, the  $T_d$  was shifted to higher temperatures. Moreover, the final weight loss of the CS/GPTMS, CS/DSP and CS/GPTMS\_DSP samples was lower than that of CS and CS/GP specimens. TGA analysis confirmed the improvement of the thermal stability of crosslinked CS, especially when both GPTMS and DSP crosslinking agents were used.

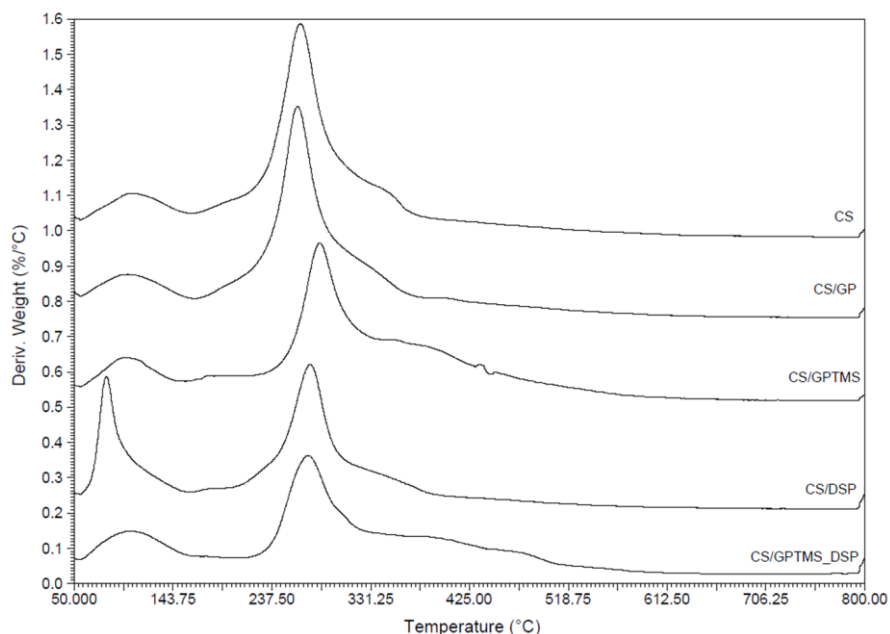


**Fig. 2.6.** First derivative of TGA curves of CS, CS/GP, CS/GPTMS, CS/DSP and CS/GPTMS\_DSP films.

**Table 2.1.** Maximum degradation rate temperature ( $T_d$ ) and corresponding weight loss for CS and crosslinked CS.

Sample	$T_d$ (°C)	Weight loss (%)
CS	265	35
CS/GP	264	34
CS/GPTMS	281	28
CS/DSP	271	31
CS/GPTMS_DSP	273	32

### 2.3.7 Differential scanning calorimetry (DSC)

DSC analysis was performed to analyze the thermal behavior of CS based materials as it is influenced by the different crosslinking treatments. The DSC thermograms, shown in Fig. 2.7, compare the first heating traces for pure CS and CS crosslinked samples in the temperature range from 30°C to 200°C. The maximum temperature of 200°C was selected in order to limit possible CS degradation, as confirmed by thermogravimetric analysis (see paragraph 2.3.6). All DSC traces presented an endothermic event in the temperature range of 90°C-100°C which features were collected in Table 2.2. For all CS based membranes, the endothermic event was not directed in the second DSC run (data not shown in Fig. 2.7), confirming the hypothesis that water evaporation occurred during the first cycle [40, 46]. A detailed examination of Fig. 2.7 revealed differences among the samples in the endothermic peak enthalpy and temperature. This result is attributable to different water holding capacity and to water–material interactions ascribed to the physical and molecular changes as a consequence of the crosslinking process. CS heating trace showed an endothermic peak at 95°C while the DSC heating trace of CS/GPTMS was characterized by the presence of a splitted endothermic event at around 100°C. CS and CS/GPTMS possess polar groups, which are able to adsorb water and establish onto hydrogen bonds with it. According to literature [47], upon heating, the thermally activated water molecules tend to be released: water molecules which are bound to amino groups are removed easier than those bound to hydroxyl groups. In CS/GPTMS films, some amino groups reacted with the oxirane group of GPTMS and, thus the number of amine groups available to interact with the water molecules decreased. Therefore, the amount of released water was lower than CS. Furthermore, as the hydrogen bonds between water molecules and CS hydroxyl groups were stronger compared to the ones with CS amino groups, CS/GPTMS endothermic peak shifted to a higher temperature value compared to the case of pure CS. On the contrary, for CS/GP samples, the DSC endothermic peak was shifted to lower temperature compared to the case of pure CS, in agreement with scientific literature [48]. The DSC heating traces of CS/DSP and CS/GPTMS\_DSP films were characterized by an endothermic peak centered at around 85-88°C. This event, again associated with the evaporation of water molecules, was shifted to lower temperatures compared to uncrosslinked CS due to weaker water–material interactions caused by the addition of DSP. The enthalpy value measured for uncrosslinked CS was 140 J/g. CS/GP enthalpy value did not change significantly upon crosslinking showing that GP did not affect the water holding capacity of CS. Following the introduction of GPTMS, DSP and GPTMS\_DSP, enthalpy value changed indicating a definite correlation between the water holding capacity and chemical and supramolecular structures of this natural polymer. CS/GPTMS showed the lowest enthalpy value (80.8 J/g) compared to other CS membranes (Table 2.2); the use of GPTMS as crosslinker forms ordered and organized structures that significantly contribute to the decrease in the content of adsorbed water. On the contrary, the presence of DSP in CS/DSP and CS/GPTMS\_DSP films led to higher enthalpy values of about 208 J/g and 184 J/g

respectively, indicating a stronger interaction with water molecules (and consequently an higher water uptake) due to the higher hydrophilicity associated with the ionic crosslinker.

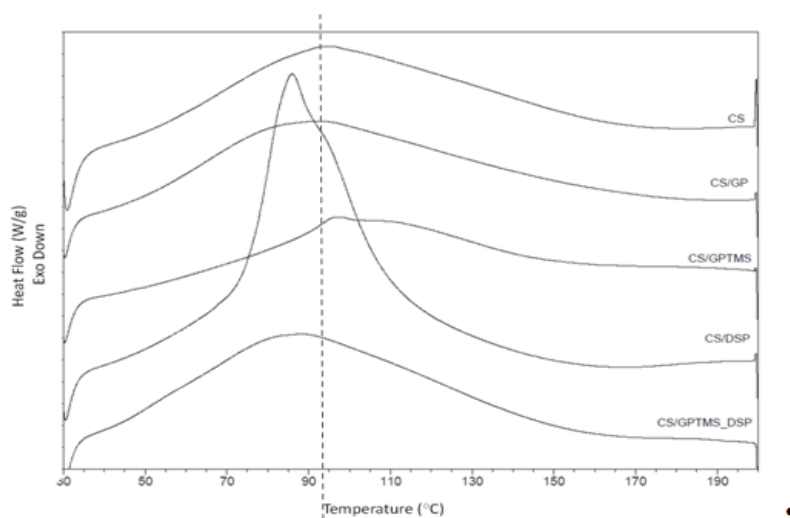


**Fig. 2.7.** The first heating scan DSC curve of CS, CS/GP, CS/GPTMS, CS/DSP and CS/GPTMS\_DSP.

**Table 2.2.** Differential scanning calorimetry (DSC) measurements for cross-linked films.

Sample	Peak temperature (°C)	Enthalpy (J/g)
CS	95.0	140.0
CS/GP	85.0	160.0
CS/GPTMS	100.0	80.8
CS/DSP	85.0	208.2
CS/GPTMS_DSP	87.0	184.4

### 2.3.8 Mechanical properties

Tensile tests were performed on control and crosslinked CS flat films both in dry and in wet conditions to determine the effect of crosslinking on sample stiffness. Dried CS based samples had a uniform thickness in the range of 60-90  $\mu\text{m}$  while wet CS samples showed an increase in thickness reaching values within 90-130  $\mu\text{m}$ . For all samples, at low strains (lower than 6%) the stress increased linearly with an increase in the strain. In this region, the  $\sigma$ - $\epsilon$  slope was calculated to obtain the elastic modulus. At strains >6%, the stress increased slowly with increasing strain until failure occurred (data not shown). Table 2.3 shows the elastic moduli of CS samples in dry and wet state. In dry condition, the Young's modulus of CS was around 1900-2800 MPa and the typical  $\sigma$ - $\epsilon$  behavior of a brittle and rigid material was observed [49]. The elastic modulus for CS/GP films did not show significant difference compared to pure CS confirming the brittleness and the poor flexibility of the CS membranes crosslinked with GP. The introduction of GPTMS, DSP or a combination of both in CS samples significantly decreased the Young's modulus compared

to CS (\*\* $p < 0.001$ ) by obtaining values of  $1643 \pm 92$  MPa,  $1090 \pm 72$  MPa and  $1250 \pm 100$  MPa, respectively. These results revealed that the mechanical resistance and flexibility of CS based films were altered by the addition of different crosslinkers because of the reorganization of the polymer structure. Furthermore, more hydrophilic CS membranes (CS/DSP and CS/GPTMS\_DSP) showed a less brittle behavior thanks to the ability of water to plasticise the CS matrix. In wet condition the elastic modulus of CS significantly decreased and an opposite trend was observed compared to dry samples. The Young's modulus of wet CS samples was about 0.212 MPa suggested a dramatical loss of stiffness. On the contrary, the crosslinking of CS films enhanced the mechanical resistance in wet state, and the elastic modulus calculated was  $5.7 \pm 0.8$  MPa for CS/GP,  $21.3 \pm 2.9$  MPa for CS/GPTMS,  $3.5 \pm 1.1$  MPa for CS/DSP and  $23.0 \pm 2.7$  MPa for CS/GPTMS\_DSP samples. The significant stiffening of the crosslinked specimens was associated to the formation of a more organized structure following the addition of GP and GPTMS (statistical significant compared to CS, CS/GP and CS/DSP samples, \*\*\* $p < 0.0001$ ) respect to pure CS. By adding DSP, an improved deformability of the samples was observed probably due to a water adsorption behaviour. CS/GPTMS\_DSP showed an intermediate behavior compared to CS/GPTMS and CS/DSP films and samples (statistical significance, \* $p < 0.05$  and \*\*\* $p < 0.0001$  respectively) were found to be both highly elastic and resistant.

**Table 2.3.** Elastic modulus calculated from the corresponding stress-strain curves of dry and wet CS based samples (average value  $\pm$  standard deviation).

Sample	$E_{dry}$ (MPa)	$E_{wet}$ (MPa)
CS	$2300 \pm 438$	$0.22 \pm 0.06$
CS/GP	$2030 \pm 208$	$5.73 \pm 0.84$
CS/GPTMS	$1465 \pm 172$	$18.10 \pm 4.14$
CS/DSP	$1402 \pm 300$	$3.47 \pm 1.06$
CS/GPTMS_DSP	$1300 \pm 126$	$23.03 \pm 2.62$

## 2.4 Conclusion

The results obtained in the present study provides the basis for choosing a crosslinking reagent that could impart the requisite properties to the CS membranes in the design of a biomaterial for different biomedical application. CS based matrices were treated with different crosslinking agents (GP, GPTMS, DSP and a combination of GPTMS and DSP) to investigate the effect on the physical and mechanical properties of CS following the chemical or the ionic crosslinking treatment. In details:

- GP and GPTMS did not affect the surface wettability and the thermal degradation kinetics of samples respect to uncrosslinked CS. Both GPTMS and GP based crosslinking treatments allowed to significantly reduce the CS swelling and dissolution behavior and to enhance its mechanical resistance under wet condition;

- DSP contributed to increase the hydrophilicity of CS/DSP and CS/GPTMS\_DSP samples as compared to CS, CS/GP and CS/GPTMS. The stronger interaction existing between water and CS chains after ionic crosslinking was confirmed by a higher water uptake degree and higher enthalpy values. Moreover, the higher water–material interaction following the addition of DSP to CS and CS/GPTMS solutions allowed to obtain more flexible membranes. The simultaneous use of GPTMS and DSP permitted to combine the features obtained both from GPTMS and DSP crosslinkers. Lower degree of swelling and dissolution respect to pure CS and CS/DSP were associated to the addition of the covalent crosslinker while the improved surface wettability for CS/GPTMS\_DSP samples was attributable to the ionic agent. Concerning the mechanical properties, GPTMS enhanced the resistance of CS while DSP allowed to obtain more flexible specimens.

In summary, these different crosslinkers for CS based membranes could offer a broad range of choices to be potentially used in biomedical applications such as biomaterial, drug delivery vehicles and skin tissue engineering.

## References

1. Minuth, W.W., M. Sittinger, and S. Kloth, Tissue engineering: generation of differentiated artificial tissues for biomedical applications. *Cell and Tissue Research*, 1998. **291**(1): p. 1-11.
2. Muzzarelli, Natural chelating polymers; alginic acid, chitin and chitosan. 1973: New York: Pergamon Press Oxford. 254.
3. Dash, M., et al., Chitosan-A versatile semi-synthetic polymer in biomedical applications. *Progress in Polymer Science*, 2011. **36**(8): p. 981-1014.
4. Chatelet, C., O. Damour, and A. Domard, Influence of the degree of acetylation on some biological properties of chitosan films. *Biomaterials*, 2001. **22**(3): p. 261-268.
5. Breyner, N.M., et al., Effect of a Three-Dimensional Chitosan Porous Scaffold on the Differentiation of Mesenchymal Stem Cells into Chondrocytes. *Cells Tissues Organs*, 2010. **191**(2): p. 119-128.
6. Bhattarai, N., J. Gunn, and M.Q. Zhang, Chitosan-based hydrogels for controlled, localized drug delivery. *Advanced Drug Delivery Reviews*, 2010. **62**(1): p. 83-99.
7. Subramanian, A., et al., Preparation and evaluation of the electrospun chitosan/PEO fibers for potential applications in cartilage tissue engineering. *Journal of Biomaterials Science-Polymer Edition*, 2005. **16**(7): p. 861-873.
8. Zhang, Y.Z., et al., Electrospun biomimetic nanocomposite nanofibers of hydroxyapatite/chitosan for bone tissue engineering. *Biomaterials*, 2008. **29**(32): p. 4314-4322.
9. Bhattarai, N., et al., Electrospun chitosan-based nanofibers and their cellular compatibility. *Biomaterials*, 2005. **26**(31): p. 6176-6184.
10. Chen, X.G., et al., Preparation and biocompatibility of chitosan microcarriers as biomaterial. *Biochemical Engineering Journal*, 2006. **27**(3): p. 269-274.
11. Denuziere, A., D. Ferrier, and A. Domard, Interactions between chitosan and glycosaminoglycans (chondroitin sulfate and hyaluronic acid): physicochemical and biological studies. *Ann Pharm Fr*, 2000. **58**(1): p. 47-53.
12. Oyarzun-Ampuero, F.A., et al., Chitosan-hyaluronic acid nanoparticles loaded with heparin for the treatment of asthma. *International Journal of Pharmaceutics*, 2009. **381**(2): p. 122-129.
13. Kawamura, Y., et al., Adsorption of Metal-Ions on Polyaminated Highly Porous Chitosan Chelating Resin. *Industrial & Engineering Chemistry Research*, 1993. **32**(2): p. 386-391.
14. Singh, A., et al., External stimuli response on a novel chitosan hydrogel crosslinked with formaldehyde. *Bulletin of Materials Science*, 2006. **29**(3): p. 233-238.
15. Beppu, M.M., et al., Crosslinking of chitosan membranes using glutaraldehyde: Effect on ion permeability and water absorption. *Journal of Membrane Science*, 2007. **301**(1-2): p. 126-130.
16. Deng, Y., et al., Preparation and characterization of hyaluronan/chitosan scaffold crosslinked by 1-ethyl-3-(3-dimethylaminopropyl) carbodiimide. *Polymer International*, 2007. **56**(6): p. 738-745.
17. Wang, G., et al., Preparation of cross-linked carboxymethyl chitosan for repairing sciatic nerve injury in rats. *Biotechnology Letters*, 2010. **32**(1): p. 59-66.
18. Kuboe, Y., et al., Quinone cross-linked polysaccharide hybrid fiber. *Biomacromolecules*, 2004. **5**(2): p. 348-357.
19. Chiono, V., et al., Genipin-crosslinked chitosan/gelatin blends for biomedical applications. *Journal of Materials Science-Materials in Medicine*, 2008. **19**(2): p. 889-898.
20. Muzzarelli, R.A.A., Genipin-crosslinked chitosan hydrogels as biomedical and pharmaceutical aids. *Carbohydrate Polymers*, 2009. **77**(1): p. 1-9.
21. Mi, F.L., et al., In vitro evaluation of a chitosan membrane cross-linked with genipin. *Journal of Biomaterials Science-Polymer Edition*, 2001. **12**(8): p. 835-850.

22. Tonda-Turo, C., et al., Comparative analysis of gelatin scaffolds crosslinked by genipin and silane coupling agent. *International Journal of Biological Macromolecules*, 2011. **49**(4): p. 700-6.
23. Sung, H.W., et al., In vitro evaluation of cytotoxicity of a naturally occurring cross-linking reagent for biological tissue fixation. *Journal of Biomaterials Science-Polymer Edition*, 1999. **10**(1): p. 63-78.
24. Tonda-Turo, C., et al., Crosslinked gelatin nanofibres: preparation, characterisation and in vitro studies using glial-like cells. *Mater Sci Eng C Mater Biol Appl*, 2013. **33**(5): p. 2723-35.
25. Shiroasaki, Y., et al., Physical, chemical and in vitro biological profile of chitosan hybrid membrane as a function of organosiloxane concentration. *Acta Biomaterialia*, 2009. **5**(1): p. 346-355.
26. Liu, Y.L., Y.H. Su, and J.Y. Lai, In situ crosslinking of chitosan and formation of chitosan-silica hybrid membranes with using gamma-glycidoxypropyltrimethoxysilane as a crosslinking agent. *Polymer*, 2004. **45**(20): p. 6831-6837.
27. Suzuki, T. and Y. Yamada, Effect of end group modification on gas transport properties of 6FDA-TAPOB hyperbranched polyimide-silica hybrid membranes. *High Performance Polymers*, 2007. **19**(5-6): p. 553-564.
28. Tian, D., P. Dubois, and R. Jerome, Biodegradable and biocompatible inorganic-organic hybrid materials .1. Synthesis and characterization. *Journal of Polymer Science Part a-Polymer Chemistry*, 1997. **35**(11): p. 2295-2309.
29. Berger, J., et al., Structure and interactions in covalently and ionically crosslinked chitosan hydrogels for biomedical applications. *European Journal of Pharmaceutics and Biopharmaceutics*, 2004. **57**(1): p. 19-34.
30. Hanna, J.R. and J.A. Giacomelli, A review of wound healing and wound dressing products. *J Foot Ankle Surg*, 1997. **36**(1): p. 2-14; discussion 79.
31. Peniche, C., C. Elvira, and J.S. Roman, Interpolymer complexes of chitosan and polymethacrylic derivatives of salicylic acid: preparation, characterization and modification by thermal treatment. *Polymer*, 1998. **39**(25): p. 6549-6554.
32. Mi, F.L., et al., Synthesis and characterization of biodegradable TPP/genipin co-crosslinked chitosan gel beads. *Polymer*, 2003. **44**(21): p. 6521-6530.
33. Zha, F., et al., Preparation and adsorption kinetics of porous gamma-glycidoxypropyltrimethoxysilane crosslinked chitosan-beta-cyclodextrin membranes. *Journal of Membrane Science*, 2008. **321**(2): p. 316-323.
34. Larkin, J., *INFRARED AND RAMAN SPETROSCOPY PRINCIPLES AND SPECTRAL INTERPRETATION*, ed. s. edition 2011: ELSEVIER.
35. Kato, M., et al., Synthesis of organosiloxane-based inorganic/organic hybrid membranes with chemically bound phosphonic acid for proton-conductors. *Electrochimica Acta*, 2007. **52**(19): p. 5924-5931.
36. van Wachem, P.B., et al., Interaction of cultured human endothelial cells with polymeric surfaces of different wettabilities. *Biomaterials*, 1985. **6**(6): p. 403-8.
37. Bumgardner, J.D., et al., Contact angle, protein adsorption and osteoblast precursor cell attachment to chitosan coatings bonded to titanium. *Journal of Biomaterials Science-Polymer Edition*, 2003. **14**(12): p. 1401-1409.
38. Otulakowska, J. and J.W. Nicholson, Scanning electron microscopy and energy dispersive X-ray study of a recovered dental implant. *Journal of Materials Science-Materials in Medicine*, 2006. **17**(3): p. 277-279.
39. Qin, D.Q., et al., Microscopic Composition Maps of Poly(styrene-co-2-hydroxyethyl methacrylate) Colloidal Crystals and Interconnected Colloidal Arrays. *Langmuir*, 2010. **26**(9): p. 6256-6261.
40. Neto, C.G.T., et al., Thermal analysis of chitosan based networks. *Carbohydrate Polymers*, 2005. **62**(2): p. 97-103.

41. Nunes, C., et al., Chitosan-caffeic acid-genipin films presenting enhanced antioxidant activity and stability in acidic media. *Carbohydr Polym*, 2013. **91**(1): p. 236-43.
42. Xi, F.N., J.M. Wu, and X.F. Lin, Novel nylon-supported organic-inorganic hybrid membrane with hierarchical pores as a potential immobilized metal affinity adsorbent. *Journal of Chromatography A*, 2006. **1125**(1): p. 38-51.
43. de Jager, H.J. and L.C. Prinsloo, The dehydration of phosphates monitored by DSC/TGA and in situ Raman spectroscopy. *Thermochimica Acta*, 2001. **376**(2): p. 187-196.
44. Chen, C.H., et al., Studies of chitosan: II. Preparation and characterization of chitosan/poly(vinyl alcohol)/gelatin ternary blend films. *International Journal of Biological Macromolecules*, 2008. **43**(1): p. 37-42.
45. de Britto, D. and S.P. Campana, A kinetic study on the thermal degradation of N,N,N-trimethylchitosan. *Polymer Degradation and Stability*, 2004. **84**(2): p. 353-361.
46. Chao, A.C., Preparation of porous chitosan/GPTMS hybrid membrane and its application in affinity sorption for tyrosinase purification with *Agaricus bisporus*. *Journal of Membrane Science*, 2008. **311**(1-2): p. 306-318.
47. Rueda, D.R., T. Secall, and R.K. Bayer, Differences in the interaction of water with starch and chitosan films as revealed by infrared spectroscopy and differential scanning calorimetry. *Carbohydrate Polymers*, 1999. **40**(1): p. 49-56.
48. Kawadkar, J. and M.K. Chauhan, Intra-articular delivery of genipin cross-linked chitosan microspheres of flurbiprofen: Preparation, characterization, in vitro and in vivo studies. *European Journal of Pharmaceutics and Biopharmaceutics*, 2012. **81**(3): p. 563-572.
49. Sarasam, A. and S.V. Madihally, Characterization of chitosan-polycaprolactone blends for tissue engineering applications. *Biomaterials*, 2005. **26**(27): p. 5500-5508.

## **Section III**

# **Chitosan for peripheral nerve regeneration**



# Chapter 3

## Peripheral nerve tissue engineering: state of the art and chitosan based biomaterials

### 3.1 Introduction

Regeneration in the peripheral nervous system offers unique opportunities and challenges to medicine. Compared to the central nervous system (CNS), peripheral axons can regenerate resulting in functional recovery, especially if the distance to target is shorter than 3 cm as in distal limb injuries. However, this regenerative capacity is often incomplete and functional recovery with proximal lesions is limited. Autologous nerve graft transplantation is a feasible treatment in several clinical cases, but it is limited by donor site morbidity and insufficient donor tissue, impairing complete functional recovery. TE has introduced innovative approaches to promote and guide peripheral nerve regeneration by using biomimetic constructs inducing favorable microenvironments for nervous ingrowth. Promising strategies using nanotechnology have been recently proposed, such as the use of scaffolds with functionalized cell-binding domains, the use of guidance channels with cell-scale internally oriented fibers, and the possibility of sustained release of GFs and encapsulation of SCs. This chapter addresses: i) an overview of the biology of peripheral nerve and type of injuries and ii), the most recent TE approaches in view of future solutions for peripheral nerve repair.

### 3.2 Biology of the peripheral nerve and injuries

#### 3.2.1 Central and peripheral nervous systems

The nervous system is composed of organized group of cells specialized for the conduction of electrochemical stimuli from sensory receptors through a network to the site at which a response occurs. The nervous system includes both the CNS and peripheral nervous system (PNS). The two systems work together to collect information from inside the body and from the environment outside it. The CNS and PNS process the collected

information and then dispatch instructions to the rest of the body, making it respond. The CNS is the primary control center for the body and is made up of the brain and spinal cord. Injuries in these locations have only a very limited capacity to heal, because nerve regeneration tends not to occur. The PNS consists of a network of nerves that connect the CNS to the limbs and peripheral organs. The PNS is divided into:

- the sensory nervous system which sends information to the CNS from internal organs or from external stimuli;
- the motor nervous system which carries information from the CNS to organs, muscles, and glands. This latter one is divided into: i) the somatic nervous system (responsible for coordinating the skeletal muscle movements, and also for controlling external sensory organs such as the skin; it is the system that regulates activities that are under conscious control); ii) the autonomic nervous system (responsible for coordinating involuntary functions, such as breathing and digestion). This system is also called the involuntary nervous system. The autonomic nervous system can further be separated into the parasympathetic and sympathetic divisions. The parasympathetic division controls various functions including inhibiting heart rate, constricting pupils, and contracting the bladder. The nerves of the sympathetic division often have an opposite effect when they are located within the same organs as parasympathetic nerves.

The CNS is contained within the dorsal cavity, with the brain in the cranial cavity and the spinal cord in the spinal cavity. Both the brain and the spinal cord are protected by bones: the brain by the bones of the skull, and the spinal cord by a set of ring-shaped bones called vertebrae. Unlike the CNS, the PNS is not protected by bones, leaving it exposed to toxins and mechanical injuries.

The PNS has a much greater capacity than the CNS for natural regeneration after an injury, in large part because the glial microenvironment both secretes inhibitory factors preventing myelin and neuronal regeneration and lacks the ability to express necessary GFs [1]. Therefore, in response to small injuries, peripheral nerves can regenerate on their own over relatively short distances under appropriate conditions.

### **3.2.2 Nervous tissue cells types**

The nervous system is primarily composed of two categories of cells: neurons and glial cells.

The neuron is the basic unit in the nervous system. It is a specialized conductor cell that receives and transmits electrochemical nerve impulses. Chemical signaling occurs via synapses, specialized connections with other cells. Neurons connect to each other to form networks. This type of cell is highly specialized and amitotic. Functionally, neurons are classified as:

- motor (efferent) neurons transmit impulses from the CNS to the effector organs such as muscles and glands. They usually have short dendrites and long axons;

- sensory (afferent) neurons respond to touch, sound, light and numerous other stimuli effecting sensory organs and transfer impulses from peripheral sense receptors to the CNS. They usually have long dendrites and relatively short axons;
- interneurons (association neurons) are located entirely within the CNS in which they form the connecting link between afferent and efferent neurons. They have short dendrites and they may have either short or long axon.

A typical neuron possesses a cell body (often called the soma), dendrites, an axon, and synapses (Fig. 3.1). Dendrites are short extensions that arise from the cell body, often extending for hundreds of  $\mu\text{ms}$  and branching multiple times, giving rise to a complex "dendritic tree". They receive information from another cell and transmit the message to the cell body. The soma ensures the vital functions of the neuron and integrates signals from the dendrites. The cell body has a nucleus with at least one nucleolus and contains many of the typical cytoplasmic organelles typical of eukaryotic cells. However, it lacks centrioles. The axon is a special cellular protrusion that arises from the cell body at a site called the axon hillock and travels for a distance, as far as 1 m in humans or even more in other species. Its main function is to carry the electrical signals produced by the cell body. The cell body of a neuron frequently gives rise to multiple dendrites, but never to more than one axon, although the axon may branch hundreds of times before it terminates. The synapses are branched terminations responsible for the transmission of the signals from the axon of one neuron to a dendrite of another. They release neurotransmitters.

Glial cells compose a voluminous support system that is essential to the proper operation of nervous tissue and the nervous system. Unlike neurons, glial cells do not conduct nerve impulses. Their main functions include providing support for the brain, assisting in nervous system repair and maintenance, assisting in the development of the nervous system, and providing metabolic functions for neurons. They are far more numerous than neurons (in the human brain glia are estimated to outnumber neurons by about 10 to 1) and, unlike neurons, are capable of mitosis. There are four types of glial cells in the human body depending on their location in the body and their function. The oligodendrocytes, the astrocytes and the microglia are three kind of glial cells located in the CNS. The astrocytes (also called astroglia) have numerous projections that anchor neurons to their blood supply. They regulate the external chemical environment of neurons by removing excess ions (notably potassium) and recycling neurotransmitters released during synaptic transmission. The current theory suggests that astrocytes may be the predominant "building blocks" of the blood-brain barrier. The microglia are extremely small cells of the central nervous system that remove cellular waste and protect against microorganisms. The oligodendrocytes are central nervous system structures that wrap some neuronal axons to form a specialized membrane called myelin, producing the so-called myelin sheath. The SCs are the glial cells located in the PNS. They surround the peripheral nerve axon and maintain the vitality of peripheral nerve fibers (both myelinated and unmyelinated). In myelinated axons, SCs form the myelin sheath.

The myelin sheath, both in the CNS and in the PNS, provides insulation to the axon that allows electrical signals to propagate more efficiently. This type of layer is not continuous but interrupted (at intervals corresponding to the length of the SCs and the uncovered parts of the axon are called nodes of Ranvier. Due to the presence of the nodes of Ranvier, impulses propagate by saltation.

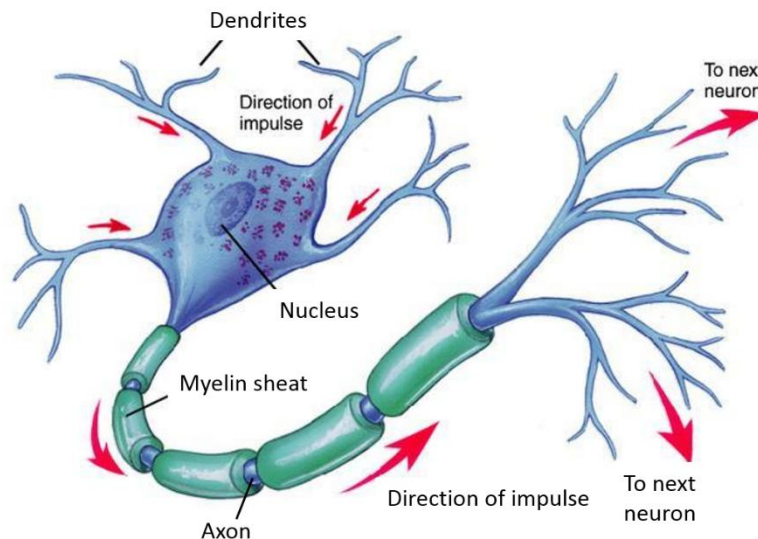


**Fig. 3.1.** Scheme of a neuron. Each neuron has three basic parts: cell body called soma, one or more dendrites and a single axon. SCs (in PNS) and oligodendrocytes (in CNS) surround the axon forming not continuous myelin sheath.

### 3.2.3 Structure of the nerve

The PNS is composed of nerves, which are cylindrical bundles of fibers that start at the brain and central cord and branch out to every other part of the body forming the communication network between the CNS and the surrounding (muscles, organs of the digestive system...).

The primary function of a peripheral nerve is to transmit signals from the spinal cord to the rest of the body (motor nerves), or to transmit sensory information from the rest of the body to the spinal cord (sensory nerves). The peripheral nerve is made up of connective tissue and nerve components. These connective tissue structures the endoneurium, perineurium, and epineurium, all form the framework that organizes and protects the nerve fibers and the axons (Fig. 3.2). The epineurium is a layer of dense connective tissue that covers and holds together the outer surface of nerves. The main function of the epineurium is to maintain the structural continuity of the nerve and to protect the nerve. Each bundle of nerve fibers is called a fasciculus (set of 10-100 axons) and is enclosed by the perineurium, a connective tissue sheath formed mainly of collagenous fibers. Important functions of the perineurium are to maintain the intrafascicular pressure and to regulate the local environment in the intrafascicular space by acting as a diffusion barrier to several substances. Within the fasciculus, each

individual nerve fiber, with its myelin and neurolemma, is surrounded by connective tissue called the endoneurium.

The peripheral nerve is supplied by both an external segment blood supply and an intrinsic longitudinal blood supply. The intrinsic blood supply exists in the epineurium, perineurium, and endoneurium. Whereas large vessels can be found in the epineurium and endoneurium, only capillaries are found in the perineurium.

A nerve conveys information in the form of electrochemical impulses (known as action potentials) carried by the individual neurons that make up the nerve. These impulses are extremely fast, with some myelinated neurons conducting at speeds up to 120 m/s. The impulses travel from one neuron to another by crossing a synapse, the message is converted from electrical to chemical and then back to electrical.

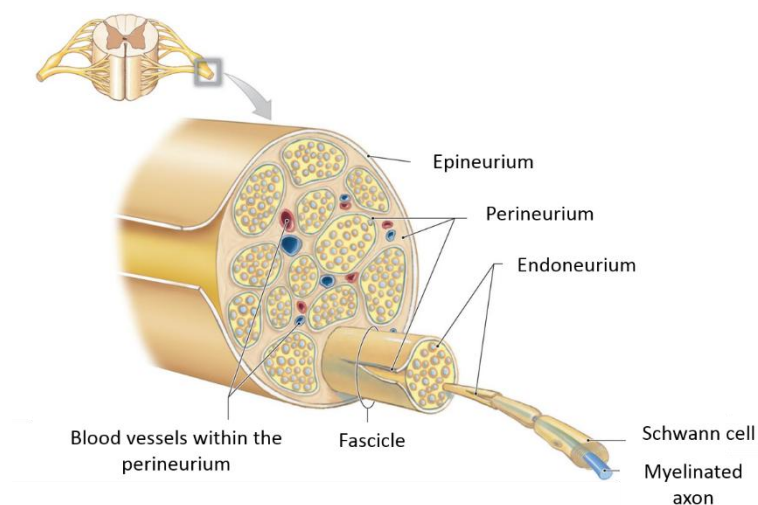


**Fig 3.2.** Section of a spinal nerve: see the epineurium surrounding the nerve, each bundle of nerve is called fasciculus and is surrounded by the perineurium. Each nerve fiber of the fasciculus is surrounded by the endoneurium.

### 3.2.4 Nerve injuries classification

Nerve injuries can be produced by various mechanisms such as crush trauma, direct laceration, stretching and compression. The two most widely accepted classifications of nerve injuries are Seddon and coworker's [2] and Sunderland's classification [3]. The latter one expanded the previous classification of Seddon, which described three types of lesion named neuropraxia, axonotmesis, and neurotmesis, into a more detailed subdivision according to the connective and fibrous structures that are damaged.

Neurapraxia and axonotmesis, or first- and second- degree Sunderland injury, have a good prognosis. Neurapraxia (Fig. 3.3A) involves a local conduction block at the site of injury along the course of the nerve, with normal conduction both proximal and distal to the site of injury. The nerve remains in continuity and no axonal injury is present. In more severe instances of neuropraxia, local myelin abnormalities or even segmental demyelination may be involved. This type of injury may result from exposure to a wide

range of conditions including heat, cold, irradiation or electrical injuries, but is most commonly due to mechanical stress, such as concussion, compression or traction injuries, and is often associated with some degree of ischemia. Full functional recovery is to be expected within a few days to a few weeks. Axonotmesis (Fig. 3.3B), involves severance or destruction to peripheral axons, but connective tissue structures remain intact thus facilitating nerve regeneration and functional recovery. The SCs enveloping the injured axons also remain intact, which allow regeneration to restore full motor and sensory function. The interruption of axons is often the result of nerve pinching, crushing or prolonged pressure. Recoveries in these injuries will occur at the classic rate of nerve regeneration of approximately 1mm/day to 1.5 mm/day [2].

The neurotmesis (Fig. 3.3C-E) is a complete transection of the nerve and can range from a disruption of a subset of endoneurial tubes to a complete transection of the nerve. Therefore, axons must regenerate through some degree of scar tissue. This can lead to incomplete regeneration, as some of the regenerating fibers do not achieve contacts with distal receptors or end organs because of interposed scarring within the endoneurium. The basal lamina of the SCs is also damaged in this type of injury which can lead to mismatching of regenerating nerve fibers to inappropriate distal receptors. In this case, the functional recovery does not easily occur because of the extent of endoneurial tube disruption. Nonetheless, successful regeneration into appropriate (or the original) endoneurial tubes might result in the re-establishment of target reinnervation. In neurotmesis the spontaneous re-innervation is often incomplete and absent.

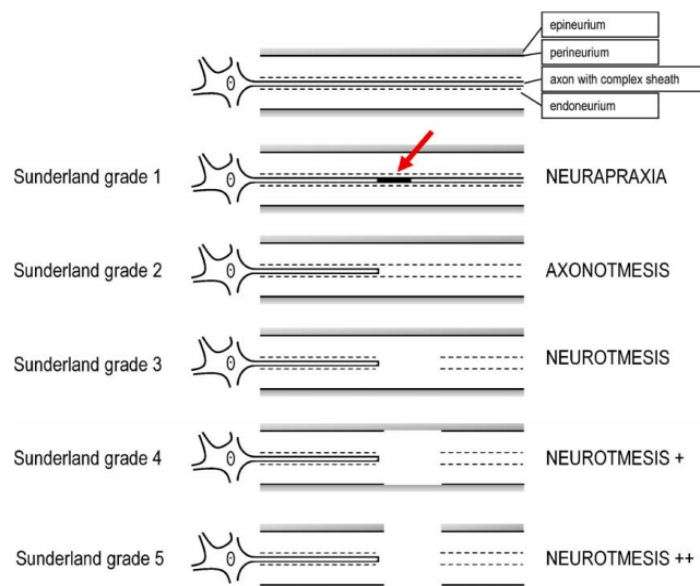


**Fig. 3.3.** Schematic representation of the five degrees of nerve injury according to Sunderland [3]. Grade 1: conduction block indicated by red arrow (neurapraxia), Grade 2: transection of axon with an intact endoneurium (axonotmesis), Grade 3: transection of the nerve fiber (axon and endoneurium) within an intact perineurium (neurotmesis), Grade 4: transection of funiculi, epineurial tissue maintains nerve trunk continuity (neurotmesis +), Grade 5: transection of the whole nerve trunk (neurotmesis ++).

### 3.2.5 Peripheral nerve regeneration after injuries

Functional recovery after nerve injury involves a complex series of pathophysiologic changes, including morphologic and metabolic alterations, each of which may delay or impair the neuronal regenerative process. These complex changes occur: i) in the nerve cell body, ii) in the segments proximal and distal to the injury site, iii) at the site of injury itself and iv) in the distal endings of both muscle end-plates and sensory receptors. The regeneration and repair phase following nerve injury may last for many months. In detail, following axonal disruption, degenerative changes, including axon and myelin breakdown, are initiated proximally and distally to the injury site (Fig. 3.4A). Retrograde axonal degeneration in the proximal nerve stump may extend for several millimeters, or even several centimeters following severe injuries. The remaining axons in the proximal nerve may also demonstrate a reduction in diameter, the extent of which depends on the time taken to re-establish functional connections (Fig. 3.4B). Pathophysiologic alteration can be seen in the nerve cell body as early as several hours after injury. The series of morphological changes that ensue in the cell body after injury are known as chromatolysis, and entail cell body and nucleolar swelling, and nuclear eccentricity. This is accompanied by the loss of Nissl substance from the cytoplasm (Fig. 3.4B). Such changes represent reactive alterations in neuronal biochemistry and function and they are indispensable for subsequent axon regeneration. Chromatolytic changes involve an alteration of metabolic machinery from being primarily concerned with transmitting nerve impulses to fabricating structural components for reconstruction of the injured nerve. Recovery from such changes takes a number of weeks (or even months) and has been reported to depend on the re-establishment of appropriate functional connections in the periphery [4]. Failure of axotomised neurons to re-establish appropriate connections may result in them persisting in an atrophic, chromatolytic state (Fig. 3.4E) or even in their degeneration. After nerve transection, the distal nerve undergoes a slow process of degeneration known as Wallerian degeneration which starts immediately after injury and involves myelin breakdown and proliferation of SCs. SCs and macrophages are recruited to the injury site, and over a period of 3 to 6 weeks, they phagocytize all the myelin and cellular debris, and ultimately leave endoneurial tubes, which essentially consist of the basement membrane of these SCs (Figure 3.4A-B). The newly generated SCs, together with pre-existing SCs that survived the nerve injury form the bands of Büngner (Fig. 3.4C). The bands of Büngner in the distal nerve segment are highly aligned and this topographical property is thought to be crucial for the direction of axon growth. Apart from their orientated topography, the molecular characteristics of SCs afford them their axon-growth promoting properties. SCs produce a basal lamina, which is a specialized and complex network of ECM proteins capable of supporting axon regrowth. The growth cones of sprouting axons use these tubes, delineated by the continuous SC basal laminae, as a regenerative substrate through which they extend at an average rate of 1–3 mm/day. Changes in the levels of neurotrophins within both the proximal and distal stump occur, too. Neurotrophin 4/5 mRNA, nerve growth factor (NGF), brain

derived neurotrophic factor (BDNF) and in the distal stump are increased. NGF is known to be secreted by SCs after axotomy [5].

In neurotmesis (Fig. 3.4C-E), the severity of disorganisation to local ECM or cellular architecture can range from a disruption of a subset of endoneurial tubes to a complete transection of the nerve. In this case, endoneurial SCs and fibroblasts proliferate and migrate from both ends of the damaged nerve in an attempt to form a cellular and connective tissue bridge across the lesion site. Distal nerve stumps, as well as denervated target tissues, such as skeletal muscle, exert an attractive influence on axonal sprouts, presumably by providing chemotactic cues. However, functional recovery does not easily occur because of the extent of endoneurial tube disruption. Nonetheless, successful regeneration might result in the re-establishment of target reinnervation with, in the case of skeletal muscle, neurotransmission at the neuromuscular junction, reversal of muscle fiber atrophy as well as of motoneuronal chromatolysis (Fig. 3.4C). The maturing SC–axon interactions in the regenerated distal nerve stump include the formation of myelin with significantly shorter internodes (Fig. 3.4C). Since these types of peripheral nerve injuries also involve connective tissue scarring, regenerative attempts of severed axons are often destined to fail and aberrant sprouting is frequently observed, often leading to the development of a neuroma at the proximal nerve stump that causes neuropathic pain symptoms (Fig. 3.4E).

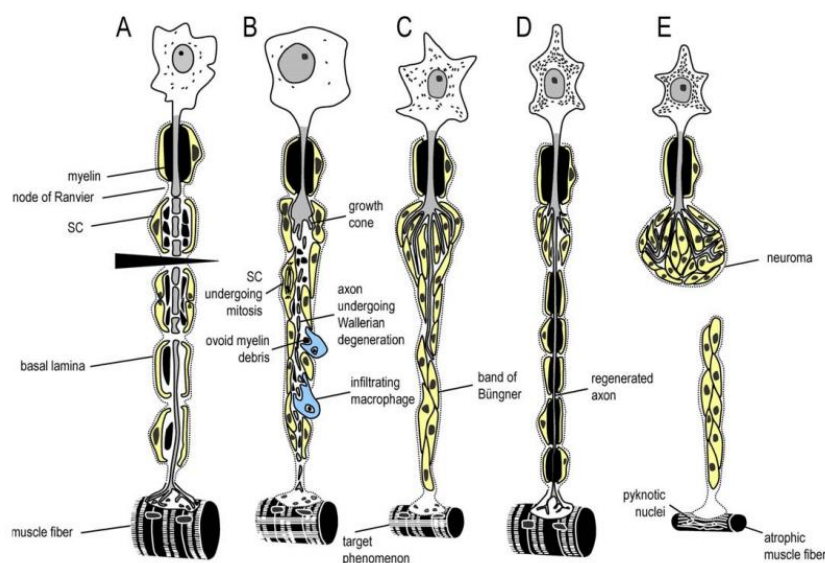


**Fig. 3.4.** Schematic representation of the degenerative and regenerative events associated with peripheral nerve injury. A: During the early phase (first few days) after axonal injury (arrowhead), local degenerative events are accompanied by both retrograde and anterograde degeneration of axon and myelin. B: During the intermediate phase (a few days to weeks), the anterograde pattern of Wallerian degeneration proceeds to completion with infiltrating macrophages contributing to the removal of tissue debris and SC undergoing mitosis. The axotomised neuronal cell body undergoes reactive, chromatolytic changes and the severed proximal end of the axon develops regenerative axonal sprouts. C: Of the numerous axonal sprouts that successfully traverse the injury site (during the first few weeks to months), some re-enter appropriate

endoneurial tubes and continue to extend through the distal nerve stump, supported by SC in the bands of Büngner. The target organ/tissue (in this case skeletal muscle) undergoes disuse atrophy. D: Successful axon regeneration through the bands of Bungner and the re-establishment of neurotransmission at the neuromuscular junction results in the retraction or dying-back of unsuccessful axon sprouts, the reversal of muscle fiber atrophy, of neuronal cell body chromatolysis and the establishment of maturing SC–axon interactions (including reduced internodal spacing). E: Failure of regenerating axonal sprouts to cross the injury site (possibly due to the formation of a physical scarring barrier or the loss of a large segment of nerve) results in neuroma formation. The permanently denervated muscle fibers demonstrate severe atrophy, loss of their characteristic striations and pyknotic nuclei.

### **3.2.6 Surgical approaches**

Peripheral nerve injury greatly compromises the quality of life of affected individuals and has a significant socioeconomic impact [6]. Nerve gaps caused by neurotmesis is undoubtedly the most challenging type of peripheral nerve lesion repair and requires surgical intervention. Satisfactory results are obtained when the nerves are purely motor or purely sensory and when the amount of intraneural connective tissue is relatively small. For optimal nerve regeneration after repair, nerve stumps must be properly prepared, aligned without tension, and repaired atraumatically with minimal tissue damage and minimal number of sutures. For nerve gaps of a few millimeters in length, end-to-end tension-free nerve suture repair is preferred clinically [7]. This surgical process consists of primary anastomosis of a divided nerve at the epineural or fascicular level, through end-to-end or end-to side and is applicable to short nerve gaps because the fascicular coaptation may cause excessive tension over the suture line, which would inhibit nerve regeneration [8]. In such cases, the regenerative process can be enhanced surgically through the use of nerve conduits, either using autologous or engineered tissue, that bridge the gap in the damaged nerve. Entubulization minimizes unregulated axonal growth at the site of injury by providing a distinct environment, and allows diffusion of trophic factors emitted from the distal stump to reach the proximal segment, which recreates the physiological conditions for nerve regeneration. Among the entubulization choices, autograft is still the gold standard technique in repairing injured peripheral nerve as it provides a scaffold containing both SCs and their basal lamina. The basal lamina contains many adhesion molecules, such as laminin, fibronectin, proteoglycans, that can promote neurite elongation. The sural, lateral antebrachial cutaneous, and terminal branch of the posterior interosseus nerve are common donor sites for nerve grafts. However, autograft is limited by the inherent drawbacks, such as limited availability of donor nerves, the need for a second surgery to obtain the donor nerve, donor site morbidity and secondary deformities, as well as mismatch between the injured nerve and the donor nerve [9]. Allografts and xenograft have also been used, but they are accompanied by the need for immunosuppression and have very poor success rate [10]. Autologous and autogenous blood vessel have also been used as conduits for nerve regeneration because of vein similarity to that of nerve tissue including the ability

to furnish important neurotrophic and neurotropic factors [11]. Although veins have shown good results, their parameters are limited and should be used only in sensory nerves with a defect of less than 30 mm [11]. Muscle-in-vein conduit (a vein segment filled with a skeletal muscle) has been developed to prevent the collapse of the lumen of the blood vessel [12]. The muscle offers strut to the vein and its basal lamina attract the regenerating axons. When the muscle degenerates, the gap is filled by the proliferation of SCs. Although such combined vein-muscle nerve conduits show the good biocompatible, the shortage of these materials limit the use of them in clinic, because these tissue must be removed from the patients.

Avoiding the problems of availability and immune rejection, artificial nerve guidance channels (NGCs) seems to be a promising alternative to autologous choices for extending the length over which nerves can successfully regenerate. In the next paragraph, the current status and future development directions of TE NGCs will be discussed.

### **3.2.7 Tissue engineering in peripheral nerve injury**

Developments in the field of TE offer the possibility to use artificial NGCs for reconstruction of nerve gaps. NGCs are small cylindrical structures composed of either natural or synthetic biomaterials that are used to facilitate axon regeneration: the ends of the damaged nerve are inserted into either end of the cylinder, and the NGC acts both as a connecting bridge for the severed nerve ends as well as a protective shelter for the regenerating nerve. Artificial NGCs seems to be a promising alternative to conventional treatments since these conduits serve to: i) direct axons sprouting from the proximal to distal nerve stump; ii) maintain adequate mechanical support for the regenerating nerve fibers; iii) provide a conduit channel for the diffusion of neurotropic and neurotrophic factors secreted by the damaged nerve stump and a conduit wall for the exchange of nutrients and waste products; iv) avoid the risk of fibroblasts infiltration and scar tissue formation that hinders axonal regeneration; and v) create an optimal microenvironment for nerve regeneration through the accumulation and release of exogenous and endogenous biochemical effects [10, 13]. In addition, the efficiency of NGCs can be improved by the presence of internal matrices inside the conduit which acts as physical guidance for axonal growth by providing a structured environment for cell regeneration and organization. Moreover, the conduits can also be functionalized with contact-mediated cues, such as proteins and peptides, chemotactic cues, such as neurotrophic factors and biological or cellular cues, such as SCs, neural stem cells and astrocytes (satellite cells of the PNS and CNS) [14]. An ideal neural scaffold should satisfy many biological and physicochemical requirements, among which biocompatibility, biodegradability into nontoxic products, permeability to ensure supply of nutrients, low degree of swelling, sufficient mechanical stability during nerve regeneration, flexibility (with a Young's modulus close to that of nerve tissues to prevent compression of the regenerating nerve) are the major concerns. Moreover, the neural scaffold is hoped to be easy to fabricate and sterilize, and simple to implant in the body by microsurgical

techniques. These required properties are mainly determined by the scaffold material and scaffold structure. As regard the former, a wide variety of biomaterials have been attempted, which are of either natural or synthetic origin. Moreover, both non-degradable [15] and (bio)degradable [13] materials have been used for NGC fabrication. The main objection for using non-degradable conduits is that they remain in situ as foreign bodies after the nerve has regenerated showing a higher risk of infection, a possible chronic inflammatory response, and having the potential to compress the nerve after regeneration. A second surgery might then be necessary to remove the conduits, causing possible damage to the nerve. Biodegradable materials offer several advantages, such as the possibility of attaching bioactive molecules or cells on the biomaterial surface through physicochemical modifications and to deliver them during biodegradation. Biodegradable polymers, both synthetic and natural polymers, have been extensively investigated as biodegradable polymeric biomaterials. Biodegradation of polymeric biomaterials involves cleavage of hydrolytically or enzymatically sensitive bonds in the polymer leading to polymer erosion. Depending on the mode of degradation, polymeric biomaterials can be further classified into hydrolytically degradable polymers and enzymatically degradable polymers. Hydrolytically degradable polymers are generally preferred as implants due to their minimal site-to-site and patient-to-patient variations compared to enzymatically degradable polymers [16]. However, most of the naturally occurring polymers undergo enzymatic degradation. Natural biomaterials are useful for nerve TE as they stimulate adhesion, migration, growth and proliferation of cells, and enable avoidance of toxic effects [17, 18]. Although the use of these natural materials would be ideal, there are some inherent difficulties generally associated to the necessity of extensive purification and characterization of the extracted materials and to the lack of adequate mechanical strength and water stability of the natural based material [19]. Synthetic polymers constitute another class of promising biomaterials for fabricating neural scaffolds due to their tunable chemical and physical properties. However, some synthetic materials, shows poor biocompatibility in terms of cell adhesion and tissue repair. Some natural and synthetic based NGCs have been approved by regulatory authorities for use in human [20]; they include, *e.g.*, NeuraGen® (Integra) and NeuroMatrix®/Neuroflex® (Stryker) both made of the cross-linked collagen, Neurotube® (Synovis) made of poly(glycolic acid), SaluBridge® and SaluTunnel® (SaluMedica) made of Salubria® hydrogel, and Neurolac® (Ascension) made of poly(d,l-lactide-co-caprolactone). The main advantages and disadvantages of the more commonly investigated polymers for NGCs (including both non-biodegradable and biodegradable synthetic and natural polymers) will be evidenced hereafter. In Table 3.1 biomaterials, both of synthetic or natural origin, used in peripheral nerve regeneration are reported.

### **3.2.7.1 Biomaterials in nerve regeneration**

#### **3.2.7.1.1 Synthetic biomaterials used for NGCs**

##### **Nonbiodegradable materials**

Silicone rubber has been studied since 1960s for peripheral nerve repair, and silicone tubes represent one of the first and most frequently used NGCs prepared with synthetic materials because of the bioinert and elastic properties of silicone. Although they are nondegradable in the body and impermeable to large molecules, silicone tubes provide an important model system for studying nerve regeneration under controlled conditions of nerve tubulization, and have been applied in clinical trials to bridge short nerve gaps (few mm in length) with some success [21, 22]. Chen et al. have recently shown that silicone rubber tubes containing a gel of collagen, laminin and fibronectin led to a successful nerve regeneration across the gap as compared to a empty silicone tube [23]. Non-degradable scaffolds have also been fabricated using plastic such as acrylic polymer, polyethylene, elastomer, etc.[16, 24, 25]. Disadvantages of the use of nondegradable NGCs include chronic foreign body reaction, inflexibility, and lack of stability. Particularly, the inflammatory response of nonbiodegradable NGCs may lead to fibrotic capsule formation around the guide and consequent nerve compression [26].

##### **Biodegradable synthetic materials**

In order to overcome the disadvantages associated with non-degradable materials, research has been concentrated on biodegradable synthetic materials used to prepare neural scaffolds. Materials applied should degrade within the regeneration period and degradation products should be no toxic and they should be absorbed by the body with no foreign body reaction. Moreover, the physiochemical and biological properties of biodegradable synthetic materials can be tailored to match different application requirements, and some chemical modifications enable the materials effectively to entrap support cells or bioactive molecules for controlled delivery during nerve regeneration. Among the bioresorbable materials, aliphatic polyesters and copolyesters have been frequently used for nerve regeneration. Aliphatic polyesters represent a class of the common degradable synthetic polymers, among which poly(L-lactic acid) (PLLA) [27], poly(glycolic acid) (PGA) [28], polycaprolactone (PCL) [29, 30] and their copolymers, including poly(lactic acid- $\epsilon$ -caprolactone) [31], poly(L-lactic-co-glycolic acid) (PLGA) [32] and poly(1,3-trimethylenecarbonate- $\epsilon$ -caprolactone) [33], have become the U.S. FDA-approved biomaterials used in the field of medical devices. Thanks to the possibility of finely tuning their properties by varying the block structure, copolymers are gaining more and more attention. Several investigations have been also focused on other copolymers, such as poly(DL-lactic-co- $\epsilon$ -caprolactone) (poly(DLLA-CL)), synthesized poly(ester-urethane)s (PU) with polyester macrodiols, poly(trimethylenecarbonate-co- $\epsilon$ -caprolactone) (poly(TMC-CL)), and microbial polyhydroxyalkanoates (e.g.,

poly(hydroxybutyrate-co-hydroxyhexanoate), PHBHHx). PGA, PLA, and PCL degrade primarily via hydrolysis in aqueous medium, but they can be cleaved enzymatically upon implantation by esterases as well.

The biocompatibility of PLLA has been demonstrated *in vitro* by the survival of SCs that were seeded onto the polymer surface and their subsequent expression of a range of ECM-related proteins, e.g. collagen IV, laminins-I and -II [34]. PLLA NGCs degradation products, particularly crystalline debris and lactic acid, may adversely cause long-term problems, affecting axon growth and nerve function [35]. In a recent study, Koh et al. have developed a new functionalized scaffold by coupling laminin onto PLLA nanofibers. Laminin was successfully added to nanofibers using covalent binding, physical adsorption or blended electrospinning procedures. The new functionalized fibers were able to enhance axonal extension by PC12 cell viability and neurite outgrowth assays [36].

PCL has been widely used in medical devices and drug delivery systems. However, the relatively slow degradation rate has resulted in being sub-optimal for some tissue-engineering applications. The *in vitro* affinity of this polymer has been recently demonstrated toward the adhesion and proliferation of PC12 cells [37], SCs and rat cortical neurons [38]. In a recent study, Ciardelli et al. [30] have shown that PCL supports the *in vitro* adhesion and proliferation of S5Y5 neuroblastoma cells and neonatal olfactory bulb ensheathing cells and can be shaped into tubular guides by dip-coating of a rotating mandrel. Interestingly, adding mesenchymal stem cells in a PCL conduit have been shown to enhance median-nerve regeneration, prevent decrease of creatine phosphokinase levels in muscle and improve functional recovery in mice [39].

PGA conduits filled with laminin-soaked collagen scaffolds have been shown to promote axonal regeneration over the 8 cm gaps with the same efficiency as the PGA-collagen fiber-filled conduits [40, 41]. Hollow guides made from PCL and poly(DLLA-CL) have also demonstrated promise of full morphometric and functional recovery at levels similar to autograft controls in 10-mm rat sciatic nerve defects [42]. In particular, poly(DLLA-CL) scaffolds have been found to be advantageous for peripheral nerve repair, as they are transparent and possess suitable mechanical properties allowing to accommodate movements over surrounding tissues. Poly(DLLA-CL) NGCs degrade completely within 1 year from implantation; however, this type of scaffold is suitable for the repair of short nerve gaps (e.g. digital nerves) because of their brief mechanical performance (negligible after only 2 months) and their high swelling during degradation, especially during the first 3 months [43]. Innovative biocompatible PUs have been investigated because they can be synthesized by a proper selection of block composition which allows a fine tuning of their mechanical properties, degradation rate, biocompatibility, and biomimicry [44].

An alternative method of stimulating neuronal tissue regeneration includes the application of electrical stimulation treatments through nerve conduits made from electrically conductive materials. Hence some important electrically conducting polymers, including polypyrrole (Ppy), polyaniline and polythiophene, have been tried to prepare neural scaffolds due to their tailored electrical and antioxidant properties [45-

47]. Ppy possesses good electrical conductivity, biocompatibility, high electrical stability, and it can be easily synthesized. When electrically stimulated *in vitro*, Ppy may attract serum proteins, such as fibronectin, which promote neurite expression: this provides a means for controlled chemical stimulation. However, its poor mechanical properties, lack of biodegradability, and difficulties associated with processing it into complex three-dimensional shape. In a recent study, Moroder et al. have investigated the mechanical and electrical properties of polycaprolactone fumarate–polypyrrole (PCLF–Ppy) scaffolds under physiological conditions. PC12 cells cultured on PCLF–Ppys scaffolds were electrically stimulated with regimens of 10  $\mu$ A of either a constant or a 20 Hz frequency current passed through the scaffolds for 1 h per day. PCLF–Ppy scaffolds exhibited excellent mechanical properties at 37°C which would allow suturing and flexibility. The scaffolds were electrically stable during the application of ES. *In vitro* studies showed the capability to significantly enhance and direct neurite extension by passing an electrical current through PCLF–PPy scaffolds [48].

#### **3.2.7.1.2 Natural polymers for NGCs**

Natural polymers are advantageous materials for TE of nerves as they are biocompatible, favour the migration of supporting cells, and avoid the occurrence of toxic effects. However, the poor mechanical properties, the high swelling behavior, and the relatively fast *in vivo* biodegradation rate of natural polymers generally limit their applications as constituent materials of the external tubular structure of NGCs. In some cases, blends between natural and synthetic polymers have been proposed for neural guides, to combine the biocompatibility of the natural component with the advantageous processing properties and mechanical performance of the synthetic material. Insoluble ECM molecules, such as collagen, gelatin, laminin, and fibronectin, play an important role in the development and growth of axons [49, 50], and many other proteoglycans and glycosaminoglycans of the ECM can modulate neural activity and neurite extension, providing either stimulatory or inhibitory effects [51, 52]. As a result, ECM components have become very important candidate materials for neural scaffolds, and they were predominantly processed into lumen fillers of NGCs in the form of fibers, channels, porous sponges, or hydrogels to serve as delivery vehicles for support cells, GFs, or drugs. Collagen is one of the major ECM proteins, accounting for up to 30% of the total body protein. In its native environment, collagen interacts with cells in connective tissues and transduces essential signals for the regulation of cell anchorage, migration, proliferation, differentiation, and survival [53]. Biomaterials made from collagen offer several advantages, including biocompatibility, non-toxic degradation and a weak antigenic activity, due to its phylogenetically conserved primary sequence and a helical structure. Disadvantages of collagen include its relatively high cost and mechanical weakness. Among the realized NGCs based on natural polymers, collagen conduits, such as NeuroMatrix<sup>®</sup>, Neuroflex<sup>®</sup> [Collagen Matrix Inc.], and NeuraGen<sup>®</sup> [Integra Life sciences Corp.] have been approved by FDA. Collagen conduits have been reported to be as

effective as autografts when repairing peripheral nerve defects as small as 4 mm in length [54]. However, Stang et al., showed that axon regeneration across the 2 cm resection injury was relatively poor in comparison to the autografts [55]. Collagen, in the form of a hydrogel, has been used to fill the lumen of conduits made from a range of materials to promote improved axon regeneration and tissue repair [56]. Collagen gel filled conduits were found to improve the extent of functional recovery across 4 mm and 6 mm lesions of the mouse sciatic nerve when compared to saline filled conduits. Interestingly, the concentration of the gel significantly affected the extent of the repair process; lower concentration gels supported the best degree of functional recovery. Moreover, collagen filaments have been found to guide axon repair. Madison et al. reported bridging of nerve gap distances of 3 cm in rat sciatic nerve [57]. In a recent work, collagen-based microstructured three-dimensional NGC containing numerous longitudinal guidance channels with dimensions resembling natural endoneurial tubes have been produced [58]. The NGCs have been functionalized by SC seeding. Viable SCs within the guidance channels formed cellular columns reminiscent of bands of Büngner, which are crucial structures in the natural process of peripheral nerve regeneration during the Wallerian degeneration. The orientated 3D nerve guides (decorated with SCs) with their physical and molecular properties showed great promise in the repair of peripheral nerve lesion.

Gelatin (GL) is a protein derived from collagen by thermal denaturation or physical and chemical degradation. GL does not express antigenicity in physiological conditions and is cheaper and easier to obtain in concentrated solutions than collagen. Other interesting properties of GL are its biocompatibility, biodegradability, and adhesiveness. The mechanical and chemical properties of GL can be modulated by proper crosslinking. GL conduits have been produced using crosslinked GL by photocuring [59] or genipin (GP) treatment [60, 61]. In both cases, NGCs have been implanted for the repair of a 10 mm nerve gap in the rat sciatic nerve. Neural regeneration was assessed in terms of functional recovery, electrophysiological responses, and tissue morphological regeneration. GL-based neural scaffolds can be covalently incorporated with additional bioactive cues, which are gradually released during the scaffold biodegradation [62].

Laminin is the first ECM protein expressed during embryogenesis, and can guide developing neurites and promote neurite outgrowth. Found in the basal lamina (basement membrane) and produced by SCs, it is an important adhesion molecule for growth and regeneration of neural tissue. Laminin plays a crucial role in the developing and maturing central nervous system, for example, in cell migration, differentiation, and axonal growth [63].

Fibronectin is an ECM protein that is dispersed in interstitial matrices. It is composed of several rod-like domains, one of which contains a repeating sequence of peptides that regulates cell adhesion, the RGDS sequence (L-arginine, L-glycine, L-aspartic acid, and L-serine). Fibronectin has been found to play a role in axonal growth and cell migration. Tong et al. have shown that the presence of laminin and fibronectin in collagen grafts can

dramatically increase the ability of neural components to regenerate effectively over long nerve gaps [64]. In a recent study, the incorporation of fibronectin into hollow conduits was able to improve axon regeneration across 18 mm gaps of the adult rat sciatic nerve. Greater numbers of regenerated axons and more retrogradely labeled motoneurons and dorsal root ganglia sensory neurons could be detected 4 months after implantation when compared to the saline filled hollow conduits.

Other naturally derived molecules investigated for their application in nerve repair include hyaluronic acid, alginate, agarose, CS and silk fibroin.

CS, has been investigated for a variety of TE applications because it is structurally similar to naturally occurring GAGs and it is degradable by enzymes in humans. It is a linear polysaccharide of (1–4)-linked d-glucosamine and N-acetyl-d-glucosamine residues derived from chitin. The similarity in the molecular structure between CS and glycosaminoglycans allows interactions between CS and ECM molecules including laminin, fibronectin and collagen. CS possesses favorable TE properties as biomaterials. This is due to its antibacterial activity, biodegradability, and biocompatibility [65]. Since CS is fragile in its dry form, it has to undergo chemical crosslinking or to be used jointly with other materials before scaffold fabrication. The biocompatibility of CS-based biomaterials with the cells in CNS or PNS has been investigated [66, 67]. Yuan et al. showed that CS fibers supported the adhesion, migration and proliferation of SCs [17]. Blending CS with a protein (or a peptide) has been proposed as an effective method to enhance nerve cell attachment and to make the mechanical properties of scaffolds more similar to those of nerve tissues. In a recent study, CS/poly(L-lysine) composite materials with various compositions have been prepared with the aim of enhancing CS nerve cell affinity. PC12 cells cultured on the composite substrates showed an improved attachment, differentiation and growth when compared to cells cultured on CS membranes. The effectiveness of CS/poly(L-lysine) composite materials in the nerve regeneration field has been attributed to the increased hydrophilicity and positive surface charge of blends with respect to pure CS [68]. Recently, NGCs have been obtained consisting of CS conduits filled with porous collagen sponges simulating the 3D structure of ECM [69]. The inner sponge was imbued with NGF. Conduits have been tested for the repair of a 10 mm defect in the rabbit facial nerve: in one case, a suspension of neural stem cells (NSCs) has been injected into the tube during *in vivo* implantation, whereas, in the control test, a saline solution has been used. Autograft has been employed as a positive control. After 12 weeks from implantation, nerves treated with autografts have shown similar recovery as compared to the ones treated with NGCs containing NSCs.

Alginate is a biodegradable polysaccharide with repeat units of mannuronic acid and glucuronic acid. It is extracted from brown sea-weed and bacteria [70]. The physical properties of alginate gels vary widely depending on the proportion of guluronic to mannuronic acid residues and the overall molecular weight of the polymer. Matsuura et al., have demonstrated the potential of alginate as a scaffold for promoting autonomic

nerve regeneration [71]. The alginate foam has been developed and implanted into a 7-mm sciatic nerve gap in rats or a 50-mm sciatic nerve gap in cats [72]. The results suggest that alginate foams could promote peripheral nerve regeneration even without being sutured to nerve stumps. Recently, alginate has been also used to deliver GFs such as FGF over a number of weeks [73].

Agarose is a polysaccharide derived from red algae. Agarose hydrogel has been found to support neurite extension *in vitro* [74]. The advantage of agarose derives from the possibility to easily couple proteins and GAGs to the polymer, resulting in improved cell response. In a recent study polysulfone NGCs have been filled with anisotropic agarose hydrogels containing gradients of laminin and NGF and used for the repair of 2 cm defects in the rat sciatic nerve. The NGCs investigated were then compared with syngenic grafts and NGCs filled with isotropic agarose hydrogels with uniform concentration of NGF and laminin. After 4 months from surgery, NGCs containing anisotropic agarose hydrogels with gradients of both laminin and NGF have shown much better results than for isotropic fillers [75].

Silk fibroin (SF), a core protein of natural silk, has found rapidly increasing applications in TE because of its biocompatibility, high resilience, and slow biodegradation. SF is water soluble and becomes water insoluble by physical induction of  $\beta$ -sheet formation. Besides serving as a biochemical delivery substrate, SF has also been used to prepare NGCs for investigating the *in vitro* biocompatibility of SF with neural tissues and cells, and for bridging a sciatic nerve gap in a mouse model [76, 77]. Recently, Yang et al., have developed a novel biomimetic design of the SF-based nerve graft which was composed of a SF-NGC inserted with oriented SF filaments, serving as a skeleton for regrowing nerve tissues. The SF-NGC was used for bridge implantation across a 10-mm long sciatic nerve defect in rats, and the outcome of peripheral nerve repair at 6 months post-implantation was evaluated. The examined functional and morphological parameters show that SF grafts could promote peripheral nerve regeneration with effects approaching those elicited by nerve autografts. Just like silk fibroin, keratins and other matrix proteins extracted from human hair, wool, nail and feather have also been tried as new scaffold materials in the clinical repair of damaged tissues. It has been reported that they are likely to become candidate materials for neural scaffolds as well [78].

**Table 3.1** Most widely studied materials for NGCs with related properties and selected studies where they were used.

<b>NGC material</b>	<b>Characteristics</b>	<b>Reference</b>
<b>Synthetic</b>		
Silicone	Highly elastomeric polymer, non-biodegradable, bioinert, impermeable, hydrophobic	[21-23, 26]
Poly( $\epsilon$ -caprolactone)	Aliphatic polyester, biodegradable by hydrolysis, commercial NGC (CultiGuide®)	[29, 30, 37-39]
Poly(glycolic acid)	Aliphatic polyester, biodegradable by hydrolysis, commercial NGC approved by FDA (Neurotube®)	[28, 40, 41]
Poly(DL-lactic-co- $\epsilon$ -caprolactone)	Aliphatic polyester, biodegradable by hydrolysis, commercial NGC approved by FDA (Neurolac®)	[31, 43]
Poly(L-lactic acid)	Aliphatic polyester, very slowly biodegradable by hydrolysis	[27, 34-36]
Polyester urethane	Elastomeric polymer, biodegradable	[44]
Polypyrrole	Electrically conducting polymer, biocompatible, high electrical stability, lack of biodegradability	[47]
<b>Natural</b>		
Alginate	Polysaccharide, water-soluble, biodegradable by hydrolysis	[70-73]
Agarose	Polysaccharide, water-soluble, biodegradable by hydrolysis	[74, 75]
Chitosan	Polysaccharide, enzymatically degradable, positively charged, good cell interactions	[65-69, 79]
Collagen	ECM protein, enzymatically degradable, good cell interaction, commercial NGC approved by FDA (Neuroflex®, Neuromatrix®, Neurogen®)	[53-58]
Fibronectin	ECM protein, enzymatically degradable, good cell interaction	[64]
Gelatin	ECM protein, enzymatically degradable, good cell interaction	[59-62]
Laminin	ECM protein, enzymatically degradable, good cell interaction	[63]
Silk fibroin	Silk protein, enzymatically degradable	[76, 77]

### 3.2.7.2 The structure of a neural scaffold

The structure of a neural scaffold, as well as the scaffold material, is a critical factor that determines the efficacy of neural guides to aid peripheral nerve regeneration. The neural scaffold can be simply fabricated into a basic structure, that is a tubular NGC with a single hollow lumen. Single hollow lumen NGCs are fabricated with natural or synthetic biomaterials by a range of polymer processing methods, among which a common technique is melt extrusion [30], the process of converting a thermostable polymer into a product by forcing it through a die of desired shape. Alternative techniques suitable for those polymers with low thermal stability are dipping spinning-mandrel into the polymer solution followed by air-drying to obtain a tube [80], injection molding, physical film rolling, crosslinking braiding, and electrospinning. All these processes have been employed for preparing neural scaffolds with the basic structure, i. e., hollow NGCs [81, 82]. Inappropriate target reinnervation following the dispersion of regenerating axons is the main drawback associated to hollow lumen NGC [83]. As a result, this type of conduit is mostly used for the repair of small injuries of sensory nerves with a less than 30-mm long nerve gap, such as digital nerve lesions [84]. Therefore, considerable efforts have been focused on the development of more complex scaffold structures in which the NGC lumen shows an intricate internal architecture, and then physical fillers are introduced into the NGC lumen, or a multichannel NGC is created to replace a single hollow lumen NGC. These modifications to the basic structure, shown in Fig 3.5, attempt to generate a substrate able to reproduce several of the important physical and molecular characteristics of nerves observed during nerve spontaneous regeneration.

The development of multichannel NGCs, through the incorporation of one or more intraluminal channels into the hollow conduit, is mainly based on the idea of mimicking the architecture of nerve fascicles. Multichannel NGCs are commonly fabricated by an injection-molding technique [85]. Multi-channel NGCs provide greater surface areas for cell attachment [86] and local release of GFs [87]. Multichannel conduits, fabricated from PLGA, have shown promising results in directing nerve growth over short observation times (six weeks) and limited gap size (7 mm) [86]. However, the extra internal structure may interfere with some important properties of the neural scaffold, such as permeability, bending and deformation properties, swelling, and degradation. Swelling has been shown *in vitro* and *in vivo* studies to close the conduit cavities and block axonal growth over long-term study (12 weeks) and larger gap sizes (10 mm) [85, 88]. In a recent study, Yao et al. have investigated the influence of channel number on the axonal regeneration using a series of 1-, 2-, 4, and 7-channel collagen conduits and commercial (NeuraGen®) single channel conduits. The multichannel collagen conduits were fabricated by molding and crosslinking (with 1-ethyl-3-(3-dimethylaminopropyl)carbodiimide (EDC) and N-hydroxysuccinimide (NHS)). Crosslinking led to control the biodegradation rate and to limit swelling. The results of this study clearly demonstrated the potential influence that multichannel nerve tube structure have

on limiting axonal dispersion across the conduit without decreasing the quantitative results of regeneration [89].

The incorporation of physical lumen fillers, typically supportive GFs or accessory cells, has been largely investigated with the aim to provide a permissive environment which mimic the endoneurial-like substructure by the presence of an adequate amount of SCs to support, through the release of neurotrophic factors and the formation of bands of Büngner, the axonal regeneration inside the NGCs. The failure of non-neuronal cells, such as SCs, to migrate across lesion gaps (longer >15 mm) is often the reason for the poor regeneration outcome in non-filler-containing nerve conduits. An array of biomaterial-based fillers with different physical forms (such as fibers, filaments, gel, or sponges) have been included into the lumen as topological cues [40, 41, 56, 74, 75]. For all these different types of biomaterial-based fillers, there seems to be a need to create an internal aligned architecture of matrix within the NGC lumen. To do this, a range of method including polymer extrusion or polymer alignment by magnetic fields, injection molding, phases separation and micropatterning have been used to orient the fiber, filament or gel fillers inside the NGC lumen [57, 90, 91]. Magnetically aligned collagen (or other ECM protein) matrices within the NGC lumen have been shown to promote axonal outgrowth *in vitro* and *in vivo* as compared to random isotropic counterparts that are usually prepared in a handmade way [92, 93]. Moreover, the number of filaments or fibers and the gel concentration introduced to the NGC lumen should be optimized because dense intraluminal matrices may impede the migration of regenerating axons and non neuronal cells, and occupy space within the NGC lumen where new initial regenerative cables are formed and distributed [56].

Longitudinally oriented filaments or fiber bundles, both of synthetic [32, 94, 95] or biological materials [57, 59], have been inserted into the NGC lumen to guide the longitudinally directed growth of regenerating axons. Several manufacture methods, including electrospinning, phase separation, and self-assembly, have been used for the fabrication of such biofunctional nanofibrous scaffolds. Wang et al. prepared a microporous CS NGC with internal oriented filaments of PGA. This NGC was used to bridge 30-mm dog sciatic nerve gap, achieving the repair outcome similar to that by autologous nerve grafting [96]. *In vitro* studies have demonstrated the influence of fiber diameter on the orientation of process outgrowth. The greater surface curvature of small diameter fibers prompted an increasing tendency for neurite outgrowth to follow the longitudinal axis of the fibers. Thus, small caliber fibers (5–30  $\mu\text{m}$  diameter) supported a greater degree of orientated process growth than large caliber fibers (up to 500  $\mu\text{m}$  diameter) [97]. Interestingly, Ribeiro-Resende et al. have reported that PCL NGCs inserted with laminin-coated PCL filaments (22  $\mu\text{m}$  diameter) or with poly-D-lysine-coated fibers (22  $\mu\text{m}$  diameter) could support nerve regeneration [90]. In this study, researchers have also shown that the alignment of SCs can be induced more efficiently by physical means, i.e. polymer filament topography, than by biological means such as the application of individual soluble factors.

Besides being processed into the physical form of fibers or filaments, the ECM protein-based intraluminal matrix is also shaped as gels or three-dimensional sponges due to the ease of fabrication. In a recent work, Tonda-Turo et al. have developed artificial NCGs consisting of porous PCL hollow tube and an internal GP-crosslinked GL sponge (GL/GP). GP crosslinking increased the GL-sponge stability in water and improved the mechanical properties under compression, as compared to uncrosslinked GL sponge. GL/GP films were found to support the *in vitro* adhesion, the survival and the proliferation of NOBEC and PC12 cells [98]. Hydrogels, serving both as space lumen filler and as delivery vehicles for bioactive molecules and cells, have been developed by using natural based biomaterial such as collagen, GL, and laminin gels, showing an improve in the recovery of neural gaps in rat or mouse sciatic nerve [40, 41, 68]. In a recent study, Pawar et al., have developed an alginate-based anisotropic hydrogels [99]. The incorporation of GL into hydrogel, by simple immersion of alginate gels in 2g/l GL solution, has been shown to promote directed axon outgrowth and SC migration *in vitro*. The author has recently collaborated to the development of a agar/gelatin based hydrogel for the loading and release of growth factors (Tonda Turo et al) The prepared developed showed shear-thinning properties and was applied as filler of NCGs. *In vitro* experiments showed that the GL based hydrogel was able to promote Schwann- like cell adhesion, proliferation and migration.

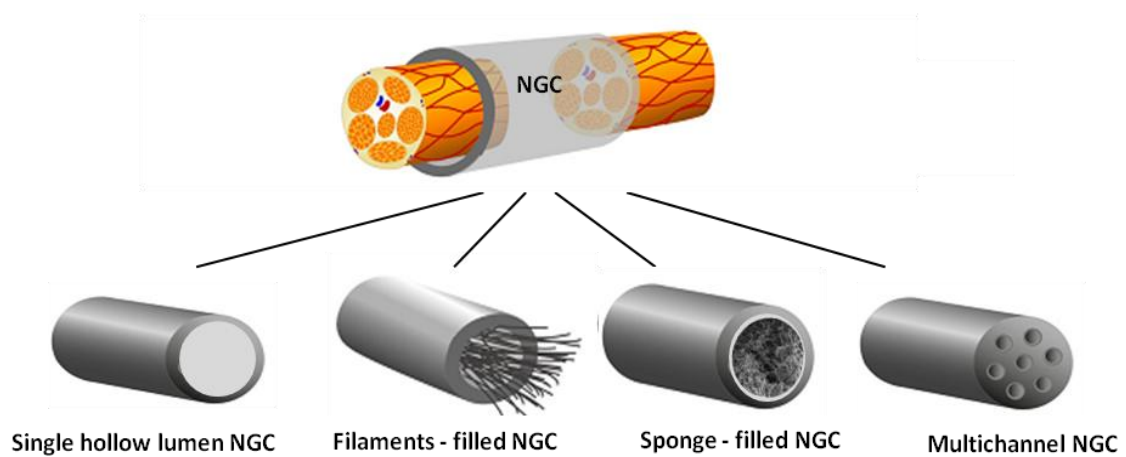


**Fig. 3.5.** Schematic representation of structural repair strategies used for improving existing hollow nerve guidance conduits. Repair strategies include the use of intraluminal guidance structures and multichannel designs to provide additional structure support and topographical guidance to regenerating axons and migrating SCs.

### 3.2.7.3 Cellular therapy: support cells

The success of simple tubulization is dependent on the length of the gap between the two nerve stumps. When the length of nerve gaps is consistent (>30 mm in primate ulnar nerve), empty NGCs alone will not suffice unless support cells or GFs are incorporated into them [100]. Support cells implanted into the injury nerve may clearly act as the source of a range of particular neurotrophic factors, and may also generate beneficial, axon growth promoting environments by the production of important ECM molecules such as collagen, laminin and fibronectin. Moreover, the donor cells obtained from patients themselves may be acutely dissociated from the injured nerve and added to an implant or expanded in tissue culture prior to implantation [101]. SCs, neural stem cells (NSCs) and marrow stromal cells (MSCs) are the most studied candidates of support cells among others.

SCs are the first and most widely used support cells in peripheral nerve TE because of their pivotal role in the neuronal process of regeneration (see paragraph 3.2.5) [102]. SCs are also able to produce a high level of different GFs, such as NGF, BDNF, and erythropoietin in the sensory system and glial derived GFs in the motor system [103, 104]. SCs suspended in GL within PGA conduits and autogenous SC suspension in venous grafts have supported nerve regeneration over a 30 mm gap in rabbits [105]. Hadlock et al. developed artificial NGCs consisting of multichannel conduits seeded with SCs isolated from neonatal Fisher rats. The NGCs seeded with SCs increased the average fiber diameter in the polymer conduits, as compared to autografts, favouring regeneration of myelinated motor fibers [86]. As well, neural scaffolds with different structures are attempted to include SCs, it has been reported that SCs introduced into NGCs with lumen fillers or multiple channels, could form the ordered arrangement of SC columns to imitate Bands of Bungner [106]. However, the long-term effects have, so far, proved unremarkable [107].

Since isolation and culture of primary SCs is a time-consuming process, the growing applicability of stem cells has opened new frontiers to nerve regeneration: the advantage of using these cell lines is that cell differentiation may be stimulated by advancing axons and pluripotency, allows multiple differentiation paths, which can create a positive environment for axonal regeneration has been taken into account by researchers. Among the multipotent stem cells, NSCs have the potential to differentiate into three major cellular elements of the nervous system, including neurons, astrocytes and oligodendrocytes; moreover they can proliferate unlimitedly and undergo rapid cellular expansion in response to nerve injuries. Markedly increased functional and morphological recovery has been observed following the incorporation of NSCs into conduits [108]. In a recent study, CS based NGCs seeded with NSCs have been used as a nerve graft to bridge 10-mm facial nerve gaps in rabbits. Nerve regeneration at 12 weeks after implantation was similar to that by autologous nerve grafting [69]. MSCs are pluripotent stem cells easily obtained through the aspiration of the bone marrow and expanded in a large scale by *in vitro* culture [109]. Several *in vitro* studies have reported

that MSCs can be induced to differentiate into non-mesenchymal cells, such as SCs, improving myelin formation and nerve regeneration *in vivo* after their transplantation into different models of peripheral nerve injury [110-113]. Moreover, morphological and functional recovery have been observed following the tubulization with a PCL conduit filled with MSC in a mouse median nerve [39].

#### **3.2.7.4 Biomolecular therapy**

Because nerve regeneration is modulated by many complex interactions between cells, ECM molecules and GFs, the local presence of neurotrophic factors at the nerve injury sites plays a vital and complex role in controlling the survival, proliferation, migration and differentiation of various cell types involved in nerve regeneration. After nerve injury the endogenous GFs secreted by neural cells in the distal nerve stump can support axon regeneration, but this supportive action may not be sustained indefinitely due to an obvious decline with time in cellular production of GFs [114]. Besides the neurotrophic actions that are indirectly provided by support cells within the neural scaffold, exogenous GFs may be ideally combined with a NGC. Nerve regeneration has been found to be enhanced by filling nerve guides with the neurotrophins, such as nerve growth factors (NGF) [75, 115-118], brain-derived neurotrophic factor (BDNF) [116, 119] and neurotrophin -3 (NT-3) [114, 116], the glial cell line-derived neurotrophic factor (GDNF) (a member of the glial cell line-derive neurotrophic factor family ligands)[117, 120], and cytokines as fibroblast growth factor-1 and -2 (FGF) [73]. Vascular endothelial growth factor (VEGF) has been fully investigated in terms of its promoting actions on peripheral nerve regeneration [121]. NGF and GDNF are two prominent used GFs. They differ in their spectrum of action when applied as a single factor. While NGF promotes primarily survival and axonal outgrowth of sensory neurons, both *in vitro* and *in vivo* [122], GDNF is a key factor for motor axonal regeneration [123]. Another striking difference between NGF and GDNF relates to their effects on axonal branching, as primarily induced by NGF, and axonal elongation, as mostly promoted by GDNF [124, 125]. However, the sustained delivery of either GDNF or NGF from synthetic NGC have been found to enhance nerve regeneration over long gaps *in vivo* [117]. In a recent work, Bloch et al. demonstrated the ability of ethylene-vinyl acetate based NGC to promote sensory nerve regeneration in the rat transected dorsal root by releasing bioactive NGF, BDNF, or NT-3. By comparing the effects of the three different types of neurotrophins, NGF was found to powerfully promote regeneration of both myelinated and unmyelinated axons after dorsal root axotomy, while NT-3 significantly increase regeneration of myelinated axons only; BDNF has no significant effect on either myelinated or unmyelinated axons [116].

GFs must be locally administered to ensure an adequate effect with little adverse reactions because the factors have several traits, including high biological activity, pleiotrophic effects (acting on various targets), short half-lives, slow tissue penetration, and potential toxicity at high systemic levels [126, 127]. Moreover, the inherent

instability of GFs is generally a very limiting factor so that denaturation and partial or complete loss of biological activity are frequently events observed in processing and formulating these compounds [128]. Therefore, GFs require mild processing conditions such as ambient or low temperatures, little exposure to organic solvents or chemical reagents, and presence of stabilizing additives. Moreover, to obtain sterile dosage forms or delivery systems for GFs, all processes have to be performed aseptically because terminal sterilization through  $\gamma$ -rays or heat would destroy the proteins.

For all these reasons, a variety of delivery systems (Fig. 3.6) with sustained neurotrophic factors release have been tested in peripheral nerve injury models. Direct delivery of GFs from the NGC has been implemented by either conjugating [129] or physically adsorbing [130] the proteins to the NGC wall. For example, PLA-based NGCs for delivery of FGF-2 fabricated with a relatively simple design consisting of an inner porous PLA layer loaded with FGF-2 and an outer densely structured PLA tube. The FGF-2 releasing NGCs promoted sciatic nerve regeneration in a 15 mm nerve gap in rats [131]. Prolonged delivery of GFs has been also achieved by embedding the drug substances into gel structures filled into the lumen of NGCs. Often used gel forming materials include alginate, Matrigel<sup>®</sup>, collagen, heparin, laminin, and fibronectin [132, 133]. Tonda Turo et al. developed an injectable hydrogel based on GL for delivery of VEGF-A165 into the NGC lumen [134]. *In vitro* results confirmed a sustained VEGF-A165 release in a bioactive form, inducing capillary-like tube formation and axonal outgrowth *ex vivo* [135]. To control GF release independently of NGC wall type and structure, the proteins can be microencapsulated into microspheres embedded in the NGC wall or into electrospun nanofibers. Kokai et al. developed double-walled PLGA microspheres for localized release of GDNF [136]. The microspheres were embedded into the wall of PCL based NGCs during fabrication. The NGCs with embedded microspheres sustained the GDNF release over the study period of 16 weeks and exhibited no initial burst release. The NGCs with improved release kinetics ameliorated also axonal regeneration and functional recovery. As regard the loading of nanofibres with proteins, the main advantage is based on the combination of localized release of growth promoting compounds and immediate axonal guidance. GFs can be added into the polymer solution prepared to produce nanofibres [137] or by co-axial spinning [138], which affords embedding of GFs in the core of the fibres.

Another approach for loading and releasing GFs in NGCs is by using the binding affinity of GFs to heparin or heparin sulfate and to ECM components like collagen or laminin. Recently, Sakiyama-Elbert et al. developed a drug delivery system consisted of heparin-binding peptides covalently immobilized within a fibrin matrix. NGF was bound by affinity to the immobilized heparin [139]. Collagen or laminin binding domain were bound to NGF or CNTF domains and used as a delivery strategy to support sciatic nerve regeneration in rat [140, 141]. The scaffolds provided slow release of the GFs at the site of nerve injury. All the studies demonstrated that prolonged release of GFs over several days or weeks can be achieved by NGC-integrated, polymer-based delivery systems.

**Table 3.2** GFs used in peripheral nerve regeneration are reported.

Growth factor	Major target	References
NGF	Sensory neurons, small axons	[75, 115-118]
NT-3	Sensory neurons, small-and medium size axons	[114, 116]
BDNF	Sensory neurons, large axons	[116, 119]
GDNF	Motor neurons	[117, 120, 136]
FGF-1 (acidic FGF)	Vascular endothelial cells	[142]
FGF-2 (basic FGF)	Vascular endothelial cells	[73, 131]
VEGF	Vascular endothelial cells	[121, 143]
IGF-1	Inflammatory cells (anti-inflammatory)	[144]

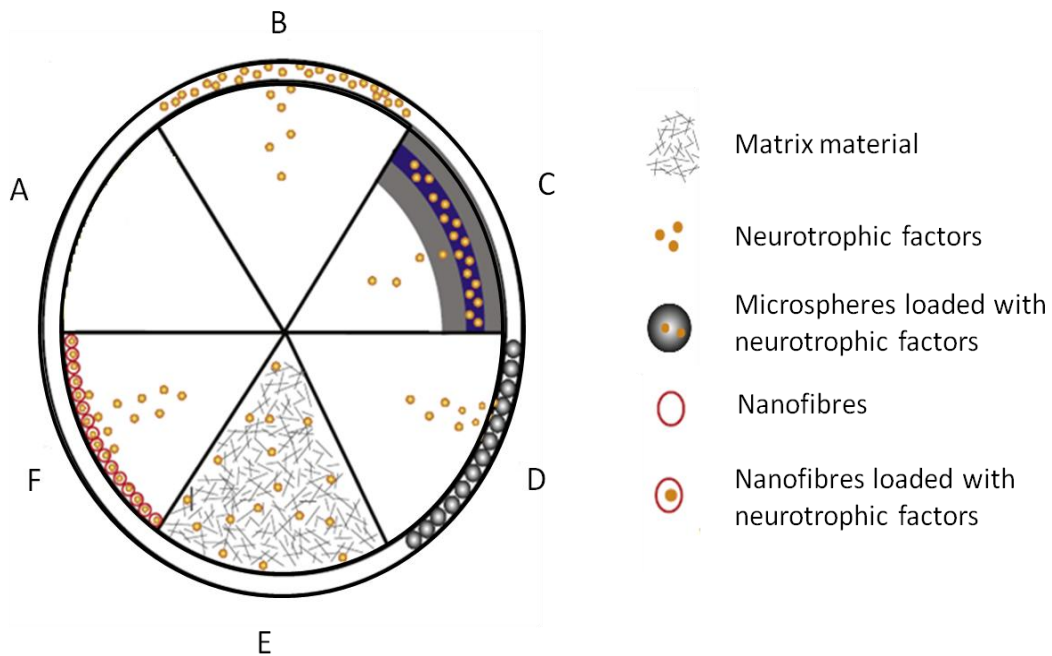


**Fig. 3.6** Design of delivery systems for neurotrophic factors inside NCs: A) NGC empty wall; B) neurotrophic factors embedded in NC wall; C) neurotrophic factors embedded in polymeric coatings of NGC wall; D) neurotrophic factors encapsulated in biodegradable microspheres embedded in NGC wall; E) neurotrophic factors embedded in ECM material in NGC lumen; F) neurotrophic factors entrapped in biodegradable nanofibres that are mounted on the NGC wall.

## References

1. Yiu, G. and Z. He, Glial inhibition of CNS axon regeneration. *Nat Rev Neurosci*, 2006. **7**(8): p. 617-27.
2. Seddon, H.J., P.B. Medawar, and H. Smith, Rate of regeneration of peripheral nerves in man. *J Physiol*, 1943. **102**(2): p. 191-215.
3. Sunderland, S., Rate of regeneration in human peripheral nerves; analysis of the interval between injury and onset of recovery. *Arch Neurol Psychiatry*, 1947. **58**(3): p. 251-95.
4. Deumens, R., et al., Repairing injured peripheral nerves: Bridging the gap. *Prog Neurobiol*, 2010. **92**(3): p. 245-76.
5. Funakoshi, H., et al., Differential expression of mRNAs for neurotrophins and their receptors after axotomy of the sciatic nerve. *J Cell Biol*, 1993. **123**(2): p. 455-65.
6. Taylor, R.S., Epidemiology of refractory neuropathic pain. *Pain Pract*, 2006. **6**(1): p. 22-6.
7. Lee, S.K. and S.W. Wolfe, Peripheral nerve injury and repair. *J Am Acad Orthop Surg*, 2000. **8**(4): p. 243-52.
8. Nan, J.N., et al., Use of nerve conduits for peripheral nerve injury repair A Web of Science-based literature analysis. *Neural Regeneration Research*, 2012. **7**(35): p. 2826-2833.
9. Mackinnon, S.E. and A.R. Hudson, Clinical application of peripheral nerve transplantation. *Plastic and Reconstructive Surgery*, 1992. **90**(4): p. 695-9.
10. Evans, G.R., Challenges to nerve regeneration. *Semin Surg Oncol*, 2000. **19**(3): p. 312-8.
11. Stahl, S. and N. Rosenberg, Digital nerve repair by autogenous vein graft in high-velocity gunshot wounds. *Mil Med*, 1999. **164**(8): p. 603-4.
12. Marcoccio, I. and A. Vigasio, Muscle-in-vein nerve guide for secondary reconstruction in digital nerve lesions. *J Hand Surg Am*, 2010. **35**(9): p. 1418-26.
13. Johnson, E.O. and P.N. Soucacos, Nerve repair: experimental and clinical evaluation of biodegradable artificial nerve guides. *Injury*, 2008. **39** Suppl 3: p. S30-6.
14. Miller, C., S. Jeftinija, and S. Mallapragada, Synergistic effects of physical and chemical guidance cues on neurite alignment and outgrowth on biodegradable polymer substrates. *Tissue Eng*, 2002. **8**(3): p. 367-78.
15. Wang-Bennett, L.T. and N.J. Coker, Analysis of axonal regeneration through the silicone regeneration chamber: a retrograde tracing study in the rabbit facial nerve. *Exp Neurol*, 1990. **107**(3): p. 222-9.
16. Katti, D.S., et al., Toxicity, biodegradation and elimination of polyanhydrides. *Adv Drug Deliv Rev*, 2002. **54**(7): p. 933-61.
17. Yuan, Y., et al., The interaction of Schwann cells with chitosan membranes and fibers in vitro. *Biomaterials*, 2004. **25**(18): p. 4273-4278.
18. Li, G.C., et al., Effect of silanization on chitosan porous scaffolds for peripheral nerve regeneration. *Carbohydrate Polymers*, 2014. **101**: p. 718-726.
19. Taras, J.S., V. Nanavati, and P. Steelman, Nerve conduits. *J Hand Ther*, 2005. **18**(2): p. 191-7.
20. Kehoe, S., X.F. Zhang, and D. Boyd, FDA approved guidance conduits and wraps for peripheral nerve injury: A review of materials and efficacy. *Injury-International Journal of the Care of the Injured*, 2012. **43**(5): p. 553-572.
21. Lundborg, G., et al., Nerve regeneration in silicone chambers: influence of gap length and of distal stump components. *Exp Neurol*, 1982. **76**(2): p. 361-75.
22. Williams, L.R., et al., Spatial-temporal progress of peripheral nerve regeneration within a silicone chamber: parameters for a bioassay. *J Comp Neurol*, 1983. **218**(4): p. 460-70.
23. Chen, Y.S., et al., Peripheral nerve regeneration using silicone rubber chambers filled with collagen, laminin and fibronectin. *Biomaterials*, 2000. **21**(15): p. 1541-7.
24. Gulati, D., A. Aggarwal, and A.P. Singh, Complications of titanium and stainless steel elastic nail fixation of pediatric femoral fractures. *J Bone Joint Surg Am*, 2009. **91**(8): p. 2040-1; author reply 2041.

25. Mink, J.R., The stainless steel crown revisited. *Alpha Omegan*, 2005. **98**(4): p. 38-42.
26. Braga-Silva, J., The use of silicone tubing in the late repair of the median and ulnar nerves in the forearm. *J Hand Surg Br*, 1999. **24**(6): p. 703-6.
27. Wang, H.B., et al., Creation of highly aligned electrospun poly-L-lactic acid fibers for nerve regeneration applications. *J Neural Eng*, 2009. **6**(1): p. 016001.
28. Waitayawinyu, T., et al., A comparison of polyglycolic acid versus type 1 collagen bioabsorbable nerve conduits in a rat model: an alternative to autografting. *J Hand Surg Am*, 2007. **32**(10): p. 1521-9.
29. Mligiliche, N.L., et al., Poly lactic acid--caprolactone copolymer tube with a denatured skeletal muscle segment inside as a guide for peripheral nerve regeneration: a morphological and electrophysiological evaluation of the regenerated nerves. *Anat Sci Int*, 2003. **78**(3): p. 156-61.
30. Chiono, V., et al., Melt-extruded guides for peripheral nerve regeneration. Part I: Poly(epsilon-caprolactone). *Biomed Microdevices*, 2009.
31. Den Dunnen, W.F., et al., Peripheral nerve regeneration through P(DLLA-epsilon-CL) nerve guides. *J Mater Sci Mater Med*, 1998. **9**(12): p. 811-4.
32. Bini, T.B., et al., Peripheral nerve regeneration by microbraided poly(L-lactide-co-glycolide) biodegradable polymer fibers. *J Biomed Mater Res A*, 2004. **68**(2): p. 286-95.
33. Pego, A.P., et al., Copolymers of trimethylene carbonate and epsilon-caprolactone for porous nerve guides: synthesis and properties. *J Biomater Sci Polym Ed*, 2001. **12**(1): p. 35-53.
34. Pierucci, A., E.A. Duek, and A.L. de Oliveira, Expression of basal lamina components by Schwann cells cultured on poly(lactic acid) (PLLA) and poly(caprolactone) (PCL) membranes. *J Mater Sci Mater Med*, 2009. **20**(2): p. 489-95.
35. Evans, G.R., et al., In vivo evaluation of poly(L-lactic acid) porous conduits for peripheral nerve regeneration. *Biomaterials*, 1999. **20**(12): p. 1109-15.
36. Koh, H.S., et al., Enhancement of neurite outgrowth using nano-structured scaffolds coupled with laminin. *Biomaterials*, 2008. **29**(26): p. 3574-82.
37. Waddell, R.L., et al., Using PC12 cells to evaluate poly(caprolactone) and collagenous microcarriers for applications in nerve guide fabrication. *Biotechnol Prog*, 2003. **19**(6): p. 1767-74.
38. Bender, M.D., et al., Multi-channeled biodegradable polymer/CultiSpher composite nerve guides. *Biomaterials*, 2004. **25**(7-8): p. 1269-78.
39. Oliveira, J.T., et al., Mesenchymal stem cells in a polycaprolactone conduit enhance median-nerve regeneration, prevent decrease of creatine phosphokinase levels in muscle, and improve functional recovery in mice. *Neuroscience*, 2010. **170**(4): p. 1295-303.
40. Toba, T., et al., Evaluation of peripheral nerve regeneration across an 80-mm gap using a polyglycolic acid (PGA)--collagen nerve conduit filled with laminin-soaked collagen sponge in dogs. *Int J Artif Organs*, 2002. **25**(3): p. 230-7.
41. Toba, T., et al., Regeneration of canine peroneal nerve with the use of a polyglycolic acid-collagen tube filled with laminin-soaked collagen sponge: a comparative study of collagen sponge and collagen fibers as filling materials for nerve conduits. *J Biomed Mater Res*, 2001. **58**(6): p. 622-30.
42. Jenny, L., "Tissue-engineered Peripheral Nerve", in *Wiley Encyclopedia of Biomedical Engineering* 2006.
43. Vitale-Brovarone, C., et al., Novel phosphate glasses with different amounts of TiO<sub>2</sub> for biomedical applications: Dissolution tests and proof of concept of fibre drawing. *J Mater Sci Eng*, 2011. **31**(2), 434-442.
44. Rechichi, A., et al., Degradable block polyurethanes from nontoxic building blocks as scaffold materials to support cell growth and proliferation. *J Biomed Mater Res A*, 2008. **84**(4): p. 847-55.

45. Gizdavic-Nikolaidis, M., et al., The antioxidant activity of conducting polymers in biomedical applications. *Current Applied Physics*, 2004. **4**(2-4): p. 347-350.
46. Kotwal, A. and C.E. Schmidt, Electrical stimulation alters protein adsorption and nerve cell interactions with electrically conducting biomaterials. *Biomaterials*, 2001. **22**(10): p. 1055-1064.
47. Wang, X.D., et al., Evaluation of biocompatibility of polypyrrole in vitro and in vivo. *Journal of Biomedical Materials Research Part A*, 2004. **68A**(3): p. 411-422.
48. Moroder, P., et al., Material properties and electrical stimulation regimens of polycaprolactone fumarate-polypyrrole scaffolds as potential conductive nerve conduits. *Acta Biomaterialia*, 2011. **7**(3): p. 944-953.
49. Grimpe, B. and J. Silver, The extracellular matrix in axon regeneration. *Prog Brain Res*, 2002. **137**: p. 333-49.
50. Rutishauser, U., Adhesion molecules of the nervous system. *Curr Opin Neurobiol*, 1993. **3**(5): p. 709-15.
51. Asher, R.A., et al., Chondroitin sulphate proteoglycans: inhibitory components of the glial scar. *Prog Brain Res*, 2001. **132**: p. 611-9.
52. Bovolenta, P. and I. Feraud-Espinosa, Nervous system proteoglycans as modulators of neurite outgrowth. *Progress in Neurobiology*, 2000. **61**(2): p. 113-132.
53. Yang, C., et al., The application of recombinant human collagen in tissue engineering. *BioDrugs*, 2004. **18**(2): p. 103-19.
54. Archibald, S.J., et al., A collagen-based nerve guide conduit for peripheral nerve repair: an electrophysiological study of nerve regeneration in rodents and nonhuman primates. *J Comp Neurol*, 1991. **306**(4): p. 685-96.
55. Stang, F., et al., Collagen nerve conduits--assessment of biocompatibility and axonal regeneration. *Biomed Mater Eng*, 2005. **15**(1-2): p. 3-12.
56. Labrador, R.O., M. Buti, and X. Navarro, Influence of collagen and laminin gels concentration on nerve regeneration after resection and tube repair. *Exp Neurol*, 1998. **149**(1): p. 243-52.
57. Yoshii, S., et al., 30 mm regeneration of rat sciatic nerve along collagen filaments. *Brain Res*, 2002. **949**(1-2): p. 202-8.
58. Bozkurt, A., et al., In vitro cell alignment obtained with a Schwann cell enriched microstructured nerve guide with longitudinal guidance channels. *Biomaterials*, 2009. **30**(2): p. 169-79.
59. Gamez, E., et al., Photofabricated gelatin-based nerve conduits: nerve tissue regeneration potentials. *Cell Transplant*, 2004. **13**(5): p. 549-64.
60. Bigi, A., et al., Stabilization of gelatin films by crosslinking with genipin. *Biomaterials*, 2002. **23**(24): p. 4827-32.
61. Chen, Y.S., et al., An in vivo evaluation of a biodegradable genipin-cross-linked gelatin peripheral nerve guide conduit material. *Biomaterials*, 2005. **26**(18): p. 3911-8.
62. Chen, P.R., et al., Biocompatibility of NGF-grafted GTG membranes for peripheral nerve repair using cultured Schwann cells. *Biomaterials*, 2004. **25**(25): p. 5667-73.
63. Martin, G.R., R. Timpl, and K. Kuhn, Basement membrane proteins: molecular structure and function. *Adv Protein Chem*, 1988. **39**: p. 1-50.
64. Tong, X.J., et al., Sciatic nerve regeneration navigated by laminin-fibronectin double coated biodegradable collagen grafts in rats. *Brain Res*, 1994. **663**(1): p. 155-62.
65. Rinaudo, M., Chitin and chitosan: Properties and applications. *Progress in Polymer Science*, 2006. **31**(7): p. 603-632.
66. He, Q.R., et al., In vitro biocompatibility of chitosan-based materials to primary culture of hippocampal neurons. *Journal of Materials Science-Materials in Medicine*, 2009. **20**(7): p. 1457-1466.
67. Yuan, Y., et al., The interaction of Schwann cells with chitosan membranes and fibers in vitro. *Biomaterials*, 2004. **25**(18): p. 4273-8.

68. Ciardelli, G. and V. Chiono, Materials for peripheral nerve regeneration. *Macromol Biosci*, 2006. **6**(1): p. 13-26.
69. Guo, B.F. and M.M. Dong, Application of neural stem cells in tissue-engineered artificial nerve. *Otolaryngol Head Neck Surg*, 2009. **140**(2): p. 159-64.
70. Remminghorst, U. and B.H. Rehm, Bacterial alginates: from biosynthesis to applications. *Biotechnol Lett*, 2006. **28**(21): p. 1701-12.
71. Matsuura, S., et al., Cavernous nerve regeneration by biodegradable alginate gel sponge sheet placement without sutures. *Urology*, 2006. **68**(6): p. 1366-71.
72. Sufan, W., et al., Sciatic nerve regeneration through alginate with tubulation or nontubulation repair in cat. *J Neurotrauma*, 2001. **18**(3): p. 329-38.
73. Ohta, M., et al., Novel heparin/alginate gel combined with basic fibroblast growth factor promotes nerve regeneration in rat sciatic nerve. *J Biomed Mater Res A*, 2004. **71**(4): p. 661-8.
74. Labrador, R.O., M. Buti, and X. Navarro, Peripheral nerve repair: role of agarose matrix density on functional recovery. *Neuroreport*, 1995. **6**(15): p. 2022-6.
75. Dodla, M.C. and R.V. Bellamkonda, Differences between the effect of anisotropic and isotropic laminin and nerve growth factor presenting scaffolds on nerve regeneration across long peripheral nerve gaps. *Biomaterials*, 2008. **29**(1): p. 33-46.
76. Yang, Y., et al., Development and evaluation of silk fibroin-based nerve grafts used for peripheral nerve regeneration. *Biomaterials*, 2007. **28**(36): p. 5526-35.
77. Yang, Y., et al., Biocompatibility evaluation of silk fibroin with peripheral nerve tissues and cells in vitro. *Biomaterials*, 2007. **28**(9): p. 1643-52.
78. Apel, P.J., et al., Peripheral nerve regeneration using a keratin-based scaffold: long-term functional and histological outcomes in a mouse model. *J Hand Surg Am*, 2008. **33**(9): p. 1541-7.
79. Guo, L., Z.X. Quan, and Y.L. Tang, [Biomechanical evaluation of three-dimensional stability of anterior approach screw fixation through C2 vertebral body to C1 lateral mass]. *Zhongguo Gu Shang*, 2008. **21**(5): p. 353-5.
80. Chen, G.Q. and Q. Wu, The application of polyhydroxyalkanoates as tissue engineering materials. *Biomaterials*, 2005. **26**(33): p. 6565-78.
81. Li, J. and R. Shi, Fabrication of patterned multi-walled poly-L-lactic acid conduits for nerve regeneration. *J Neurosci Methods*, 2007. **165**(2): p. 257-64.
82. Zhu, Y., et al., Engineering bi-layer nanofibrous conduits for peripheral nerve regeneration. *Tissue Eng Part C Methods*, 2011. **17**(7): p. 705-15.
83. Brushart, T.M., et al., Joseph H. Boyes Award. Dispersion of regenerating axons across enclosed neural gaps. *J Hand Surg Am*, 1995. **20**(4): p. 557-64.
84. Weber, R.A., et al., A randomized prospective study of polyglycolic acid conduits for digital nerve reconstruction in humans. *Plast Reconstr Surg*, 2000. **106**(5): p. 1036-45; discussion 1046-8.
85. de Ruitter, G.C., et al., Accuracy of motor axon regeneration across autograft, single-lumen, and multichannel poly(lactic-co-glycolic acid) nerve tubes. *Neurosurgery*, 2008. **63**(1): p. 144-53; discussion 153-5.
86. Hadlock, T., et al., A polymer foam conduit seeded with Schwann cells promotes guided peripheral nerve regeneration. *Tissue Eng*, 2000. **6**(2): p. 119-27.
87. Liao, C.Y., et al., Multi-channel chitosan-polycaprolactone conduits embedded with microspheres for controlled release of nerve growth factor. *Reactive & Functional Polymers*, 2013. **73**(1): p. 149-159.
88. de Ruitter, G.C., et al., Methods for in vitro characterization of multichannel nerve tubes. *J Biomed Mater Res A*, 2008. **84**(3): p. 643-51.
89. Yao, L., et al., Controlling dispersion of axonal regeneration using a multichannel collagen nerve conduit. *Biomaterials*, 2010. **31**(22): p. 5789-97.

90. Ribeiro-Resende, V.T., et al., Strategies for inducing the formation of bands of Bungner in peripheral nerve regeneration. *Biomaterials*, 2009. **30**(29): p. 5251-9.
91. Lee, D.Y., et al., Nerve regeneration with the use of a poly(l-lactide-co-glycolic acid)-coated collagen tube filled with collagen gel. *J Craniomaxillofac Surg*, 2006. **34**(1): p. 50-6.
92. Dubey, N., P.C. Letourneau, and R.T. Tranquillo, Guided neurite elongation and schwann cell invasion into magnetically aligned collagen in simulated peripheral nerve regeneration. *Exp Neurol*, 1999. **158**(2): p. 338-50.
93. Ceballos, D., et al., Magnetically aligned collagen gel filling a collagen nerve guide improves peripheral nerve regeneration. *Exp Neurol*, 1999. **158**(2): p. 290-300.
94. Wang, W., et al., Effects of Schwann cell alignment along the oriented electrospun chitosan nanofibers on nerve regeneration. *J Biomed Mater Res A*, 2009. **91**(4): p. 994-1005.
95. Hu, W., et al., Polyglycolic acid filaments guide Schwann cell migration in vitro and in vivo. *Biotechnol Lett*, 2008. **30**(11): p. 1937-42.
96. Wang, X.D., et al., Dog sciatic nerve regeneration across a 30-mm defect bridged by a chitosan/PGA artificial nerve graft. *Brain*, 2005. **128**: p. 1897-1910.
97. Smeal, R.M. and P.A. Tresco, The influence of substrate curvature on neurite outgrowth is cell type dependent. *Exp Neurol*, 2008. **213**(2): p. 281-92.
98. Tonda-Turo, C., et al., Comparative analysis of gelatin scaffolds crosslinked by genipin and silane coupling agent. *Int J Biol Macromol*, 2011. **49**(4): p. 700-6.
99. Pawar, K., et al., Increasing capillary diameter and the incorporation of gelatin enhance axon outgrowth in alginate-based anisotropic hydrogels. *Acta Biomater*, 2011. **7**(7): p. 2826-34.
100. Hood, B., H.B. Levene, and A.D. Levi, Transplantation of autologous Schwann cells for the repair of segmental peripheral nerve defects. *Neurosurg Focus*, 2009. **26**(2): p. E4.
101. Brandt, J., et al., Acutely-dissociated Schwann cells used in tendon autografts for bridging nerve defects in rats: a new principle for tissue engineering in nerve reconstruction. *Scand J Plast Reconstr Surg Hand Surg*, 2005. **39**(6): p. 321-5.
102. Webber, C.A., et al., Schwann cells direct peripheral nerve regeneration through the Netrin-1 receptors, DCC and Unc5H2. *Glia*, 2011. **59**(10): p. 1503-17.
103. Hammarberg, H., et al., Expression of insulin-like growth factors and corresponding binding proteins (IGFBP 1-6) in rat spinal cord and peripheral nerve after axonal injuries. *J Comp Neurol*, 1998. **400**(1): p. 57-72.
104. Li, X., S.L. Gonias, and W.M. Campana, Schwann cells express erythropoietin receptor and represent a major target for Epo in peripheral nerve injury. *Glia*, 2005. **51**(4): p. 254-65.
105. Chiu, D.T.W., Autogenous venous nerve conduits - A review. *Hand Clinics*, 1999. **15**(4): p. 667-+.
106. Shen, Z.L., et al., Establishment of Schwann cell culture from newborn and adult rats - First step towards the "living bioartificial nerve graft". *Langenbecks Archives of Surgery*, 1999: p. 145-152.
107. Arino, H., J. Brandt, and L.B. Dahlin, Implantation of Schwann cells in rat tendon autografts as a model for peripheral nerve repair: long term effects on functional recovery. *Scand J Plast Reconstr Surg Hand Surg*, 2008. **42**(6): p. 281-5.
108. Alessandri, G., C. Emanuelli, and P. Madeddu, Genetically engineered stem cell therapy for tissue regeneration. *Ann N Y Acad Sci*, 2004. **1015**: p. 271-84.
109. Ringden, O., et al., Mesenchymal stem cells for treatment of therapy-resistant graft-versus-host disease. *Transplantation*, 2006. **81**(10): p. 1390-7.
110. Lu, L., et al., Morphological and functional characterization of predifferentiation of myelinating glia-like cells from human bone marrow stromal cells through activation of F3/Notch signaling in mouse retina. *Stem Cells*, 2008. **26**(2): p. 580-90.
111. Munoz-Elias, G., D. Woodbury, and I.B. Black, Marrow stromal cells, mitosis, and neuronal differentiation: stem cell and precursor functions. *Stem Cells*, 2003. **21**(4): p. 437-48.

112. Suzuki, H., et al., Neurospheres induced from bone marrow stromal cells are multipotent for differentiation into neuron, astrocyte, and oligodendrocyte phenotypes. *Biochem Biophys Res Commun*, 2004. **322**(3): p. 918-22.
113. Wislet-Gendebien, S., et al., Plasticity of cultured mesenchymal stem cells: switch from nestin-positive to excitable neuron-like phenotype. *Stem Cells*, 2005. **23**(3): p. 392-402.
114. Gordon, T., The role of neurotrophic factors in nerve regeneration. *Neurosurg Focus*, 2009. **26**(2): p. E3.
115. Rich, K.M., et al., Nerve growth factor enhances regeneration through silicone chambers. *Exp Neurol*, 1989. **105**(2): p. 162-70.
116. Bloch, J., et al., Nerve growth factor- and neurotrophin-3-releasing guidance channels promote regeneration of the transected rat dorsal root. *Experimental Neurology*, 2001. **172**(2): p. 425-432.
117. Fine, E.G., et al., GDNF and NGF released by synthetic guidance channels support sciatic nerve regeneration across a long gap. *European Journal of Neuroscience*, 2002. **15**(4): p. 589-601.
118. Pfister, L.A., et al., Controlled nerve growth factor release from multi-ply alginate/chitosan-based nerve conduits. *European Journal of Pharmaceutics and Biopharmaceutics*, 2008. **69**(2): p. 563-572.
119. Terris, D.J., et al., Brain-derived neurotrophic factor-enriched collagen tubule as a substitute for autologous nerve grafts. *Arch Otolaryngol Head Neck Surg*, 2001. **127**(3): p. 294-8.
120. Barras, F.M., et al., Glial cell line-derived neurotrophic factor released by synthetic guidance channels promotes facial nerve regeneration in the rat. *J Neurosci Res*, 2002. **70**(6): p. 746-55.
121. Hobson, M.I., Increased vascularisation enhances axonal regeneration within an acellular nerve conduit. *Ann R Coll Surg Engl*, 2002. **84**(1): p. 47-53.
122. Rich, K.M., et al., Nerve Growth-Factor Protects Adult Sensory Neurons from Cell-Death and Atrophy Caused by Nerve Injury. *Journal of Neurocytology*, 1987. **16**(2): p. 261-268.
123. Henderson, C.E., et al., Gdnf - a Potent Survival Factor for Motoneurons Present in Peripheral-Nerve and Muscle. *Science*, 1994. **266**(5187): p. 1062-1064.
124. Zahedi, K., et al., The role of spermidine/spermine N1-acetyltransferase in endotoxin-induced acute kidney injury. *Am J Physiol Cell Physiol*, 2010. **299**(1): p. C164-74.
125. Madduri, S., M. Papaloizos, and B. Gander, Synergistic effect of GDNF and NGF on axonal branching and elongation in vitro. *Neuroscience Research*, 2009. **65**(1): p. 88-97.
126. Pfister, L.A., et al., Nerve conduits and growth factor delivery in peripheral nerve repair. *J Peripher Nerv Syst*, 2007. **12**(2): p. 65-82.
127. Tayalia, P. and D.J. Mooney, Controlled growth factor delivery for tissue engineering. *Adv Mater*, 2009. **21**(32-33): p. 3269-85.
128. Nguyen, C.B., et al., Stability and interactions of recombinant human nerve growth factor in different biological matrices: In vitro and in vivo studies. *Drug Metabolism and Disposition*, 2000. **28**(5): p. 590-597.
129. Ho, P.R., et al., Repair with collagen tubules linked with brain-derived neurotrophic factor and ciliary neurotrophic factor in a rat sciatic nerve injury model. *Archives of Otolaryngology-Head & Neck Surgery*, 1998. **124**(7): p. 761-766.
130. Aebischer, P., A.N. Salessiotis, and S.R. Winn, Basic Fibroblast Growth-Factor Released from Synthetic Guidance Channels Facilitates Peripheral-Nerve Regeneration across Long Nerve Gaps. *Journal of Neuroscience Research*, 1989. **23**(3): p. 282-289.
131. Wang, S.G., et al., Acceleration effect of basic fibroblast growth factor on the regeneration of peripheral nerve through a 15-mm gap. *Journal of Biomedical Materials Research Part A*, 2003. **66A**(3): p. 522-531.
132. Malone, E., et al., Surveillance study of a number of synthetic and natural growth promoters in bovine muscle samples using liquid chromatography-tandem mass

- spectrometry. *Food Addit Contam Part A Chem Anal Control Expo Risk Assess*, 2011. **28**(5): p. 597-607.
133. Hawkes, K., et al., A reappraisal of grandmothering and natural selection. *Proc Biol Sci*, 2011. **278**(1714): p. 1936-8; discussion 1939-41.
  134. Tonda-Turo, C., et al., Development and characterization of novel agar and gelatin injectable hydrogel as filler for peripheral nerve guidance channels. *J Tissue Eng Regen Med*, 2014.
  135. Kennedy, R., W. Arthur, and B.F. Keegan, Long-term trends in benthic habitat quality as determined by Multivariate AMBI and Infaunal Quality Index in relation to natural variability: a case study in Kinsale Harbour, south coast of Ireland. *Mar Pollut Bull*, 2011. **62**(7): p. 1427-36.
  136. Zahedi, K., et al., Polyamine catabolism is enhanced after traumatic brain injury. *J Neurotrauma*, 2010. **27**(3): p. 515-25.
  137. Xia, J.J., et al., A new method to orient 3-dimensional computed tomography models to the natural head position: a clinical feasibility study. *J Oral Maxillofac Surg*, 2011. **69**(3): p. 584-91.
  138. Logeart-Avramoglou, D. and J. Jozefonvicz, Carboxymethyl benzylamide sulfonate dextrans (CMDDBS), a family of biospecific polymers endowed with numerous biological properties: a review. *Journal of Biomedical Materials Research*, 1999. **48**(4): p. 578-90.
  139. Sakiyama-Elbert, S.E. and J.A. Hubbell, Controlled release of nerve growth factor from a heparin-containing fibrin-based cell ingrowth matrix. *Journal of Controlled Release*, 2000. **69**(1): p. 149-158.
  140. Hodgins, D., et al., Biocompatible materials developments for new medical implants. *Med Device Technol*, 2007. **18**(6): p. 30, 32-5.
  141. Cao, J.I., et al., The use of laminin modified linear ordered collagen scaffolds loaded with laminin-binding ciliary neurotrophic factor for sciatic nerve regeneration in rats. *Biomaterials*, 2011. **32**(16): p. 3939-3948.
  142. Cordeiro, P.G., et al., Acidic fibroblast growth factor enhances peripheral nerve regeneration in vivo. *Plast Reconstr Surg*, 1989. **83**(6): p. 1013-9; discussion 1020-1.
  143. Sondell, M., G. Lundborg, and M. Kanje, Vascular endothelial growth factor stimulates Schwann cell invasion and neovascularization of acellular nerve grafts. *Brain Res*, 1999. **846**(2): p. 219-28.
  144. Fansa, H., et al., Influence of insulin-like growth factor-I (IGF-I) on nerve autografts and tissue-engineered nerve grafts. *Muscle Nerve*, 2002. **26**(1): p. 87-93.

# Chapter 4

## Chitosan crosslinked flat membranes as scaffolds for peripheral nerve regeneration

### Abstract

Chitosan (CS) has been widely used in a variety of biomedical applications including peripheral nerve repair because of its excellent biocompatibility, biodegradability, readily availability and antibacterial activity. In this study, CS flat membranes, crosslinked with dibasic sodium phosphate (DSP) alone (CS/DSP) or in association with the  $\gamma$ -glycidoxypropyltrimethoxysilane (CS/GPTMS\_DSP) were fabricated with a solvent casting technique. The constituent ratio of crosslinking agents and CS was previously selected to obtain a composite material having both proper mechanical properties and good biocompatibility. Furthermore, the diffusion of nutrients through the CS/DSP and CS/GPTMS\_DSP flat films were tested.

*In vitro* cytotoxicity tests showed that CS membranes were not cytotoxic. CS/GPTMS\_DSP provided a favorable environment for nerve RT4-D6P2T adhesion, proliferation, and function. Moreover, developed CS based membranes showed to direct cell attachment resulting in characteristic cell morphology typical of SCs and to support the neurite outgrowth of dorsal root ganglia (DRG) cultured on this biomaterial. Finally, *in vivo* tests were carried out on both the two types of nerve scaffolds made by CS/DSP and CS/GPTMS\_DSP flat membranes due to their easily manipulation and suturability.

During *in vivo* tests CS/GPTMS\_DSP tubes were detached from the distal suturing site and functional recovery did not occurred. On the other hand, crushed nerve encircled with CS/DSP membranes, allowed nerve fiber regeneration and functional recovery, obtaining results comparable to median nerve repaired with reversed autologous graft, used as control.

## 4.1 Introduction

Peripheral nerve injuries (PNI) are a serious health problem. Generally, an end-to-end anastomosis method can be used to bridge the PNI with small gaps, however, it is still difficult to completely cure the long nerve gaps [1]. Autologous nerve grafts is the “gold standard” technique in bridging peripheral nerve defects [2]. However there are unavoidable drawbacks associated to it such as the limited availability and donor-site morbidity. In recent years, a variety of biomaterials for better recovery of nerve functions have been developed as previously described in chapter 3. CS, as a natural polysaccharide, has attracted more and more attention due to its good biocompatibility, biodegradability, non-toxicity, readily availability and unique physicochemical properties [3-5].

Recent *in vitro* studies revealed the suitability of CS membranes as substrate for survival and oriented SC growth [6] as well as survival and differentiation of neuronal cells [7, 8]. CS NGCs alone or in combination with other biomaterials have been found to efficiently bridge peripheral nerve defects [9]. For example, CS/gelatin nerve grafts have been developed for delivering SCs and NGF to explore the feasibility of improving sciatic nerve regeneration, the results showed that the nerve conduction velocity, average regenerated myelin area, and myelinated axon count were all promoted [10, 11]. In addition, the differentiation of induced pluripotent stem cells into neuron-like cells was found to be accelerated by the chitin–CS–gelatin scaffolds [12]. However, pure CS is brittle and degrades rapidly [13, 14]: improved technologies and different crosslinking methods have been developed to overcome the poor mechanical strength of CS nerve guide channel under physiological conditions, which is one of the main factors limiting the use of such for neural clinical applications until now [11]. In the first section of this thesis (Chapter 2), CS flat membranes, crosslinked with DSP and GPTMS\_DSP were prepared and characterized to have suitable properties for peripheral nerve TE.

In this work, DSP and GPTMS\_DSP crosslinked CS flat membranes were prepared by solvent casting technique and biologically characterized by *in vitro* and preliminary *in vivo* tests. Permeability to nutrients was evaluated using FITC-dextran as a model of nutrients having a Stokes radius of 14 Å that is superior to glucose Stokes radius (3.8 Å) [15] and NaCl Stokes radius (1.4 Å) [16]. Culture studies of RT4-D6P2T cells were also performed on these degradable CS based flat membranes to ensure their potential applicability as nerve repair conduits.

In addition to the fine-tuned manufacturing of the CS samples and their evaluation with regard to biocompatibility, CS flat membranes were used to bridge a 10 mm defect in rat sciatic nerves: *in vivo* studies were performed by analyzing the outcome of peripheral nerve repair at 12 weeks post-implantation through a combination of electrophysiological assessment, immunohistochemical and histological investigations.

## **4.2 Experimental**

### **4.2.1 Materials**

CS (medium molecular weight, 75%-85% deacetylation degree), GPTMS and DSP were supplied from Sigma Aldrich. All solvents used were of analytical grade and used without further purification. RT4-D6P2T schwannoma cell line was purchased from American Type Culture Collection (ATCC- catalog number CRL-2768) and cultured following manufacturer's instruction.

### **4.2.2 Methods**

CS was dissolved in acetic acid solution 0.5M at room temperature by continuous stirring to obtain a 2.5 % (w/v) solution. The crosslinked membranes were prepared according to the following procedures as previously described in chapter 2. Briefly:

- I. DSP-crosslinked samples (CS/DSP) were obtained by adding DSP 1M (one drop per second) to the CS solution with a concentration of 7.5 % v/v with respect to the natural polymer solution volume. The mixed solution was kept under stirring at room temperature for about 10 minutes.
- II. GPTMS\_DSP crosslinked samples (CS/GPTMS\_DSP) were obtained adding GPTMS (50% w/w) to the CS solution. The resulting CS/GPTMS solution was kept under stirring for 1 hour, followed by the dropwise addition (one drop per second) of DSP 1M (concentration 7.5 % v/v) and maintained under moderate stirring for 10 minutes.

Then, 10 ml of each solution (CS/DSP and CS/GPTMS\_DSP) was poured into 6 cm Petri dishes and air-dried for 48 h to obtain flat membranes. All crosslinked dried samples were dipped into demineralised water for 10 minutes and then the water pH values were measured to evaluate the presence of acidic residues.

### **4.2.3 Sample characterization**

#### **4.2.3.1 Evaluation of CS based membranes permeability**

Permeability of CS flat membranes for FITC-labelled dextrans (Sigma Aldrich) of 4400 Da (FD-4) was determined in the following way. First, CS/DSP and CS/GPTMS\_DSP membranes were rolled and glued to obtain a tube having a 3 mm diameter and a 1.5 cm length, then one end of the tube was closed with cyanoacrylate glue. A 10% w/v solution of FD-4 in phosphate buffer saline (PBS) was prepared, and 180  $\mu$ l of FD-4 solution were inserted into the lumen, then the second opening was closed with a cyanoacrylate glue. The tube was then placed in 3 ml of PBS at pH 7.4, and FITC-dextran concentration in the incubation medium was measured through UV spectroscopy (CARY 500 SCAN UV-VIS-NIR Spectrophotometer) after 1, 3, 6, 24, 48 and 96 hours. The FD-4 release concentration in the external PBS solution was reported as a percentage respect

to the initial concentration (10% w/v) in the tube (Fig. 4.1). Five measures for samples were used and the data were reported as mean value and standard deviation. The concentration of FD-4 was calculated from the absorption values using the calibration curves that was prepared starting from FD-4 solution of known concentrations.

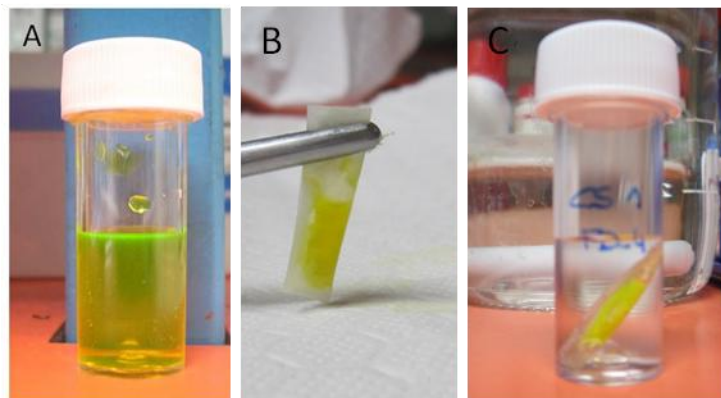


**Fig. 4.1.** Sample preparation for permeability test: A) solution of FD-4 in PBS was prepared, B) CS/DSP and CS/GPTMS\_DSP films were rolled and glued to obtained a tube and one end of the tube was closed with cyanoacrylate glue; FD-4 solution was inserted into the lumen, then the second opening was closed with a cyanoacrylate glue; C) the tubes was placed in PBS.

#### **4.2.3.2 *In vitro* cell tests on CS based samples**

*In vitro* cell tests were performed using RT4-D6P2T, a schwannoma cell line derived from N-ethyl-N-nitrosourea (ENU) induced rat peripheral neurotumor RT4 [17]. Cytotoxicity test was carried out on both CS/DSP and CS/GPTMS\_DSP while, RT4-D6P2T adhesion, proliferation and function were evaluated on CS/GPTMS\_DSP due to the higher mechanical stability of the biomaterial under physiological condition and because they were considered as “the worst case” (biomaterials employed for CS/GPTMS\_DSP fabrication were the same of CS/DSP supplemented with GPTMS). Neurite outgrowth of dorsal root ganglia (DRG) cultured on CS/GPTMS\_DSP was examined.

##### **4.2.3.2.1 Cytotoxicity study on CS/GPTMS\_DSP and CS/DSP**

The effect of the CS based material extracts was studied on RT4-D6P2T. CS/DSP and CS/GPTMS\_DSP samples were first sterilized with a 20 minutes exposure to ultraviolet (UV) irradiation (UV lamp, wavelength 254 nm; Technoscientific Co., El- Haram Giza - Egypt). Material extracts were prepared by incubating both crosslinked CS samples in Dulbecco’s Modified Eagle Medium (DMEM, Sigma Aldrich) supplemented with 100 U/ml penicillin (Sigma), 0.1 mg/ml streptomycin (Sigma), 1 mM sodiumpyruvate (Sigma), 4 mM L-glutamine (Sigma) and 10% heat-inactivated fetal bovine serum (FBS; all from Invitrogen) and stored at 37 °C in a humidified atmosphere of 5% CO<sub>2</sub> for 13 days. As control media, samples of culture medium without CS were maintained in the same conditions of CS/DSP and CS/GPTMS\_DSP samples and then collected after 13 days. Then proliferation assay on cell line was carried out using media collected. In details, RT4-

D6P2T cells were seeded in the previous prepared extract media, at a density of  $2 \times 10^3$  cells/cm<sup>2</sup> on Petri dishes. After 2, 3, 5 and 7 days *in vitro* (DIV), cells were trypsinized and counted in a Burker's hemocytometer chamber. Experiments were performed as technical and biological triplicates. The counts obtained from assays were analysed, averaged and expressed as logarithmic scale of viable cells/mm<sup>2</sup>  $\pm$  SD.

#### **4.2.3.2.2 Cell adhesion on CS/GPTMS\_DSP samples**

Immunocytochemistry analysis was performed to qualitatively evaluate cell adhesion and morphology. RT4-D6P2T were seeded at a density of  $1.05 \times 10^4$ /cm<sup>2</sup> on films and control glass slides. After 24 hours of culture, culture medium was removed, substrates with attached cells were rinsed with PBS and fixed by the addition of 4% paraformaldehyde solution (PAF; Sigma-Aldrich). After 20 min the PAF was removed and each plate was washed with PBS. Fixed cells were permeabilized with 0.1% Triton X-100 and blocked with 1% Normal goat serum in 0.01M PBS (pH 7.4) for 1 h at room temperature. F-actin was detected using fluorescein isothiocyanate (FITC)- conjugated phalloidin diluted 1:1000 in blocking solution (Chemicon-Millipore) by 1 h incubation at room temperature following three wash steps of 5 min each. Vinculin was detected by overnight incubation with vinculin monoclonal antibody (Millipore) diluted 1:200 in PBS followed by 1-h incubation with goat-anti-mouse Alexa 488 secondary antibody (Invitrogen) diluted 1:200 in PBS. All the fluorescently-labeled cells were examined under a LSM 510 confocal laser microscopy system (Zeiss, Jena), which incorporates two lasers (argon and HeNe) and is equipped with an inverted Axiovert 100 M microscope.

#### **4.2.3.2.3 Proliferation assay on CS/GPTMS\_DSP samples**

RT4-D6P2T cells were seeded in DMEM containing 10% FBS, at a density of  $2.5 \times 10^3$  cells/cm<sup>2</sup> on both CS/GPTMS\_DSP and poly-d-lysine coated glass plates (positive control). After 1, 3 and 4 DIV, culture medium was removed, substrates with attached cells were rinsed with PBS and fixed by the addition of 4% PAF. After 20 min the PAF was removed and each plate was washed with PBS. RT4-D6P2T cells were stained with 1% crystal violet (a deep purple nucleic acid stain) solution in 200 mM boric solution (pH 9) for 10 min at room temperature. Cells were photographed at DFC 320 Leica microscope with a 30 images were taken at a low magnification (10X) for each sample. The images were then acquired through the program Image Manager IM50 (Leica). The counts obtained from proliferation assay were analysed, averaged and expressed as logarithmic scale of viable cells/mm<sup>2</sup>  $\pm$  SD.

#### **4.2.3.2.4 Real Time Reverse-Transcriptase-Polymerase-Chain-Reaction (Real Time RT-PCR) analysis on CS/GPTMS\_DSP**

RT4-D6P2Ts were cultured in DMEM containing 10% FBS on polystyrene plates and CS/GPTMS\_DSP flat membranes and were allowed to reach confluence. The total RNA was isolated from the confluent culture by extraction with TRIzol (Invitrogen). The RNA

concentration was quantified by measuring the absorbance at 260/280 nm. The total RNA (1 µg per sample) was reverse-transcribed in a reaction volume of 25 µl with 7.5 mM of random hexamers (Thermo Scientific). Each reaction consisted of cDNA synthesis buffer (50x10<sup>-3</sup> M Tris-HCl, pH 8.3, 75x10<sup>-3</sup> M KCl, 3x10<sup>-3</sup> M MgCl<sub>2</sub>), 1 mM deoxynucleotide triphosphate (dNTP), Thermo Scientific), 1.3 U/µl ribonuclease inhibitor (RNAsin, Ribolock Thermo Scientific) and 8 U/µl Moloney murine leukaemia virus (M-MLV) reverse transcriptase (RevertAid Thermo Scientific). The samples were then exposed to a first cycle: 25°C for 10 min, 42°C for 90 min and 90°C for 10 min. Specific primers designed to amplify B cell lymphoma 2 (Bcl2)-associated X protein (BAX), Bcl2 (two proteins involved in the cascade of caspases, which regulates cellular apoptosis), superoxide dismutase (SOD, an important antioxidant defense in nearly all living cells exposed to oxygen) and mammalian target of rapamycin (mTor, a protein encoded by the MTOR gene involved in the regulation of cell growth, cell proliferation, cell motility, cell survival, protein synthesis, and transcription) are listed in Table 4.1. For normalisation to multiple housekeeping genes, ubiquitin gene C (UBC) and TATA-binding protein (TBP) were used. The reaction mixture of PCR included 7.5µg forward and reverse primers, 12.5 µl SYBR Green (Life Technologies) and 5 µl cDNA. The PCR conditions were as following: initial step at 95°C for 25 s, then 40 cycles at 95 °C for 15 s, 60 °C for 1 min. The results were obtained from three independent experiments.

**Table 4.1.** Primers designed to amplify BAX, Bcl2 and G3PDH cDNA.

cDNA	Primer	Oligonucleotide primers	Annealing temperature (°C)
<b>BAX</b>	Forward	5'-TTGCTGATGGCAACTTCAAC-3'	60
	Reverse	5'-GATCAGCTCGGGCACTTTAG-3'	
<b>Bcl2</b>	Forward	5'-GCATCTGCACACCTGGATC-3'	60
	Reverse	5'-GGGCCATATAGTTCCACAAAGG-3'	
<b>SOD</b>	Forward	5'-GAGGCCATCCCTTATCCAAG	60
	Reverse	5'-GATGCCACAGGCCAACC-3'	
<b>mTOR</b>	Forward	5'-GCAGCAACAGTGAAAGTGAAG-3'	60
	Reverse	5'-GCCTCTCGACAAGGAGATAG-3'	
<b>UBC</b>	Forward	5'-CCACCAAGAAGGTCAAACAGG-3'	60
	Reverse	5'-CCCATCACACCCAAGAACAAG-3'	
<b>TBP</b>	Forward	5'-GATCAAACCCAGAATTGTTCTCC-3'	60
	Reverse	5'-GGGGTAGATGTTTTCAAATGCTTC-3'	

#### **4.2.3.2.5 Neurite outgrowth assay on CS/GPTMS\_DSP**

DRGs explants were harvested from adult female Wistar rats, weighing approximately 250 g, reduced and maintained in Ham's nutrient mixture F12 (Gibco) for 1 hour under sterile conditions. Experiment was performed in technical and biological triplicate. Rats were sacrificed by a lethal i.m. injection of tiletamine + zoletil, according with the Ethics Committee and the European Communities Council Directive of 24 November 1986 (86/609/ EEC). Adequate measures were taken to minimize pain and discomfort taking into account human endpoints for animal suffering and distress. DRG explants were cultured onto matrigel-coated coverslips (BD Biosciences) and CS/GPTMS\_DSP flat membranes and incubated at 37 °C for 1 hour. The matrigel was diluted 1:1 in the culture medium. Explants were maintained for 4 days in defined serum-free medium (SFM) at 37 °C with 5% CO<sub>2</sub> [18] supplemented with 50 ng/ml of NGF. As control no 50 ng of NGF/ml of medium were added according to literature data [19, 20]. After 4 days, explants were fixed with 4% PAF for 15 minutes at room temperature. For the immunohistochemistry, briefly, the specimens were incubated overnight in a solution containing both anti-neurofilament-H (anti-NF-H, monoclonal mouse, 1:200, Sigma) that specifically recognizes both phosphorylated and non-phosphorylated NF-H subunits, and anti-peripherin (polyclonal rabbit, 1:1000, Chemicon International) primary antibodies. After washing in PBS, double immunolabeling was carried out by incubating sections for 1 h in a solution containing two secondary antibodies: anti-rabbit IgG Cy3 (Jackson Immunoresearch Laboratory) and anti-mouse IgG Alexa-Fluor-488-conjugated (Molecular Probes). All samples were observed with a LSM 510 confocal laser microscopy system (Zeiss, Jena), which incorporates two lasers (argon and HeNe) and is equipped with an inverted Axiovert 100 M microscope. For quantification, the whole explants were acquired through an optical video-confocal microscope and the supporting software ImageJ.

#### **4.2.3.3 *In vivo* tests on CS/GPTMS\_DSP and CS/DSP**

All procedures were performed in accordance with the Ethics Committee and the European Communities Council Directive of 24 November 1986 (86/609/ EEC).

##### **4.2.3.3.1 *In vivo* qualitative analysis on: biocompatibility, rolling up and suturability**

Prior to their use on crushed median nerves, the biocompatibility, the rolling up and the suturability of CS/DSP and CS/GPTMS\_DSP flat membranes were tested *in vivo* in 2 adult female Wistar rats, weighing approximately 250 g. First, CS/DSP and CS/GPTMS\_DSP membranes were immersed in PBS solution, rolled up and glued with biomedical cyanoacrylate glue to obtain a tube having a 1.1 mm diameter and a 1 cm length (Fig 4.2 A, B,C, D). Under general anesthesia, 1-cm-long incisions was made on the median nerve of the left forelimb and CS tubes were implanted (Fig. 4.2 E,F). Throughout the 8-week follow-up time, animals remained healthy, and none developed local or systemic signs of infection and/or inflammation.

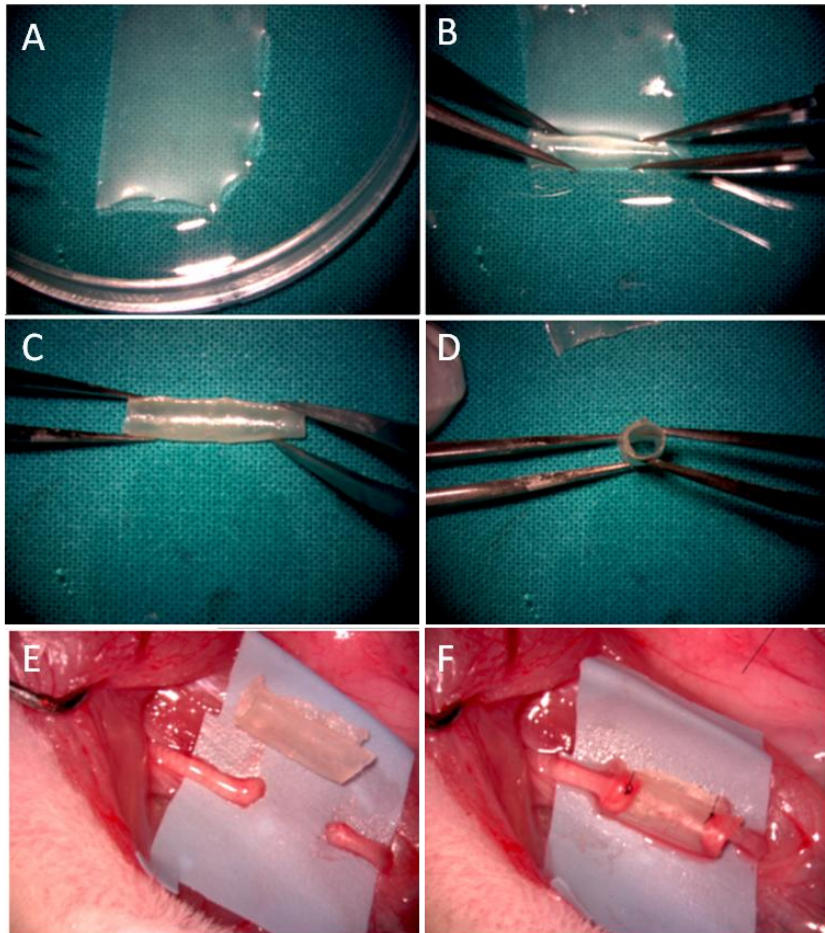


**Fig. 4.2** Sample preparation for *in vivo* qualitative analysis on biocompatibility, rolling up and suturability: A) CS/DSP film was immersed in PBS solution, B), C), D) CS/DSP film was rolled and glued with a cyanoacrylate glue to obtain a tube; E) F) CS/DSP tube immediately before and after implantation.

#### 4.2.3.3.2 Animals and surgery

*In vivo* nerve regeneration assays were carried out with both CS/DSP and CS/GPTMS\_DSP membranes because of their higher elasticity which proved to facilitate surgery. A total of 12 adult female Wistar rats weighing approximately 250 g at the start of the experiment were used. The animals were divided by three experimental groups of 4 animals each. The experimental groups were set according to treatment after nerve median crush injury. In two groups, the crushed median nerve was encircled by CS/DSP or CS/GPTMS\_DSP films. Finally, in an additional group, the median nerve was repaired with reversed autologous graft. The surgery procedure was the one previously described by Tos et al. [21]. Similar to the procedure used for rats [22], in order to prevent interferences with the grasping test device during testing due to the use of the contra-lateral forepaw, the contra-lateral median nerve was transected at the middle third of the brachium and its proximal stump was sutured in the pectoralis major muscle to avoid spontaneous reinnervation. After 12-weeks post-operative, rats were sacrificed: CS/GPTMS\_DSP were found to be detached from the distal suturing site (Fig. 4.3E). For

this reason, light and transmission electron microscope analysis was carried out on CS/DSP samples.

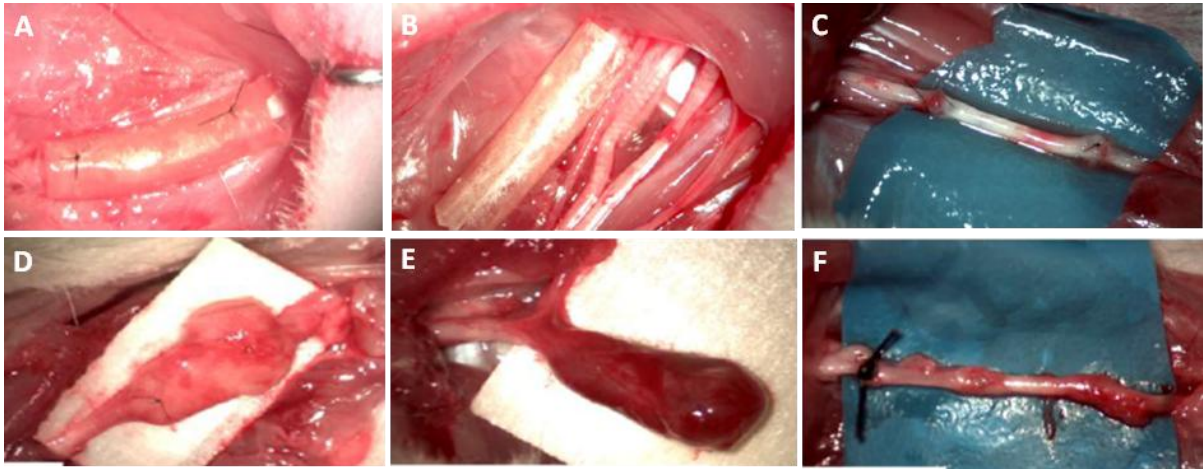


**Fig. 4.3** Pictures taken from CS/DSP (A, D), CS/GPTMS\_DSP(B,E) and autograft (C, F) in situ immediately after post-operative (A, B, C) and 12 weeks post-injury (D, E, F).

#### **4.2.3.3.3 Postoperative assessment of functional recovery**

Grasping test sessions were carried out every 3 weeks until week 12. Grasping test was performed following the same procedure previously described [22] using the BS-GRIP Grip Meter (2Biological Instruments, Varese, Italy). Equipment for grasping test is basically represented by a precision balance connected to a grid. The test is carried out by holding the mouse by the tail and lowering it towards the device and then, when the animal grips the grid, pulling it upward until it loses its grip. When the median nerve function is impaired, the animal's paw approaches the grid in complete finger extension. The balance records the maximum weight that the animal manages to hold up before losing the grip. Each animal was tested three times and the average value was recorded. Since assessment of animal welfare was one of the main objectives of this study, a careful daily animal surveillance was adopted for passive and active movement, auto-mutilation and joint contracture, especially during early post-operative times.

#### **4.2.3.3.4 Resin embedding and electron microscopy**

After the 12-week follow-up time, animals were euthanized and a 10-mm long segment of the median nerve distal to the site of lesion was collected, fixed, and prepared for design-based stereological analysis of myelinated nerve fibers and for electron microscopy. The week-12 end-point was chosen since functional recovery measured by the grasping test was stabilized by this post-operative time. Nerve samples were fixed by immediate immersion in 2.5% purified glutaraldehyde and 0.5% saccarose in 0.1 M Sorensen phosphate buffer for 6–8 hours. Specimens were then washed in a solution containing 1.5% saccarose in 0.1 M Sorensen phosphate buffer, post-fixed in 1% osmium tetroxide, dehydrated and embedded in resin. From each nerve, series of semi-thin

transverse sections (2- $\mu\text{m}$  thickness) were cut starting from the distal stump of each median nerve specimen, using an Ultracut UCT ultramicrotome (Leica Microsystems, Wetzlar, Germany) and stained using Toluidine blue for high resolution light microscopy examination and design-based stereology. For transmission electron microscopy, ultra-thin sections (50–90-nm thick) were cut using the same ultramicrotome and stained with saturated aqueous solution of uranyl acetate and lead citrate. Ultra-thin sections were analyzed using a JEM-1010 transmission electron microscope (JEOL, Tokyo, Japan).

#### **4.2.3.3.5 Design-based quantitative morphology of nerve fiber regeneration**

In each nerve treated with reversed autograft or encircled with CS/DSP, design-based stereological analysis was carried out using one randomly selected toluidine blue stained semithin section. A DM4000B microscope equipped with a DFC320 digital camera and an IM50 image manager system (Leica Microsystems, Wetzlar, Germany) was used for stereology. The final magnification was 6600X enabling accurate identification and morphometry analysis of myelinated nerve fibers. One semi-thin section from each nerve was randomly selected and the total cross-sectional area of the nerve was measured. The sample of fibers in each nerve was then randomly selected using a previously described stereological method [23]. Mean fiber density was then calculated by dividing the total number of nerve fibers within the sampling field by its area ( $N/\text{mm}^2$ ). Total fibers number ( $N$ ) was finally estimated by multiplying the mean fiber density by the total cross-sectional area of the whole nerve cross section.

Two-dimensional disector probes were also used to select an unbiased representative sample of myelinated nerve fibers. In each fiber, both fiber and axon area were measured and the circle-fitting diameter of fiber ( $D$ ) and axon ( $d$ ) were calculated. These data were used to calculate myelin thickness  $[(D-d)/2]$ , myelin thickness/axon diameter ratio  $[(D-d)/2d]$ , and axon/fiber diameter ratio, the  $g$ -ratio ( $D/d$ ). The precision of the estimates was evaluated by calculating the coefficient of error (CE) as previously described [24, 25]. The sampling scheme was designed in order to keep the CE below 0.10, which assures enough accuracy for neuromorphological studies [26].

#### **4.2.3.3.6 Immunohistochemistry and confocal laser microscopy**

From all animals, a 3-mm long nerve specimen withdrawn proximal to the segment was used for resin embedding, was fixed in PAF 4% and PBS and routinely embedded in paraffin for immunohistochemistry and confocal laser microscopy. Series of 8–10  $\mu\text{m}$  thick sections were cut by a RM2135 microtome (Leica Microsystems, Wetzlar, Germany). Sections were then incubated overnight in a solution containing anti-neurofilament-200kD ( $\alpha$ -NF) primary antibody (monoclonal, mouse, which recognizes the 200 kD subunit of neurofilaments, dilution 1:200, Sigma) and then, after washing in PBS, incubated for 1 hour in a solution containing TRITC-conjugated anti-rabbit IgG (dilution 1:200, Dako). The sections were finally mounted with a Dako fluorescent mounting medium and analyzed by a LSM 510 confocal laser microscopy system (Zeiss, Jena, Germany), which

incorporates two lasers (Argon and HeNe) and is equipped with an inverted Axiovert 100M microscope. To visualize TRITC, we used excitation from 543 nm HeNe laser line and emission passing through a high-pass (LP) 560 filter which passes wavelengths superior to 560 nm to the detector.

#### **4.2.3.4 Statistics**

*For vitro* experiments, data were expressed as mean  $\pm$  SEM. For *in vivo* studies, the number of animals used in the experiments (12) was calculated in order to meet the Ethical Committee requirements for a minimum number of animals used with the 'Three Rs' (replacement, reduction and refinement of animal studies) concept put forward by Russel and Burch and adopted by the European Community. Statistical analysis was carried out using single-factor analysis of variance (ANOVA) post hoc Bonferroni. Values of  $*p \leq 0.05$ ,  $**p \leq 0.01$ ,  $***p \leq 0.001$  were considered as statistically significant.

### **4.3 Results and discussion**

#### **4.3.1 Evaluation of CS based membranes permeability**

One critical properties of NGCs is the wall permeability for solutes and nutrients. The NGCs have to facilitate the permeation of small molecules from the outside to the inside of the tube and viceversa to allow cell metabolism and growth. The FD-4 was used as a model of nutrients having a Stokes radius of 14 Å that is superior to glucose Stokes radius (3.8 Å) [15] and NaCl Stokes radius (1.4 Å) [16]. In Fig. 4.4 the release concentration of the FD-4 in the PBS after 1, 3, 6, 24, 48 and 96 hours are reported. Results showed that the release of FD-4 from CS crosslinked tubes increased with time: an initial burst release (about 50%) from the inside to the outside of CS/DSP and CS/GPTMS\_DSP conduits was followed by a sustained release stage of FD-4 contained into CS tubes, reaching a final value of 80% of model molecule released in 96 hours. The prolonged release observed after the initial burst release can be ascribed to the penetration of the FD-4 inside the tubes after PBS absorption during CS swelling. Moreover, different crosslinking method slightly influenced the FD-4 release kinetics. CS/DSP showed an easier permeation of the model molecules from the inside to the outside of the tube respect to CS crosslinked with both covalent (GPTMS) and ionic (DSP) agents. In detail, after 3 hours, a higher permeation of FD-4 was observed for CS/DSP compared to CS/GPTMS\_DSP. This trend is also confirmed after 6, 24, 48 and 96 hours where a higher release was observed for CS/DSP. The addition of the covalent crosslinker in CS/GPTMS\_DSP could slow down the FD-4 release in time for the hydrophobic properties of the GPTMS and for formation of a more organized structure as a consequence of a double crosslinker.

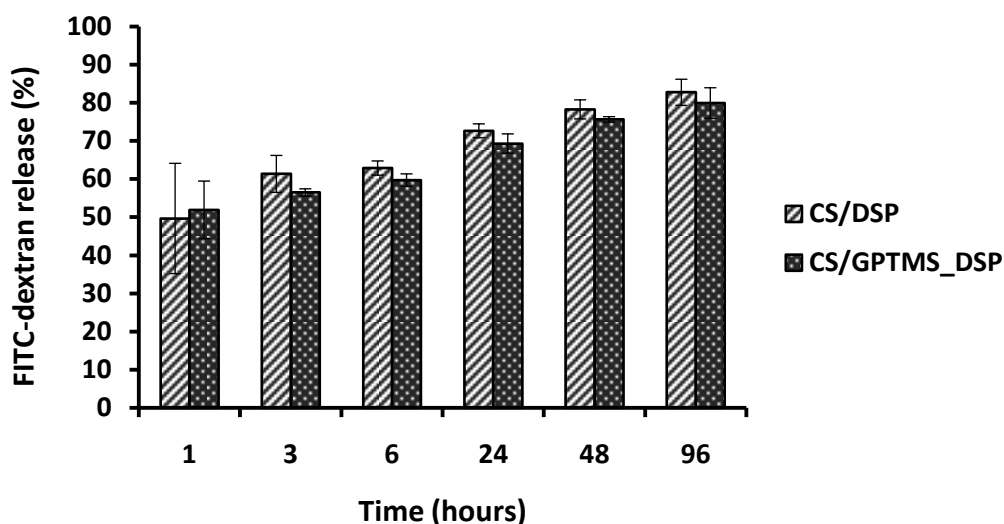


**Figure 4.4.** FITC–dextran release concentration in the incubation medium reported as a percentage respect to the dextran initially loaded into CS/DSP and CS/GPTMS\_DSP tubes.

### 4.3.2 *In vitro* cell tests on CS based samples

#### 4.3.2.1 Cytotoxicity study on CS/GPTMS\_DSP and CS/DSP

The effect of the CS based material extracts was studied by RT4-D6P2T proliferation assay counting the number of proliferating cells after 2, 3, 5 and 7 DIV (Fig 4.5). RT4-D6P2Ts treated with extracts of CS/DSP and CS/GPTMS\_DSP showed no cytotoxic effects as no significant differences in the cells numbers were evidenced in these two culture conditions compared to the control used as reference.

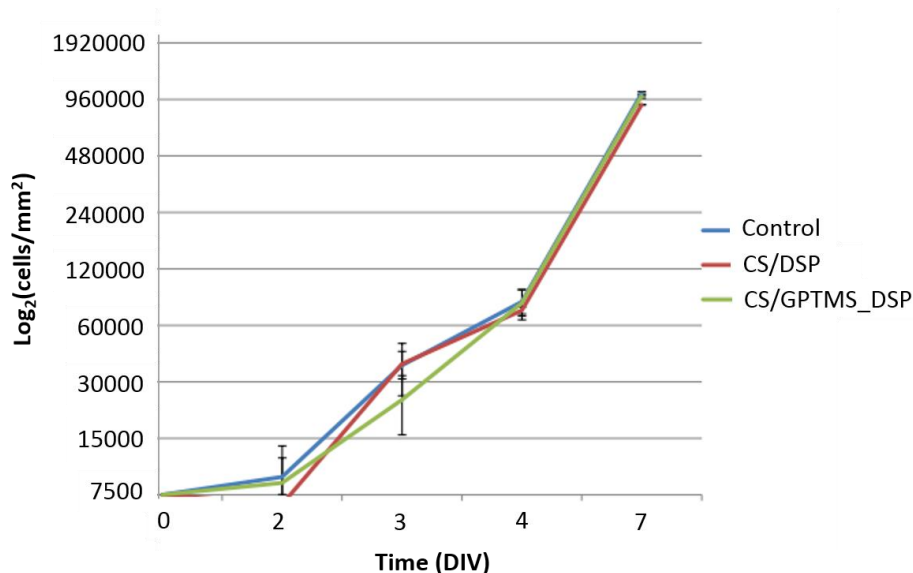


**Fig.4.5.** Logarithmic scale of RT4-D6P2Ts/mm<sup>2</sup> proliferated after 1, 3, 5 and 7 DIV seeded in control, CS/DSP and CS/GPTMS\_DSP extract media. Cells were counted in a Burker's hemocytometer chamber.

#### 4.3.2.2 Cell adhesion on CS/GPTMS\_DSP samples

RT4-D6P2Ts were seeded on CS/GPTMS\_DSP and on control glass; immunocytochemistry analysis was performed after 24 hours of culture to qualitatively evaluate cell adhesion and morphology. The actin cytoskeleton is a highly dynamic network composed of actin polymers and a large variety of associated proteins. The function of the actin cytoskeleton is to mediate a variety of essential biological functions, including intracellular and extracellular movement and structural support. The orientation distribution of actin filaments within a cell is, therefore, an important determinant of cellular shape, adhesion and motility. In order to obtain a more detailed evaluation of cell adhesion, the actin cytoskeleton and focal adhesion complex were stained using FITC-conjugated phalloidin and antivinculin antibody, respectively. RT4-D6P2T cells interacted and integrated well with both the control and CS/GPTMS\_DSP substrates. However, differing morphologies and dimensions were seen when RT4-D6P2T cells were cultured on control glass and CS/GPTMS\_DSP (Fig. 4.6). Cells on control glass displayed a higher dimension and more spreading with no particular orientation of the actin cytoskeleton (Fig. 4.6A and C), while RT4-D6P2Ts cultured on CS/GPTMS\_DSP displayed a more condensed and elongated morphology characterized by a typical oval-shaped cell body with long extensions, giving an overall spindle shape that is typical with SCs morphology (Fig. 4.6B and D). Vinculin immunostaining was performed for RT4-D6P2T cells to visualize the exact location of focal adhesion sites. Vinculin-positive sites were observed on cells seeded both on control and CS/GPTMS\_DSP. However CS/GPTMS\_DSP presented an higher accumulation of vinculin around the nucleus of RT4-D6P2T cells (Fig. 4.6F) while protein accumulation at the edges of cells was also showed in control (Fig. 4.6E).

These data provide qualitative information about cell adhesion, morphology and spreading on the biomaterial surface: 24 hours after seeding cells are still attached to the CS/GPTMS\_DSP and display a different morphology and vinculin accumulation compared to RT4-D6P2Ts cultured on control glass, allowing to hypothesize a lower adhesion and a higher motility of cells on the developed biomaterial.

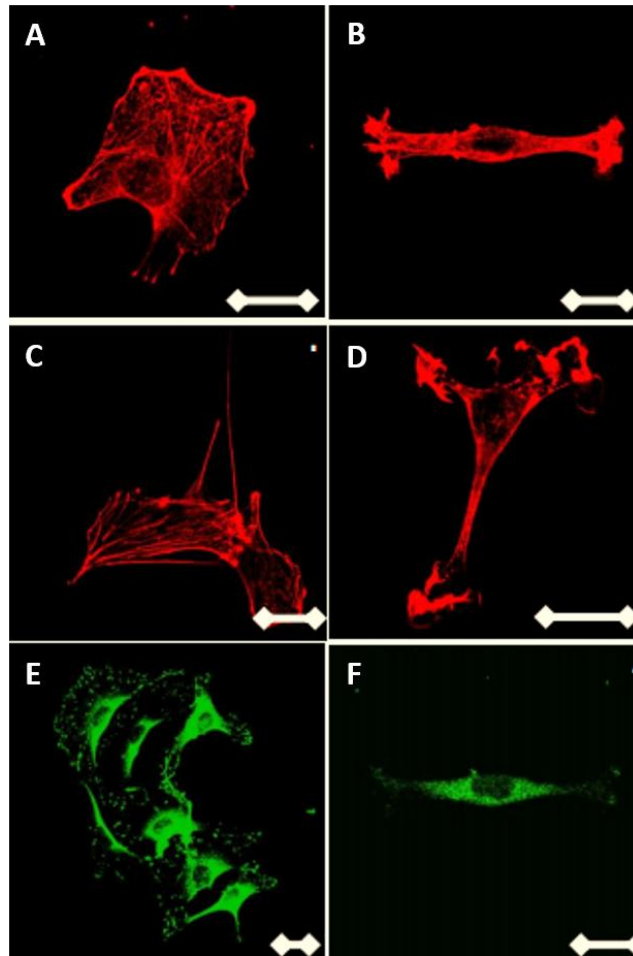


**Fig. 4.6.** Confocal fluorescence microscopy images of RT4-D6P2T cells attached on control glass (A, C, E) and CS/GPTMS\_DSP (B, D, F) after 24 hours of cell culture. Representative pictures of RT4-D6P2T, cultured after phalloidin staining (A, B, C, D) and anti-vinculin (E, F). Scale bar 20  $\mu\text{m}$ .

#### 4.3.2.3 Proliferation assay on CS/GPTMS\_DSP samples

As for cell adhesion (paragraph 4.3.1.2.2), proliferation assay was performed on CS/GPTMS\_DSP samples. RT4-D6P2T cells were cultured on both CS/GPTMS\_DSP and poly-d-lysine coated glass plates (positive control). The number of proliferating cells was then counted after 1, 3 and 4 DIV. RT4-D6P2Ts seeded on CS/GPTMS\_DSP showed lower cell proliferation rate and significant differences in the cells numbers were evidenced in this culture condition after 3 (\*\* $p < 0.01$ ) and 4 DIV (\*\* $p < 0.001$ ) compared to the positive control. However, an increase in cell number on CS/GPTMS\_DSP samples was observed at each time point. The obtained results are probably correlated with the lower adhesion and higher motility of RT4-D6P2T on the biomaterial at initial culture time.

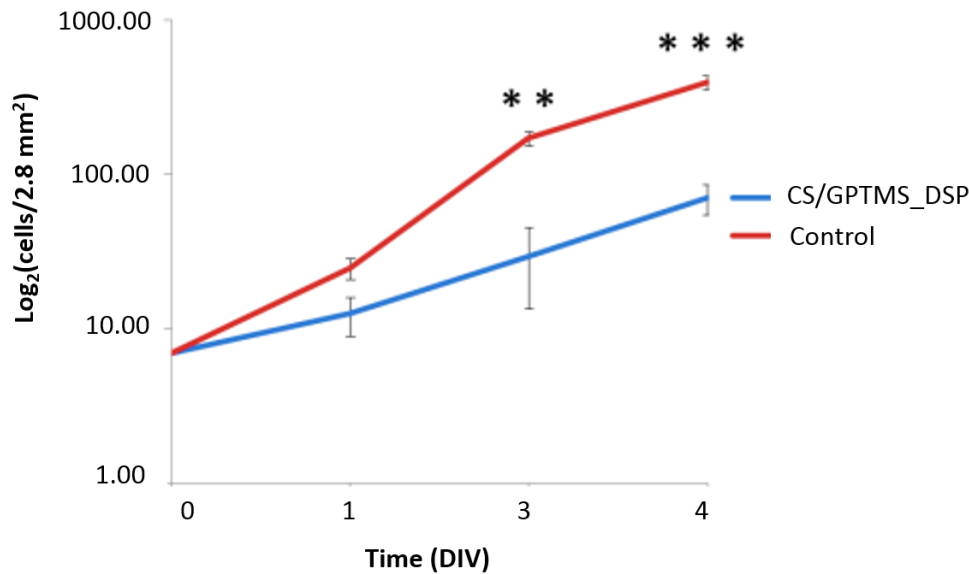


**Fig.4.7** RT4-D6P2T proliferation ratio after 1, 3 and 4 DIV on poly-d-lysine coated glass plates (control) and on CS/GPTMS\_DSP films. RT4-D6P2T significant differences between CS/GPTMS\_DSP substrates and control samples were observed (\*\*p<0.01; \*\*\*p<0.001).

#### 4.3.2.4 Real Time Reverse-Transcriptase-Polymerase-Chain-Reaction (Real Time RT-PCR) analysis on CS/GPTMS\_DSP

Bax, Bcl2, mTOR and SOD mRNA expression changes were evaluated to study proapoptotic and cell survival signaling after 3 and 6 days of culture. Bax is a cytosolic protein that plays a pro-apoptotic role, whereas Bcl2 is a pro-survival protein that has been shown to heterodimerize with BAX, which counters the death-repressor activity of Bcl2 [27]. SOD enzyme participates in the first line of defence against superoxide anions ( $O_2^{\cdot-}$ ) generated in different cell compartments. mTOR is a protein encoded by the MTOR gene involved in the regulation of cell growth, cell proliferation, cell motility, cell survival, protein synthesis, and transcription.

The relative values of BAX, mTOR and SOD mRNA expression were not significantly different to RT4\_D6P2T cells seeded on the CS/GPTMS\_DSP samples and control condition both after 3 and 6 days of culture, providing confirmation of the viability of the cells cultured on CS/GPTMS\_DSP (Fig. 4.8A, B, E, F, G and H). Significant difference in the Bcl2 mRNA expression was evidenced in the culture condition after 3 days of culture (\*p<0.05) compared to the positive control. However, this difference was not observed after 6 days.

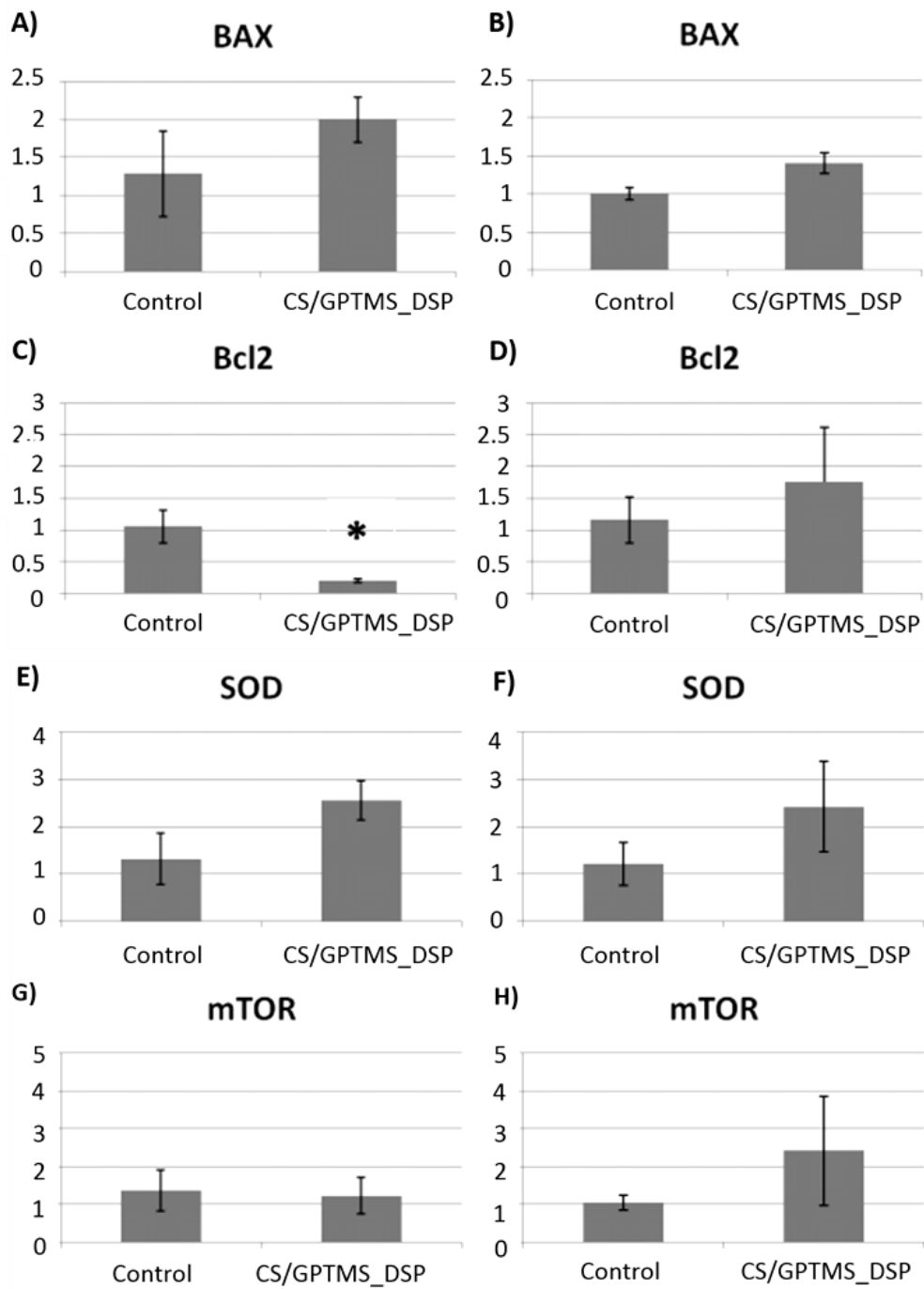


**Fig.4.8.** RT PCR expression profiles of BAX (A, B), Bcl2 (C, D), SOD (E, F) and mTOR (G, H) messengers in RT4-D6P2T seeded respectively on control plates, and CS/GPTMS\_DSP films after 3 and 6 days of culture. Significant difference between the biomaterial and control was observed for Bcl2 after 3 days of culture (\* $p < 0.05$ ).

#### 4.3.2.5 Neurite outgrowth assay on CS/GPTMS\_DSP

DRG explants were harvested from adult female Wistar rats and cultured for 4 days onto matrigel-coated coverslips and CS/GPTMS\_DSP flat membranes. The cultures were fixed and immunostained for neurofilaments NF-H (yellow) and peripherin (red) and then analyzed in toto using the laser confocal microscopy. Neurofilaments are the intermediate filaments of neurons and in mature neurons comprise neurofilament light, middle and heavy chains (NF-L, NF-M and NF-H) as their major proteins; peripherin is a 57 kDa type III neuronal intermediate filament protein particularly expressed in the peripheral nervous system [28-30]. In common with other members of the intermediate filament protein family, each neurofilament subunit comprises a central  $\alpha$ -helical rod domain of 310–352 amino acids that is flanked by an N-terminal globular head domain and non- $\alpha$ -helical C-terminal domains. The C-terminal domains are the most variable with those of NF-H being the longest and forming side-arms that project from the filament and which appear to form crossbridges between neurofilaments and between neurofilaments and other cytoskeletal organelles. Moreover, previous data in literature have suggested that all DRG neurons express NF-H [31]. Peripherin immunolabeling has been employed for the study of peripheral nerve development and regeneration, since this intermediate filament protein is highly over-expressed during axon elongation [32]. Both peripherin and all NF-H have been reported to co-existing in several neuronal types [31, 33, 34]. A double labeling in immunofluorescence revealed that these two neuronal intermediate filament proteins were both expressed within the DRG stained neurons (Fig. 4.9). High magnification showed that the axonal outgrowth onto CS/GPTMS\_DSP flat membranes (Fig. 4.9D) apparently exceeds in length compared to that of the matrigel-coated coverslips (Fig. 4.9C).

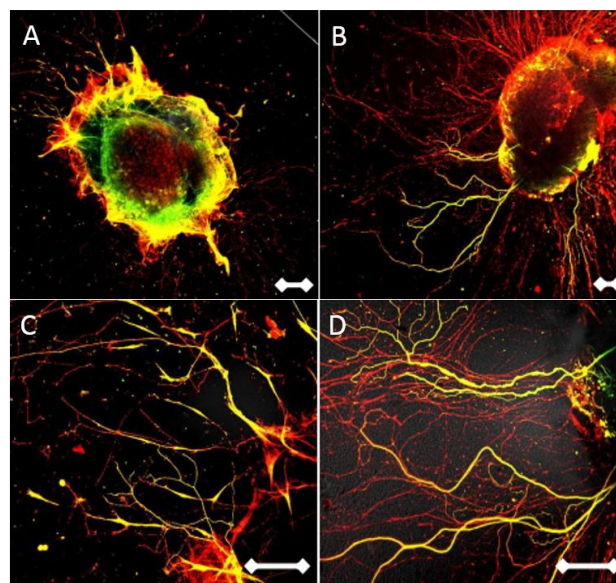


**Fig. 4.9** Representative immunostaining image of axonal outgrowth at 4 days after co-culture onto matrigel-coated coverslips (A, C) and CS/GPTMS\_DSP flat membranes (B, D) using anti-NF-H antibody (yellow) and anti-peripherin (red). Scale bar 100  $\mu$ m.

### 4.3.3 *In vivo* tests on CS/GPTMS\_DSP and CS/DSP

#### 4.3.3.1 Postoperative assessment of functional recovery

*In vivo* nerve regeneration experiments were carried out with both CS/DSP and CS/GPTMS\_DSP flat membranes. The crushed median nerve of female Wistar rats were encircled by CS/DSP or CS/GPTMS\_DSP films or repaired with reversed autologous graft, used as control. Functional recovery of the left forepaw was assessed every 3 weeks until the end of the experiment at week-12 postoperative using the grasping test. Grasping test was performed following the same procedure previously described [22] using the BS-GRIP Grip Meter (2Biological Instruments, Varese, Italy). Fig. 4.10 reports the post traumatic time course of functional recovery for rats treated using CS/DSP and autologous graft. At week-3 post-crush, animal performance in the behavioral test dropped to zero confirming a complete nerve fiber transection from the crush lesion. The function of finger flexor muscles innervated by the median nerve started to recover faster for autograft reaching a performance statistically different from CS/DSP at week-6 after lesion ( $*p<0.05$ ). However, functional recovery also started for CS/DSP at week-9 and progressively increased arriving at 60% and 80% of the pre-operative values by week-9 and until the end of the experiment (week-12), respectively. No significant differences were evidenced between autograft and CS/DSP treatment at these time points (week-9 and 12). CS/GPTMS\_DSP tubes were detached from the distal suturing site and functional recovery of finger flexor muscles did not occurred.

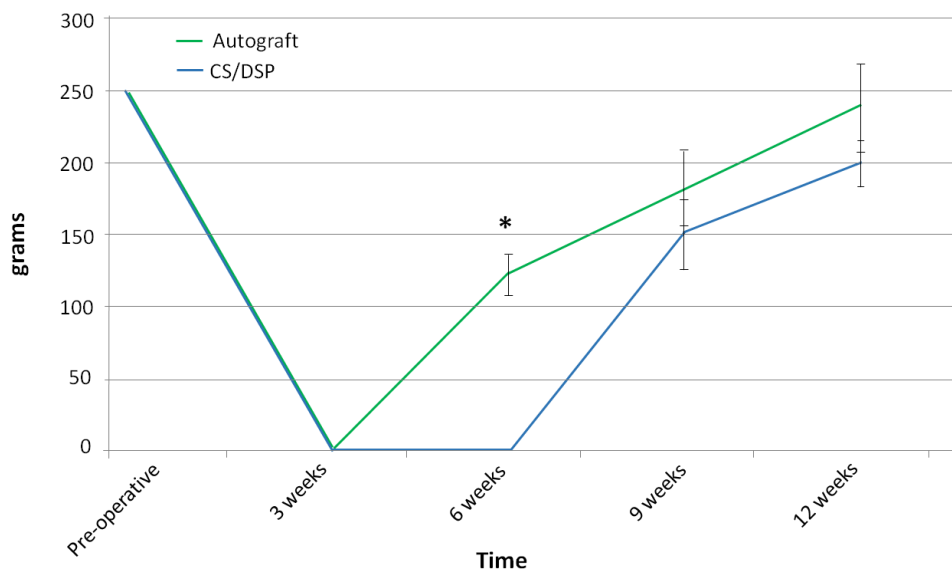
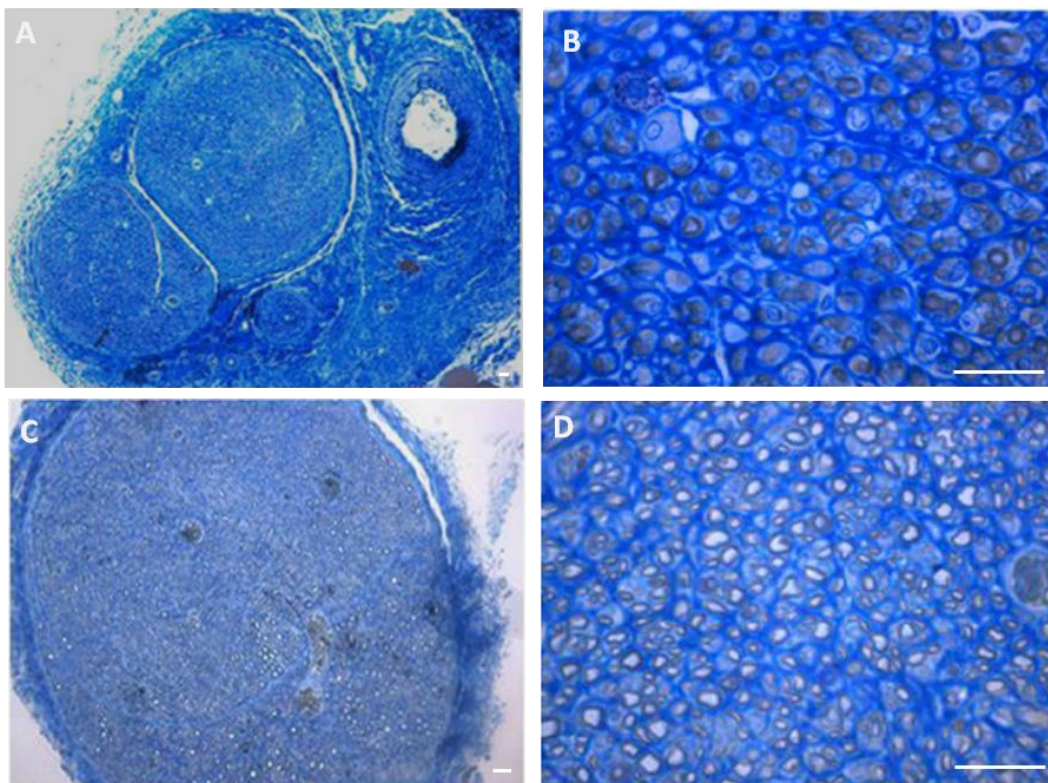


**Fig. 4.10** Line graph reporting the posttraumatic time course of functional recovery as assessed by the grasping test. Values are mean  $\pm$  standard deviation. Significant difference between CS/DSP and autograft treated functional recovery was observed after 6 weeks ( $*p<0.05$ ).

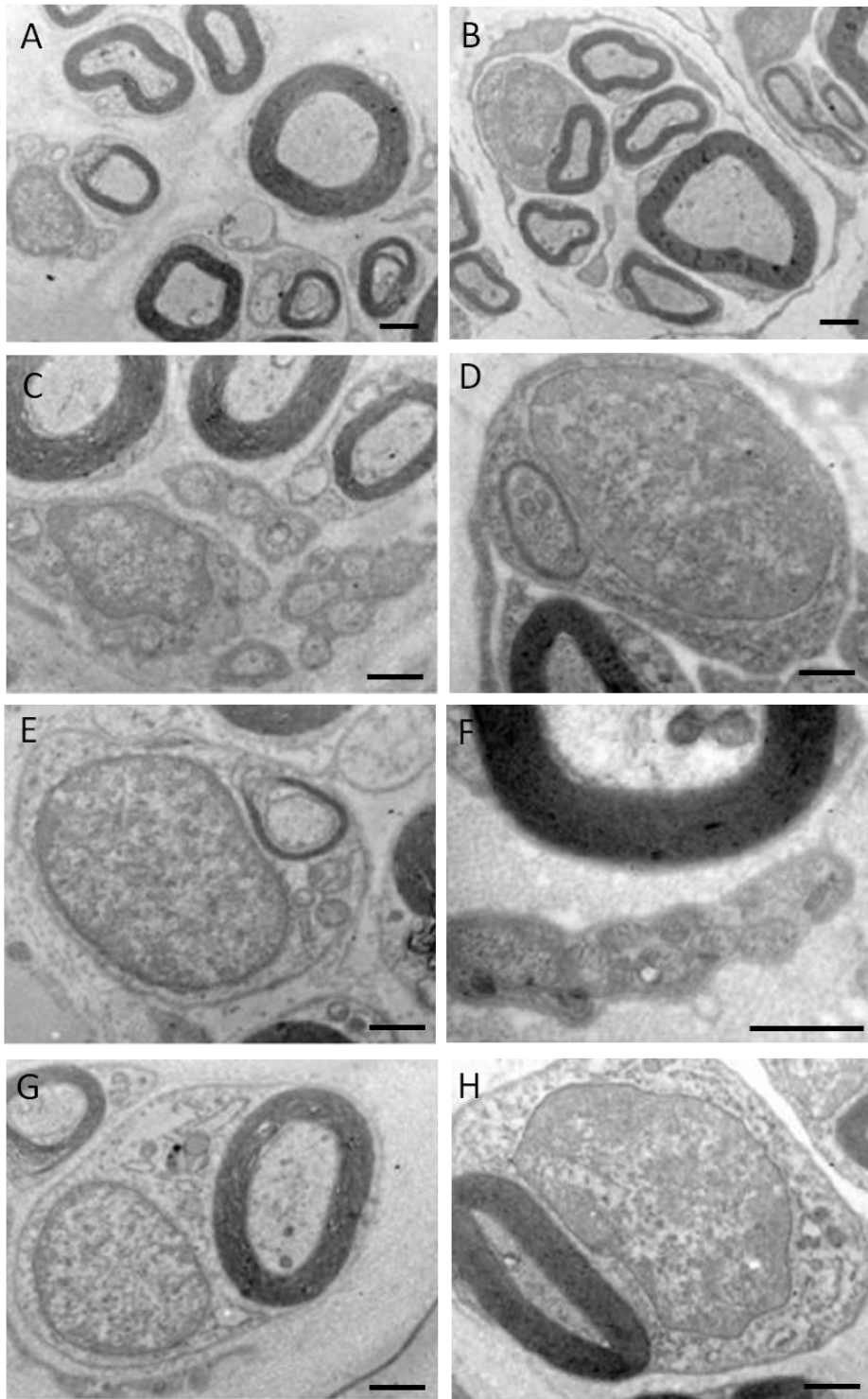
#### 4.3.3.2 Light and transmission electron microscope analysis

Fig. 4.11 shows high-resolution light photomicrographs of rat median nerves injured, treated with reversed autologous graft or encircled by CS/DSP film and harvested at 12 weeks post-operative. Distal median nerves treated with CS/GPTMS\_DSP were not harvested because conduits were found to be detached from the distal suturing site (Fig.4.3E). From each nerve, series of semi-thin transverse sections (2- $\mu$ m thickness) were cut starting from the distal stump of each median nerve specimen and stained using Toluidine blue. Small myelinated axons and microfasciculation typical of regenerated nerve fibers was detected both on samples treated with CS/DSP (Fig. 4.11A, B) and autologous graft (Fig. 4.11C, D) through light microscopy observation.

Small nerve fibers at different myelination stages (unmyelinated in Fig. 4.12C, D; in early stages of myelination in Fig. 4.12E, F and myelinated in Fig. 4.12 G, H) were detected both on the median nerve encircled with the biomaterial or repaired with reversed autologous graft through transmission electron microscopy observations. The presence of fibers that were still in the very early phase of myelination (Fig. 4.12E, F) suggested that at week-12 post-crush injury the process of maturation of regenerated nerve fibers is still incomplete.



**Fig. 4.11** Photomicrographs of semi-thin sections cut transversely to the main axis of treated median nerves using CS/DSP (A,B) and autologous graft (C, D) after 12 weeks post-operative. Scale bar: 20  $\mu$ m.



**Fig. 4.12** Electron microscope images of regenerated nerves treated using CS/DSP (A, C, E, G) and autologous graft (B, D, F, H) after 12 weeks post-operative. Scale bars: A, B, C, D, E, G and H = 1  $\mu\text{m}$ : F=0.5  $\mu\text{m}$ .

#### 4.3.3.3 Design-based quantitative morphology of nerve fiber regeneration

At 12-week post injury, design-based stereological analysis of regenerated median nerves using CS/DSP tubes or reversed autologous grafts (Table 4.2) showed comparable results in terms of total number of myelinated fibers, fiber diameters and myelin thickness. Regarding density of fibers and axon diameters, both parameters decreased significantly ( $*p<0.05$ ) for median nerve encircled with CS/DSP tubes compared to control. Interestingly, the mean g-ratio was not significantly different from both the surgical approaches.

**Table 4.2.** Comparison of stereological parameters of myelinated nerve fibers in regenerated median nerve (12-week post-injury) using autograft and CS/DSP tubes. Values are expressed as mean  $\pm$  S.D. Significant differences between the bioengineered and the gold standard approach were observed for the density of fibres and axons diameter ( $*p<0.05$ ).

Regenerated median nerve	Autograft	CS/DSP
Total number of myelinated fibers	6916 $\pm$ 817	7059 $\pm$ 219
Density of fibers (#/mm <sup>2</sup> )	37763 $\pm$ 2450	26677 $\pm$ 2766*
Fibers diameter ( $\mu$ m)	2.98 $\pm$ 0.11	2.62 $\pm$ 0.14
Axons diameter ( $\mu$ m)	2.08 $\pm$ 0.09	1.68 $\pm$ 0.04*
Myelin thickness ( $\mu$ m)	0.45 $\pm$ 0.02	0.47 $\pm$ 0.05
g-ratio	0.68 $\pm$ 0.01	0.63 $\pm$ 0.02

#### 4.3.3.4 Immunohistochemistry and confocal laser microscopy

Axonal regeneration onto CS/GPTMS\_DSP and CS/DSP conduits was examined by confocal laser microscopy on longitudinal nerve frozen sections (Fig. 4.11) after neurofilaments staining. After 12-week post-injury, in middle segments of regenerated nerves, CS/DSP conduit exhibited NF200-positive axons that were linearly oriented in the longitudinal sections (Fig. 4.13B). The CS/GPTMS\_DSP treated rats displayed poor axonal regeneration, irregular orientation, or disordered but NF positive staining for axons in the longitudinal sections (Fig. 4.13A).

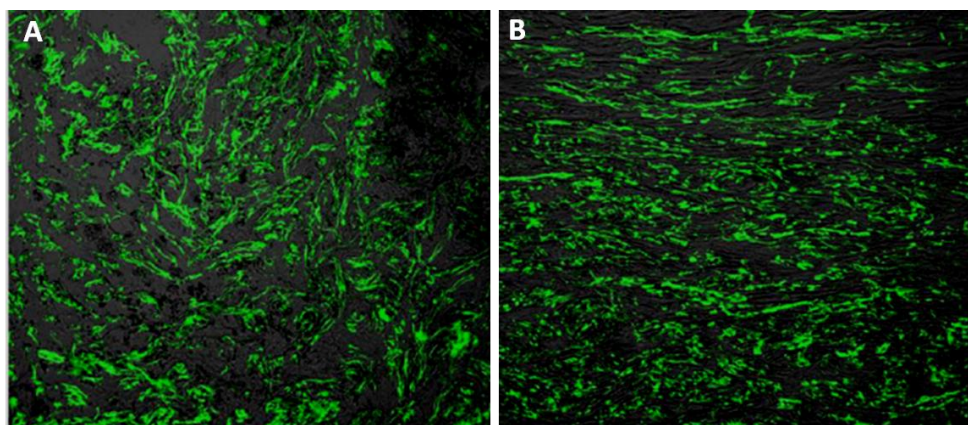


**Fig. 4.13** Neurofilament staining on longitudinal sections at 12 weeks revealed that CS/DSP and CS/GPTMS\_DSP were densely populated with axons. Properly linearly aligned NF axons were found in CS/DSP (B) while CS/GPTMS\_DSP displayed axons that were haphazardly oriented and disorder (A).

#### 4.4 Conclusion

In this chapter CS/GPTMS\_DSP and CS/DSP flat membranes were studied *in vitro* and *in vivo* for the development of CS based nerve conduit scaffolds. Both the crosslinked films were fabricated by solvent casting technique and they can be easily enwrapped to form a NGC in wet state. CS/DSP and CS/GPTMS\_DSP showed a good permeability to molecules having a Stokes radius around 14 Å guarantying the permeation of nutrients and metabolites from the outside to the inside of the tube and viceversa.

*In vitro* characterization performed on model membranes showed that CS/DSP and CS/GPTMS\_DSP do not exert any cytotoxic effects on RT4-D6P2T. The higher mechanical stability of CS/GPTMS\_DSP under physiological condition allowed to evaluate the RT4-D6P2T proliferation on the CS materials: a high tendency to RT4-D6P2T to migrate emerged, phenomenon that is crucial in the lesion site for promoting nerve regeneration. Moreover, the compatibility of CS/GPTMS\_DSP with axonal regrowth was tested culturing explants of rat dorsal root ganglia (DRG): the presence of neurite outgrowth in the samples grown on the CS films was assessed after only four days of culture with ppherin and neurofilament positive axons.

Finally, *in vivo* tests were carried out on both the two types of nerve scaffolds made by CS/DSP and CS/GPTMS\_DSP flat membranes due to their easily manipulation and suturability. CS/DSP and CS/GPTMS\_DSP nerve membranes were used for bridge implantation across 10-mm long median nerve defects in rats, and the outcome of peripheral nerve repair at 12 weeks post-implantation was evaluated by a combination of electrophysiological assessment, immunohistochemical and histological investigation. During *in vivo* tests CS/GPTMS\_DSP tubes were detached from the distal suturing site and functional recovery did not occurred. This result was confirmed by confocal laser microscopy which displayed poor axonal regeneration and irregular orientation but NF positive staining for axons in the longitudinal nerve sections. However, the examined

functional and morphological parameters showed that CS/DSP grafts could promote peripheral nerve regeneration with effects approaching those elicited by nerve autografts which are generally considered as the gold standard for treating large peripheral nerve defects, thus raising a potential possibility of using these newly developed nerve grafts as a promising alternative to nerve autografts.

## References

1. Ichihara, S., et al., Development of New Nerve Guide Tube for Repair of Long Nerve Defects. *Tissue Engineering Part C-Methods*, 2009. **15**(3): p. 387-402.
2. Ignatiadis, I.A., et al., Diverse types of epineural conduits for bridging short nerve defects. An experimental study in the rabbit. *Microsurgery*, 2007. **27**(2): p. 98-104.
3. Hsu, S.H., T.T. Ho, and T.C. Tseng, Nanoparticle uptake and gene transfer efficiency for MSCs on chitosan and chitosan-hyaluronan substrates. *Biomaterials*, 2012. **33**(14): p. 3639-50.
4. Hsu, S.H., et al., New nerve regeneration strategy combining laminin-coated chitosan conduits and stem cell therapy. *Acta Biomaterialia*, 2013. **9**(5): p. 6606-15.
5. Busilacchi, A., et al., Chitosan stabilizes platelet growth factors and modulates stem cell differentiation toward tissue regeneration. *Carbohydrate Polymers*, 2013. **98**(1): p. 665-676.
6. Yuan, Y., et al., The interaction of Schwann cells with chitosan membranes and fibers in vitro. *Biomaterials*, 2004. **25**(18): p. 4273-4278.
7. Freier, T., et al., Controlling cell adhesion and degradation of chitosan films by N-acetylation. *Biomaterials*, 2005. **26**(29): p. 5872-5878.
8. Simoes, M.J., et al., In Vitro and in Vivo Chitosan Membranes Testing for Peripheral Nerve Reconstruction. *Acta Medica Portuguesa*, 2011. **24**(1): p. 43-52.
9. Xu, H., Y. Yan, and S. Li, PDLA/chondroitin sulfate/chitosan/NGF conduits for peripheral nerve regeneration. *Biomaterials*, 2011. **32**(20): p. 4506-16.
10. Nie, X., et al., Axonal regeneration and remyelination evaluation of chitosan/gelatin-based nerve guide combined with transforming growth factor-beta1 and Schwann cells. *Cell Biochem Biophys*, 2014. **68**(1): p. 163-72.
11. Ao, Q., et al., The regeneration of transected sciatic nerves of adult rats using chitosan nerve conduits seeded with bone marrow stromal cell-derived Schwann cells. *Biomaterials*, 2011. **32**(3): p. 787-96.
12. Kuo, Y.C. and C.C. Lin, Accelerated nerve regeneration using induced pluripotent stem cells in chitin-chitosan-gelatin scaffolds with inverted colloidal crystal geometry. *Colloids and Surfaces B-Biointerfaces*, 2013. **103**: p. 595-600.
13. Wang, A., et al., Physical properties and biocompatibility of a porous chitosan-based fiber-reinforced conduit for nerve regeneration. *Biotechnology Letters*, 2007. **29**(11): p. 1697-702.
14. Yang, Y., et al., Fabrication and properties of a porous chitin/chitosan conduit for nerve regeneration. *Biotechnology Letters*, 2004. **26**(23): p. 1793-7.
15. Schultz, S.G. and A.K. Solomon, Determination of the effective hydrodynamic radii of small molecules by viscometry. *J Gen Physiol*, 1961. **44**: p. 1189-99.
16. Boyle, M.D. and T. Borsos, Studies on the terminal stages of immune hemolysis. V. Evidence that not all complement-produced transmembrane channels are equal. *Journal of Immunology*, 1979. **123**(1): p. 71-6.
17. Imada, M. and N. Sueoka, Clonal sublines of rat neurotumor RT4 and cell differentiation. IV. Cell surface proteins. *Dev Biol*, 1980. **79**(1): p. 199-207.
18. Gazdik, F., et al., Decreased levels of coenzyme Q(10) in patients with bronchial asthma. *Allergy*, 2002. **57**(9): p. 811-4.
19. Deister, C. and C.E. Schmidt, Optimizing neurotrophic factor combinations for neurite outgrowth. *J Neural Eng*, 2006. **3**(2): p. 172-9.
20. Gorokhova, S., et al., Uncoupling of Molecular Maturation from Peripheral Target Innervation in Nociceptors Expressing a Chimeric TrkA/TrkC Receptor. *PLoS Genet*, 2014. **10**(2): p. e1004081.

21. Tos, P., et al., Employment of the mouse median nerve model for the experimental assessment of peripheral nerve regeneration. *J Neurosci Methods*, 2008. **169**(1): p. 119-27.
22. Papalia, I., et al., On the use of the grasping test in the rat median nerve model: a re-appraisal of its efficacy for quantitative assessment of motor function recovery. *J Neurosci Methods*, 2003. **127**(1): p. 43-47.
23. Geuna, S., D. Gigo-Benato, and C. Rodrigues Ade, On sampling and sampling errors in histomorphometry of peripheral nerve fibers. *Microsurgery*, 2004. **24**(1): p. 72-6.
24. Schmitz, C., Variation of fractionator estimates and its prediction. *Anatomy and Embryology*, 1998. **198**(5): p. 371-397.
25. Geuna, S., et al., Methodological issues in size estimation of myelinated nerve fibers in peripheral nerves. *Anat Embryol (Berl)*, 2001. **204**(1): p. 1-10.
26. Pakkenberg, B. and H.J. Gundersen, Neocortical neuron number in humans: effect of sex and age. *J Comp Neurol*, 1997. **384**(2): p. 312-20.
27. Becker, E.B.E. and A. Bonni, Cell cycle regulation of neuronal apoptosis in development and disease. *Progress in Neurobiology*, 2004. **72**(1): p. 1-25.
28. Portier, M.M., B. de Nechaud, and F. Gros, Peripherin, a new member of the intermediate filament protein family. *Dev Neurosci*, 1983. **6**(6): p. 335-44.
29. Portier, M.M., et al., Peripherin and Neurofilaments - Expression and Role during Neural Development. *Comptes Rendus De L Academie Des Sciences Serie Iii-Sciences De La Vie-Life Sciences*, 1993. **316**(9): p. 1133-1140.
30. Troy, C.M., et al., Regulation of Peripherin and Neurofilament Expression in Regenerating Rat Motor Neurons. *Brain Research*, 1990. **529**(1-2): p. 232-238.
31. Goldstein, M.E., S.B. House, and H. Gainer, Nf-L and Peripherin Immunoreactivities Define Distinct Classes of Rat Sensory Ganglion-Cells. *Journal of Neuroscience Research*, 1991. **30**(1): p. 92-104.
32. Terao, E., et al., In vivo expression of the intermediate filament peripherin in rat motoneurons: Modulation by inhibitory and stimulatory signals. *Neuroscience*, 2000. **101**(3): p. 679-688.
33. Troy, C.M., et al., Ontogeny of the Neuronal Intermediate Filament Protein, Peripherin, in the Mouse Embryo. *Neuroscience*, 1990. **36**(1): p. 217-237.
34. Beaulieu, J.M., J. Robertson, and J.P. Julien, Interactions between peripherin and neurofilaments in cultured cells: disruption of peripherin assembly by the NF-M and NF-H subunits. *Biochemistry and Cell Biology-Biochimie Et Biologie Cellulaire*, 1999. **77**(1): p. 41-45.

# Chapter 5

## Bi-layer CS membranes for nerve tissue engineering

### Abstract

The purpose of this study was to develop bi-layer CS flat membranes that can be easily manipulated and rolled to obtain flexible nerve guidance channels (NGCs). These bi-layer membranes were prepared via solvent casting technique and their chemical composition was optimized to realize malleable membranes to be enwrapped for NGC formation. Two kinds of CS films crosslinked with different crosslinking agents were combined to produce scaffold structures with good biocompatibility in the inner layer and with the desired mechanical strength imparted by the outer. A tight connection between the two layers was achieved and the physicochemical, thermal, mechanical properties of CS bi-layer membranes were investigated. Additionally, bi-layer membranes were used for bridge implantation across 10-mm long median nerve defects in rats, and the outcome of peripheral nerve repair at 12 weeks post-implantation was evaluated by a combination of electrophysiological assessment, immunohistochemical and histological investigations.

### 5.1 Introduction

Despite over 150 years of experience in modern surgical management of the peripheral nerve, repair of a nerve gap remains a problem in microsurgery [1]. Usually, peripheral nerve injuries that result in gaps or defects require surgical implantation of a bridge or guidance channel between the proximal nerve end and the distal stump in order to restore full function and organ regeneration [2]. Autologous nerve grafts have been commonly used in bridging peripheral nerve defects [3, 4]. However, unavoidable disadvantages, such as the limited availability and donor-site morbidity of autografts, still remained. Although allografts have also been used, these were accompanied by the usual need for immunosuppression and have lower success rates [5]. Due to the shortcomings associated with these approaches to nerve repair, artificial NGCs have been widely accepted as a method to create a favorable micro-environment for nerve regeneration.

However, there are many requirements for an ideal nerve scaffold, including proper mechanical strength to avoid local guide collapse and detachment at guide/nerve interface, porosity in the range of few microns to allow nutrients exchange minimizing the infiltration of fibrous tissue, good biocompatibility to avoid inflammation and other adverse reactions, desirable degradable rate to avoid long-term foreign body existence and internal porous structures to encourage nerve fibers or cells to grow inside [6]. To satisfy these requires, a bi-layer CS flat membrane with CS/DSP film as inner layer and CS/GPTMS\_DSP as outer layer was developed. The two layers were selected on the basis of results reported in the second section of this thesis. In chapter 4, CS/DSP films were proved to enhance nerve fibre regeneration and functional recovery, obtaining results comparable to the autologous graft which is consider the gold standard technique, while CS/GPTMS\_DSP samples showed improved mechanical resistance under wet condition due to the presence of the covalent crosslinker (see chapter 2) and were found to be permeable to nutrients and biocompatible (see chapter 4). The composition of the bi-layer membrane was selected since the CS/DSP provides a substrate to promote cell adhesion, proliferation and migration as a template to guide the formation of new neural tissue and the CS/GPTMS\_DSP membrane works as a temporary scaffold, which imparts the desired mechanical strength to the conduits.

In this chapter the development of CS bi-layer membranes was described. The obtained membranes were analyzed for their physicochemical properties by FT-IR analysis and static contact angle measurements, their water stability was studied by swelling and dissolution tests in PBS, their mechanical properties were evaluated by tensile tests. Finally, conduits were fabricated by rolling the developed membranes to bridge the 10 mm defects in the median nerve of female Wistar rats, and autograft nerves were taken as positive controls.

## **5.2 Experimental**

### **5.2.1 Materials**

CS (medium molecular weight, 75%-85% deacetylation degree), GPTMS and DSP were supplied from Sigma Aldrich. All solvents used were of analytical grade and used without further purification.

### **5.2.2 Methods**

CS was dissolved in acetic acid solution 0.5 M at room temperature by continuous stirring to obtain a 2.5% (w/v) solution. Single (CS/DSP and CS/GPTMS25\_DSP) layer membranes were prepared according to the procedures described in paragraph 2.2.2. For the realization of CS/GPTMS25\_DSP membrane, the amount of GPTMS was decreased from 50% to 25% w/w compared to CS/GPTMS\_DSP samples (developed in chapter 2) with the final aim to reduce compositional differences and optimize the adhesion among the inner and outer side in the bi-layer structure.

Bi-layer flat membranes were prepared by a two-step coating technique. CS/DSP samples were obtained following the procedures described in chapter 2 and were used as the base component of the bi-layer films, whereas CS/GPTMS25\_DSP solutions were poured on top of them. Finally, samples were air-dried for 48 hours to obtain bi-layered membranes.

### 5.2.3 Sample characterization

#### 5.2.3.1 Fourier transform infrared-attenuated total reflectance spectroscopy (FTIR-ATR)

The FTIR-ATR spectra of CS/GPTMS25\_DSP, CS/DSP and bi-layer samples were recorded at room temperature in a Perkin Elmer Spectrometer in the range 2000-600  $\text{cm}^{-1}$  at a resolution of 4  $\text{cm}^{-1}$ .

#### 5.2.3.2 Surface wettability

The static contact angle of CS/DSP, CS/GPTMS25\_DSP and bi-layer films were measured at room temperature using a KSV instrument equipped with a CAM 200 software for data acquisition. Sessile drop method was applied, using a 5  $\mu\text{L}$  double distilled water droplet. For each angle reported, at least five measurements on different surface locations were measured and results were expressed as average value  $\pm$  standard deviation.

#### 5.2.3.3 Mechanical properties

The tensile mechanical properties were performed on wet flat membranes using MTS QTest/10 device equipped with load cells of 10 N, respectively. Rectangular strips of 30x10 mm size were cut from each films and strained to break at a constant crosshead speed of 2 mm/min. Prior to tensile testing, samples were immersed in PBS for 10 min at 25°C. Using the associated software Test Works, break stress and strain were determined. The elastic modulus was calculated from the slope of the linear portion of the stress–strain curve. To measure the thickness of the films, digital calibrator was used. Four specimens for each kind of material were tested. The results were expressed as average values  $\pm$  standard deviation.

#### 5.2.3.4 Swelling and dissolution tests

The swelling and dissolution behavior of single and double layer samples were evaluated by immersing the samples in PBS (pH 7.4) at 37°C. The swelling degree was measured after 1, 3, 6, 9 and 24 hours while the dissolution degree was evaluated after 1, 3, 5, 7, 14, 28 and 56 days. The swelling percentage was calculated as:

$$\Delta W_s (\%) = (W_s - W_0) / W_0 * 100$$

where  $W_0$  and  $W_s$  are the sample weights before and after swelling respectively. The dissolution percentage was calculated as:

$$\Delta W_d (\%) = (W_0 - W_d) / W_0 * 100$$

where  $W_d$  is the dried sample weight after dissolution. The solution pH was measured at the same time intervals during the swelling and the dissolution tests, and its stable value at around 7 (physiological pH) was verified. For each experimental time, three samples were measured and the results were expressed as averages value  $\pm$  standard deviation.

### 5.2.3.5 Permeability of bi-layer CS based membranes

Permeability of CS/DSP, CS/GPTMS25\_DSP25 and bi-layer membranes for FITC-labelled dextrans (Sigma Aldrich) of 4400 Da (FD-4) was determined following the procedure described in paragraph 4.2.3.1. Briefly, all samples were rolled and glued with a cyanoacrylate glue to obtained a tube closed to one end. A 10% w/v solution of FD-4 in PBS was prepared, and 180  $\mu$ l of the solution were inserted into the lumen, then the second opening was with a cyanoacrylate glue. The tube was then placed in 3 ml of PBS at pH 7.4, and FITC-dextran concentration in the incubation medium was assayed fluorimetrically (CARY 500 SCAN UV-VIS-NIR Spectrophotometer) after 1, 3, 6, 24, 48 and 96 hours. The FD-4 release concentration in the external PBS solution was reported as a percentage respect to the initial concentration (10% w/v) in the tube (Fig. 5.1). Five measures for samples were used and the data were reported as mean value and standard deviation. The concentration of FD-4 was calculated from the absorption values using the calibration curves that was prepared starting from FD-4 solution of known concentrations.

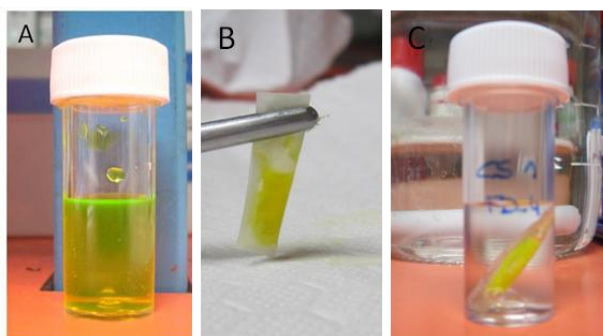


**Figure 5.1.** Sample preparation for permeability test: A) solution of FD-4 in PBS was prepared, B) CS/DSP, CS/GPTMS25\_DSP and bi-layer membranes were rolled and glued to obtained a tube and one end of the tube was closed with cyanoacrylate glue; FD-4 solution was inserted into the lumen, then the second opening was closed with a cyanoacrylate glue; C) the tubes was placed in PBS.

### 5.2.3.6 Preliminary *in vivo* tests

#### 5.2.3.6.1 Animals and surgery

*In vivo* nerve regeneration assay was carried out with CS/DSP, CS/GPTMS25\_DSP and bi-layer membranes. A total of 16 adult female Wistar rats weighing approximately 250 g at the start of the experiment were used. The animals were divided by three experimental groups of 4 animals each. The experimental groups were set according to treatment after nerve median crush injury. In three groups, the crushed median nerve was encircled by

CS/DSP, CS/GPTMS25\_DSP and bi-layered films. Finally, in an additional group, the median nerve was repaired with reversed autologous graft. The surgery procedure was the one previously described by Tos et al. [7]. After 12-weeks post-operative, rats were sacrificed: CS/GPTMS25\_DSP were found to be detached from the distal suturing site (Fig. 5.2F). For this reason, light and transmission electron microscope analysis was carried out on CS/DSP and bi-layer samples.

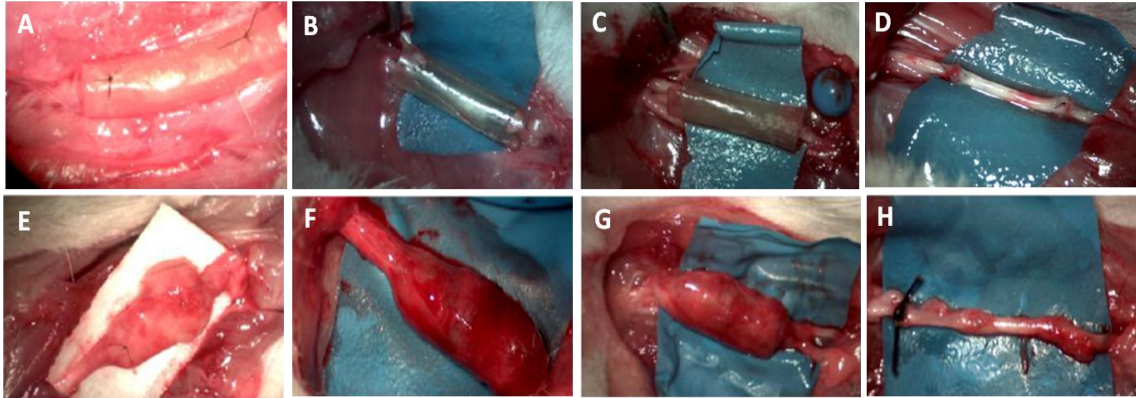


**Fig. 5.2** Pictures taken from CS/DSP (A, E), CS/GPTMS25\_DSP (B, F) and bi-layer (C, G) nerve conduits and autograft (D, F) in situ immediately after post-operative (A, B, C, D) and 12 weeks post-injury (E, F, G, H).

#### 5.2.3.6.2 Resin embedding and electron microscopy

After the 12-week follow-up time, animals were euthanized and a 10-mm long segment of the median nerve distal to the site of lesion was collected, fixed, and prepared for design-based stereological analysis of myelinated nerve fibers and for electron microscopy. Nerve samples were fixed by immediate immersion in 2.5% purified glutaraldehyde and 0.5% saccarose in 0.1 M Sorensen phosphate buffer for 6–8 hours. Specimens were then washed in a solution containing 1.5% saccarose in 0.1 M Sorensen phosphate buffer, post-fixed in 1% osmium tetroxide, dehydrated and embedded in resin. From each nerve, series of semi-thin transverse sections (2- $\mu$ m thickness) were cut starting from the distal stump of each median nerve specimen, using an Ultracut UCT ultramicrotome (Leica Microsystems, Wetzlar, Germany) and stained using Toluidine blue for high resolution light microscopy examination and design-based stereology. For transmission electron microscopy, ultra-thin sections (50–90-nm thick) were cut using the same ultramicrotome and stained with saturated aqueous solution of uranyl acetate and lead citrate. Ultra-thin sections were analyzed using a JEM-1010 transmission electron microscope (JEOL, Tokyo, Japan).

### 5.2.3.6.3 Immunohistochemistry and confocal laser microscopy

From all animals, a 3-mm long nerve specimen withdrawn proximal to the segment was used for resin embedding, was fixed in PAF 4% and PBS and routinely embedded in paraffin for immunohistochemistry and confocal laser microscopy. Series of 8–10  $\mu\text{m}$  thick sections were cut by a RM2135 microtome (Leica Microsystems, Wetzlar, Germany). Sections were then incubated overnight in a solution containing  $\alpha$ -NF-200kD primary antibody (monoclonal, mouse, which recognizes the 200 kD subunit of neurofilaments, dilution 1:200, Sigma) and then, after washing in PBS, incubated for 1h in a solution containing TRITC-conjugated anti-rabbit IgG (dilution 1:200, Dako). The sections were finally mounted with a Dako fluorescent mounting medium and analyzed by a LSM 510 confocal laser microscopy system (Zeiss, Jena, Germany), which incorporates two lasers (Argon and HeNe) and is equipped with an inverted Axiovert 100M microscope. To visualize TRITC, we used excitation from 543 nm HeNe laser line and emission passing through a high-pass (LP) 560 filter which passes wavelengths superior to 560 nm to the detector.

### 5.2.3.7 Statistics

Experiments were repeated three times and results expressed as a mean  $\pm$  standard deviation. Statistical analysis was carried out using single-factor analysis of variance (ANOVA) post hoc Bonferroni. Values of  $*p \leq 0.05$ ,  $**p \leq 0.01$ ,  $***p \leq 0.001$  were considered as statistically significant. For *in vivo* tests, the number of animals used in the experiments (16) was calculated in order to meet the Ethical Committee requirements for a minimum number of animals used with the 'Three Rs' (replacement, reduction and refinement of animal studies) concept put forward by Russel and Burch and adopted by the European Community.

## 5.3 Results and discussion

### 5.3.1 Fourier transform infrared-attenuated total reflectance spectroscopy (FTIR-ATR)

In fig. 5.3 the FTIR-ATR spectra of CS based film samples are reported. CS/DSP, CS/GPTMS25\_DSP, internal and external side bi-layer spectra showed the characteristics bands of both CS and DSP, as described at paragraphs 2.3.2. In details, the peak at  $1674\text{ cm}^{-1}$ ,  $1542\text{ cm}^{-1}$  and  $1414\text{ cm}^{-1}$  were associated respectively to the C=O stretching bond, the amide and amine bending vibrations and O-H bending vibrations typical of CS. DSP crosslinking was confirmed by the detection of bands at  $1000\text{ cm}^{-1}$  and at  $989\text{ cm}^{-1}$  and  $943\text{ cm}^{-1}$  due to the  $\text{PO}_3$  out-of-phase and in-phase stretching; typical absorption peaks at  $861\text{ cm}^{-1}$  and at  $814\text{ cm}^{-1}$  were associated with P-OH stretching and P-O-P asymmetric stretching vibration, respectively [8]. Moreover, the CS/GPTMS25\_DSP and external side of the bi-layer FTIR-ATR spectrum showed bands at  $1196\text{ cm}^{-1}$  due to the Si-O-Si bonds of the covalent crosslinking chains, confirming the successful crosslinking of CS by GPTMS.

The absorption band at  $1720\text{ cm}^{-1}$  was observed in all spectra and could be attributed to the stretching vibration of C=O groups, probably due to acetic acid residuals [9].

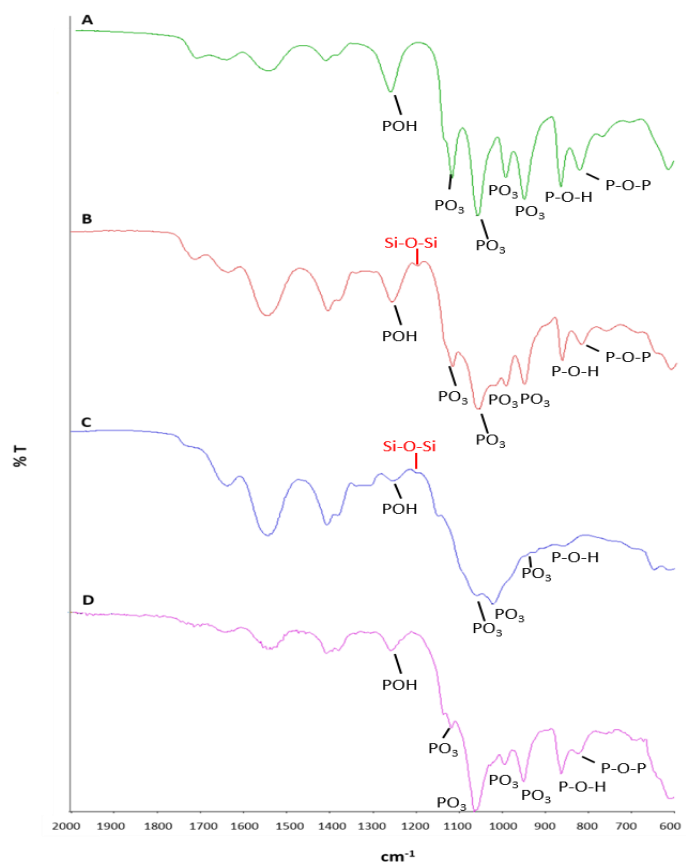


**Fig. 5.3.** FTIR-ATR spectra of CS/DSP (A), CS/GPTMS25\_DSP (B), external (C) and internal side (D) bilayer membrane.

### 5.3.2 Surface wettability

The static water contact angles of model CS/DSP, CS/GPTMS25\_DSP, internal and external side of bi-layer samples are reported in Fig. 5.4. The average contact angles of CS/DSP and CS/GPTMS\_DSP were  $66^\circ \pm 9^\circ$  and  $65^\circ \pm 11^\circ$ , respectively. The development of a double layer flat membranes significantly modified the wettability of the inner layer as compared to CS/DSP and CS/GPTMS\_DSP25 films. Static water contact angles of the internal and external side of the bi-layer samples were also significantly different ( $41^\circ \pm 9^\circ$  for inner and  $64^\circ \pm 16^\circ$  for outer layer).

The enhanced hydrophilicity of the internal part of the double layer membrane could be attributed to the physicochemical interactions between the inner and outer layer that occurs during the fabrication process that increased the amount of phosphate groups and consequently the surface wettability. The measured contact angle of the bi-layer flat membrane could favour cell attachment on the studied materials [10, 11].

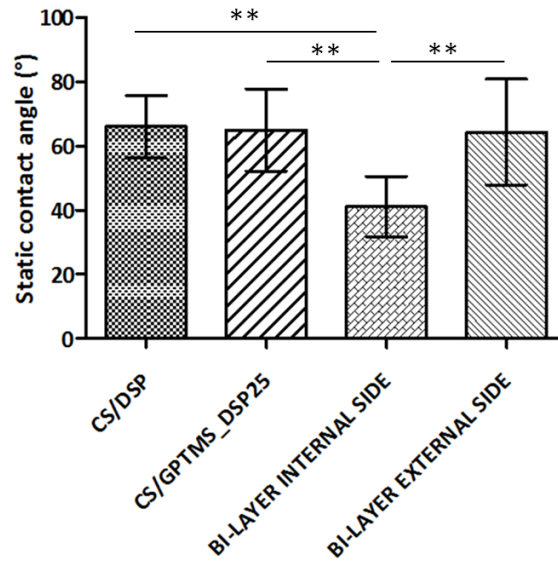


**Fig. 5.4** Static water contact angle of CS/DSP, CS/GPTMS25\_DSP, internal and external side of bi-layered film samples. Histograms reported the average values and the standard deviations. \*\*p<0.01.

### 5.3.3 Mechanical properties

CS based samples were tested under wet state since wet membranes are flexible enough to be rolled up to fabricate hollow guide. All specimens showed an elasto-plastic behaviour; the  $\sigma$ - $\epsilon$  slope was calculated to obtain the elastic modulus. Wet CS/GPTMS25\_DSP and CS/DSP samples had a uniform thickness in the range of 90-130  $\mu\text{m}$  while bi-layer membrane showed thickness values within 300-350  $\mu\text{m}$ . The presence of GPTMS enhanced the E values (E, from  $3.47 \pm 1.06$  MPa for CS/DSP to  $9.29 \pm 0.85$  MPa and  $11.01 \pm 2.08$  MPa for CS/GPTMS25\_DSP and bi-layer respectively); the increment of the elastic modulus of CS/GPTMS25\_DSP and bi-layer samples (statistical significant compared to CS/DSP samples, \*\*p<0.01 and \*\*\*p<0.001) was a consequence of the mechanical reinforcement associated with covalent crosslinking process and indicated the superior elastic behaviour of CS/GPTMS25\_DSP and double layer membranes compared to the ionic crosslinked samples. No significant differences were observed between CS/GPTMS25\_DSP and bi-layer. Moreover, the developed bi-layer samples showed an intermediate behaviour in terms of elongation at break compared to CS/GPTMS25\_DSP and CS/DSP (Fig. 5.5), indicating that the double layer is a highly elastic and resistant membrane, properties imparted by the CS/DSP internal side and CS/GPTMS25\_DSP external side respectively.

Biomaterials used to fabricate NGCs are expected to possess mechanical flexibility to favour their surgical application and the *in vivo* permanence in the body and to not collapse under compression during axonal outgrowth. The elastic modulus of the mouse sciatic nerve has been reported to be 7 MPa [12]. A nerve guide able to mimic the behaviour of the natural nerve tissue should possess a similar elastic modulus. In this work, elastic modulus values of around 10 MPa were measured for CS/GPTMS25\_DSP and bi-layer samples and showed superior mechanical properties respect to CS/DSP samples.

Moreover, the development of a bi-layer membranes allowed to improve the elongation at break compared with CS/GPTMS25\_DSP. Additionally, all the crosslinked scaffolds could be easily wrapped around the trunked nerve stumps, allowing the use of the different typologies of membranes for the preparation of NGCs during the surgical intervention and with the appropriate diameter size depending on the treated nerve size (data not shown).

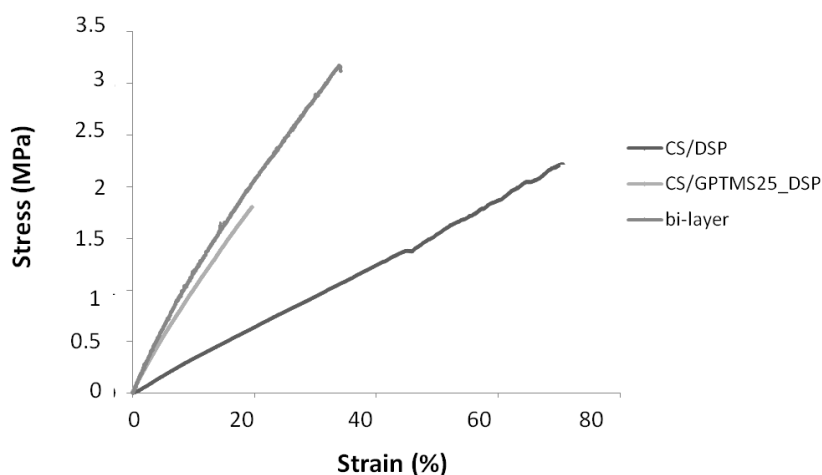


**Fig. 5.5** Stress-strain curves of the CS/DSP, CS/GPTMS25\_DSP and bi-layer flat membranes tested in wet state.

### 5.3.4 Swelling and dissolution tests

The CS based membranes prepared by solvent casting increased their weight when immersed in PBS and after 1 hour the water uptake was around 530%, 70% and 135% for CS/DSP, CS/GPTMS25\_DSP and bi-layer samples, respectively (Fig. 5.6). The CS/GPTMS25\_DSP and CS/DSP swelling values stabilized after 3 hours, while a slightly and continuous increase was measured for the bi-layer membranes reaching a water uptake value of around 130% after 24 hours. This gradual increase in swelling degree could be attributed to the higher thickness of the double layer membranes compared to single layers which slows down the water absorption in time. Moreover, an intermediate value of water uptake for the bi-layer membranes was observed and could be associated to the combination of single component behaviour: the high swelling degree attributed to the presence of phosphate groups for the inner layer and the moderate water absorption capacity of the external layer due to the presence of a GPTMS (see paragraphs 2.3.4). A comparison of the swelling percentage of CS based samples revealed that the water uptake of CS/DSP samples was significantly higher than for CS/GPTMS25\_DSP and bi-layer specimens at each time point (\*\* $p < 0.001$ ).

The dissolution profiles of CS based samples after 56 days of immersion in PBS are presented in Fig. 5.7. All membranes decreased their weight of  $44.6 \pm 5.6$  %,  $34.5 \pm 1.9$  % and  $38.2 \pm 5.2$  % for the CS/DSP, the CS/GPTMS25\_DSP and the bi-layer after 1 day incubation in PBS. CS/GPTMS25\_DSP samples showed significant lower weight loss

respect to CS/DSP specimens at this time point. The initial high weight loss was due to the release of salts into PBS solution, as described in chapter 2. CS/DSP, CS/GPTMS25\_DSP and bi-layer weight loss reached final values of  $67.3 \pm 6.6\%$ ,  $54.7 \pm 1.5\%$  and  $54.2 \pm 3.6\%$  after 56 days incubation in PBS. Compared to the CS/DSP membranes, chemical crosslinking by the addition of GPTMS agents enhanced the stability in aqueous media of CS/GPTMS25\_DSP and bi-layer membranes.

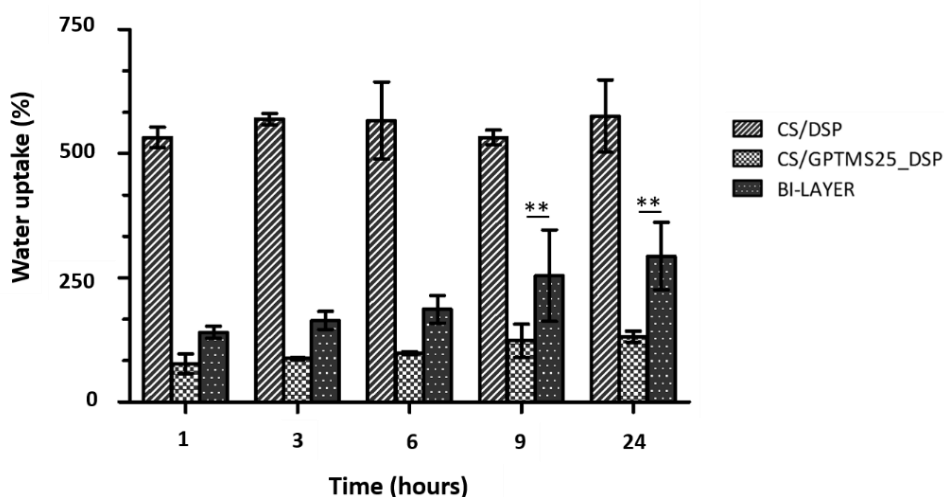


**Fig. 5.6.** Swelling degree of CS/DSP, CS/GPTMS25\_DSP and bi-layer flat membranes in PBS as a function of time. Column heights correspond to the mean values. Bars indicate standard deviations ( $n = 3$ ). \* $p < 0.05$ , \*\* $p < 0.001$ .

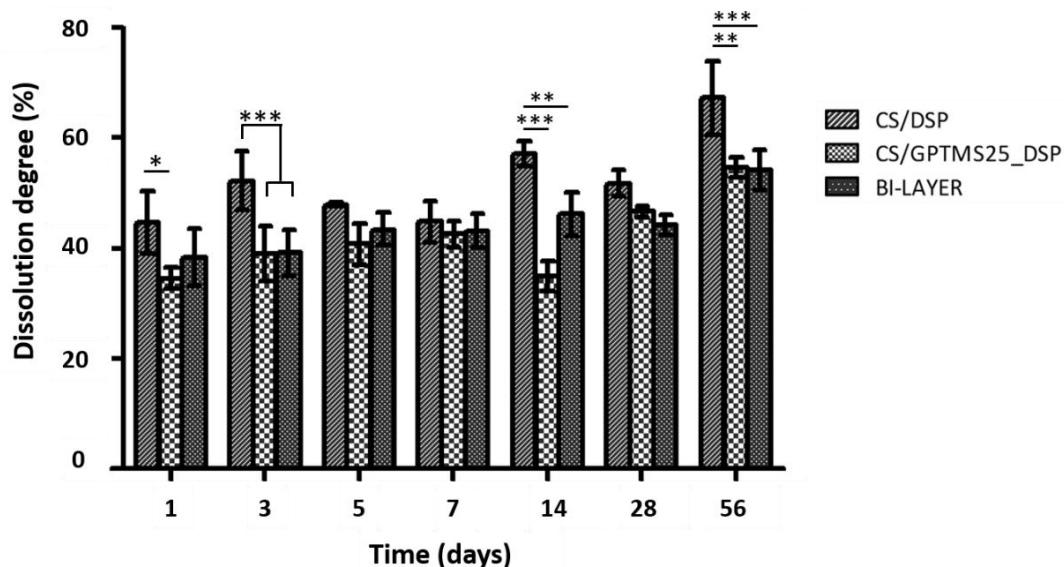


**Fig. 5.7.** Dissolution degree of CS/DSP, CS/GPTMS25\_DSP and bi-layer samples in PBS as a function of time. Columns are the average values; bars represent the standard deviation. \* $p < 0.05$ , \*\* $p < 0.001$  and \*\*\* $p < 0.001$ .

### 5.3.5 Permeability of bi-layer CS based membranes

Fig. 5.8 reports the release concentration of the FD-4 in the PBS after 1, 3, 6, 24, 48 and 96 hours. Results showed that the different structures (single or bi-layer) influenced the FD-4 release kinetics. The release of FD-4 from CS/DSP and CS/GPTMS25\_DSP tubes was characterized by an initial burst release (about 50% and 65% for CD/DSP and CS/GPTMS25\_DSP respectively) from the inside to the outside of conduits which was followed by a sustained release stage of FD-4 contained into CS tubes, reaching a final value of around 80% of model molecule released in 96 hours for both the single layer samples. No significant differences were observed between CS/DSP and CS/GPTMS25\_DSP membranes at each time point. As regard bi-layer samples, a more gradual and controlled release of FD-4 was observed in time. In detail, multi-layer tubes released about 28% of the model molecule in the earlier time (6 hours) of incubation in PBS. Then, a burst release was observed from 24 hours reaching a FD-4 release value of about 72% after 4 days (96 hours). This behavior can be ascribed to the higher thickness of double layer specimens compared to CS/DSP and CS/GPTMS25\_DSP conduits which slows down the penetration of the FD-4 inside the bi-layer tubes after PBS absorption during CS swelling, as observed in paragraph 5.3.4. However, no significant difference of model molecule release was observed between the different typologies of structure (single and by-layer) after 96 hours of immersion in PBS confirming the permeability of the bi-layer membrane for solutes and nutrients.

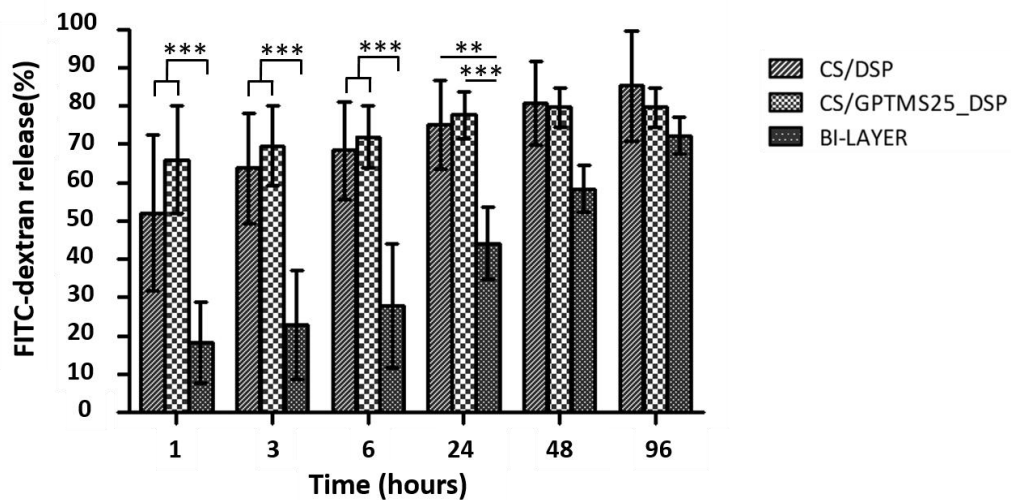


**Fig. 5.8.** FITC–dextran release concentration in the incubation medium reported as a percentage respect to the dextran initially loaded into the tube. Columns are the average values; bars represent the standard deviation (n = 4). \*p < 0.05, \*\*p < 0.01 and \*\*\*p < 0.001.

### 5.3.6 Preliminary *in vivo* tests

All procedures were performed in accordance with the Ethics Committee and the European Communities Council Directive of 24 November 1986 (86/609/ EEC).

### 5.3.6.1 Light and transmission electron microscope analysis

Fig. 5.9 shows high-resolution light photomicrographs of rat median nerves injured, treated with reversed autologous graft or encircled by CS/DSP (previously described in paragraph 4.3.1.2.6.2) or by bi-layer flat membranes and harvested at 12 weeks post-operative. From each nerve, series of semi-thin transverse sections (2- $\mu$ m thickness) were cut starting from the distal stump of each median nerve specimen and stained using Toluidine blue. Distal median nerves treated with CS/GPTMS25\_DSP were not harvested because conduits were found to be detached from the distal suturing site (Fig. 5.2F). Small myelinated axons and microfasciculation typical of regenerated nerve fibers were detected on samples treated with bi-layer membranes through light microscopy observation. These results were comparable to nerve regenerated using autologous graft (Fig. 5.9A, B) and CS/DSP (Fig. 5.9C, D) (see chapter 4). As described in paragraph 4.3.1.2.6.2, small nerve fibers at different myelination stages were detected both on the median nerve encircled with CS/DSP (Fig 5.10A, D, H) or repaired with reversed autologous graft (Fig. 5.10B, E, H) through transmission electron microscopy observations. Nerve treated with bi-layer membranes showed unmyelinated (Fig. 5.10F) and myelinated fibers (Fig.5.10I) which organized into small bundles following the perineural cells activity (Fig. 5.10 C, I).

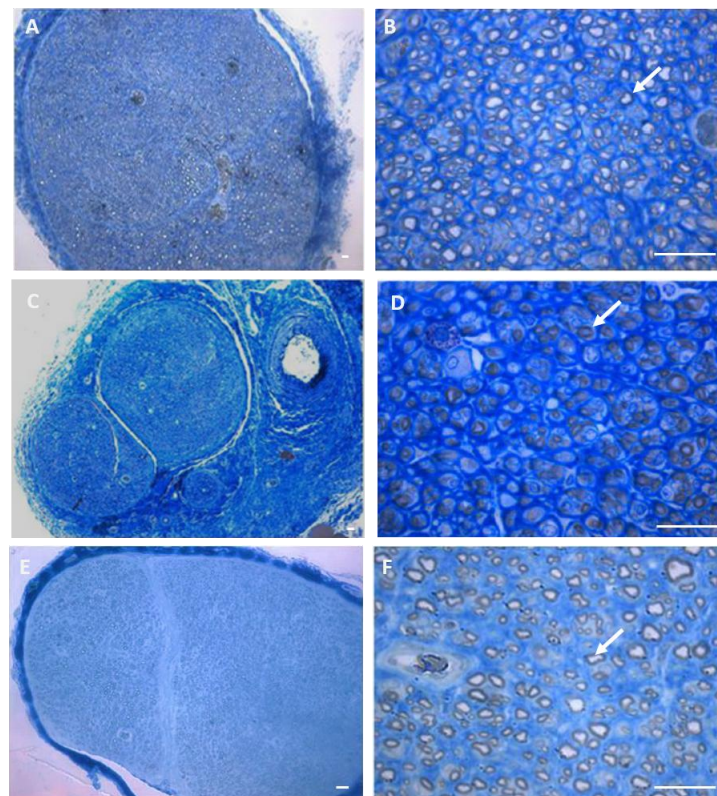


**Fig. 5.9** Photomicrographs of semi-thin sections cut transversely to the main axis of treated median nerves using autologous graft (A,B), CS/DSP (C, D) and bi-layer membranes (E, F) after 12 weeks post- operative. White arrows indicated the presence of myelinated axons. Scale bar: 20  $\mu$ m.

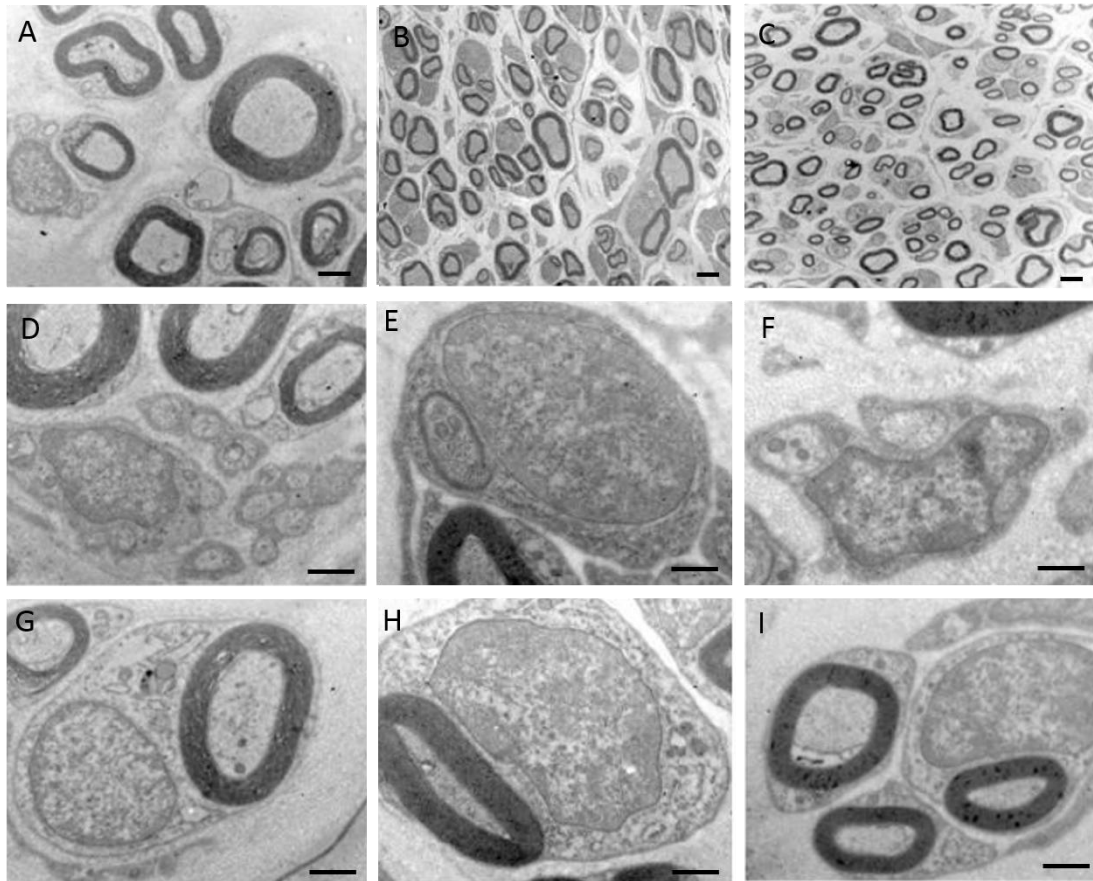


**Fig. 5.10** Electron microscope images of regenerated nerves treated using CS/DSP (A, D, G), autologous graft (B, E, H) and bi-layer membranes (C, F, I) after 12 weeks post-operative. Scale bars: 1  $\mu$ m.

### 5.3.6.2 Immunohistochemistry and confocal laser microscopy

Axonal regeneration onto bi-layer, CS/DSP and CS/GPTMS25\_DSP conduits was examined by confocal laser microscopy on longitudinal nerve frozen sections (Fig. 5.11) after NF staining. After 12-week post-operative, in middle segments of regenerated nerves, all samples exhibited a densely population of NF axons. Properly linearly alignment of NF axons was observed in CS/DSP (Fig. 5.11B) and bi-layer (Fig. 5.11C) while CS/GPTMS25\_DSP treated rats (Fig. 5.11A) displayed poor axonal regeneration and disordered orientation in the longitudinal sections. Moreover, an increase of axon alignment was observed for bi-layer membranes compared to CS/DSP single layer. These results allows to confirm that the presence of CS/DSP internal side of the bi-layer structure could be beneficial for axon regeneration from the proximal to the distal stump.

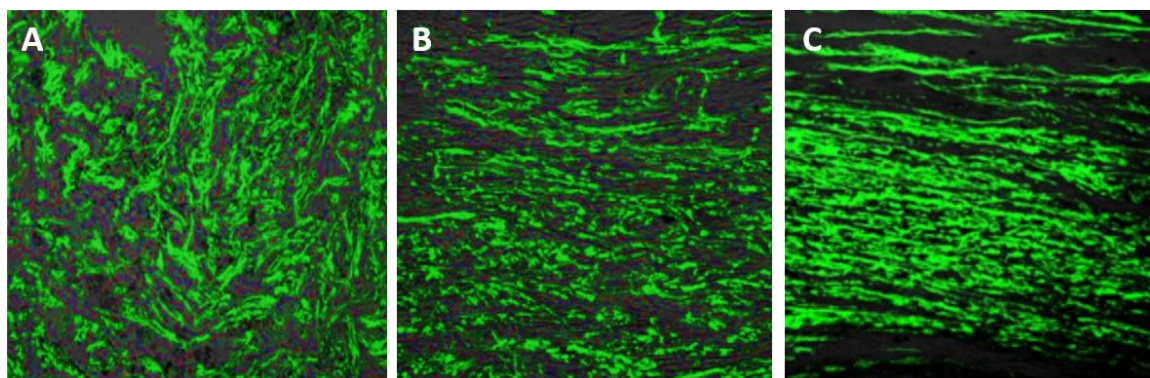


**Fig. 5.11** Neurofilament staining on longitudinal sections at 12 weeks revealed that bi-layer, CS/DSP and CS/GPTMS\_DSP were densely populated with axons. Properly linearly aligned NF axons were found in CS/DSP (B) and bi-layer (C) while CS/GPTMS25\_DSP displayed axons that were haphazardly oriented and disorder (A).

#### 5.4 Conclusion

In the present study, a novel bi-layer flat membrane based on CS was developed to enhance peripheral nerve regeneration. The bi-layer was composed of a CS/DSP inner layer and a CS/GPTMS25\_DSP outer layer with the aim to improve nerve regeneration at the internal site and to impart the desired mechanical strength to the membrane. The scaffold was fabricated by a two-step coating technique where one layer was formed for solvent casting and then the polymer solution of the second layer is poured directly on top of the previously dried layer. In the present case, CS/DSP film was used as the base component of the bi-layer membrane, whereas CS/GPTMS25\_DSP solution was poured on top of it and left dried. CS/DSP and CS/GPTMS25\_DSP single layer were used as controls.

The physico-chemical results showed that the two single layers interact during the double-layer fabrication process: an increase in the surface wettability of the structure was observed and could be associated to the strong hydrogen bonding and the higher amount of phosphate groups. The bi-layer samples tested under wet condition showed improved mechanical properties compared with the CS/DSP and higher elongation at break characteristic of CS/DSP film was also observed. Bi-layer samples permeation to small molecules and an intermediate swelling degree compared to the single layers. Finally, preliminary *in vivo* tests were carried out on the bi-layers fat membranes for bridge implantation across 10-mm long median nerve defects in rats. After 12 weeks post-operative, nerves treated with bi-layer tubes displayed regenerated and aligned fibers at the injury site through light and transmission electron microscopy and observation as well as immunohistochemistry analysis.

These attractive results, together with all the previous reported positive characteristics of CS/DSP and CS/GPTMS\_DSP based conduit (see chapter 2 and 4) indicate that the double-layer CS based conduit should be investigated further as a guide conduit for promoting peripheral nerve regeneration.

## References

1. Suematsu, N., Tubulation for Peripheral-Nerve Gap - Its History and Possibility. *Microsurgery*, 1989. **10**(1): p. 71-74.
2. Heath, C.A. and G.E. Rutkowski, The development of bioartificial nerve grafts for peripheral-nerve regeneration. *Trends in Biotechnology*, 1998. **16**(4): p. 163-168.
3. Ignatiadis, I.A., et al., Diverse types of epineural conduits for bridging short nerve defects. An experimental study in the rabbit. *Microsurgery*, 2007. **27**(2): p. 98-104.
4. Calver, J.S. and R.W. Norris, Results of Mixed Peripheral-Nerve Repair in Humans Using Freeze-Thawed Skeletal-Muscle Autografts - Discussion. *Journal of Reconstructive Microsurgery*, 1994. **10**(6): p. 438-439.
5. Mackinnon, S.E., et al., The Peripheral-Nerve Allograft - an Assessment of Regeneration in the Immunosuppressed Host. *Plastic and Reconstructive Surgery*, 1987. **79**(3): p. 436-444.
6. Schmidt, C.E. and J.B. Leach, Neural tissue engineering: Strategies for repair and regeneration. *Annual Review of Biomedical Engineering*, 2003. **5**: p. 293-347.
7. Tos, P., et al., Employment of the mouse median nerve model for the experimental assessment of peripheral nerve regeneration. *J Neurosci Methods*, 2008. **169**(1): p. 119-27.
8. Larkin, J., INFRARED AND RAMAN SPETROSCOPY PRINCIPLES AND SPECTRAL INTERPRETATION, ed. s. edition. 2011: ELSEVIER.
9. Kato, M., et al., Synthesis of organosiloxane-based inorganic/organic hybrid membranes with chemically bound phosphonic acid for proton-conductors. *Electrochimica Acta*, 2007. **52**(19): p. 5924-5931.
10. van Wachem, P.B., et al., Interaction of cultured human endothelial cells with polymeric surfaces of different wettabilities. *Biomaterials*, 1985. **6**(6): p. 403-8.
11. Bumgardner, J.D., et al., Contact angle, protein adsorption and osteoblast precursor cell attachment to chitosan coatings bonded to titanium. *Journal of Biomaterials Science-Polymer Edition*, 2003. **14**(12): p. 1401-1409.
12. Wong, J.Y., J.B. Leach, and X.Q. Brown, Balance of chemistry, topography, and mechanics at the cell-biomaterial interface: Issues and challenges for assessing the role of substrate mechanics on cell response. *Surface Science*, 2004. **570**(1-2): p. 119-133.

# Chapter 6

## CS electrospun nanofibres for nerve tissue engineering

### Abstract

Polymeric nanofibres that mimic the structure and function of the native extracellular matrix (ECM) are of great interest in tissue engineering as scaffolding materials. Chitosan (CS) has been investigated for biomedical applications because of its good biocompatibility, biodegradability, and wound healing effect. In this work, CS based nanofibers were fabricated by electrospinning solutions containing CS, polyethylene oxide (PEO), and dimethyl sulfoxide (DMSO). Spinnable CS-based solution was prepared by dissolving CS and PEO in 0.5M acetic acid with a concentration of 5% and 3% (w/v), respectively. Then, the two solutions (CS and PEO) were mixed in order to obtain blends with volume ratios of 50/50 and finally 5% (v/v) of DMSO was added. The set of electrospinning parameters composed by a voltage of 30 kV, a 30  $\mu$ L/min flow rate and a temperature of 37 – 39 °C allowed to obtain homogenous nanofibres with an average fiber diameter of 120 nm. Lastly, dibasic sodium phosphate (DSP) was introduced into CS based solution as ionic crosslinker to improve the mechanical and physiological stability of the developed nanofibres and to neutralize the electrospun membranes. Crosslinked nanofibres showed an increase in the mechanical strength (E, from 63 $\pm$ 10 MPa to 113 $\pm$ 8 MPa) and on water stability until 7 days in aqueous environment compared to uncrosslinked CS nanofibres.

### 6.1 Introduction

In artificial nerve guidance conduits (NGCs) designed, it is essential to introduce an internal filler for large nerve gaps (> 30 mm in humans). Internal fillers act as a physical axonal guidance enhancing the regeneration process and the functional recovery of injured nerves [1]. Fibrous substrates have gained increased interest in recent years since they mimic the structure of the ECM. Random or aligned fibrous matrices with fibre diameters ranging from tens of nanometres to several microns can be easily prepared by electrospinning [2-4] which is a simple and versatile method, which allows the deposition

of nanofibrous mats through the extrusion of the solution from a needle by an high voltage electric field. By tuning electrospinning processing parameters is possible to modify fibres morphology and dimension to maximize the morphology- mediated cellular response [3].

In nerve regeneration, the choice of an appropriate biomaterial is essential to satisfy the requirements of a proper biological response and scaffold processability. Among currently available polymers, natural polymers, such as proteins (gelatin, collagen and silk fibroin) and polysaccharides (chitosan, hyaluronic acid and cellulose) are functionally superior to non- informational synthetic polymers: as components of natural ECM or having a similar composition to ECM components, natural polymers provide chemical cues which facilitate cell attachment [5].

As discussed in previous chapters, CS offers many advantages and it is a promising material for TE applications (see chapter 1 and 3). The possibility to fabricate nanofibrous scaffold through electrospinning using CS have few drawbacks since processing conditions have to be carefully selected as the use of high temperatures and organic solvents may cause CS denaturation [6]. On the other hand, CS electrospinning is also critical due to the relative high viscosity of CS solutions, which limits the spinnability [7].

Studies reported in literature strongly suggest that nanofibre-based scaffolds hold a great potential as a new class of synthetic NGCs for repairing peripheral nerve injuries and defects *in vivo* since CS nanofibers not only promoted the adhesion of Schwann cells, but also helped to maintain their characteristic cell morphology and cell phenotype, providing a new class of scaffolds for neural tissue engineering [8].

Although many studies have been reported, the use of electrospun nanofibres remains largely unexplored and further experiments are necessary to define the effect of CS nanofibres on peripheral nerve repair.

In this work, CS based solution were electrospun to produce internal filler for NGCs. Low amounts of acetic acid (0.5M) were applied for CS solubilization in order to reduce the risk of polymer degradation and citotoxicity. Different blends of medical grade highly deacetylated chitosan (CS M.G.) and polyethylene oxide (PEO) were analyzed in order to identify the ideal solution for the deposition of homogeneous and uniform nanofibres suitable for peripheral nerve regeneration. PEO solution (3% w/v) and CS solutions (ranging from 3 to 7% w/v) were prepared separately by dissolving CS and PEO in 0.5M acetic acid. Then, the two solutions (CS M.G. and PEO) were mixed in order to obtain blends with volume ratios of 50/50. Among the mixtures analysed, the optimal nanofibrous scaffolds were obtained electrospinning the blend CS/PEO 50/50 vol/vol with a CS concentration of 5% w/v. Furthermore, the influence of different process parameters on fibre deposition and morphology was analyzed. Moreover, dibasic sodium phosphate (DSP) was used as CS crosslinker to increase the nanofibres stability in aqueous environment and to neutralize the electrospun membrane. The crosslinked nanofibrous mats developed were characterized from a physicochemical point of view, through

infrared spectroscopy (FTIR) analysis, then thermal, mechanical and dissolution properties were studied by thermogravimetric analysis, tensile and dissolution tests.

## **6.2 Experimental**

### **6.2.1 Materials**

Medical grade CS (molecular weight 200 – 400 kDa, deacetylation degree  $\geq 92.6\%$ ) was purchased by Kraeber GmbH & Co. PEO ( $M_w$  900000 Da), DSP, DMSO and solvents were supplied from Sigma Aldrich. All solvents used were of analytical grade and used without further purification.

### **6.2.2 Electrospun membrane preparation**

#### **6.2.2.1 Preparation of solutions for electrospinning**

3, 5 or 7 % (wt/vol) CS and 3% (wt/vol) PEO solutions were prepared separately by dissolving CS or PEO in 0.5M acetic acid solution at room temperature by continuous stirring. After complete solubilisation of each components, a 50/50 (v/v) CS/PEO solution was prepared by mixing equal volumes of CS and PEO solutions to obtain the mixtures with weight ratios of CS to PEO of 50/50, 62/38 and 70/30; the resultant mixtures were kept under stirring for about 2 hours. A 5% (v/v) of DMSO was added to the CS/PEO solution as a cosolvent to relax CS chain entanglements and increase the fiber yields and consequently improving the spinnability of the CS-based solution [9]. Finally, ionically crosslinked samples were prepared by adding DSP 1M (one drop per second) to the CS/PEO solution with a concentration of 7.5 % vol./vol. with respect to the natural polymer solution volume as previously described (Chapter 2). The CS/PEO\_DSP mixed solution was maintained under magnetic stirring at room temperature for about 10 minutes. Not crosslinked solutions were prepared as control.

#### **6.2.2.2 Electrospinning of CS nanofibres**

The electrospinning system used for fibre preparation was previously described [10]. Briefly, the system consists of a high voltage generator (PS/EL30R01.5-22 Glassman High Voltage), providing a voltage of 0 to 30 kV; a volumetric pump (KDS210 of KD Scientific); a mobile syringe support and a 1.5 mm-thick flat aluminium collector for random fibres.

### **6.2.3 Membrane preparation and optimization of solution and process parameters**

#### **6.2.3.1 Solution parameters and viscosity tests**

Preliminary tests were performed to optimize CS based solution concentration. Different CS concentrations were tested (3%, 5% and 7%) using a MCR302, Anton Paar GmbH rheometer having 50 mm parallel plate and a temperature controller. Measurements were performed by pouring 5 ml of solution on pre-heated plate (40°C), then the shear rate was set in the range of 1 to 100  $s^{-1}$ .

### **6.2.3.2 Process parameters**

Continuous nanofibres were obtained only for 5% CS solution concentration while process parameters (62/38 w/w CS/PEO mixture) were varied to reduce fibre defects and maximize the amount of collected fibres. The parameter values allowing spinnability were: (i) temperature from 25 °C to 39°C, (ii) flow rate of 25  $\mu\text{l min}^{-1}$  to 50  $\mu\text{l min}^{-1}$ , (iii) nozzle-collector distance of 12 cm and (iv) voltage of 30 kV. The effect of temperature and flow rate was evaluated to optimize the process and the fibre morphology.

### **6.2.3.3 Fibres morphology and element distribution**

The surface morphology of crosslinked and uncrosslinked CS based nanofibrous membranes was observed by scanning electron microscopy (SEM LEO – 1430, Zeiss). Qualitative compositional analysis and punctual elemental composition of materials were performed using an energy dispersive spectrometer (EDS). Samples were sputter coated with gold in a undervacuum chamber prior to SEM-EDS examination. SEM micrographs were then analysed through ImageJ software. Fibre diameters and pore size were measured on three different images and they were reported as average value  $\pm$  standard deviation.

### **6.2.4 Electrospun membranes characterization**

#### **6.2.4.1 Fourier transform infrared-attenuated total reflectance spectroscopy (FTIR-ATR)**

FTIR-ATR spectra of CS, PEO, CS/PEO, CS/PEO\_DSP electrospun matrices were recorded at room temperature in a Perkin Elmer Spectrometer in the range 4000-600  $\text{cm}^{-1}$  at a resolution of 4  $\text{cm}^{-1}$ .

#### **6.2.4.2 Thermogravimetric analysis (TGA)**

Thermogravimetric analysis was performed using a TA INSTRUMENT Q500 equipment. Thermal degradation was measured on a 10-15 mg sample in aluminum pans under a dynamic nitrogen atmosphere between 40°C and 800 C. The experiments were run at a scanning rate of 10°C/min and obtained results were analyzed using TA Universal Analysis software. Three samples were analyzed both compositions.

#### **6.2.4.3 Mechanical properties**

The tensile mechanical properties were evaluated on crosslinked and uncrosslinked CS-based nanofibrous scaffolds in dry condition using a MTS QTest/10 device equipped with load cells of 10N. Rectangular specimens of 30x5 mm size were cut from each membranes and their thickness were measured using a digital calibrator. Samples were then strained at a constant crosshead speed of 1 mm/min until breaking. Break stress and strain were determined using the associated software Test Works 4 while the elastic

moduli (E) were calculated from the slope of the linear portion of the stress–strain curve of each sample. Five specimens for each kind of material were tested. The results were expressed as an average values  $\pm$  standard deviation

#### **6.2.4.4 Fibres dissolution**

The dissolution behavior of the uncrosslinked and crosslinked CS samples was evaluated by immersing the samples in PBS (pH 7.4) at 37°C. Qualitative tests after immersion were performed analyzing the nanofibres morphology by SEM. For each sample, five rectangular nanofibrous membranes deposited on the rectangular metal collector (1 cm x 3 cm) were soaked in 5 ml of PBS and maintained at 37°C. After 1, 24 and 168 hours, samples were collected, freeze-dried and then analyzed by SEM.

Quantitative analysis were performed on crosslinked CS based nanofibres. After 1, 3, 5, 7 days immersions, samples were dried and the dissolution percentage was calculated as:

$$\Delta W_d (\%) = (W_0 - W_d) / W_0 * 100$$

where  $W_0$  and  $W_d$  are the sample weights before and after degradation respectively.

The solution pH was measured at the same time intervals during the dissolution tests confirming a stable value at around 7.2 (physiological pH). For each experimental time, three samples were measured and the results were expressed as averages value  $\pm$  standard deviation.

#### **6.2.5 Statistical Analysis**

Statistical analysis was performed applying t-Student for two group comparisons and one-way ANOVA for multiple analysis using GraphPad Prism 6.0 software. Data were considered statistically difference for p value < 0.05.

### **6.3 Results and discussion**

#### **6.3.1 Optimization of the electrospinning parameters**

##### **6.3.1.1 Solution viscosity and its effect on electrospun nanofibres**

The effect of CS solution concentration on viscosity and, consequently, spinnability was evaluated. The three mixed solutions showed a non-newtonian behavior and an increase in viscosity for more concentrate CS solutions (Fig.6.1). Homogenous nanofibres were obtained only for CS/PEO solutions obtained with a 5% CS solution (Fig 6.2B), while less viscous solution (3% CS) caused the formation on beads instead of fibres (Fig. 6.2A) and highly concentrated CS solution impeded the flow of the solution from the needle (Fig 6.2C).

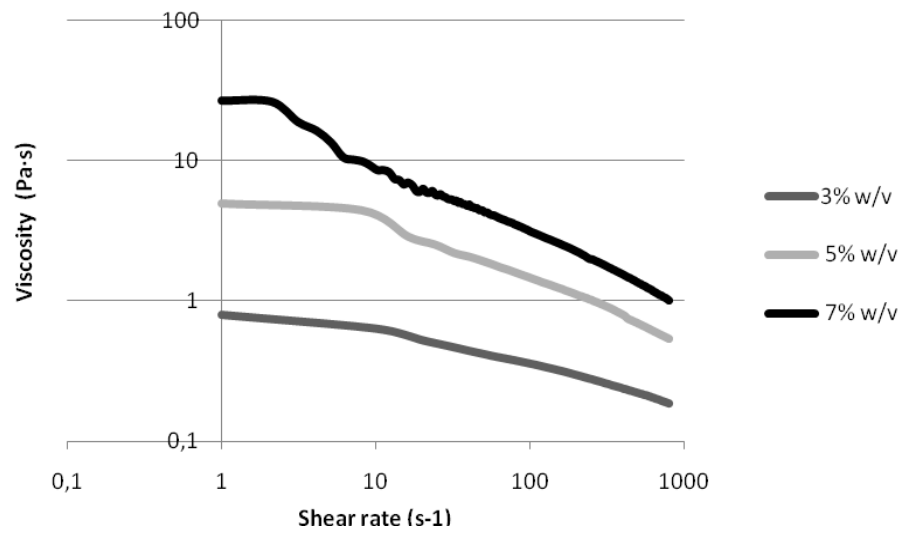


**Fig. 6.1.** Viscosity versus shear rate for three different CS concentration of the CS/PEO solutions.

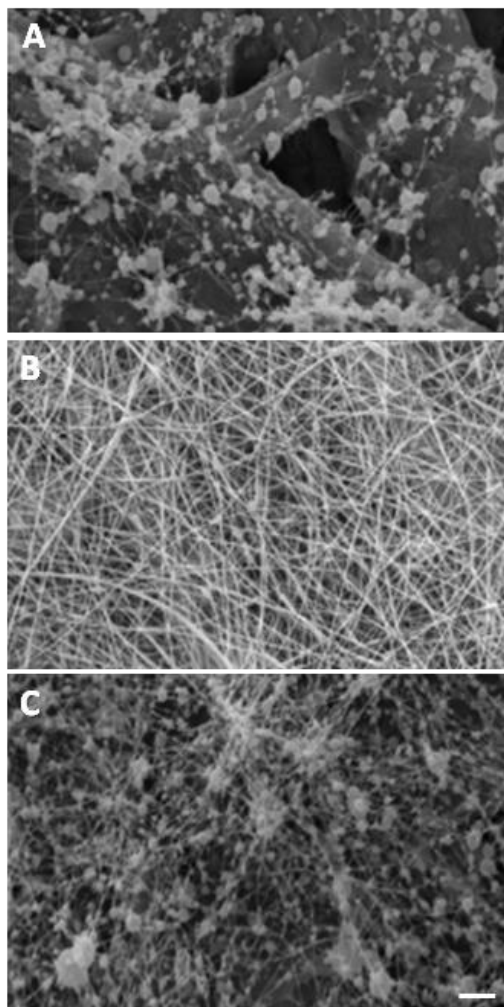


**Fig. 6.2.** SEM micrographs of electrospun CS/PEO solutions obtained with a 3% (A), 5% (B) and 7% (C) CS solutions (Parameters: 30kV, temperature 39°C, distance 12 cm, flow rate 30  $\mu$ L/min).

### 6.3.1.2 Process parameters

The optimization of the process parameters required to vary the parameters in a wide range of sets. For the fabrication of randomly oriented nanofibres, the voltage applied was fixed at 30kV and the distance between needle and collector was at 12 cm. The influence of temperature and flow rate was analyzed to maximize the formation of homogeneous fibres. The CS/PEO solution obtained with a 5% CS solution was spinnable in the range of 25 to 50  $\mu\text{L}/\text{min}$  and highly homogeneous fibres with a diameter of  $118\pm 16$  nm were observed for a flow rate of 30  $\mu\text{L}/\text{min}$  (Fig. 6.3C). Concerning temperature, an increase in temperature allowed to increase the spinnability and to reduce the number of defects on the fibres as reported in Fig. 6.4. The electrospinning process was set at  $38\pm 1^\circ\text{C}$ .

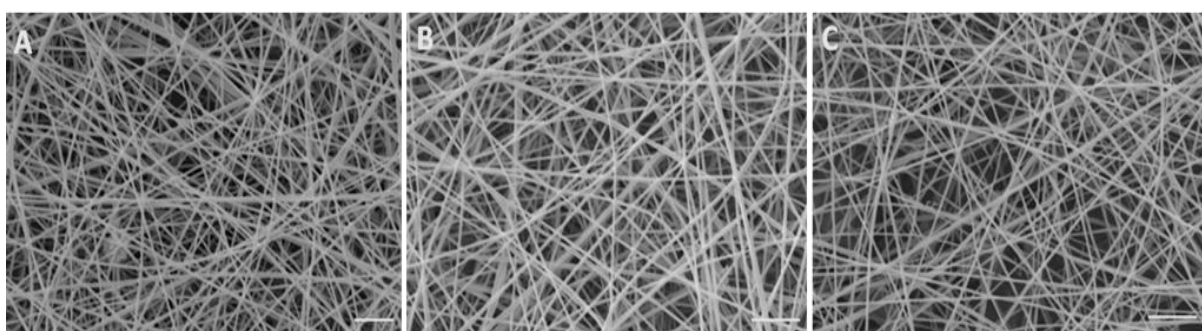


**Fig. 6.3** . SEM micrographs at different flow rates: 25  $\mu\text{L}/\text{min}$  (A), 27,5  $\mu\text{L}/\text{min}$  (B), 30  $\mu\text{L}/\text{min}$  (C). Bars: 2  $\mu\text{m}$ .

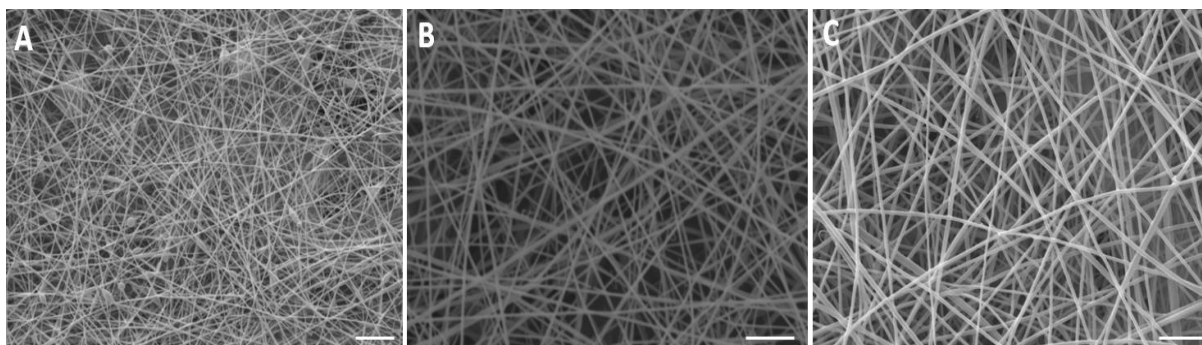


**Fig.6.4.** SEM micrographs at different temperatures: 25  $^\circ\text{C}$  (A), 32 $^\circ\text{C}$  (B), 39  $^\circ\text{C}$  (C). Bars: 2  $\mu\text{m}$ .

## 6.3.2 Characterization of CS based nanofibres

### 6.3.2.1 Fibres morphology and element distribution

Fibres with optimized parameters were visualized through SEM and qualitative analysis of phosphorus (P) element was performed using EDS. Phosphorous was homogeneously distributed within both the samples confirming the presence of DSP into the nanofibres (Fig. 6.5) and consequently the effectiveness of the crosslinking process. No green spots were detected on uncrosslinked samples (data not shown).

Crosslinked and uncrosslinked CS based nanofibres showed a comparable fiber diameter of  $109\pm 17$  nm and  $128\pm 19$  nm, respectively.

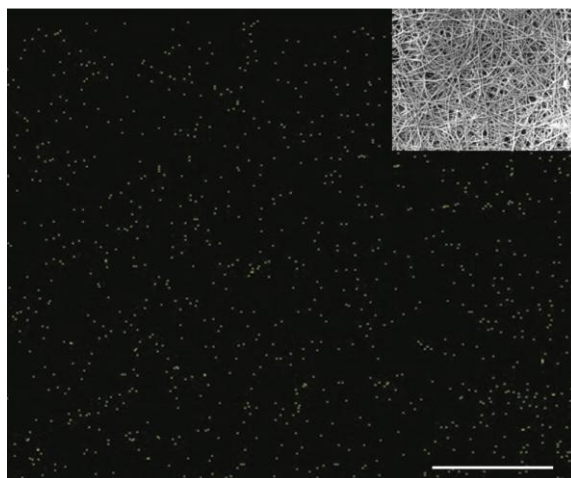


**Fig.6.5.** EDS spectra and SEM images of randomly oriented CS-based nanofibres. Green spots correspond to phosphorus (P) elements. Bars 10  $\mu$ m.

### 6.3.2.2 Fourier transform infrared-attenuated total reflectance spectroscopy (FTIR-ATR)

Fig. 6.6 reports the spectra of CS-based nanofibres and crosslinked CS-based nanofibres. Both spectra presented the peaks related to CS and PEO which are present in the CS-based nanofibres. Peak wavenumbers and their relative bond vibrations are reported in table 6.1. For CS-based nanofibres, the appearance of the peak at  $1074\text{ cm}^{-1}$  is related to the stretching of S=O bonds ( $\nu$ S=O) due to the presence of DMSO residues in the nanofibres [11]. Furthermore, in the crosslinked nanofibres the effectiveness of the crosslinking was confirmed by the appearance of peaks at  $1059\text{ cm}^{-1}$ ,  $944\text{ cm}^{-1}$  and  $858\text{ cm}^{-1}$  related to  $\text{PO}_3$  stretching ( $\nu$  $\text{PO}_3$ ), O-P-O bending ( $\delta$ O-P-O) and P-OH bending ( $\nu$ P-OH), respectively [12].

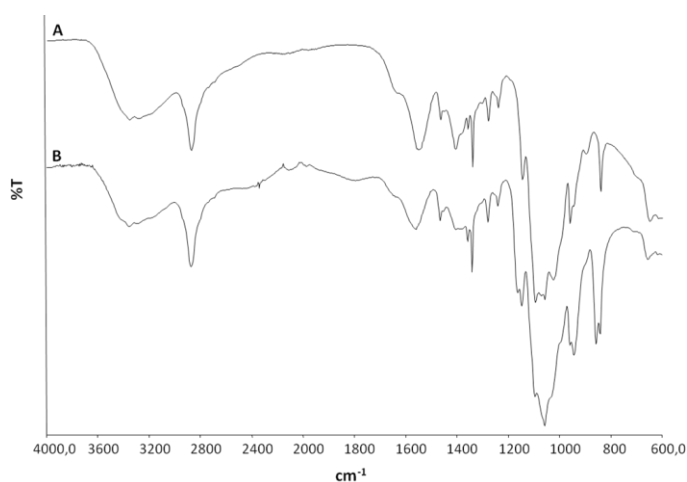


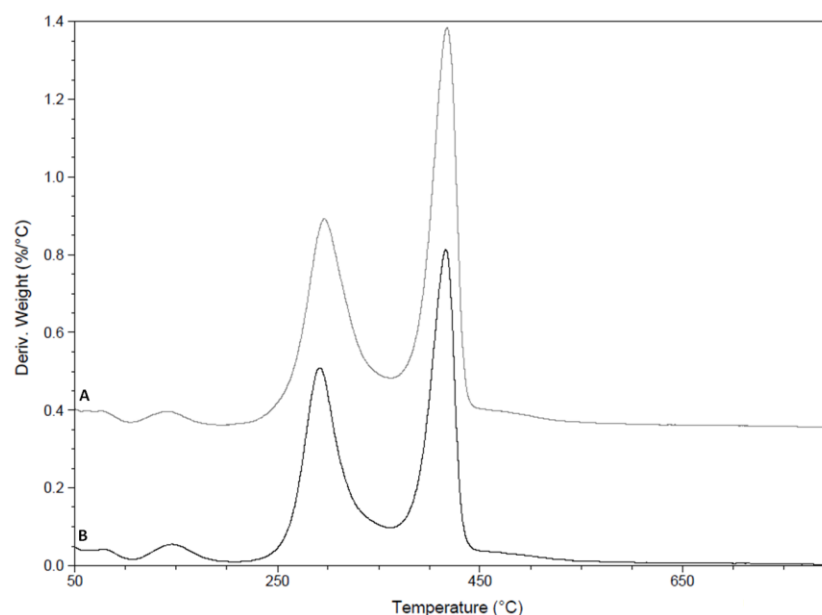
**Fig.6.6.** FTIR spectra of aligned CS-based nanofibres (A) and crosslinked CS-based nanofibres (B).

**Table 6.1.** FTIR peaks and their relative bond vibrations

Bond vibration	Wavenumber (cm <sup>-1</sup> )	Material	ref
vO-H	3222	CS	[13]
vN-H			
vC-H	2883	CS and PEO	[14, 15]
vC=O	1634	CS	[13, 14, 16]
δN-H	1547	CS	[13, 14, 16, 17]
δCH <sub>2</sub>	1466	PEO	[18]
vC-N	1410	CS	[17]
ωCH <sub>2</sub>	1360	PEO	[18]
τCH <sub>2</sub>	1280; 1241	PEO	[18]
vC-O-C	114; 1095; 1060	CS and PEO	[14, 19]
ρCH <sub>2</sub>	959; 947	PEO	[18]
δC-O-C	842	PEO	[19]

### 6.3.2.3 Thermogravimetric analysis (TGA)

The derivative of TGA curves (DTG) revealed four separate degradation phenomena both for crosslinked and uncrosslinked CS nanofibres. The first decomposition step, started at around 80°C, was related to the water evaporation; the second and then third weight loss were observed at 140°C and 290°C and were attributed to the decomposition of CS main chains, while the weight loss at 417°C was related to PEO [19-21]. The presence of the DSP did not modify the thermal phenomena significantly. Compared to results obtained in chapter 2, the use of a different CS (having an increased degree of deacetylation) showed a different thermal behavior with two decomposition temperatures related to CS instead of one at 238°C.

**Fig 6.7.** DTG curves of CS-based nanofibres (A) and crosslinked CS-based nanofibres (B).

### 6.3.2.4 Mechanical properties

The mechanical properties of both the uncrosslinked and crosslinked randomly oriented CS fibrous matrices were determined using a MTS QTest/10 device; after tensile test, samples were examined through SEM. Figure 6.8 displays a typical stress-strain plot for both the CS based nanofibres and crosslinked CS based nanofibres. The average Young's modulus (tensile elastic modulus) of the CS electrospun matrices were determined from the slope of the linear elastic region of the stress-strain curve. The E value of the crosslinked CS based nanofibres was found to be significantly higher ( $113.03 \pm 8.35$  MPa) compared to the uncrosslinked nanofibrous matrices ( $63.28 \pm 9.87$  MPa). However, the crosslinked mats showed a decreased in ultimate tensile strength and elongation at break in comparison with the as-spun nanofibres (Fig. 6.8), indicating that the individual fibres following DSP addition to the CS/PEO solution become locked together and therefore they can not slip past each other.

The previously described distinct difference in the elasticity of the uncrosslinked versus crosslinked CS nanofibres was also supported by the SEM images (Fig. 6.9). These images were taken in close proximity to the failure point of the nanofibrous matrices so that changes in individual fibre morphology could be observed. Uncrosslinked CS nanofibres after mechanical testing displayed both aligned fibres and a multitude of cracks or locations where extensions occurred on the fibres prior to their ultimately breaking (Fig. 6.9B). On the contrary, crosslinked CS nanofibres retained their randomly oriented fibre composition and did not demonstrate alignment prior to their failure (Fig. 6.9D), confirming the lower elasticity compared to uncrosslinked CS nanofibres.

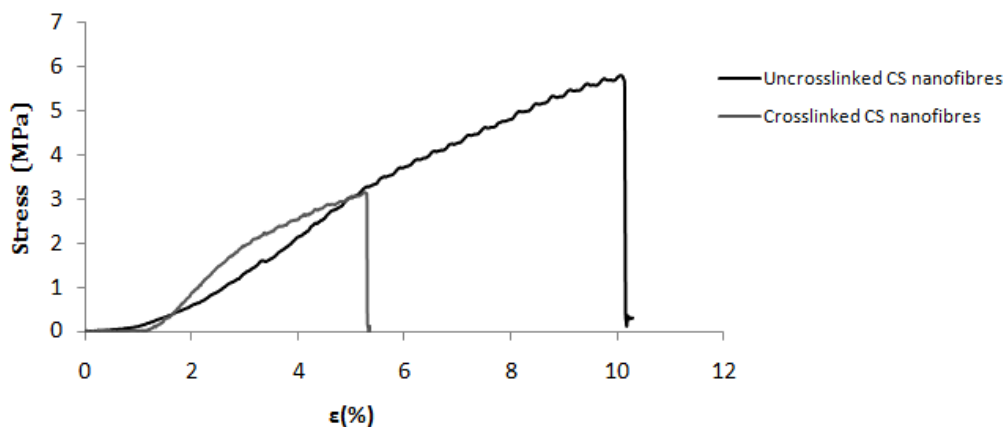


**Fig. 6.8** Stress-strain curves of CS-based nanofibres and crosslinked CS-based nanofibres.

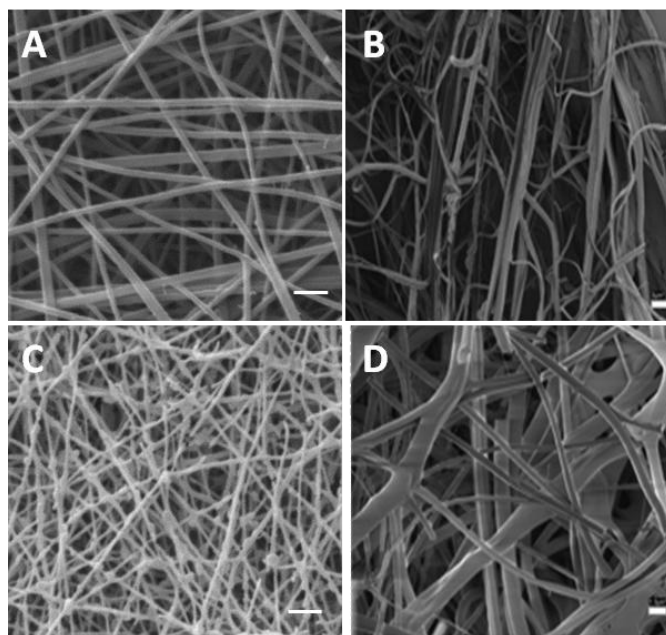


**Fig. 6.9.** SEM images of CS-based nanofibres (A, B) and crosslinked CS-based nanofibres (C, D) CS-based nanofibres before (A, C) and after (B, D) tensile testing.

### 6.3.2.5 Fibres dissolution

To confirm the efficiency of the crosslinking process and to evaluate the stability of CS based nanofibres in aqueous environment, a qualitative analysis of the dissolution behaviour crosslinked and uncrosslinked of CS-based nanofibres was performed in PBS at 37°C. After 7 days incubation in PBS, the uncrosslinked nanofibres showed a not fibrous structures (Fig. 6.10G). On the other hand, crosslinked nanofibres showed a stable morphology at 7 days confirming the effect of crosslinker on nanofibres water stability (Fig. 6.10H). Quantitative analysis showed a weight loss around 50% after 1 day immersion probably due to the dissolution of PEO, then the nanofibres weigh did not significantly vary until 7 days (Fig. 6.11).

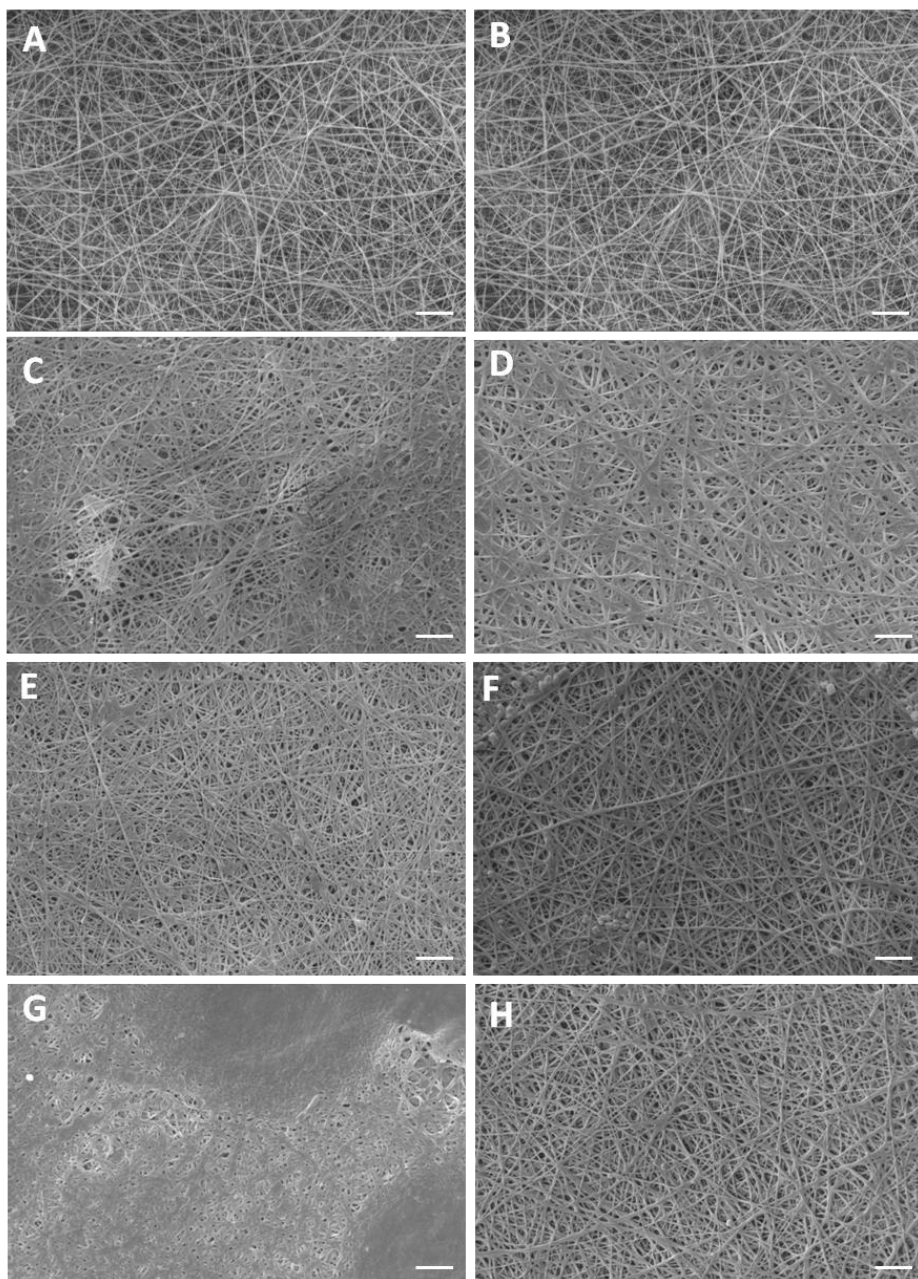


**Fig. 6.10.** SEM images of CS-based nanofibres (A, C, E, G) and crosslinked CS-based nanofibres (B, D, F, H) CS-based nanofibres before immersion in PBS (A, B) and after 1 hour (C, D), 1 day (E, F) and 7 days dissolution in PBS.

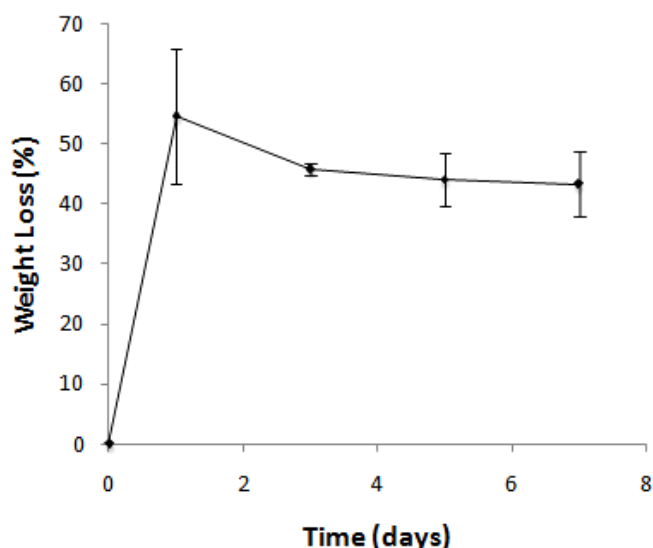


**Fig. 6.11.** Quantification of crosslinked CS-based nanofibres at different time points.

#### 6.4 Conclusion

Innovative substrates for peripheral nerve regeneration were developed within this chapter. CS electrospun nanofibres acting as NGCs internal fillers were prepared in 0.5M acetic acid solutions in the form of non-woven nanofibrous matrices with high specific surface areas and relatively small pores. Compared to previous work in literature, in this work CS was solubilized with a reduced amount of acid solution and without the use of potentially cytotoxic organic solvents. Furthermore, an innovative ionic crosslinker (DSP) able to neutralize the CS nanofibres without further process was successfully applied.

Crosslinked CS-based nanofibres were produced showing a fibre dimensions of  $109\pm 17$  nm which has been reported to be advantageous for glial cell adhesion and proliferation as compared to fibres characterized by a diameter of 700 nm [9, 22]. Furthermore, an increase in mechanical properties and water stability was observed for crosslinked nanofibres compared to uncrosslinked one.

The developed crosslinked CS based nanofibres are currently evaluated for their application as NGC internal filler in collaboration with the Neuroscience University Cavaliere Ottolenghi (Torino, Italy). *In vitro* cell tests were performed using primary Schwann cells and dorsal root ganglia (DRG) extracted from rats. Encouraging preliminary *in vitro* results were obtained confirming the ability of cells to adhere and proliferate on CS nanofibrous matrices.

Furthermore, the fabrication of aligned crosslinked CS-based nanofibres is in progress. Aligned nanofibres can improve the regeneration process by mimicking the structure of axons and by giving directional cues to cells growth.

## References

1. Chiono, V., C. Tonda-Turo, and G. Ciardelli, Chapter 9: Artificial scaffolds for peripheral nerve reconstruction. *International review of neurobiology*, 2009. **87**: p. 173-98.
2. Agarwal, S., J.H. Wendorff, and A. Greiner, Use of electrospinning technique for biomedical applications. *Polymer*, 2008. **49**(26): p. 5603-5621.
3. Koh, H.S., et al., Enhancement of neurite outgrowth using nano-structured scaffolds coupled with laminin. *Biomaterials*, 2008. **29**(26): p. 3574-3582.
4. Teo, W.E. and S. Ramakrishna, A review on electrospinning design and nanofibre assemblies. *Nanotechnology*, 2006. **17**(14): p. R89-R106.
5. Caracciolo, P.C., et al., Electrospinning of novel biodegradable poly(ester urethane)s and poly(ester urethane urea)s for soft tissue-engineering applications. *Journal of Materials Science-Materials in Medicine*, 2009. **20**(10): p. 2129-2137.
6. Ghasemi-Mobarakeh, L., et al., Electrospun poly(epsilon-caprolactone)/gelatin nanofibrous scaffolds for nerve tissue engineering. *Biomaterials*, 2008. **29**(34): p. 4532-4539.
7. Homayoni, H., S.A.H. Ravandi, and M. Valizadeh, Electrospinning of chitosan nanofibers: Processing optimization. *Carbohydrate Polymers*, 2009. **77**(3): p. 656-661.
8. Xie, J., et al., Electrospun nanofibers for neural tissue engineering. *Nanoscale*, 2010. **2**(1): p. 35-44.
9. Bhattarai, N., et al., Electrospun chitosan-based nanofibers and their cellular compatibility. *Biomaterials*, 2005. **26**(31): p. 6176-6184.
10. Tonda-Turo, C., et al., Cross linked gelatin nanofibres: Preparation, characterisation and in vitro studies using glial-like cells. *Materials Science & Engineering C-Materials for Biological Applications*, 2013. **33**(5): p. 2723-2735.
11. Markarian, S.A., L.S. Gabrielyan, and K.R. Grigoryan, FT IR ATR study of molecular interactions in the urea/dimethyl sulfoxide and urea/diethyl sulfoxide binary systems. *Journal of Solution Chemistry*, 2004. **33**(8): p. 1005-1015.
12. Larkin, P., *Infrared and Raman Spectroscopy; Principles and Spectral Interpretation*. 1st ed. 2011: Elsevier.
13. Rubilar, J.F., et al., Physico-mechanical properties of chitosan films with carvacrol and grape seed extract. *Journal of Food Engineering*, 2013. **115**(4): p. 466-474.
14. Duan, B., et al., Electrospinning of chitosan solutions in acetic acid with poly(ethylene oxide). *Journal of Biomaterials Science-Polymer Edition*, 2004. **15**(6): p. 797-811.
15. Ojha, S.S., et al., Fabrication and characterization of electrospun chitosan nanofibers formed via templating with polyethylene oxide. *Biomacromolecules*, 2008. **9**(9): p. 2523-2529.
16. Kjm, K.M., et al., Properties of chitosan films as a function of pH and solvent type. *Journal of Food Science*, 2006. **71**(3): p. E119-E124.
17. Leceta, I., P. Guerrero, and K. de la Caba, Functional properties of chitosan-based films. *Carbohydrate Polymers*, 2013. **93**(1): p. 339-346.
18. Dey, A., et al., Vibrational spectroscopy and ionic conductivity of polyethylene oxide-NaClO<sub>4</sub>-CuO nanocomposite. *Spectrochimica Acta Part a-Molecular and Biomolecular Spectroscopy*, 2011. **83**(1): p. 384-391.
19. Caykara, T., et al., Poly(ethylene oxide) and its blends with sodium alginate. *Polymer*, 2005. **46**(24): p. 10750-10757.
20. Neto, C.G.T., et al., Thermal analysis of chitosan based networks. *Carbohydrate Polymers*, 2005. **62**(2): p. 97-103.
21. de Carvalho, M.R.P., et al., Effects of supervised cardiovascular training program on exercise tolerance, aerobic capacity, and quality of life in patients with systemic lupus erythematosus. *Arthritis & Rheumatism-Arthritis Care & Research*, 2005. **53**(6): p. 838-844.

22. Christopherson, G.T., H. Song, and H.Q. Mao, The influence of fiber diameter of electrospun substrates on neural stem cell differentiation and proliferation. *Biomaterials*, 2009. **30**(4): p. 556-64.

## **Section IV**

# **Chitosan for wound dressing**



# Chapter 7

## Wound healing dressing: state of the art

### 7.1 Introduction

The amount of knowledge and understanding concerning the wound healing process and dressing practices has expanded and changed dramatically over the past four decades. Wound care dressings aim to restore the milieu required for skin regeneration and to protect the wound from environmental threats and penetration of bacteria. Any single type of wound dressing can not address the need and management of all types of wounds. For an effective design of a functional wound bandage, characteristics of the wound type, wound healing time, physical, mechanical, and chemical properties of the bandage must be taken into consideration. This chapter offers a review of the common and advanced wound management dressings, their key advantages and shortcomings. It also reviews many of the dressings and novel polymers used for the delivery of drugs to acute, chronic and other types of wound. These include hydrocolloids, alginates, hydrogels, polyurethane, collagen, chitosan, pectin and hyaluronic acid. The definition and classification of wounds together with the different stages of wound healing are also briefly described, as they directly affect the choice of a particular dressing. In addition to that this chapter also compiles the list of wound care product available in the market.

### 7.2 Structure and function of the skin

The skin is a complex, multilayered organ, which produces several specialized derivative structures called appendages (hair follicles, eccrine sweat glands, sebaceous glands, apocrine glands) and consists of heterogeneous cell types and extracellular components. The skin constitutes about the 15% of total human weight and in adult it shows a surface of about 2 m<sup>2</sup>. It is important to recognize, when considering either normal or abnormal skin structure and function, that there also regional variation in the skin which is primarily manifested in terms of thickness, composition and density of appendages. Skin is made of three overlapping layers: epidermis, dermis and hypodermis (Fig. 7.1). Interaction among

these layers is important during development and for maintenance of homeostasis in the adult.

The epidermis or outer layer is composed for the 95% of only one kind of cells, the keratinocytes; the remaining 5% of the tissue is made of melanocytes, Langerhans and Merkel cells. Epidermis is made up of stratified layers of keratinocytes (basal, spinous, granular, lucidum and cornified layers). The differentiation of keratinocytes toward a terminally differentiated corneocyte is very tightly regulated. Basal keratinocytes divide with daughter cells, migrating into the overlying spinous layer. Keratinocytes in the spinous layer subsequently move into a granular layer, and eventually move into the outer cornified layer of the epidermis (Fig.7.1). The epidermis is a barrier, preventing the penetration in the wound bed of water, microorganisms, extraneous substances and in the same time, avoiding the loss of water and electrolytes from the injured tissue. Average thickness of epidermis is 70-120  $\mu\text{m}$ , but it can reach values of 1-2 mm in some regions of the body, such as on the hand palm; this layer is separated from the dermis below by the basement membrane zone (BMZ), which has a thickness of about 200 nm and is composed of a complex network, in which macromolecules, proteins and glycoproteins guarantee the adhesion between the two superimposed layers. The dermis or middle layer is the thick layer (average thickness of about 0.55 mm) of collagen rich connective tissue component of the skin and provides its pliability, elasticity and tensile strength. It protects the body from mechanical injury, binds water, aids in thermal regulation and includes receptor of sensory stimuli. The dermis is less cellular than the epidermis, being composed primarily of fibrous and amorphous ECM surrounding the epidermally derived appendages, neurovascular networks, sensory receptor and dermal cells. About the 70% of the dermis is made of collagen, mainly type I and III, which supports the tissue and assures mechanical resistance; whereas the 5% of dermis weight derives from elastin fibers which provide elasticity to the tissue. Epidermis and dermis are separated by the basement membrane, a sheet composed of specialized collagens and matrix proteins such as laminins and collagen IV. The hypodermis is the deepest cutaneous layer, situated between the dermis and the muscular and adipose tissues. As dermis, the hypodermis is composed of connective tissue and it is particularly rich of mesenchymally adipocytes, which are cells responsible of fats synthesis. Due to the presence of this kind of cells, the hypodermis insulates the body, serves as a reserve energy supply and allows for its mobility over underlying structures. In this stratum, follicles and sudoriferous glandes originate.

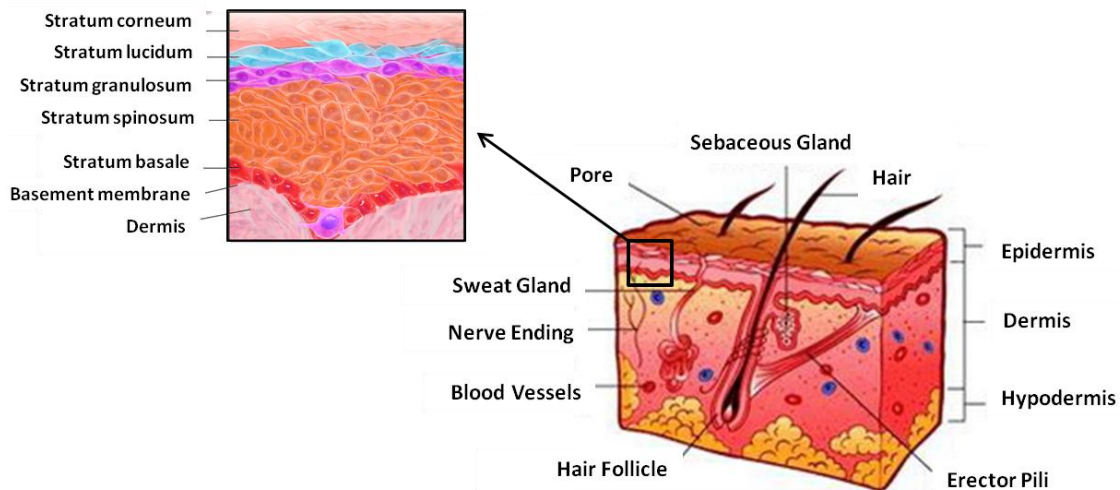


**Fig.7.1.** Stratified structure of the skin.

### 7.3 Wounds and wound healing process

A wound can be described as a defect or a break in the skin, resulting from physical or thermal damage or as a result of the presence of an underlying medical or physiological condition. According to the Wound Healing Society, a wound is the result of ‘disruption of normal anatomic structure and function’ [1]. On the basis of wound healing processes, there are two types of wounds: acute and chronic wounds. Acute wounds are usually tissue injuries that heal completely, with minimal scarring usually in 8–12 weeks [2]. Acute wounds are generally caused by mechanical injuries but can be also formed by burns and chemical injuries which arise from a variety of sources such as radiation, electricity, corrosive chemicals and thermal sources. Chronic wounds on the other hand arise from specific diseases such as diabetes, tumors, and persistent infections [3]. They also include decubitus ulcers (bedsores or pressure sores) and leg ulcers (venous, ischaemic or of traumatic origin). Healing of chronic wounds could take more than 12 weeks [4] and recurrence of the wounds is not uncommon [5]. Wounds are also classified based on the number of skin layers and area of skin affected [5, 6]. Injury that affects the epidermal skin surface alone is referred to as a superficial wound, whilst injury involving both the epidermis and the deeper dermal layers, including the blood vessels, sweat glands and hair follicles is referred to as partial thickness wound. Full thickness wounds occur when the underlying subcutaneous fat or deeper tissues are damaged in addition to the epidermis and dermal layers.

The healing of a wound is defined by the Wound Healing Society as “a dynamic and complex process leading to the re-establishment of the structure and the functionality of the injured tissue” [1]. A healed wound shows peculiar characteristics, connective tissue appears completely restored and the epithelium is regenerated; skin structure and functionality are re-established, without requiring continuous drainage and tissue protection with a dressing. Wound healing progresses through a series of interdependent and overlapping stages in which a variety of cellular and matrix components act together

to reestablish the integrity of damaged tissue and replacement of lost tissue. There are 4 major stages of wound healing after a full-thickness skin wound: hemostasis, inflammation, proliferation and remodeling (Fig. 7.2). Hemostasis is the first stage of wound healing. Wounds cause leakage of blood from damaged blood vessels. The formation of plasma clot is necessary to stop local hemorrhages immediately. It is initiated by proteolytic conversion of fibrinogen into fibrin by thrombin. As fibrin molecules assemble into fibrin fibers, platelets and neutrophils are entrapped in a mesh of fibrin fibers. It act as a temporally shield protecting the denuded tissue [7, 8]. The process of clotting induces platelet degranulation and release of cytokines and GFs, including platelet derived growth factor (PDGF), insulin-like growth factor-1 (IGF-1), epidermal growth factor (EGF) and transforming growth factor- $\beta$  (TGF- $\beta$ ) [9]. Plasma clot is served as a provisional matrix for invading cells as well as a reservoir of cytokines and GFs that are released from activated platelets [9]. These GFs act as chemotactic factors for lymphocytes, fibroblasts and keratinocytes, and promote various processes of reepithelialization and wound contraction. Inflammation occurred simultaneously with hemostasis, sometimes from within a few minutes of injury to 24 hours and lasts for about 3 days. The main goal of the inflammatory phase is the removal of bacteria, foreign debris and other microorganism from wound bed. This process is activated by a variety of mediators released by cells and capillaries of the injured tissue, platelets, cytokines and products of hemostasis. Neutrophils and polymorphonuclear leukocytes (PMN) infiltrate at injured sites from the surrounding microvasculature and start the elimination process of microorganisms and wound repair by activating local fibroblasts and epithelial cells. Neutrophils appear first at the wound site and are predominant for the first few days, then disappear when the wound is no more infected. In presence of infection, neutrophil infiltration continues until the wound is not completely clean and the infective process is controlled; in absence of infection, the existing monocytes differentiate into macrophages, which become predominant phagocytic cells at the wound bed. Macrophage tasks include phagocytosis of any remaining pathogenic organisms and other cell and matrix debris; in addition they stimulate two fundamental mechanisms of inflammatory stage: angiogenesis and fibroplasia. The first one, that is the physiological process involving the growth of new blood vessels and the formation of capillary buds, starts 3 days after injury and are essential for providing metabolic substances that wound needs for a complete healing. The fibroplasia, that is the formation of fibrous tissue and collagen synthesis, starts by the third to the fifth day after injury. Moreover, macrophages synthesize nitric oxide and secrete different cytokines to initiate the wound repair process, including GFs involved in migration, proliferation and organization of new connective tissue and vascular beds. As they can secrete cytokines over time, they assure the continuity of the tissue repair process. In this phase the release of the protein-rich exudates from the wound site causes vasodilatation through the release of histamine and serotonin. Histamine and serotonin allows phagocytes to enter the wound and engulf dead cells (necrotic tissue). At the end of the inflammation stage, bleeding is controlled

and the wound bed is clean and moist, obtaining suitable conditions for the next stage of cell proliferation and repair. In the proliferation phase (3-21 days), angiogenesis, fibroplasia, and re-epithelialization occur [10]. Within this phase, fibroplasia and angiogenesis take place concurrently in a closely orchestrated manner to form ECM and granulation tissue. By the fifth day, maximum formation of blood vessels and formation of granulation tissue occur. Mesenchymal cells transform into fibroblasts, which lay fibrin strands to act as a framework for cellular migration. Fibroblasts and keratinocytes play a pivotal role in this stage. Fibroblasts produce collagen and proteoglycans and the neovasculature forms granulation tissue which fills wound defects. The early collagen secretion results in an initial rapid increase in wound strength, which continues to increase more slowly as the collagen fibers reorganize according to the stress on the wound. During this phase, the wounded tissue contracts, reducing the size of defect and approaching wound edges. This process is mediated by special fibroblasts with contractile properties called myofibroblasts. Finally, epithelial cells migrate over the granulation tissue and cover the wound bed, providing in this way a barrier to bacterial invasion and preventing fluid loss. Basal epithelial cells flatten and migrate across the open wound. The epithelial cells may slide across the defect in small groups, or “leapfrog” across one another to cover the defect. Migrating epithelial cells secrete mediators, such as transforming GFS  $\alpha$  and  $\beta$ , which enhance wound closure. Although epithelial cells migrate in random directions, migration stops when contact is made with other epithelial cells on all sides (i.e., contact inhibition). Epithelial cells migrate across the open wound and can cover a properly closed surgical incision within 48 hours. In an open wound, epithelial cells must have a healthy bed of granulation tissue to cross. Epithelialization is retarded in a desiccated wound [11]. Remodeling, also called maturation, is the final stage of wound healing and begins 21 days after injury and can last until 1 or 2 years. This phase involves the formation of cellular connective tissue and strengthening of the new epithelium which determines the nature of the final scar. During this period, the newly laid collagen fibers and fibroblasts reorganize along lines of tension. Fibers in a nonfunctional orientation are replaced by functional fibers. The density of cells such as macrophages, keratinocytes, fibroblasts and myofibroblasts is reduced by apoptosis.

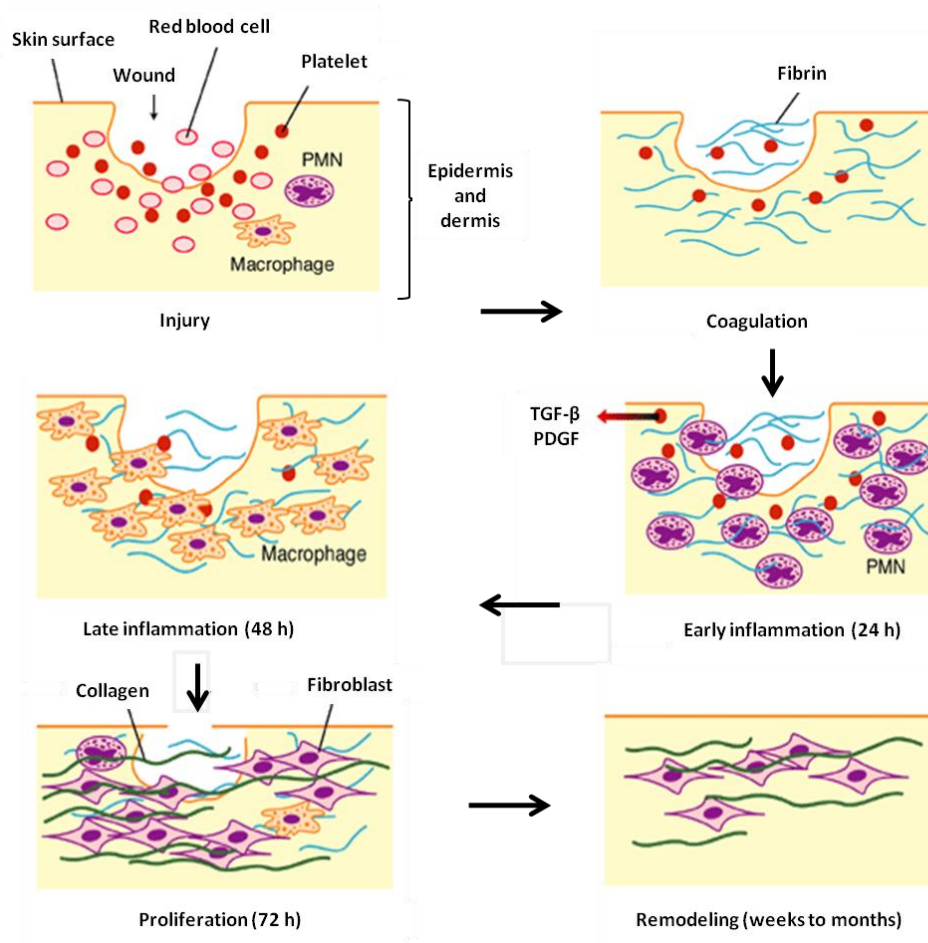


**Fig. 7.2.** The phases of cutaneous wound healing.

#### 7.4 Factors which impair wound healing chronic wounds

Although most wounds will heal uneventfully, the failure of the wound to heal or a prolonged healing time usually results in a chronic wound. A chronic wound fails to heal because the orderly sequence of events is disrupted at one more of the phases of wound healing. Excessive production of exudates can cause maceration of healthy skin tissue around the wound [12] and inhibit wound healing. In addition, exudate from chronic wound differs from acute wound fluid with relatively higher levels of tissue destructive proteinase enzymes [13] and therefore more corrosive. Furthermore, the presence of foreign bodies into the wound injury site can cause chronic inflammatory responses delaying healing and sometimes leading to granuloma or abscess formation. Other problems associated with wound healing include the formation of keloid (raised) scars resulting from excess collagen production in the latter part of the wound healing process [7]. Pathogenic bacteria such as *Staphylococcus aureus*, *Pseudomonas aeruginosa*, *Streptococcus pyogenes* and some *Proteus*, *Clostridium* and *Coliform* species can be detrimental to the healing process. *P. aeruginosa* and *S. aureus* have been shown to significantly reduced skin graft healing [14]. Inadequate control measures to manage

infected wounds can lead to cellulitis (cell inflammation) and ultimately bacteraemia and septicaemia, both of which can be fatal.

Krasner et al., outlined the necessity to control factors that could impair wound healing: preventing infection, optimising exudate control and removing foreign bodies have to be satisfied in order to manage efficiently the wound injury and to promote healing [15].

Poor nutritional status and ageing also reduce the ability to fight infection [16]. Protein, vitamin (e.g. vitamin C) and mineral deficiencies impair the inflammatory phase and collagen synthesis, leading to prolonged healing times [17]. In addition, underlying diseases such as diabetes [18] and anaemia delay wound healing because compromised circulation results in the delivery of inadequate nutrients, blood cells and oxygen to the wound. Treatment with drugs such as steroids suppress the body's inflammatory responses and thereby impede the inflammatory stage of wound healing, which eventually leads to a compromised immune system [19]. Glucocorticoids for example have been shown to impair wound healing in both rats and humans [20].

Dressings used to protect wounds may establish and maintain favorable conditions for the healing process. Before applying the dressing on the injury, foreign matter, necrotic tissue, contaminating microorganisms should be removed from the wound site, in order to reduce the risk of infection. This can be carried out applying a sterile, atraumatic surgical technique and, in case of traumatic wounds, performing initial debridement and irrigation. The dressing has the function of protecting the wound site from further contamination and it may be produced in order to stimulate the rapid complete regeneration of the injured tissue and healing of the wound.

## **7.5 Wound dressing**

### **7.5.1 Classification of wound dressings**

For years, different materials such as linen, honey, animal fats, and vegetable fibers have been used for wound dressing [21, 22]. However, most plants, could have many drawbacks associated to the presence of microorganism or chemicals which might be detrimental to the wound healing process. For this reason, continuous developments have led to extensive use of new bandages with improved performance. The attention has been focused on finding biocompatible materials, mainly polymers, able to help the restoration of the tissue and, once the healing process is terminated, degrading without releasing toxic products. Wound dressings are classified in a number of ways depending on their function in the wound (debridement, antibacterial, occlusive, absorbent, adherence) [23], type of material employed to produce the dressing (e.g. hydrocolloid, alginate, collagen) [24] and the physical form of the dressing (ointment, film, foam, gel) [25]. Dressings are further classified into primary, secondary and island dressings [26]. Dressings which make physical contact with the wound surface are referred to as primary dressings while secondary dressings cover the primary dressing. Island dressings possess a central absorbent region that is surrounded by an adhesive portion.

In this chapter, dressings are classified according to traditional or modern (moist wound environment) dressings. Modern dressings are discussed under the type of material (hydrocolloid, alginate, hydrogel) employed to produce the dressing and the physical form (film, foam) of the dressing.

#### **7.5.1.1 Traditional dressings**

Ordinary dressings, such as cotton wool, natural or synthetic bandages and gauzes, act as a common cover on a wound so that the wound can rehabilitate underneath. Cotton wool is used to absorb exudate and applied over a primary wound dressing to avoid contaminating the wound with cellulose fibres. Bandages are made from natural (cotton wool and cellulose) and synthetic (e.g. polyamide) materials which perform different functions (i.e. retention of light, sustained compression in the treatment of venous insufficiency, leg ulcers). Gauze dressings are made from woven and nonwoven fibres of cotton, rayon polyester or a combination of both. Sterile gauze pads are used for packing open wounds to absorb fluid and exudates with the fibres in the dressing acting as a filter to draw fluid away from the wound. Gauze dressings need to be changed regularly to prevent maceration of the healthy underlying tissue and have been reported to be less cost effective compared with the more modern dressings. [27]. Though gauze dressings can provide some bacterial protection, this is lost when the outer surface of the dressing becomes moistened either by wound exudate or external fluids. All these dressings are dry and do not provide a moist wound environment. They may be used as primary or secondary dressings, or form part of a composite of several dressings with each performing a specific function. The conventional wound dressing materials are not suitable for acute and chronic wounds as far as rapid healing of a wound is concerned. Moreover, traditional wound dressings can adhere to wounds as exudate dries, and capillary loops and granulation tissue can grow through the dressing fabrics causing trauma and pain to wounds upon removal [28]. Despite these limitations, many conventional dressings are actually available on market in the form of bandages and gauzes [27].

#### **7.5.1.2 Modern dressings**

Modern dressings have been developed as an improvement upon the traditional wound dressing because they aim to: i) maintain the most suitable environment at the wound/dressing interface, ii) absorb excess exudates without leakage to the surface of a dressing, iii) provide thermal insulation, iv) mechanical and bacterial protections, v) allow gaseous and fluid exchanges and vi) be non adherent to the wound and easily removable without trauma. The modern dressings are mainly classified according to the materials from which they are produced including hydrocolloids, alginates and hydrogels, and generally occur in the form of gels, thin films and foam sheets.

### 7.5.1.2.1 Hydrocolloids

Hydrocolloids dressing are among the mostly wide used dressings. The term 'hydrocolloid' describes the family of wound products obtained from colloidal materials (gel forming agents) combined with elastomers and adhesives. Typical colloidal materials are carboxymethylcellulose (CMC), gelatin and pectin. They occur in the form of thin films and sheets (Fig. 7.3). Hydrocolloid has the ability to form gels upon contact with wound exudates and the high absorption occurs via strong hydrophilic gel formation [29]. The formation of gel allows excess fluid to escape without permitting wound desiccation. However, the fluid handling capacity of hydrocolloid dressings depends on many factors such as the physicochemical properties and the design of the dressing [30]. For their intrinsic properties, hydrocolloids dressing are clinically useful for partial- or full-thickness acute and chronic wounds [31]. As they are occlusive, hydrocolloid dressings do not allow water, oxygen, or bacteria into the wound. This may help facilitate a wound to granulate or epithelialize and encourage autolytic debridement in wounds with necrotic or sloughy tissue present. However, because of their occlusive nature, hydrocolloids should not be used if the wound or surrounding skin is infected and are not recommended for use in diabetic foot ulceration. Hydrocolloids also cause the pH of the wound surface to drop; the acidic environment can inhibit bacteria growth. Hydrocolloid dressings are conformable to the patient's body and adhere well to high-friction areas, such as the sacrum and heels. Examples of hydrocolloids dressing include Granuflex™ and Aquacel™ (Conva Tec, Hounslow, UK), Comfeel™ (Coloplast, Peterborough, UK) and Tegaserb™ (3M Healthcare, Loughborough, UK).



**Fig. 7.3** A typical hydrocolloid dressing. The dressing combines moisture vapour permeability with absorbency and conformability.

### 7.5.1.2.2 Alginates

Alginate dressings are produced from the calcium and sodium salts of alginic acid, a polysaccharide comprising mannuronic and guluroinic acid units. Various alginate dressings are available which possess different chemical and physical properties dependent upon the proportion and arrangement of mannuronic and guluronic acid

residues and the content of calcium and sodium ions. They occur in the form of porous sheets or as flexible fibers. When the alginate dressing comes into contact with wound exudate, ion exchange occurs between the calcium ions of the dressing and the sodium ions in the exudate resulting in the formation of a gel on the surface of the wound [32]. This gel absorbs moisture and maintains an appropriately moist environment which is considered to promote optimal healing [33], limit wound secretion and minimize bacterial contamination [31]. As alginates are highly absorbent, they should not be used with dry wounds or those covered with hard necrotic tissue. Alginates require a secondary dressing; foams or hydrocolloids will secure the alginate and keep it from drying out. Moreover, the calcium component of the dressing have been found to improve many cellular aspects of wound healing [34]. The role of calcium alginate in the wound healing process was investigated by Schmidt who suggested that it may help in the production of mouse fibroblast [34]. Thomas et al., have reported that some alginate dressings activate human macrophages to produce tumour necrosis factor- $\alpha$  (TNF- $\alpha$ ) which initiates inflammatory signals, as part of the wound healing process. Calcium ions present in alginate dressings, when released into the wound, also play a physiological role aiding in the clotting mechanism (haemostat) during the first stage of wound healing [35].

#### **7.5.1.2.3 Synthetic hydrogels**

Synthetic hydrogel dressings are insoluble, swellable hydrophilic materials made from synthetic polymers such as poly(methacrylates) and polyvinylpyrrolidone. Hydrogel dressings are commonly available in two forms: amorphous gel and sheet hydrogel and can be useful when managing painful wounds. When applied to a wound as a gel, hydrogel dressing usually require a secondary covering such as gauze and need to be changed frequently [36]. On the contrary, the sheets do not need a secondary dressing as a semi-permeable polymer film backing controls the transmission of water through the dressing. Hydrogel dressings contain significant amounts of water (70–90%) and as a result they cannot absorb much exudate, thus they are used for light to moderately exuding wounds (i.e. pressure ulcers, skin tears, surgical wounds, and burns). Fluid accumulation can lead to skin maceration and bacterial proliferation which produces a foul smell in infected wounds. Hydrogels have been found to promote moist healing, to be malleable, non adherent and improve reepithelisation of wounds [36].

#### **7.5.1.2.4 Semi-permeable adhesive films**

Film dressings are flexible sheets of transparent polyurethane coated with an acrylic adhesive. They can be used as a primary or secondary dressing. These dressings are semipermeable, vary in size and thickness, and have an adhesive that holds the dressing on the skin. They conform easily to the patient's body. As films are transparent, the wound can be easily monitored. Film dressings generally require a border of dry, intact skin for the adhesive edge of the dressing; film dressings will not adhere to moist skin or moist wound beds because the moisture inactivates the adhesive. Therefore, the

condition of the periwound skin should be assessed before application to determine if a film dressing is appropriate. As film dressings are semi-occlusive and trap moisture, they allow autolytic debridement of necrotic wounds and create a moist healing environment for granulating wounds. Most of the existing brands differ in terms of vapour permeability, adhesiveness, conformability and extensibility [37]. Opsite™ (Smith and Nephew, Hull, UK) which is a thin semi-permeable film made from polyurethane covered with hypoallergenic acrylic derivatives and is more porous and permeable to water vapour and gases but no liquid from exudates [38].

#### **7.5.1.2.5 Foam dressings**

Foam dressings are semipermeable and either hydrophilic or hydrophobic with a bacterial barrier. They consist of porous polyurethane foam or polyurethane foam film and are capable of handling moderate to high volumes of wound exudates [39]. Foam dressings provide thermal insulation to the wound, maintain a moist environment around the wound, are non-adherent, and allow atraumatic dressing removal [40]. They are highly absorbent, property that can be controlled by foam texture, thickness and pore size. The open pore structure also gives a high moisture vapour transmission rate [41]. Foam dressing are used as primary wound dressings for absorption and insulation and a secondary dressing is usually not required due to their high absorbency and moisture vapour permeability but they can be used in conjunction with a topical antimicrobial for infected wounds. Foam dressings may be manufactured with an adhesive border, which eliminates the need for a securing device or without an adhesive boarder. Foam dressings are also available which release agents such as antimicrobials, moisturizers or anti-inflammatory analgesics into the wound. Examples of foam dressing include: Lyofoam (Conva Tec), POLYDERM (DeRoyale) and Allevyn1 (Smith and Nephew).

#### **7.5.1.2.6 Tissue engineered skin substitutes**

Traditional and modern dressings though useful, cannot replace lost tissue, particularly missing dermis as occurs in severe burns. Advances in the fabrication of biomaterials, mainly polymers, and the culturing of skin cells have led to the development of a new generation of engineered skin substitutes (biosynthetic dressing) [42]. Nanofibrous matrices, microspheres, hydrogels, films and solid foams obtained from polymeric materials should not simply protect and cover the wound site but also allow tissue regeneration and cell proliferation, stimulating the physiological processes on which the complete healing of the wound is based [43]. For this reason, TE skin substitutes seems to be a promising alternative to conventional treatments since these scaffolds aim to: i) provide a tough and self- maintaining surface to the body; ii) provide initial contact between the outside world and the defensive systems of the body; iii) allow physiological functions such as temperature control and neurological sensing; iv) host to structures such as sweat glands and hair follicles; and v) create an optimal microenvironment for skin regeneration through the delivery of bioactive molecules. Skin substitutes are

developed starting from biocompatible and bioresorbable polymeric dermal scaffolds such as CS–gelatin composite films, poly(d,L-lactic acid), poly(d, L-lactic acid)–polyethylene glycol–poly(d, L-lactic acid), poly(lactic co-glycolic acid) membranes containing (1→3),(1→6)-β-d-glucans [44, 45], porous scaffolds composed of gelatin, hyaluronic acid and (1→3),(1→6)-β-d-glucans crosslinked with 1-ethyl-(3-3-dimethylaminopropyl) carbodiimide hydrochloride for artificial dermis [46]. The use of these polymers either in the natural biological form or semi-synthetic forms are reported to be able to mimic normal physiologic responses during wound healing [47]. Moreover, engineered scaffolds are potentially useful for the release of additional bioactive molecules, such as GFs and genetic materials [48, 49], as well as, for the accommodation of living cells [50, 51].

Two major matrices are employed in TE skin substitutes: acellular and cell containing matrices. Acellular matrices are produced either from synthetic collagen and ECM combinations such as hyaluronic acid [52] for example Integra<sup>TM</sup>, or native dermis with the cellular components removed but preserving the dermal architecture [41] for example Alloderm<sup>TM</sup>. Cell containing TE dressings include biodegradable films formed from, for example, collagen and GAGs (e.g. Apligraf<sup>TM</sup>) as scaffolds onto which skin cells (patient derived or from recombinant sources) can be seeded for the growth of new tissues. Some of the developed TE products and skin substitutes available are summarized in Table 7.1. Though these advanced dressings have great potential for treating chronic wounds and third degree burns, they are still limited by the high costs involved, the risk of infection carry over and antigenicity as well as having to create a second wound in the case of harvesting patient's own cells to aid wound healing. These shortcomings in addition to the legal and ethical issues surrounding stem cell research have probably contributed to the slow adoption of these dressings in routine clinical practice [53].

**Table 7.1** Tissue engineered skin substitutes available commercially.

<b>Dressing</b>	<b>Type</b>	<b>Major components</b>	<b>Manufacturers</b>
Integra™	Artificial skin	Collagen/chondroitin-6 sulphate matrix overlaid with a thin silicone sheet	Integra LifeScience (Plainsborough, NJ)
Biobrane™	Biosynthetic skin substitute	Silicone, nylon mesh, collagen	Dow Hickham/Berte Pharmaceuticals (Sugar Land, TX)
Alloderm™	Acellular dermal graft	Normal human dermis with all the cellular material removed	Lifecell Corporation (Branchberg, NJ)
Dermagraft™	Dermal skin substitute	Cultured human fibroblasts on a biodegradable polyglycolic acid or polyglactin mesh	Advanced Tissue Sciences (LaJolla, CA)
Epicel™	Epidermal skin substitute	Cultured autologous human keratinocytes	Genzyme Biosurgery (Cambridge, MA)
Myskin™	Epidermal skin substitute	Cultured autologous human keratinocytes on medical grade silicone polymer substrate	Celltran Limited (University of Sheffield, Sheffield, UK)
TranCyte™	Human fibroblast derived skin substitute (synthetic epidermis)	Polyglycolic acid/polylactic acid, ECM proteins derived from allogenic human fibroblasts and collagen	Advanced Tissue Sciences
Hyalograft 3-D™	Epidermal skin substitute	Human fibroblasts on a laser-microperforated membrane of benzyl hyaluronate	Fidia Advanced Biopolymers (Padua, Italy)
Bioseed™	Epidermal skin substitute	Fibrin sealant and cultured autologous human keratinocytes	BioTissue Technologies (Freiburg, Germany)

#### 7.5.1.2.6.1 Biocompatible polymers for wound dressings

Dressings for wound healing can be produced using different materials, generally both natural and synthetic polymers. In this biomedical field, the use of biodegradable materials is preferred because skin substitutes should remain on the wound bed until the healing process is over, then they are resorbed without requiring the removal of the dressing, avoiding to traumas to the healing new tissue. In the last years, starting from natural or synthetic polymers, the production of biomimetic ECM micro/nanoscale fibers (80 nm–1.5 µm) through electrospinning process has been found to be effective for

wound healing [54, 55]. Natural macromolecules show a relatively low mechanical strength compared to synthetic polymers. By cross-linking or blending with synthetic polymers, the mechanical properties of natural polymers can be improved; however, their biocompatibility is somewhat affected. Modern bandage materials, such as electrospun nanofibrous polymeric bandages, hydrogels, porous scaffolds and foams are also used for active wound dressings by releasing local active principles such as antimicrobial and anti-inflammatory drugs [56]. In Table 7.2 biodegradable materials, both of synthetic or natural origin, used in wound dressing application are reported.

#### **7.5.1.2.6.1.1 Natural polymers for wounds healing**

Natural polymers are widely used in the regenerative medicine field, for wounds and burns dressing because of their biocompatibility, biodegradability and similarity to the ECM [57]. Inducing and stimulating the wound healing process, natural polymers are involved in the repair of damaged tissues and consequently in skin regeneration [58]. For the regeneration of full-thickness wounds, polysaccharides and proteins are the most common natural polymers used.

Polysaccharides are extensively used for the management of wounds and burns: neutral (i.e. glucans, dextrans, cellulose), acidic (alginic acid, hyaluronic acid), basic (chitin, chitosan) or sulfated polysaccharides (heparin, chondroitin, dermatan sulfate, keratan sulfate) [59]. Among dextrans, carboxymethyl benzylamide sulfonate dextran (CMDBS) is a soluble polymer structurally similar to GAG heparin which stimulates wound healing in various *in vivo* experimental models, controls the proliferation of *S. aureus* biofilm and affects proliferation and metabolism of endothelial cells [60]. Moreover, hydrated cyclodextrins are used for modern odor-control dressings because of their peculiar (bucket-shaped) conformation. Cellulose is used especially as healing scaffold/matrix for chronic wound dressings, reducing pain and shortening healing time. For partial and full thickness wounds, it stimulates the granulation and epithelialization process. Wound dressings with modified cellulose can incorporate by co-immobilization different active molecules such as enzymes, antioxidants, hormones, vitamins, antimicrobial drugs [61]. Biosynthesized in high amounts by *Acetobacter xylinum* (Acetobacteraceae), microbial cellulose (MC) is a biocompatible, biodegradable, antimicrobial, hypoallergenic and non-toxic polymer which exhibits a great potential for wound dressings and tissue engineered skin due to its similarity with ECM [62-64]. MC is an innovative product, recommended as an alternative dressing for superficial partial thickness burn wounds [65, 66]. In a recent study, different composites were prepared through impregnation of MC sheets with 2% and 4% suspensions of montmorillonite (MMT), Na-MMT, Ca-MMT and Cu-MMT. Modified MMTs were obtained through cation exchange technique. MC-MMTs nanoreinforced composite films are novel wound dressing materials showing a powerful antibacterial effect against *Escherichia coli* and *S. aureus* and a potential therapeutic importance for wound healing and tissue regeneration [67]. Chitin is the most abundant natural amino polysaccharide (poly-N-acetyl-glucosamine) produced annually almost as

much as cellulose while CS is a poly N-acetyl-glucosaminoglycan obtained by alkaline deacetylation of chitin (see chapter 2). Different formulations of chitin and CS have been obtained: water-soluble chitin ointment as a wound healing assistant [68], microcrystalline partially deacetylated chitin hydrochloride as promising hemostatic material [69], bactericidal films based on chitin and silver nanoparticles for wound dressing applications [70], chitin hydrogel–nano zinc oxide composite bandage [71], bioactive chitin/CS hydrogel membranes and scaffolds cocultured with keratinocyte and fibroblast cells [72], films, sponges and hydrogels of microcrystalline CS with antimicrobial and wound-healing effects for wounds and burns [73], CS–gelatin sponge like/composite films for wound-healing dressing [74], ciprofloxacin loaded chitosan–gelatin composite films [75], CS gel formulation containing epidermal growth factor (EGF) for burn wound healing [76]. Alginates are linear unbranched polysaccharides which contain different amounts of (1→4′)-linked β-D-mannuronic acid and α-L-guluronic acid residues. Alginate-based wound dressings are commonly used for their haemostatic properties in exudation/bleeding wounds and burns and for their high capacity to absorb exudates as previously described in paragraph 7.5.1.2.2. Glycosaminoglycans (hyaluronic acid, heparin and chondroitin sulfate) are the most important components of ECM, essential to skin regeneration. According to the structure (polymer length, degree of sulfation), they modulate the attraction of skin precursor cells and their potential in TE for wounds and burns is well known [77]. Hyaluronic acid (HA) is a naturally occurring non-immunogenic linear polysaccharide made from N-acetyl-dglucosamine and glucuronic acid. It has remarkable effects in scar-free wound healing, supporting angiogenesis and neuritis out growth/repair [78]. HA and silver sulfadiazine-impregnated polyurethane foams have been used for wound dressing applications. After one week of foams application in experimental model, the wound size decreased around 77% at the rat skin level without inflammation [79]. Heparin-coated aligned nanofibers increase endothelial cell infiltration in three-dimensional structures and tissue remodeling in vitro and in vivo, in a full-thickness dermal wound model [80].

Among the proteins, collagen and gelatin are widely used in skin TE. Collagen is the most abundant protein in the human body and the skin. It is produced by fibroblasts and stimulates the wound healing cellular and molecular cascade, development of new tissue and wound debridement. Collagen dressings are recommended for the treatment of partial and full-thickness wounds with minimal to moderate exudates. Different collagen dressings formulations have been developed for wounds and burns: collagen sponges in the healing of experimental deep skin wounds [81], collagen–GAG complex (Glycogen), collagen–minocycline based hydrogels potentially applicable for the treatment of cutaneous wound infections [82], denatured collagen microfiber scaffold seeded with human fibroblasts and keratinocytes for skin grafting [83], electrospun collagen nanofibrous scaffolds for wound repair [84]. Gelatin is administered in various formulations: crosslinked gelatin–alginate and gelatin–hyaluronate sponges with wound healing properties on the full-thickness dorsal skin defects of Wistar rat [85], EGF

containing gelatin based wound dressings in case of bulk loss of tissue or non-healing wounds such as burns, trauma, diabetic [86]. Keratin defines all intermediate filament-forming proteins found in vertebrate epithelia and corneous tissues like horns, claws, hooves [87, 88]. Keratin derivatives are used for chronic wound dressing because of their interaction with the proteolytic wound environment facilitating the healing process. Novel keratin-based wound dressings with improved properties have been found to the release of antibiotics and GFs in a controlled manner [89]. Silk fibroin is widely used for wound dressings due to its unique properties such as biocompatibility, biodegradability, flexibility, adherence, absorption of exudates and minimal inflammatory reaction. Different types of dressing based on SF have been developed: CS blend three dimensional scaffolds for tissue regeneration [90], electrospun SF nanofibers with multiwalled carbon nanotubes for wound dressing [91, 92], SF–alginate-blended sponges/membranes with wound healing effect in full-thickness skin defect of rat [93].

#### **7.5.1.2.6.1.2 Synthetic polymers for wound healing**

Synthetic polymers (composite nanobiomaterials with small pores, 2-3  $\mu\text{m}$  diameter, and very high specific surface area) used for wounds and burns dressing are obtained by various techniques but mainly by electrospinning [54, 55]. Among the bioresorbable synthetic materials, PUs, aliphatic polyesters (PLGA, PLA, PGA, PCL), polyvinylpyrrolidone (PVP), polyvinyl alcohol (PVA) and polyethylene glycol (PEG) have been frequently used for wound healing applications [94, 95]. Some of these polymeric materials can overcome the problems typically associated with natural polymers as they can be synthesized and processed in a highly controlled way, thus leading to homogeneous materials that will present constant and reproducible chemical and physical properties [56]. PUs are synthesized by condensation and polymerization methods from a wide range of bifunctional or higher-order functional monomers. PUs can lead to hard, flexible or elastomeric materials and are also non-toxic, sterilizable, non-adherent and non-allergenic [96]. They are frequently used in wound dressings because of their good barrier properties and oxygen permeability [97]. Research has reported that semi-permeable dressings, many of which are PUs, enhance wound healing [98]. Wound-dressing materials with antibacterial activity from electrospun PU-dextran nanofiber mats containing ciprofloxacin hydrochloride [99], novel absorptive and antibacterial PU membranes [100], PU foam combined with pH-sensitive alginate/bentonite hydrogel [101], fatty acid-based PU films [102] have been recently developed for wound dressing applications. Unnithan et al., prepared an antibacterial electrospun nanofibrous scaffolds by physically blending PU with two biopolymers such as cellulose acetate and zein. Desirable properties such as better hydrophilicity, excellent cell attachment, proliferation and blood clotting ability were obtained by combining PU with natural components [103]. Tegaderm™ (3M Medical) is an available polyurethane wound dressing.

PLA, PGA and PLGA aliphatic polyesters have been extensively investigated because they demonstrate good toxicological safety and biodegradability [104]. These polymers when

degraded through hydrolysis of their ester bonds result in the formation of lactic and glycolic acids, which are safely metabolized into carbon dioxide and water *in vivo*. As such, they have been widely studied for wound dressing [105]. These polymers are administered in various formulations for wound dressing applications: curcumin-loaded PLA [106] and PLGA/collagen nanofibers [107], fusidic acid-loaded PLGA ultrafine fibres [108], collagen–PLLA composite material [109].

PCL has been studied for tissue regeneration and wound healing applications since it promotes a faster healing and reduced inflammatory infiltrate [110]. Extensive research had been conducted on its biocompatibility and efficacy, both *in vitro* and *in vivo*, resulting in FDA approval of a number of medical and drug delivery devices that are composed of PCL. At present, PCL is being regarded as a soft- and hard-tissue-compatible bioresorbable material [111] non-woven matrices from PCL homopolymers and poly-L-lactide– $\epsilon$ -caprolactone [112], silicone-coated non-woven polyester dressing have been found to enhance re-epithelialization in a sheep model of dermal wounds [113].

PVA is a water-soluble synthetic polymer obtained from vinyl acetate by alcoholysis, hydrolysis or aminolysis. It has been applied in several advanced biomedical applications among which wound dressing [114] and wound management [115]. However, PVA exhibits some unfavorable mechanical properties (e.g. strength and flexibility), as well as a relatively poor thermal stability [116] which restrict its use alone as a wound dressing polymeric material. Blending PVA with natural polymers (polysaccharides or proteins) and some other synthetic polymers is attractive because of the abundance of such polymers, easy for chemical derivatization or modification, and in most cases good biocompatibility [117]. Different PVA dressings formulations have been developed for wounds and burns: PVA–gelatin esterified hydrogel membrane for wound dressing compatible with the L929 fibroblast cell line and mice splenocytes [118], PVA–sodium carboxymethylcellulose membranes loaded with fucidic acid [119], novel porous cryo-foam for potential wound healing application starting from PVA and polyacrylic acid based hydrogels [120].

PEG is a hydrophilic, biocompatible, flexible, non-toxic and non-immunogenic polyether. PEG is widely used in various TE applications and applied as co-solvents, lubricants and stabilizers, bases in topical products, precipitants and crystallization agents for proteins, and as chemical agents for pegylation of proteins. PEG macromers have low toxicity, and can be coupled with peptides or GFs and placed *in situ* to fill irregular sites [121]. Ciprofloxacin hydrochloride loaded PEG/CS scaffold [122], PEG functionalized with low molecular weight heparin [123], PEG–protein conjugates was evaluated as an occlusive wound dressing material [124], PEG–gelatin based semi-interpenetrating networks [125] have been recently investigated for the development of wound dressings. Like PVA and PEG, PVP has been extensively used for a wide variety of pharmaceutical and biomedical applications (including wound dressings). This is mostly due to its water absorption and oxygen permeability properties [126, 127]. Like the two above-described hydrophilic synthetic polymers (i.e. PVA and PEG), PVP is usually blended with other polymers (e.g. agar, cellulose or PEG) or cross-linked with carbodiimides in order to modify its solubility,

delivery and erosion profiles, mechanical properties, softness and elasticity [128]. PVP–alginate hydrogel containing nanosilver [129], resveratrol in immobilization on PVP hydrogel dressing [130] have been developed for drug delivery and accelerating wound healing.

**Table 7.2** Most widely studied biodegradable materials for wound dressings with related properties and selected studies where they were used.

<b>Wound material</b>	<b>dressing</b>	<b>Characteristics</b>	<b>Reference</b>
<b>Natural</b>			
Cellulose		Polysaccharide, water-soluble, biodegradable by hydrolysis	[59-65]
Chitosan		Polysaccharide, enzymatically degradable, positively charged, good cell interactions	[66-74] [143][145]
Alginates		Polysaccharide, enzymatically degradable, highly absorbent	[32-35] [131]
Hyaluronic acid		Glycosaminoglycan, ECM component, enzymatically degradable, non immunogenic,	[76, 77]
Collagen		ECM protein, enzymatically degradable, good cell interaction	[79-82] [141][132]
Gelatin		ECM protein, enzymatically degradable, good cell interaction	[83, 84]
Keratin		Fibrous structural proteins, enzymatically degradable	[85-87]
Silk fibroin		Silk protein, enzymatically degradable	[88-91]
<b>Synthetic</b>			
Polyester urethane		Elastomeric polymer, biodegradable	[96-103] [140]
Poly(L-lactic acid)		Aliphatic polyester, very slowly biodegradable by hydrolysis	[106, 109][144]
Poly(glycolic acid)		Aliphatic polyester, biodegradable by hydrolysis	
Poly(lactic-co-glycolic acid)		Copolymer of poly(L-lactic acid) and poly(glycolic acid), biodegradable by hydrolysis	[107, 108]
Poly( $\epsilon$ -caprolactone)		Aliphatic polyester, biodegradable by hydrolysis	[110-113]
Polyvinyl alcohol		Hydrophilic polymer obtained from vinyl acetate biodegradable by hydrolysis	[114-120] [133]
Poly(vinyl pyrrolidone)		Hydrophilic polymer, water-soluble	[128-130]
Poly(ethylene glycol)		Polyether, water soluble	[122-130]

## **7.6 Medicated dressings for wound delivery**

Despite advances in the development of wound dressings, no single dressing is suitable for all types of wounds, and often, different types are needed during the healing of a single wound [134]. Current strategies for wound dressings have aimed at the development of the medicated dressings, which combines the use of pharmaceutical and bioactive agents and dressings used to deliver them. Topical pharmaceutical agents in the form of solutions, creams and ointments are generally applied to wound sites. For example, solutions such as thymol and hydrogen peroxide used commonly for cleansing and debridement, also possess antiseptic and antibacterial actions [135]. The new generation of medicated dressings incorporate new chemicals which have therapeutic value, and overcome some of the disadvantages associated with topical pharmaceutical agents such as short residence times on the wound area. The modern dressings used to deliver active agents (both therapeutic and GFs) to wounds include hydrocolloids, hydrogels, alginates, polyurethane foam/films and gels [136]. Incorporated drugs and proteins play an active role in the wound healing process either directly or indirectly as cleansing or debriding agents for removing necrotic tissue, antimicrobials which prevent or treat infection or growth factors to aid tissue regeneration.

Moreover, the development of medicated dressing aims to prolong the action of active agents over time by allowing consistent and sustained release from a polymeric matrix without the need for frequent dressing change [137]. Drug release from polymeric dressings is generally controlled by: i) hydration of the polymer by fluids, ii) swelling to form a gel, iii) diffusion of drug through the swollen gel and iv) dissolution of the polymer [138-141]. Swelling, drug diffusion and dissolution kinetics are typical of hydrocolloids, alginates, hydrogels and PU. Upon contact of a dry dressing with a moist wound surface, wound exudates penetrates into the polymer matrix. This causes hydration and subsequent swelling of the dressing to form a gel over the wound surface [142]. In aqueous medium, the polymer also undergoes a relaxation process resulting in slow, dissolution of the hydrated polymer containing the drug [143]. Hydrolytic activity of enzymes present in the wound exudates [144] or from bacteria in the case of infected wounds [145] could also influence the mechanism of release of drug from polymeric dressings. Some of the commonly used active compounds and the dressings (and novel polymer systems) used to deliver them to wound sites are described below.

### **7.6.1 Antimicrobials**

The purpose of applying antibiotics and other antibacterials is mainly to prevent or combat infections especially for diabetic foot ulcers [146] surgical and accident [147] wounds. In some cases, the delivery of certain antibiotics from paraffin based ointments such as bismuth subgallate are known to take active part in the wound healing process [148]. The delivery of antibiotics to local wound sites may be a preferred option to systemic administration since aims to: i) reduce the risk of systemic toxicity such as the

cumulative cell and organ toxicity of the aminoglycosides in the ears and kidneys [149, 150], ii) provide tissue compatibility, low occurrence of bacterial resistance and reduced interference with wound healing [151] and iii) overcome the problem of ineffective systemic antibiotic therapy resulting from poor blood circulation at the extremities in diabetic foot ulcers.

Common antibiotics incorporated into available dressings for delivery to wounds include dialkylcarbamoylechloride which is incorporated into Cutisorb® a highly absorbent cotton wool dressing, povidone-iodine used with fabric dressing and silver used with most of the modern dressings [152]. Other antibiotics delivered to wounds include gentamycin from collagen sponges [153], ofloxacin from silicone gel sheets [154] and minocycline from CS film dressings [155]. Some of the reported novel antimicrobial wound healing dressings reported include lactic acid based system for the delivery of ofloxacin and the inhibition of *S. aureus* and *P. aeruginosa* in split-thickness wounds in rats [156]. A CS-PU film dressing incorporating minocycline has also been developed for treating severe burn wounds [142]. Nanofibrous mats composed of PVA and poly(vinyl acetate) fibres loaded with ciprofloxacin HCl (CipHCl) have been also investigated for controlled drug release at targeted sites of injury [133].

The antimicrobial effects of silver are well established, and dressings designed to elute silver ions have been shown to be effective at reducing bacterial colonisation of wounds [157-159]. In particular silver dressings are extensively used in the management of burn wounds following surgical excision [160]. Several products incorporate silver for use as a topical antibacterial agent, such as silver nitrate, silver sulphadiazine (Flammazine™) [161], silver sulphadiazine/chlorhexidine (Silverex®), and silver sulphadiazine-impregnated lipidocolloid wound dressing Urgotul SSD® [159, 162]. Silver impregnated modern dressings available on the UK Drug Tariff include various forms such as fibrous hydrocolloid, PU foam film and silicone gels [152]. Moreover, newly developed products such as Acticoat™ and Silverlon® have a more controlled and prolonged release of nanocrystalline silver to the wound area. This mode of silver delivery allows the dressings to be changed with less frequency, thereby reducing risk of nosocomial infection, cost of care, further tissue damage and patient discomfort [163]. However, consideration of the cytotoxic effects of silver and silver-based products should be taken when deciding on dressings for specific wound care strategies.

### **7.6.2 Growth factors**

GFs take a physiological role in the wound healing process because they are involved with cell division, migration, differentiation, protein expression and enzyme production. The wound healing properties of GFs are mediated through the stimulation of angiogenesis and cellular proliferation, which affects both the production and the degradation of the ECM and also plays a role in cell inflammation and migratory phases of wound healing [164]. A variety of GFs have been reported to participate in the process of wound healing including EGF, PDGF, fibroblast growth factor (FGF), TGF- $\beta$ , IGF-1 and granulocyte-

macrophage colony-stimulating factor (GM-CSF) [165]. Different formulation of dressings have been developed to topically administer some of the above GFs to wound sites. These include hydrogel dressings for delivering TGF- $\beta$ 1 [166], collagen film for delivering PDGF [132], alginate dressings in the form of beads used to deliver EGF [131] PU and collagen film dressings for delivery of EGF [167]. Moreover, the combined use of antimicrobials and GFs has been found to significantly enhance wound healing compared with dressing containing only the antibiotic agents [168].

### 7.6.3 Supplements

Other active compounds applied to enhance the wound healing process are vitamins (A, C and E) and curcumin [169]. The dressings employed for the delivery of vitamins and curcumin include oil based liquid emulsions, creams, ointments, gauze, hydrogels and sheets.

Vitamin A is involved with epithelial cell differentiation [170], collagen synthesis and bone tissue development [171]. It has also been shown to facilitate normal physiological wound healing [172]. Vitamin C is an essential compound for the synthesis of collagen and other organic components of the intra cellular matrix of tissues such as bones, skin and other connective tissues [170]. It is also involved with normal responses to physiological stressors such as in accident and surgical trauma and the need for ascorbic acid increases during times of injury [173]. In addition, vitamin C aids in improving immune function particularly during infection [174]. Lazovic et al., have reported the application of collagen sheet dressings wetted with vitamin A and C solutions over burn wounds and showed significant improvements in the healing of wounds [175]. Vitamin E is an antioxidant and an intermediary in arachidonic acid and prostaglandin metabolism, which are important in inflammatory processes, including burns [176, 177] Vitamin E also promotes angiogenesis and reduces scarring [178]. Aloe vera/vitamin E/ CS microparticles loaded into HA hydrogels have been used for the treatment of skin burns [179]. The release of vitamin E from the polymeric matrices allowed to make one oxidative interruption in the healing cascade thus leading to an improvement of the structural quality and a reduction in the time of healing compared to HA hydrogels alone [179]. Although the delivery of vitamins seems to promote wound healing, these compound are generally administered orally to supplement body stores.

Curcumin (diferuloylmethane) is a yellow crystalline compound and the active ingredient of turmeric, a traditional Asian spice. Curcumin has been reported as a promising wound healing agent both in normal and diabetic-impaired wounds when used topically [180]. Curcumin promotes wound healing by increasing granulation tissue and enhancing the biosynthesis of TGF- $\beta$ 1 and proteins in ECM [181, 182]. Also, it scavenges the free radicals, a major cause for the inflammation and inhibits the peroxide induced oxidative damage in human keratinocytes and fibroblasts [183]. Curcumin has potential antioxidant and anti-infective properties. However, there many drawbacks associated with curcumin administration such as its poor water solubility, photosensitivity and low stability [184].

Hence, several strategies including nanoparticles [185, 186], micelles [187], hydrogels [188] and films [189], have been adopted to improve the water solubility as well as bioavailability of curcumin. Chereddy et al., investigated the combined activity of PLGA and curcumin on topical wound healing. The developed curcumin loaded PLGA nanoparticles were capable to control and maintain the release of the natural compound and lactic acid and significantly accelerated the wound closure by comprehensive healing which included down regulation of inflammatory responses, expedited re-epithelialization and improved granulation tissue formation [185].

## References

1. Lazarus, G.S., et al., Definitions and Guidelines for Assessment of Wounds and Evaluation of Healing. *Archives of Dermatology*, 1994. **130**(4): p. 489-493.
2. Percival, N., Classification of Wounds and their Management. *Surgery*, 2002. **20**(5): p. 114-117.
3. Moore, K., et al., Prediction and monitoring the therapeutic response of chronic dermal wounds. *Int Wound J*, 2006. **3**(2): p. 89-96.
4. Harding, K.G., H.L. Morris, and G.K. Patel, Science, medicine, and the future - Healing chronic wounds. *British Medical Journal*, 2002. **324**(7330): p. 160-163.
5. Ferreira, M.C., et al., Complex wounds. *Clinics (Sao Paulo)*, 2006. **61**(6): p. 571-8.
6. Krasner, D., et al., The ABCs of wound care dressings. *Ostomy Wound Manage*, 1993. **39**(8): p. 66, 68-9, 72 passim.
7. Martin, P., Wound healing--aiming for perfect skin regeneration. *Science*, 1997. **276**(5309): p. 75-81.
8. Shaw, T.J. and P. Martin, Wound repair at a glance. *Journal of Cell Science*, 2009. **122**(18): p. 3209-3213.
9. Werner, S. and R. Grose, Regulation of wound healing by growth factors and cytokines. *Physiological Reviews*, 2003. **83**(3): p. 835-870.
10. Greaves, N.S., et al., Current understanding of molecular and cellular mechanisms in fibroplasia and angiogenesis during acute wound healing. *Journal of Dermatological Science*, 2013. **72**(3): p. 206-217.
11. Hanna, J.R. and J.A. Giacomelli, A review of wound healing and wound dressing products. *J Foot Ankle Surg*, 1997. **36**(1): p. 2-14; discussion 79.
12. Cutting, K.F. and R.J. White, Maceration of the skin and wound bed. 1: Its nature and causes. *J Wound Care*, 2002. **11**(7): p. 275-8.
13. Chen WY, R.A., Lydon MJ., Characterization of biological properties of wound fluid collected during early stages of wound healing, J.I. *Dermatol*, Editor 1992. p. 559-564.
14. Gilliland, E.L., et al., Bacterial colonisation of leg ulcers and its effect on the success rate of skin grafting. *Ann R Coll Surg Engl*, 1988. **70**(2): p. 105-8.
15. Krasner, D., Minimizing factors that impair wound healing: a nursing approach. *Ostomy Wound Manage*, 1995. **41**(1): p. 22-6, 28, 30; quiz 31-2.
16. Lee, J., et al., Surgical site infection in the elderly following orthopaedic surgery. Risk factors and outcomes. *Journal of Bone and Joint Surgery-American Volume*, 2006. **88**(8): p. 1705-12.
17. Patel, G.K., The role of nutrition in the management of lower extremity wounds. *Int J Low Extrem Wounds*, 2005. **4**(1): p. 12-22.
18. Falanga, V., Wound healing and its impairment in the diabetic foot. *Lancet*, 2005. **366**(9498): p. 1736-43.
19. Chedid, M., et al., Glucocorticoids inhibit keratinocyte growth factor production in primary dermal fibroblasts. *Endocrinology*, 1996. **137**(6): p. 2232-7.
20. Beck, L.S., et al., One systemic administration of transforming growth factor-beta 1 reverses age- or glucocorticoid-impaired wound healing. *J Clin Invest*, 1993. **92**(6): p. 2841-9.
21. Inngjerdigen, K., et al., An ethnopharmacological survey of plants used for wound healing in Dogonland, Mali, West Africa. *J Ethnopharmacol*, 2004. **92**(2-3): p. 233-44.
22. Mensah, A.Y., et al., In vitro evaluation of effects of two Ghanaian plants relevant to wound healing. *Phytother Res*, 2006. **20**(11): p. 941-4.
23. Purna, S.K. and M. Babu, Collagen based dressings--a review. *Burns*, 2000. **26**(1): p. 54-62.
24. Queen, D., et al., A dressing history. *Int Wound J*, 2004. **1**(1): p. 59-77.
25. Falabella, A.F., Debridement and wound bed preparation. *Dermatol Ther*, 2006. **19**(6): p. 317-25.

26. van Rijswijk, L., Ingredient-based wound dressing classification: a paradigm that is passe and in need of replacement. *J Wound Care*, 2006. **15**(1): p. 11-4.
27. VJ, J., The use of gauze: Will it ever change, I.W. J, Editor 2006. p. 79–86.
28. Hollinworth H., W.R., The clinical significance of wound pain, W.U. (Aberdeen), Editor 2006. p. 3–16.
29. Lanel, B., et al., Swelling of hydrocolloid dressings. *Biorheology*, 1997. **34**(2): p. 139-53.
30. Thomas S, L.P., A comparative study of twelve hydrocolloid dressings, W.W. Wounds, Editor 1997. p. 1–12.
31. Heenan, P.J., Sebaceous differentiation in microcystic adnexal carcinoma. *Am J Dermatopathol*, 1998. **20**(5): p. 537-8.
32. Thomas, S., Alginate dressings in surgery and wound management--Part 1. *J Wound Care*, 2000. **9**(2): p. 56-60.
33. Winter, G.D., Formation of the scab and the rate of epithelisation of superficial wounds in the skin of the young domestic pig. 1962. *J Wound Care*, 1995. **4**(8): p. 366-7; discussion 368-71.
34. Schmidt RJ, T.T., Calcium alginate dressings, P. J, Editor 1986.
35. Blair, S.D., et al., Clinical trial of calcium alginate haemostatic swabs. *Br J Surg*, 1990. **77**(5): p. 568-70.
36. Debra J.B., C.O., Wound healing: Technological innovations and market overview, 1998. p. 1–185.
37. Thomas S., L.P.A., Comparative review of the properties of six semipermeable film dressings, P. J, Editor 1988. p. 785–787.
38. Moshakis V., F.M.J., Griffiths J.D., McKinna J.A., Tegaderm versus gauze dressing in breast surgery, B.J.C. Pract, Editor 1984. p. 149–152.
39. Morgan, Wounds—What should a dressing formulary include? , H. Pharmacist, Editor 2002. p. 261–266.
40. Baeyens, T.A., Wound care guidelines and formulary for community nurses. *J Wound Care*, 2000. **9**(3): p. 106-8.
41. Ramos-e-Silva, M. and M.C. Ribeiro de Castro, New dressings, including tissue-engineered living skin. *Clinics in Dermatology*, 2002. **20**(6): p. 715-23.
42. Horch, R.E., et al., Tissue engineering of cultured skin substitutes. *J Cell Mol Med*, 2005. **9**(3): p. 592-608.
43. Stashak T. S. , F.E., Othic A., Update on Wound Dressings: Indications and Best Use, C.T.E. Pract, Editor 2004. p. 148-163.
44. Garric, X., M. Vert, and J.P. Moles, [Development of new skin substitutes based on bioresorbable polymer for treatment of severe skin defects]. *Ann Pharm Fr*, 2008. **66**(5-6): p. 313-8.
45. Kim, H.L., et al., Evaluation of electrospun (1,3)-(1,6)-beta-D-glucans/biodegradable polymer as artificial skin for full-thickness wound healing. *Tissue Eng Part A*, 2012. **18**(21-22): p. 2315-22.
46. Lee S.B., J.H.W., Lee Y.W., Cho S.K., Lee Y.M., Song K.W., Park M.H., Hong S.H, Artificial dermis composed of gelatin, hyaluronic acid and (1→3),(1→6)-β-glucan, M. Res, Editor 2003. p. 368–374.
47. Supp, D.M. and S.T. Boyce, Engineered skin substitutes: practices and potentials. *Clinics in Dermatology*, 2005. **23**(4): p. 403-12.
48. Storrie, H. and D.J. Mooney, Sustained delivery of plasmid DNA from polymeric scaffolds for tissue engineering. *Adv Drug Deliv Rev*, 2006. **58**(4): p. 500-14.
49. Nie, X., et al., Innovative strategies for tissue engineered skin based on multiple growth factors gene transfection. *Med Hypotheses*, 2009. **73**(4): p. 516-8.
50. Liu, Y., et al., Reconstruction of a tissue-engineered skin containing melanocytes. *Cell Biol Int*, 2007. **31**(9): p. 985-90.

51. Ruszczak, Z., Effect of collagen matrices on dermal wound healing. *Adv Drug Deliv Rev*, 2003. **55**(12): p. 1595-611.
52. Burke J. F., Y.I.V., Quinby W. C., Bondoc Jr. C. C., and Jung W.K., Successful use of a physiologically acceptable artificial skin in the treatment of extensive burn injury, *A. Surg*, Editor 1981. p. 413–428.
53. Stewart, Next generation products for wound management., S.M.T. Laboratory, Editor 2002, *Worldwide wounds: Wales*, UK.
54. Khang, D., et al., Nanotechnology for regenerative medicine. *Biomedical Microdevices*, 2010. **12**(4): p. 575-87.
55. Supaphol P., S.O., Sangsanoh P., Srinivasan S., Jayakumar R., Nair S.V., Electrospinning of incompatible polymers and their potentials in biomedical applications. *Adv. Polym. Sci.*, 2012. **246**: p. 213–240.
56. Zhong, S.P., Y.Z. Zhang, and C.T. Lim, Tissue scaffolds for skin wound healing and dermal reconstruction. *Wiley Interdiscip Rev Nanomed Nanobiotechnol*, 2010. **2**(5): p. 510-25.
57. Wiegand C., H.U.C., Polymer-based biomaterials as dressings for chronic stagnating wounds, *M. Symp*, Editor 2010. p. 1–13.
58. Huang, S. and X. Fu, Naturally derived materials-based cell and drug delivery systems in skin regeneration. *Journal of Controlled Release*, 2010. **142**(2): p. 149-59.
59. Kennedy J.F., K.C.J., Thorley M., Natural polymers for healing wounds., *A.i.E.C. Polymers*, Editor 2011: Woodhead Publishing, Cambridge, England, p. 97–104.
60. Logeart-Avramoglou, D. and J. Jozefonvicz, Carboxymethyl benzylamide sulfonate dextrans (CMDDBS), a family of biospecific polymers endowed with numerous biological properties: a review. *Journal of Biomedical Materials Research*, 1999. **48**(4): p. 578-90.
61. Medusheva E. O., F.V.N., Ryl'tsev V. V., Kazakova N. A., Filatov N. V., Kulagina A. S., Avagyan A. A., New medical materials with an integral lasting effect based on fibre-forming polymers. *Fibre Chemistry*, 2007. **39**(4): p. 268-271.
62. Czaja, W., et al., Microbial cellulose--the natural power to heal wounds. *Biomaterials*, 2006. **27**(2): p. 145-51.
63. Czaja, W.K., et al., The future prospects of microbial cellulose in biomedical applications. *Biomacromolecules*, 2007. **8**(1): p. 1-12.
64. Fu, L., J. Zhang, and G. Yang, Present status and applications of bacterial cellulose-based materials for skin tissue repair. *Carbohydr Polym*, 2013. **92**(2): p. 1432-42.
65. Muangman, P., et al., Efficiency of microbial cellulose dressing in partial-thickness burn wounds. *J Am Col Certif Wound Spec*, 2011. **3**(1): p. 16-9.
66. Park, S.U., et al., The possibility of microbial cellulose for dressing and scaffold materials. *Int Wound J*, 2014. **11**(1): p. 35-43.
67. Ul-Islam, M., T. Khan, and J.K. Park, Nanoreinforced bacterial cellulose-montmorillonite composites for biomedical applications. *Carbohydr Polym*, 2012. **89**(4): p. 1189-97.
68. Han, Topical formulations of water-soluble chitin as a wound healing assistant. *Fiber Polym.*, 2005. **6**(3): p. 219–223.
69. Sugamori, T., et al., Local hemostatic effects of microcrystalline partially deacetylated chitin hydrochloride. *Journal of Biomedical Materials Research*, 2000. **49**(2): p. 225-32.
70. Madhumathi, K., et al., Development of novel chitin/nanosilver composite scaffolds for wound dressing applications. *Journal of Materials Science-Materials in Medicine*, 2010. **21**(2): p. 807-813.
71. Sudheesh Kumar, P.T., et al., In vitro and in vivo evaluation of microporous chitosan hydrogel/nanofibrin composite bandage for skin tissue regeneration. *Tissue Eng Part A*, 2013. **19**(3-4): p. 380-92.
72. Paul W., R.M.R., Mohanan P.V., Sharma, C.P., Bioactive chitosan scaffold co cultured with keratinocyte and fibroblast cells., *T.B.A. Organs*, Editor 2012. p. 3–9.

73. Dai, M., et al., Chitosan-alginate sponge: preparation and application in curcumin delivery for dermal wound healing in rat. *Journal of Biomedicine and Biotechnology*, 2009. **2009**: p. 595126.
74. He L-Z., L.Y., Yang D., Preparation and performance of chitosan–gelatin sponge-like wound-healing dressing., *J.C.R.T.E. Res.*, Editor 2007. p. 5252–5256.
75. Hima Bindu T.V.L., V.M., Kavitha K., Sastry T., Suresh Kumar R.V., Preparation and evaluation of ciprofloxacin loaded chitosan–gelatin composite films for wound healing activity, *r.B.A. Organs*, Editor 2012. p. 123–130.
76. Alemdaroglu, C., et al., An investigation on burn wound healing in rats with chitosan gel formulation containing epidermal growth factor. *Burns*, 2006. **32**(3): p. 319-27.
77. Salbach, J., et al., Regenerative potential of glycosaminoglycans for skin and bone. *J Mol Med (Berl)*, 2012. **90**(6): p. 625-35.
78. Kogan, G., et al., Hyaluronic acid: a natural biopolymer with a broad range of biomedical and industrial applications. *Biotechnology Letters*, 2007. **29**(1): p. 17-25.
79. Cho, Y.S., et al., Hyaluronic acid and silver sulfadiazine-impregnated polyurethane foams for wound dressing application. *J Mater Sci Mater Med*, 2002. **13**(9): p. 861-5.
80. Kurpinski, K.T., et al., The effect of fiber alignment and heparin coating on cell infiltration into nanofibrous PLLA scaffolds. *Biomaterials*, 2010. **31**(13): p. 3536-42.
81. Sedlarik, K.M., et al., [Comparative animal experiment studies of the effect of exogenous collagen on healing of a deep skin wound]. *Unfallchirurgie*, 1991. **17**(1): p. 1-13.
82. Ghica, M.V., et al., Design and optimization of some collagen-minocycline based hydrogels potentially applicable for the treatment of cutaneous wound infections. *Pharmazie*, 2011. **66**(11): p. 853-61.
83. Kempf, M., et al., A denatured collagen microfiber scaffold seeded with human fibroblasts and keratinocytes for skin grafting. *Biomaterials*, 2011. **32**(21): p. 4782-92.
84. Fullana M.J., W.G.E., Electrospun collagen and its applications in regenerative medicine, *D.D.T. Res.*, Editor 2012. p. 313–322.
85. Choi, Y.S., et al., Studies on gelatin-based sponges. Part III: a comparative study of cross-linked gelatin/alginate, gelatin/hyaluronate and chitosan/hyaluronate sponges and their application as a wound dressing in full-thickness skin defect of rat. *J Mater Sci Mater Med*, 2001. **12**(1): p. 67-73.
86. Ulubayram, K., et al., EGF containing gelatin-based wound dressings. *Biomaterials*, 2001. **22**(11): p. 1345-56.
87. Bragulla, H.H. and D.G. Homberger, Structure and functions of keratin proteins in simple, stratified, keratinized and cornified epithelia. *J Anat*, 2009. **214**(4): p. 516-59.
88. Homberger, D.G., et al., The structure of the cornified claw sheath in the domesticated cat (*Felis catus*): implications for the claw-shedding mechanism and the evolution of cornified digital end organs. *J Anat*, 2009. **214**(4): p. 620-43.
89. Vasconcelos, A. and A. Cavaco-Paulo, Wound dressings for a proteolytic-rich environment. *Appl Microbiol Biotechnol*, 2011. **90**(2): p. 445-60.
90. Gobin, A.S., V.E. Froude, and A.B. Mathur, Structural and mechanical characteristics of silk fibroin and chitosan blend scaffolds for tissue regeneration. *Journal of Biomedical Materials Research Part A*, 2005. **74**(3): p. 465-73.
91. Kang, K., et al., Preparation and characterization of chemically functionalized silica-coated magnetic nanoparticles as a DNA separator. *Journal of Physical Chemistry B*, 2009. **113**(2): p. 536-43.
92. Zhang, X., M.R. Reagan, and D.L. Kaplan, Electrospun silk biomaterial scaffolds for regenerative medicine. *Adv Drug Deliv Rev*, 2009. **61**(12): p. 988-1006.
93. De Moraes M.A., B.M.M., Biocomposite membranes of sodium alginate and silk fibroin fibers for biomedical applications, *J.A.P. Sci*, Editor 2013. p. 3451–3457.
94. M., N., Nanofibers for skin regeneration. *Trends Biomater. Artif. Organs*, 2012. **26**: p. 86–102.

95. Sell S., B.C., Smith M., McClure M., Madurantakam P., Grant J., McManus M., Bowlin G., Extracellular matrix regenerated: tissue engineering via electrospun biomimetic nanofibers, *P. Int.*, Editor 2007. p. 1349–1360.
96. Varma A. K., B.A., Kumar H., Kesav R., Nair S., Efficacy of polyurethane foam dressing in debrided diabetic lower limb wounds, *D. Wounds*, Editor 2006. p. 300-306.
97. Lakshman L. R., S.K.T., Nair S.V., Jayakumar R., Nair S.V., Preparation of silver nanoparticles incorporated electrospun polyurethane nano-fibrous mat for wound dressing. *Journal of Macromolecular Science, Part A: Pure and Applied Chemistry*, 2010. **47**(10): p. 1012-1018.
98. Woodley, D.T., et al., Re-epithelialization. Human keratinocyte locomotion. *Dermatol Clin*, 1993. **11**(4): p. 641-6.
99. Unnithan, A.R., et al., Wound-dressing materials with antibacterial activity from electrospun polyurethane-dextran nanofiber mats containing ciprofloxacin HCl. *Carbohydr Polym*, 2012. **90**(4): p. 1786-93.
100. Yari, A., H. Yeganeh, and H. Bakhshi, Synthesis and evaluation of novel absorptive and antibacterial polyurethane membranes as wound dressing. *J Mater Sci Mater Med*, 2012. **23**(9): p. 2187-202.
101. Oh S-T., K.W.-R., Kim S-H., Chung Y-C., Park J-S., The preparation of polyurethane foam combined with pH-sensitive alginate/bentonite hydrogel for wound dressings. *Fibers and polymers*, 2011. **12**(2): p. 159-165.
102. Gultekin, G., et al., Fatty acid-based polyurethane films for wound dressing applications. *J Mater Sci Mater Med*, 2009. **20**(1): p. 421-31.
103. Unnithan, A.R., et al., Electrospun antibacterial polyurethane-cellulose acetate-zein composite mats for wound dressing. *Carbohydr Polym*, 2014. **102**: p. 884-92.
104. Athanasiou, K.A., G.G. Niederauer, and C.M. Agrawal, Sterilization, toxicity, biocompatibility and clinical applications of polylactic acid/polyglycolic acid copolymers. *Biomaterials*, 1996. **17**(2): p. 93-102.
105. Wang, X.T., et al., Effects of controlled-released sirolimus from polymer matrices on human coronary artery smooth muscle cells. *J Biomater Sci Polym Ed*, 2007. **18**(11): p. 1401-14.
106. Nguyen T.T., G.C., Hwang S-G., Tran L. D., Park J. S., Characteristics of curcumin-loaded poly (lactic acid) nanofibers for wound healing. *Journal of Materials Science*, 2013. **48**(20): p. 7125-7133.
107. Liu S-J., K.Y.-C., Choua C-Y., Chenc J-K., Wud R-C., Yehe W-L., Electrospun PLGA/collagen nanofibrous membrane as early-stage wound dressing. *Journal of Membrane Science*, 2010. **355**(1-2): p. 53-59.
108. Said, S.S., et al., Bioburden-responsive antimicrobial PLGA ultrafine fibers for wound healing. *Eur J Pharm Biopharm*, 2012. **80**(1): p. 85-94.
109. Lee J. S., K.J.K., Chang Y. H., Park S. R., Preparation of collagen/poly(L-lactic acid) composite material for wound dressing. *Macromolecular Research*, 2007. **15**(3): p. 205-210.
110. Merrell, J.G., et al., Curcumin-loaded poly(epsilon-caprolactone) nanofibres: diabetic wound dressing with anti-oxidant and anti-inflammatory properties. *Clin Exp Pharmacol Physiol*, 2009. **36**(12): p. 1149-56.
111. Yoshimoto, H., et al., A biodegradable nanofiber scaffold by electrospinning and its potential for bone tissue engineering. *Biomaterials*, 2003. **24**(12): p. 2077-82.
112. Vaseashta A., E.A., Stamatina I. Nanobiomaterials for controlled release of drugs and vaccine delivery. in *Materials Research Society Spring Meeting*. 2006. San Francisco, CA, United States: Mater. Res. Soc. Symp. Proc.
113. Losi, P., et al., Silicone-coated non-woven polyester dressing enhances reepithelialisation in a sheep model of dermal wounds. *J Mater Sci Mater Med*, 2012. **23**(9): p. 2235-43.

114. Kenawy E., K.E.A., Eldin M.S., El-Meligy M.A., Physically crosslinked poly(vinyl alcohol)-hydroxyethyl starch blend hydrogel membranes: Synthesis and characterization for biomedical applications *Arabian Journal of Chemistry*, 2014. **7**(3): p. 372-380.
115. Zhao L., M.H., Zhai M., Yoshii F., Nagasawa N., Kumec T., Synthesis of antibacterial PVA/CM-chitosan blend hydrogels with electron beam irradiation. *Carbohydrate Polymers*, 2003. **53**(4): p. 439-446.
116. Xia C., X.C., Preparation and characterization of dual responsive sodium alginate-g-poly(vinyl alcohol) hydrogel. *Journal of Applied Polymer Science*, 2011. **123**(4): p. 2244-2249.
117. Coviello, T., et al., Polysaccharide hydrogels for modified release formulations. *Journal of Controlled Release*, 2007. **119**(1): p. 5-24.
118. Pal, K., A.K. Banthia, and D.K. Majumdar, Biomedical evaluation of polyvinyl alcohol-gelatin esterified hydrogel for wound dressing. *J Mater Sci Mater Med*, 2007. **18**(9): p. 1889-94.
119. Lim, C.K., et al., In vitro biocompatibility of chitosan porous skin regenerating templates (PSRTs) using primary human skin keratinocytes. *Toxicology in Vitro*, 2010. **24**(3): p. 721-727.
120. Smith, T.J., J.E. Kennedy, and C.L. Higginbotham, Development of a novel porous cryo-foam for potential wound healing applications. *J Mater Sci Mater Med*, 2009. **20**(5): p. 1193-9.
121. Slaughter, B.V., et al., Hydrogels in regenerative medicine. *Adv Mater*, 2009. **21**(32-33): p. 3307-29.
122. Sinha M., B.R.M., Haldar C., Maiti P., Development of ciprofloxacin hydrochloride loaded poly(ethylene glycol)/chitosan scaffold as wound dressing. *Journal of Porous Materials*, 2013. **20**(4): p. 799-807.
123. Casper, C.L., et al., Functionalizing electrospun fibers with biologically relevant macromolecules. *Biomacromolecules*, 2005. **6**(4): p. 1998-2007.
124. Shingel, K.I., et al., Inflammatory inert poly(ethylene glycol)-protein wound dressing improves healing responses in partial- and full-thickness wounds. *Int Wound J*, 2006. **3**(4): p. 332-42.
125. Bader, R.A., K.T. Herzog, and W.J. Kao, A study of diffusion in poly(ethyleneglycol)-gelatin based semi-interpenetrating networks for use in wound healing. *Polym Bull (Berl)*, 2009. **62**(3).
126. Himly N., D.D., Hardiningsih L., Poly(n-vinylpyrrolidone) hydrogels: 2.Hydrogel composites as wound dressing for tropical environment. *Radiation Physics and Chemistry*, 1993. **42**(4-6): p. 911-914.
127. Lugão A. B., M.L.D.B., Miranda L.F., Alvarez M.R., Rosiak J.M., Study of wound dressing structure and hydration/dehydration properties. *Radiation Physics and Chemistry*, 1998. **52**(1-6): p. 319-322.
128. Gibas I, J.H., Review: synthetic polymer hydrogels for biomedical applications. *Chemistry and Chemical Technology*, 2010. **4**(4): p. 297-304.
129. Singh, R. and D. Singh, Radiation synthesis of PVP/alginate hydrogel containing nanosilver as wound dressing. *J Mater Sci Mater Med*, 2012. **23**(11): p. 2649-58.
130. Momesso R.G.R.A.P., M.C.S., Rogero S.O., Rogero J.R., Spencer P.J., Lugão A.B, Radiation stability of resveratrol in immobilization on poly vinyl pyrrolidone hydrogel dressing for dermatological use. *Radiat. Phys. Chem*, 2010. **79**(283-285).
131. Gu, F., B. Amsden, and R. Neufeld, Sustained delivery of vascular endothelial growth factor with alginate beads. *Journal of Controlled Release*, 2004. **96**(3): p. 463-72.
132. Koempel, J.A., et al., The effect of platelet-derived growth factor on tracheal wound healing. *Int J Pediatr Otorhinolaryngol*, 1998. **46**(1-2): p. 1-8.

133. Jannesari, M., et al., Composite poly(vinyl alcohol)/poly(vinyl acetate) electrospun nanofibrous mats as a novel wound dressing matrix for controlled release of drugs. *Int J Nanomedicine*, 2011. **6**: p. 993-1003.
134. Clark, R.A., Biology of dermal wound repair. *Dermatol Clin*, 1993. **11**(4): p. 647-66.
135. Morgan, D., Wound management products in the drug tariff. *Pharm J*, 1999. **263**: p. 820-825.
136. Joshua S. B., K.M., Howardn N.E.S., Gilliam M. E., Wound healing dressings and drug delivery systems: a review. *Journal of Pharmaceutical Sciences*, 2007. **97**(8): p. 2892–2923.
137. Nair, L.S. and C.T. Laurencin, Polymers as biomaterials for tissue engineering and controlled drug delivery. *Adv Biochem Eng Biotechnol*, 2006. **102**: p. 47-90.
138. Koizumi, T., et al., Rate of release of medicaments from ointment bases containing drugs in suspension. *Chem Pharm Bull (Tokyo)*, 1975. **23**(12): p. 3288-92.
139. Higuchi, T., Rate of release of medicaments from ointment bases containing drugs in suspension. *J Pharm Sci*, 1961. **50**: p. 874-5.
140. Hanes, J., M. Chiba, and R. Langer, Degradation of porous poly(anhydride-co-imide) microspheres and implications for controlled macromolecule delivery. *Biomaterials*, 1998. **19**(1-3): p. 163-72.
141. Sujja-areevath J., M.D.L., Cox P.J., Khan K.A., Relationship between swelling, erosion and drug release in hydrophilic natural gum mini-matrix formulations. *Eur J Pharm Sci*, 1998. **6**(3): p. 207-17.
142. Aoyagi, S., H. Onishi, and Y. Machida, Novel chitosan wound dressing loaded with minocycline for the treatment of severe burn wounds. *International Journal of Pharmaceutics*, 2007. **330**(1-2): p. 138-45.
143. Siepmann, J., et al., HPMC-matrices for controlled drug delivery: a new model combining diffusion, swelling, and dissolution mechanisms and predicting the release kinetics. *Pharm Res*, 1999. **16**(11): p. 1748-56.
144. DuBose, J.W., C. Cutshall, and A.T. Metters, Controlled release of tethered molecules via engineered hydrogel degradation: model development and validation. *Journal of Biomedical Materials Research Part A*, 2005. **74**(1): p. 104-16.
145. Suzuki, Y., et al., A new drug delivery system with controlled release of antibiotic only in the presence of infection. *Journal of Biomedical Materials Research*, 1998. **42**(1): p. 112-6.
146. O'Meara, S., et al., Systematic reviews of wound care management: (3) antimicrobial agents for chronic wounds; (4) diabetic foot ulceration. *Health Technol Assess*, 2000. **4**(21): p. 1-237.
147. Harihara, Y., et al., Effects of applying povidone-iodine just before skin closure. *Dermatology*, 2006. **212 Suppl 1**: p. 53-7.
148. Mai, L.M., et al., Synergistic effect of bismuth subgallate and borneol, the major components of Sulbogin, on the healing of skin wound. *Biomaterials*, 2003. **24**(18): p. 3005-12.
149. Chu, H.Q., et al., Aminoglycoside ototoxicity in three murine strains and effects on NKCC1 of stria vascularis. *Chin Med J (Engl)*, 2006. **119**(12): p. 980-5.
150. Patrick, B.N., M.P. Rivey, and D.R. Allington, Acute renal failure associated with vancomycin- and tobramycin-laden cement in total hip arthroplasty. *Ann Pharmacother*, 2006. **40**(11): p. 2037-42.
151. Doillon, C.J. and F.H. Silver, Collagen-based wound dressing: effects of hyaluronic acid and fibronectin on wound healing. *Biomaterials*, 1986. **7**(1): p. 3-8.
152. The Annual UK Drug Tariff. The Stationary Office, 1988(Nov),1998 (May), 2007(Feb).
153. Rutten, H.J. and P.H. Nijhuis, Prevention of wound infection in elective colorectal surgery by local application of a gentamicin-containing collagen sponge. *Eur J Surg Suppl*, 1997(578): p. 31-5.

154. Sawada, Y., et al., Treatment of dermal depth burn wounds with an antimicrobial agent-releasing silicone gel sheet. *Burns*, 1990. **16**(5): p. 347-52.
155. Galandiuk, S., et al., Absorbable, delayed-release antibiotic beads reduce surgical wound infection. *Am Surg*, 1997. **63**(9): p. 831-5.
156. Sawada, Y., et al., An evaluation of a new lactic acid polymer drug delivery system: a preliminary report. *Br J Plast Surg*, 1994. **47**(3): p. 158-61.
157. Jorgensen, B., et al., Effect of a new silver dressing on chronic venous leg ulcers with signs of critical colonisation. *J Wound Care*, 2006. **15**(3): p. 97-100.
158. Ziegler, K., et al., Reduced cellular toxicity of a new silver-containing antimicrobial dressing and clinical performance in non-healing wounds. *Skin Pharmacol Physiol*, 2006. **19**(3): p. 140-6.
159. Russell, A.D. and W.B. Hugo, Antimicrobial activity and action of silver. *Prog Med Chem*, 1994. **31**: p. 351-70.
160. Fong, J. and F. Wood, Nanocrystalline silver dressings in wound management: a review. *Int J Nanomedicine*, 2006. **1**(4): p. 441-9.
161. Monafo, W.W. and B. Freedman, Topical therapy for burns. *Surg Clin North Am*, 1987. **67**(1): p. 133-45.
162. Carsin, H., et al., A silver sulphadiazine-impregnated lipidocolloid wound dressing to treat second-degree burns. *J Wound Care*, 2004. **13**(4): p. 145-8.
163. Sheridan, R.L., et al., Once-daily wound cleansing and dressing change: efficacy and cost. *J Burn Care Rehabil*, 1997. **18**(2): p. 139-40.
164. Komarcevic, A., [The modern approach to wound treatment]. *Med Pregl*, 2000. **53**(7-8): p. 363-8.
165. Steenfos, H.H., Growth factors and wound healing. *Scand J Plast Reconstr Surg Hand Surg*, 1994. **28**(2): p. 95-105.
166. Puolakkainen, P.A., et al., The enhancement in wound healing by transforming growth factor-beta 1 (TGF-beta 1) depends on the topical delivery system. *J Surg Res*, 1995. **58**(3): p. 321-9.
167. Grzybowski, J., et al., New cytokine dressings. I. Kinetics of the in vitro rhG-CSF, rhGM-CSF, and rhEGF release from the dressings. *International Journal of Pharmaceutics*, 1999. **184**(2): p. 173-8.
168. Park, S.N., J.K. Kim, and H. Suh, Evaluation of antibiotic-loaded collagen-hyaluronic acid matrix as a skin substitute. *Biomaterials*, 2004. **25**(17): p. 3689-98.
169. Wallace, E., Feeding the wound: nutrition and wound care. *Br J Nurs*, 1994. **3**(13): p. 662-7.
170. M, L., *Nutritional biochemistry and metabolism with clinical applications*, ed. n. edition 1991, East Norwalk, CT: Appleton & Lange.
171. Flanigan, K.H., Nutritional aspects of wound healing. *Adv Wound Care*, 1997. **10**(3): p. 48-52.
172. Ehrlich, H.P., H. Tarver, and T.K. Hunt, Effects of vitamin A and glucocorticoids upon inflammation and collagen synthesis. *Annals of Surgery*, 1973. **177**(2): p. 222-7.
173. Pugliese, P.T., The skin's antioxidant systems. *Dermatol Nurs*, 1998. **10**(6): p. 401-16; quiz 417-8.
174. Delafuente, J.C., J.M. Prendergast, and A. Modigh, Immunologic modulation by vitamin C in the elderly. *Int J Immunopharmacol*, 1986. **8**(2): p. 205-11.
175. Lazovic, G., et al., The application of collagen sheet in open wound healing\*. *Ann Burns Fire Disasters*, 2005. **18**(3): p. 151-6.
176. Zampieri, N., et al., A prospective study in children: Pre- and post-surgery use of vitamin E in surgical incisions. *J Plast Reconstr Aesthet Surg*, 2010. **63**(9): p. 1474-8.
177. Thiele, J.J. and S. Ekanayake-Mudiyanselage, Vitamin E in human skin: organ-specific physiology and considerations for its use in dermatology. *Mol Aspects Med*, 2007. **28**(5-6): p. 646-67.

178. Miyazawa, T., et al., Antiangiogenic and anticancer potential of unsaturated vitamin E (tocotrienol). *J Nutr Biochem*, 2009. **20**(2): p. 79-86.
179. Pereira, G.G., et al., Microparticles of Aloe vera/vitamin E/chitosan: microscopic, a nuclear imaging and an in vivo test analysis for burn treatment. *Eur J Pharm Biopharm*, 2014. **86**(2): p. 292-300.
180. Sidhu, G.S., et al., Enhancement of wound healing by curcumin in animals. *Wound Repair Regen*, 1998. **6**(2): p. 167-77.
181. Panchatcharam, M., et al., Curcumin improves wound healing by modulating collagen and decreasing reactive oxygen species. *Mol Cell Biochem*, 2006. **290**(1-2): p. 87-96.
182. Sidhu, G.S., et al., Curcumin enhances wound healing in streptozotocin induced diabetic rats and genetically diabetic mice. *Wound Repair Regen*, 1999. **7**(5): p. 362-74.
183. Phan, T.T., et al., Protective effects of curcumin against oxidative damage on skin cells in vitro: its implication for wound healing. *J Trauma*, 2001. **51**(5): p. 927-31.
184. Sharma, R.A., A.J. Gescher, and W.P. Steward, Curcumin: the story so far. *Eur J Cancer*, 2005. **41**(13): p. 1955-68.
185. Chereddy, K.K., et al., Combined effect of PLGA and curcumin on wound healing activity. *Journal of Controlled Release*, 2013. **171**(2): p. 208-15.
186. Krausz, A.E., et al., Curcumin-encapsulated nanoparticles as innovative antimicrobial and wound healing agent. *Nanomedicine*, 2014.
187. Gong, C., et al., A biodegradable hydrogel system containing curcumin encapsulated in micelles for cutaneous wound healing. *Biomaterials*, 2013. **34**(27): p. 6377-87.
188. Li, X., et al., In situ injectable nano-composite hydrogel composed of curcumin, N,O-carboxymethyl chitosan and oxidized alginate for wound healing application. *International Journal of Pharmaceutics*, 2012. **437**(1-2): p. 110-9.
189. Li X., N.K., Li L., Zhang Z., Chen H. , In vivo evaluation of curcumin nanoformulation loaded methoxy poly(ethylene glycol)-graft-chitosan composite film for wound healing application. *Carbohydrate Polymers*, 2012. **88**(1): p. 84-90.

# Chapter 8

## Porous CS based membranes with improved antimicrobial properties for the treatment of chelonian shell injuries

### Abstract

Recently, much attention has been given to the use of CS in veterinary applications, as a wound healing agent, antimicrobial agent, bandage material, skin grafting template, hemostatic agent and drug delivery vehicle. In this chapter, CS crosslinked porous membranes with improved antimicrobial properties were prepared via freeze-drying technique to promote wound healing and to reduce the bacterial proliferation in chelonians after carapace injuries. Silver nanoparticles (AgNPs) and gentamicin sulphate (GS) were incorporated into the CS matrices to impart the proper antibacterial properties. CS based porous membranes were tested for their physicochemical, thermal, mechanical as well as swelling and degradation behavior at physiological condition. Additionally, GS release profile was investigated, showing a moderate burst effect in the first day followed by a decreasing release rate which was maintained for at least 56 days. Moreover, porous membranes loaded with GS or AgNPs showed good bactericidal activity against both of *Gram*<sup>+</sup> and *Gram*<sup>-</sup> bacteria. Preliminary *in vivo* tests were carried out *Testudo Hermanni* showing the potential use of the developed antimicrobial membranes as an alternative to wet-to-dry conventional treatment.

### 8.1 Introduction

Shell trauma is one of the most common pathological conditions encountered in chelonians and it occurs with different seriousness degrees [1]. Carapace injuries arise mostly from dog bites, automobile and mower accidents, but can also result from falls [1]. Chelonians suffering shell trauma die following internal hemorrhage, organ damage and sepsis due to the recurring bacterial proliferation on the wound site. When a tortoise is injured, the first clinical step consists in classifying the trauma seriousness [1]. Shell

trauma may result in shell fractures with or without loss of bone tissue. In case of shell fracture without loss of bone tissue, closure of the fracture is usually enough to permit resolution of the wound while in case of severe fracture with loss of bone tissue, it is necessary to replace –at least temporarily– the tissue loss, as it will not regenerate spontaneously [2]. To treat chelonian carapace injuries, two clinical approaches are currently employed: i) the immediate closure of the shell by means of screws, plates and bone cements or epoxy resins [1, 3-7] or ii) the periodical direct medication of the wound through wet-to-dry bandages [1, 8], vacuum assisted closure (VAC) [9, 10], platelet-rich-plasma (PRP) treatment [11, 12] or ointments [13, 14]. In the former, the external fixation by means of screws and bone plates is used when wound contamination and infection have been prevented and there is no loss of bone tissue [15, 16] while cements/ epoxy resins are applied to fill bone missing zone [6, 7, 14, 17]. However, epoxy resins may cause an excessive tissue heating due to the exothermic nature of the resin polymerization process, they may require potentially toxic solvents for their removal [18] and they may increase the risk of contaminations that results in infection and sepsis [19]. In the latter treatment, turtle wound is left open in order to periodically disinfect and medicate it. Wet-to-dry bandages are generally used: the primary layer of gauzes is moist with sterile saline or dilute antiseptic solution and is allowed to dry out before its removal; however, dry gauzes are preferred in the presence of wound exudates and lets out necrotic tissue or debris [20]. However, there many drawbacks associated with bandages, such as the damage of healthy tissue, the presence of disperse bacteria and fibers in the wound bed after the removal of gauzes [10]. The use of VAC technology consists on the application of an open-cell foam over the wound, secured to the site with adhesive occlusive drape, to which a suction system is attached [9]. With a constant negative pressure of about 125 mmHg [1] fluids can be collected from the wound permitting the exudate and bacteria removal and granulation tissue formation [21]. Disadvantages include the initial price and the need of proper training to use the equipment. Moreover, VAC technology is unsuitable in the case of a gross infection, lack of wound haemostasis, unprotected vascular anastomoses, foam placement over vessels, the presence of necrotic tissue with scar, exposed organs and malignancy in the wound bed [22]. PRP is a platelet concentrate derived from blood centrifugation procedures [11] which locally delivers high amounts of GFs involved in haemostasis and cell proliferation (fibroblasts, osteoblasts, endothelial cells), promoting the wound healing process [23]. PRP gel must be applied onto the wound surface and is to be protected by a sterile gauze for 48 hours [12], working as a barrier against external microorganisms. Disadvantages of this technique include the need of an initial investment, the need of a proper training to use the equipment and the lack of a thorough understanding of the biologic interactions among PRP gel and the animal tissue. Among ointments, honey and sugar, petroleum impregnated gauzes, triple antibiotic ointment, GS cream and a variety of silver based products have been widely used in managing chelonian shell wound to prevent infection, maintain moisture, enhance healing, or facilitate debridement [14, 24]. Silver (Ag) is

known for its broad antibacterial spectrum; it can be used as ointment and cream (silver sulfadiazine) [8], or it can be loaded in matrices as nanoparticles for its controlled release [25, 26]. Unfortunately, even if it shows an high antimicrobial activity, Ag has a potential toxic effect at higher dosage [27]. On the contrary, honey and sugar are cheaper and effective against a wide variety of *Gram*<sup>+</sup> and *Gram*<sup>-</sup> bacteria, explicating their action by hydrogen peroxide release [28, 29]. GS also exerts antibacterial effects against both *Gram*<sup>+</sup> and *Gram*<sup>-</sup> bacteria [30] but it has a potential nephrotoxic effect depending on its concentrations [31].

In this contest, skin TE could be a promising alternative approach to treat chelonian shell injuries. However, only few studies have been investigated in reptiles [14, 32]. During the wound healing process, the dressing protects the injury and it is supposed to improve dermal and epidermal tissue regeneration [33]. The implantation of biodegradable membranes can overcome the clinical approaches above described, since they completely cover the wound site, avoiding dirt and bacterial infiltration, and their removal is not required at the end of the treatment due to the material biodegradability [33]. Moreover, biodegradable membranes can be loaded using proper drugs acting as drug delivery systems to guarantee an antibiotic time and space controlled release [34]. The localized drug release achieved using biodegradable membranes guarantees lower antibiotic concentrations compared to systemic therapy due to the direct drug release in the wound site, thus assuming a lower toxicity. Alginates, hydrocolloids, hydrogels and foams are the most popular wound dressing in veterinary applications [20] Among the natural polymers, CS (alone or coupled with antimicrobial or antibiotic agents) has been widely used in wound management both in humans (see paragraph 7.5.1.2.6.1.1) and animals. CS stimulates the migration of PMNs and macrophages, explicating an anti-inflammatory effect and is a hemostatic effect, as described in chapter 7.

In this study, CS based porous membranes with improved antimicrobial properties were developed to promote the wound healing process and to reduce the bacterial proliferation in chelonian shell injury site. To improve the mechanical properties and water stability of CS, DSP and GPTMS were used (see chapter 2). GS and AgNPs were loaded into the developed membranes to improve the antibacterial effect against *Gram*<sup>+</sup> and *Gram*<sup>-</sup> bacteria and to guarantee drug controlled release in time and in space without exceeded the toxic dosage for systemic circulation. The obtained porous membranes were analyzed for their physicochemical and morphological properties by SEM and Energy Dispersive X-ray Spectrometry (EDS), their thermal properties by TGA and their mechanical properties were evaluated by tensile and compressive tests. Swelling and dissolution measurements were investigated in media simulating physiological conditions. GS release from CS porous membranes was evaluated by means of UV-VIS spectroscopy, whilst the AgNPs release was indirectly investigated from the antibacterial test results conducted *in vitro* against five different bacteria lineages: *Staphylococcus Aureus* (*Gram*<sup>+</sup>), *Escherichia Coli* (*Gram*<sup>-</sup>), *Enterococcus Faecalis*, *Pseudomonas Aeruginosa* and *Proteus Mirabilis*.

## 8.2 Experimental

### 8.2.1 Materials

CS (medium molecular weight, 75%-85% deacetylation degree), GPTMS, DSP, GS and AgNPs (<110 nm particle size) were supplied from Sigma Aldrich. All solvents used were of analytical grade and used without further purification.

### 8.2.2 Methods

CS was dissolved in acetic acid solution 0.5M to form a CS solution of 2.5% w/v. Four different typologies of CS based membranes were prepared according to the following procedures:

- i. CS/GPTMS\_DSP were obtained by adding GPTMS and DSP to the CS solution, as described in paragraph 2.2.2. Briefly, GPTMS (50% w/w) was added to the CS solution and kept under magnetic stirring for about 1 hour. Afterward, DSP 1M solution (7.5 % v/v) was added dropwise to CS/GPTMS blend (one drop per second), maintained under stirring for about 10 minutes (CS/GPTMS\_DSP).
- ii. CS/GPTMS\_DSP\_AgNPs samples were obtained by adding AgNPs to CS/GPTMS\_DSP solution. Three different amounts of AgNPs respect to the total amount of CS were added: 5%, 10% and 15% w/w (CS/GPTMS\_DSP\_AgNPs5, CS/GPTMS\_DSP\_AgNPs10 and CS/GPTMS\_DSP\_AgNPs15 respectively). Once AgNPs were incorporated, the solutions were kept under magnetic stirring till their homogeneity was reached.

Then, CS/GPTMS\_DSP and CS/GPTMS\_DSP\_AgNPs solutions were poured in multiwell (2 ml in each well for compressive tests, 1 ml for the *in vitro* tests), 20 ml in circular Petri dishes (10 cm of diameter) to obtain 2 mm thickness membranes for *in vivo* test and 90 ml in squared Petri dishes (12 x 12 cm) to obtain 5 mm thickness membranes for antibacterial tests. Once poured, samples were placed in a freezer at -20°C for 24 hours and then freeze-dried at -55°C for minimum 24h (48 hours for membranes with 5 mm thickness).

- iii. For the incorporation of the antibiotic agent, GS was dissolved in ultrapure water to obtain a solution with concentration of 3.5 mg/ml; then, the GS solution was poured dropwise onto the surface of CS/GPTMS\_DSP porous membranes allowing its homogeneous absorption into the CS matrix. Finally, CS/GPTMS\_DSP\_GS samples were cooled down a second time at -20°C for 24 hours and then freeze-dried for 48 hours depending on the thickness of membranes.

### 8.2.3 Sample characterization

#### 8.2.3.1 Morphological characterization and element distribution

The external surface and section morphology of CS/GPTMS\_DSP, CS/GPTMS\_DSP\_AgNP5, CS/GPTMS\_DSP\_AgNP10, CS/GPTMS\_DSP\_AgNP15 and CS/GPTMS\_DSP\_GS porous

membranes was observed by SEM (SEM LEO – 1430, Zeiss). Using an energy dispersive spectrometer (EDS), qualitative compositional analysis was performed and punctual elemental composition of materials with high spatial resolution was accomplished. Samples were sputter coated with gold in a undervacuum chamber prior to SEM-EDS examination.

### **8.2.3.2 Thermogravimetric analysis (TGA)**

Thermal degradation was measured using a TA INSTRUMENT Q500 equipment. The experiments were performed with a 10-15 mg sample in aluminum pans under a dynamic nitrogen atmosphere between 40°C and 800 C. The experiments were run at a scanning rate of 10°C/min and obtained results were analyzed using TA Universal Analysis software.

### **8.2.3.3 Mechanical properties**

#### **8.2.3.3.1 Tensile test**

Rectangular strips of 10X30 mm size were cut from each typology of membranes. Samples were tested in wet state because of the *in vivo* implantation procedure on chelonians requires to soak the membranes with sterile 0.9% NaCl solution before application (see paragraph 8.2.3.8). In addition, the release of exudates from wound site in time maintains the developed scaffold in a moist environment. Before testing in wet state, specimens were immersed in PBS (pH 7.4). Then, samples were strained to break at a constant crosshead speed of 2 mm/min. Using the associated software Test Works, stress-strain curves were obtained, in which the elastic modulus was calculated from the slope of the first linear portion. To measure the thickness of the strips, digital calibrator was used and thicknesses were employed for determining the stress value. Three specimens for each kind of material were tested. The result was expressed as an average value  $\pm$  standard deviation.

#### **8.2.3.3.2 Compressive test**

The compressive mechanical properties were performed on wet porous cylindrical scaffolds using MTS QTest/10 device equipped with load cells of 50 N, respectively. Before testing in wet state, specimens were immersed in PBS (pH 7.4). All samples were compressed at a constant crosshead speed of 2 mm/min to approximately 80% of their original length. Four specimen for each kind of scaffolds were tested. Young's modulus (E), collapse strength and strain ( $\sigma^*$  and  $\epsilon^*$ , respectively) and collapse modulus ( $E^*$ ) were measured from the stress-strain curves. E is the slope of the linear elastic regime,  $E^*$  is the slope of the collapse regime,  $\sigma^*$  and  $\epsilon^*$  are respectively the stress and strain of transition from linear to collapse regime (determined from the intersection of E and  $E^*$  regression lines). The resulted was expressed as an average value  $\pm$  standard deviation.

#### 8.2.3.4 Water uptake and dissolution tests

The water uptake and dissolution behavior of porous samples were evaluated by immersing the samples in PBS (pH 7.4) at 37°C. The water uptake degree was measured after 1, 3, 6, 9 and 24 hours while the dissolution degree was evaluated after 1, 3, 5, 7, 14, 28 and 56 days. The water uptake percentage was calculated as:

$$\Delta W_s (\%) = (W_s - W_0) / W_0 * 100$$

where  $W_0$  and  $W_s$  are the sample weights before and after swelling respectively. The dissolution percentage was calculated as:

$$\Delta W_d (\%) = (W_0 - W_d) / W_0 * 100$$

where  $W_d$  is the dried sample weight after dissolution. The solution pH was measured at the same time intervals during the swelling and the dissolution tests, and its stable value at around 7 (physiological pH) was verified. For each experimental time, three samples were measured and the results were expressed as averages value  $\pm$  standard deviation.

#### 8.2.3.5 Drug release evaluation

GS release from CS/GPTMS\_DSP\_GS membranes was carried out by UV-VIS spectroscopy (CARY 500 SCAN UV-VIS-NIR Spectrophotometer). Samples were immersed in 5 ml of PBS at pH 7.4 and GS concentration in the incubation media was assayed after 1, 3, 6, 24 hours and 2, 7, 14, 28, 56 days. The GS release concentration was reported as a percentage respect to the initial concentration and was calculated from the absorption values using the calibration curves that was prepared starting from GS solution of known concentrations. UV spectra were recorded in a range of 400-200 nm. Five measures for samples were used and the data were reported as mean value  $\pm$  standard deviation.

#### 8.2.3.6 Antibacterial tests

The antibacterial properties of membranes were tested against five pathogenic bacteria isolated from turtles wound infection: *Staphylococcus aureus*, *Escherichia coli*, *Enterococcus faecalis*, *Pseudomonas aeruginosa* and *Proteus mirabilis*. CS/GPTMS\_DSP, CS/GPTMS\_DSP and CS/GPTMS\_DSP\_AgNP10 samples (5 mm thickness) were prepared for antibacterial tests. Strains were stored in tryptone soy broth (TSB, Oxid, Milano) with 20% glycerol at -80°C until needed. For experimental use, the stock cultures were grown on tryptone soy agar (TSA, Oxid) slants, then each strain 2-3 colonies was transferred to 10 ml of TSB and incubated at 37°C for 18 hours to obtain early stationary phase cells. Cell cultures of each microorganism in stationary phase were diluted in TSB and incubated at 37°C until an optical density of  $0.2 \times 10^5$  colony-forming units (CFU/ml) at 600 nm was reached. Tubes with 10 ml of Mueller-Hinton broth (MHB, Oxid) were inoculated with 100  $\mu$ l of culture. Sample weighing 0.25 g were then cut into 1.5 cm<sup>2</sup> pieces and added to each tube. The tubes were then incubated at 37 °C for 18 hours. Depending on the turbidity of

the tubes, serial dilutions with peptone water were made and plated in Petri dishes with 15 mL of TSA culture medium. Colonies (CFU) were counted after incubation at 37 °C for 18 hours. Three replicate plates were used per each dilution of broth.

#### **8.2.3.7 Preliminary *in vivo* tests**

The test was performed in collaboration with the *Clinica per animali esotici* in Rome, Italy. *Testudo Hermannii* chelonians were divided into two different groups consisting of 12 animals each. The first group was treated with wet-to-dry gauzes (conventional treatment), while the second group with GS loaded CS based porous membranes. In detail, CS/GPTMS\_DSP\_GS porous membranes and gauzes were implanted in shell traumatized *Testudo Hermannii* after swab collection, wound lavage, debridement, and disinfection of the injury site.

CS/GPTMS\_DSP\_GS dry membranes were moisten with sterile 0.9% NaCl solution before their application. After CS/GPTMS\_DSP implantation on the wound site, gauzes and adhesive tape were applied over the membranes to guarantee that they were pushed against the wound site. Depending on the extension of the wound site, more than one membrane or gauze could be used. On days 21, the gauzes and CS/GPTMS\_DSP\_GS were removed to evaluate the wound healing process and a new gauze or membrane loaded with the antibiotic agent was replaced in case of the formation of granulation tissue was not occurred. Follow up: 21 days.

#### **8.2.3.8 Statistics**

Experiments were repeated three times and results were expressed as an mean  $\pm$  standard deviation. Statistical significance was calculated using analysis of variance (ANOVA). A comparison between two means was analyzed using Tukey's test with statistical significance level set at  $p < 0.05$ .

### **8.3 Results and discussion**

#### **8.3.1 Morphological characterization and element distribution**

In Fig. 8.1 the surfaces and the fractured sections of CS/GPTMS\_DSP membranes loaded with AgNPs are reported. The Petri-side surface showed a more compact structure as compared to the air-side surface due to the contact with the polystyrene substrate that probably induced a compression of the pores (data not shown). All porous scaffolds showed a typical foam-like morphology with highly interconnected pores on the sections. Mean pore dimensions of the fractured sections were  $27.7 \pm 2.4 \mu\text{m}$ ,  $30 \pm 2.5 \mu\text{m}$ ,  $16 \pm 2.03 \mu\text{m}$  and  $13 \pm 2.9 \mu\text{m}$  for CS/GPTMS\_DSP, CS/GPTMS\_DSP\_AgNP5, CS/GPTMS\_DSP\_AgNP10 and CS/GPTMS\_DSP\_AgNP15 membranes. The pores showed a spherical shape and a decreasing size and density on the surface with increasing the initial AgNPs amount from 5 to 15 wt.% (Fig. 8.1).

SEM images of fracture sections and surfaces of CS/GPTMS\_DSP and GS loaded samples are reported in Fig. 8.2. Spherical, interconnected pores were observed both on the surface and on the section of CS/GPTMS\_DSP\_GS having a pore size dimension of  $26.7 \pm 1.2 \mu\text{m}$ . Microstructure remodelling of CS/GPTMS\_DSP\_GS surface occurred after the rehydration and re-lyophilization processes used for the GS loading treatment: new pores with higher size and formation of sheets on the surface (reducing the interconnectivity) compared to control samples were detected and were associated to the removal of ice crystals during the second freeze-drying step. SEM analysis also evidenced the deposition and homogeneous distribution of the antibiotic agent into the bulk of the scaffold (insert in Fig. 8.2D).

Membrane pore size and its distribution are known to affect cell and nutrient permeability. It has been reported that highly open porous polymer matrices are required for high-density cell seeding, as well as sufficient nutrient and oxygen supply to the cells in the scaffold [35]. Pore sizes of 5-10  $\mu\text{m}$  are favourable for vascularization whilst a multi-pore size membrane (212–250  $\mu\text{m}$ , 250–300  $\mu\text{m}$ , 355–500  $\mu\text{m}$ ) has been investigated to guarantee a better environment for cell proliferation, compared with the uniform-pore size scaffold [35]. On the basis of these considerations, CS/GPTMS\_DSP\_AgNP5, CS/GPTMS\_DSP\_AgNP10 and CS/GPTMS\_DSP\_GS could be ideal candidate materials for the production of porous membranes for wound healing in chelonians. However, a selection of the optimal dressing also requires an evaluation of the mechanical performance, the water uptake behaviour of porous samples.

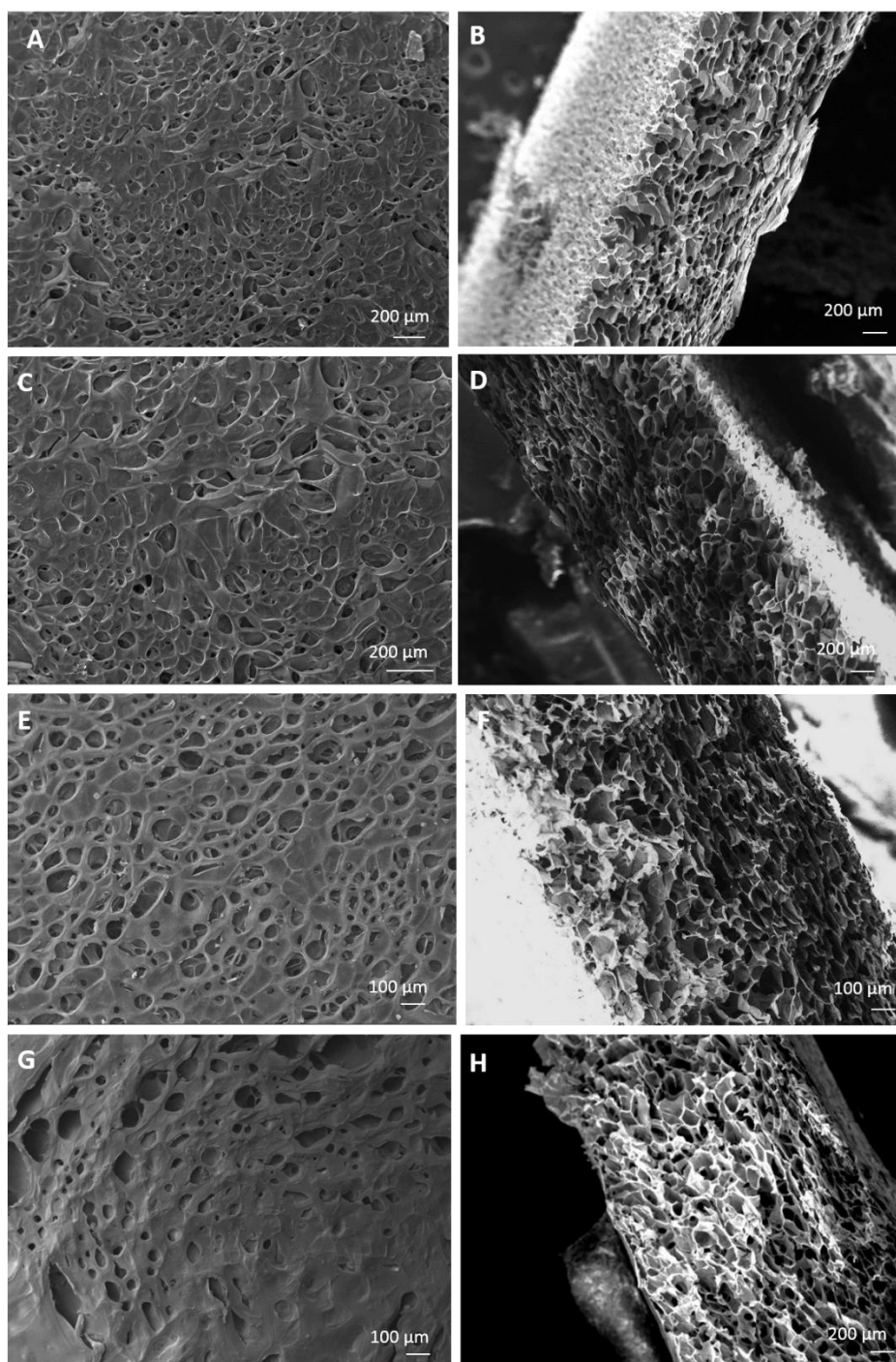


**Fig. 8.1.** SEM micrographs of CS based membrane surfaces (A, C, E, G) and sections (B, D, F, H) after AgNPs addition: (A, B) CS/GPTMS\_DSP; (C, D) CS/GPTMS\_DSP\_AgNP5; (E,F) CS/GPTMS\_DSP\_AgNP10; (G, H) CS/GPTMS\_DSP\_AgNP15.

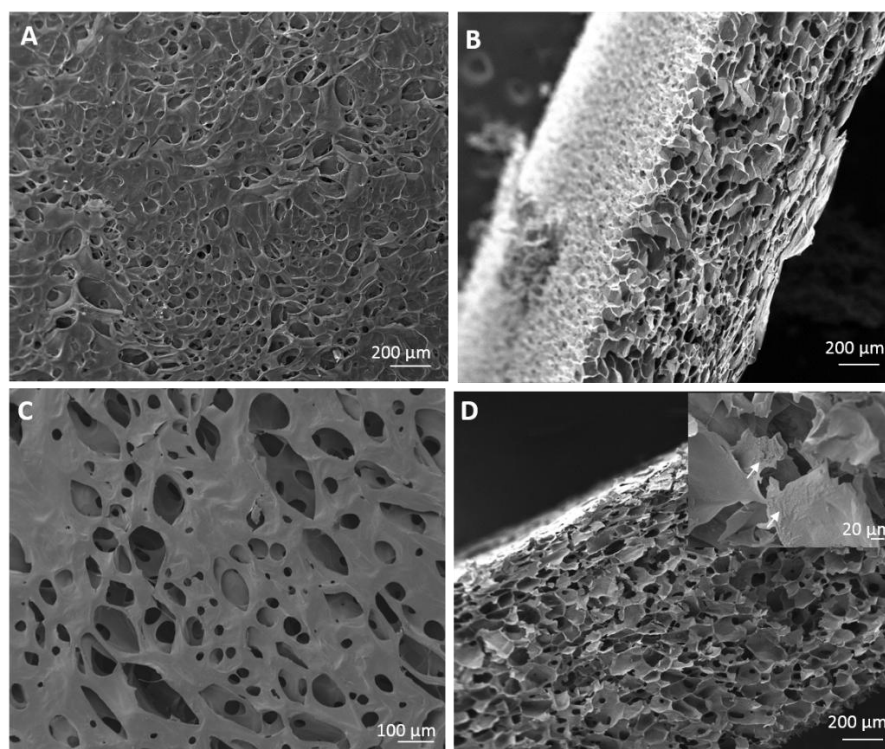


**Fig. 8.2.** SEM micrographs of CS/GPTMS\_DSP (A,B) and CS/GPTMS\_DSP\_GS (C, D) membrane surfaces (A, C) and sections (B, D).

EDS analysis was performed on CS/GPTMS\_DSP, CS/GPTMS\_AgNP5, CS/GPTMS\_AgNP10 and CS/GPTMS\_AgNP15 porous membranes to evaluate the distribution of AgNPs on the surfaces and sections of samples. Fig. 8.3 reports the EDS element-mapping on the sections and surfaces for control and AgNPs loaded CS/GPTMS\_DSP samples, respectively. EDS spectra of AgNPs loaded samples showed the characteristic elements of CS (C and O) and peaks corresponding to Si, Na and P elements associated both to the presence of GPTMS and DSP crosslinkers (data not shown). The green spots corresponding to Ag element were uniformly dispersed both on the sections (Fig. 8.3B, C, D) and surfaces (Fig. 8.3F, G, H) of CS/GPTMS\_DSP\_AgNPs5, CS/GPTMS\_DSP\_AgNPs10 and CS/GPTMS\_DSP\_AgNPs15 samples. The EDS mapping results suggested Ag homogeneous dispersion of Ag for all the analysed compositions.

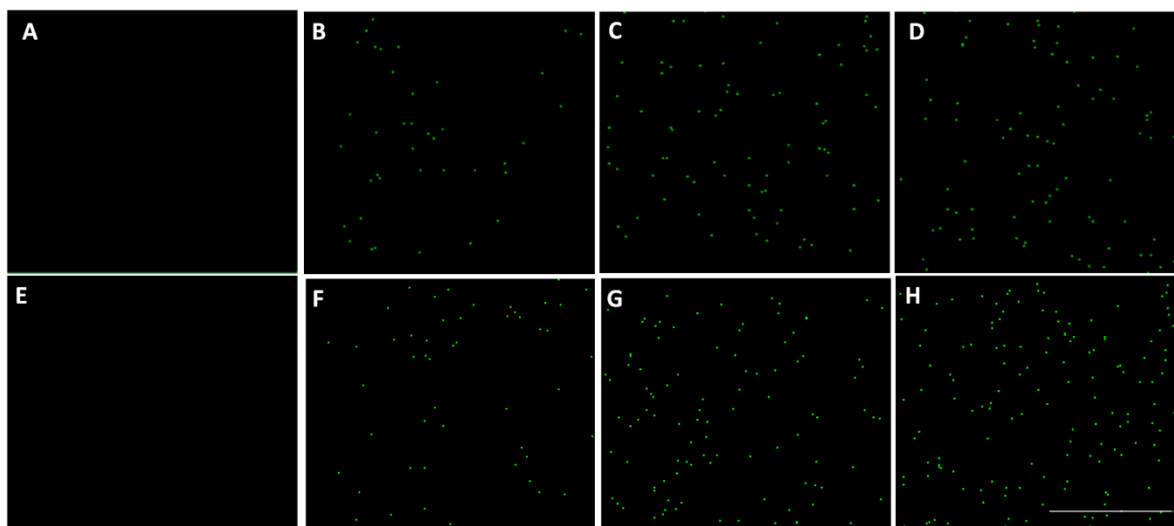


**Fig. 8.3.** EDS spectra of sections (A, B, C, D) and surfaces (E, F, G, H) of CS based porous membrane: (A, E) CS/GPTMS\_DSP; (B, F) CS/GPTMS\_DSP\_AgNP5; (C, G) CS/GPTMS\_DSP\_AgNP10; (D, H) CS/GPTMS\_DSP\_AgNP15. Scale bar: 200  $\mu\text{m}$ . Green spots represented Ag element.

### 8.3.2 Thermogravimetric analysis (TGA)

To further explore the interaction between CS/GPTMS\_DSP and both the antibacterial agents (AgNPs and GS), the prepared membranes were characterized by TGA from 40°C to 800 C. The typical DGA curves of AgNPs and GS loaded membranes are reported in Fig 8.4 and 8.5, respectively. Both the thermal curves clearly exhibited two distinctive thermal decomposition patterns (Fig. 8.4 and Fig. 8.5): the first decomposition step started from about 90°C and continued to above 150 °C and the second weight loss was observed in the 180-550 °C. The initial thermal decomposition is mainly due to the evaporation of the water retained in the membranes and the second thermal decomposition is attributed to the decomposition (oxidative and thermal) of the base membrane matrix, CS, which was completely destroyed around at temperature 550 °C. In addition, specimens exhibited small shoulders at 375 C to 550 °C, which were associated with the thermal destruction of GPTMS and DSP used as crosslinkers (see paragraph 2.3.6).

As shown in Fig. 8.4, after the addition of AgNPs, the onset temperature for the water evaporation and thermal destruction of CS/GPTMS\_DSP\_AgNP5, CS/GPTMS\_DSP\_AgNP10 and CS/GPTMS\_DSP\_AgNP15 membranes delayed slightly to higher temperatures, indicating the increase in water holding capacity and thermal stability, which is mainly due to the more heat stable metallic Ag [36] (Fig. 8.4). The residual percentages of weight of the CS/GPTMS\_DSP, CS/GPTMS\_AgNP5, CS/GPTMS\_AgNP10 and CS/GPTMS\_AgNP15 were 48.3%, 58.4%, 56.5% and 57.2%, respectively. The high residuals of all samples are mainly due to the formation of inorganic compounds containing C, N and O. Similar multi-degradation behavior of CS film was reported in the literature [37]. Additionally, the higher residual content of the AgNPs loaded CS/GPTMS\_DSP membranes is also attributed to the Ag nanoparticles in the membranes. Table 8.1 collects the maximum

water evaporation temperature ( $T_{we}$ ), the maximum degradation rate temperature ( $T_d$ ) of CS based samples and the corresponding weight losses. No differences were observed by increasing AgNPs amount from 5 to 15 wt. %. TGA analysis confirmed the improvement of the thermal stability of CS porous membranes after the addition of AgNPs.

Fig 8.5 reports the DGA curve of control and CS/GPTMS\_DSP\_GS samples. The incorporation of GS into CS/GPTMS\_DSP membranes did not affect the thermal behavior of samples. CS/GPTMS\_DSP\_GS showed a first thermal degradation at around 140 °C and a second stage, associated to the thermal and oxidative decomposition of CS and to the vaporization and elimination of volatile products, starting at 210 °C and reaching a maximum at 630 °C with a total weight loss of 43.7%. CS decomposition masked GS thermal degradation which is known to partially take place in the 200–500 C interval and to have a final oxidation between 500°C and 650 C [38].

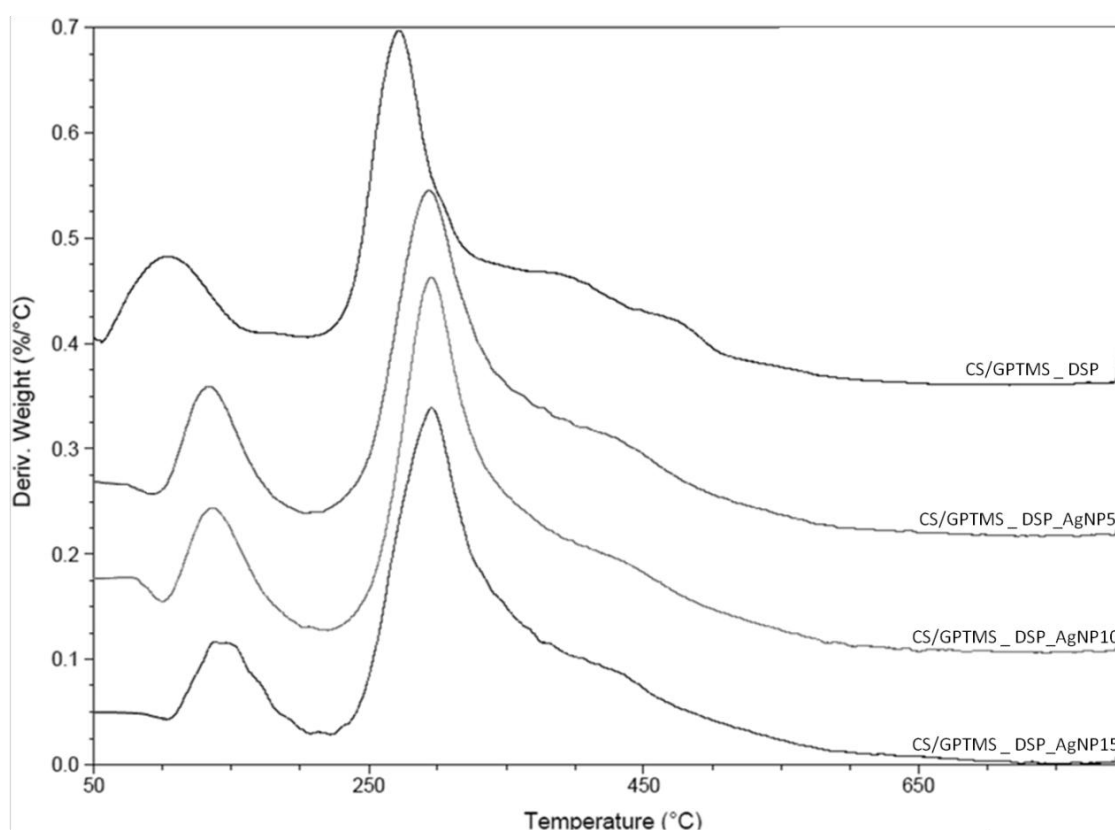


**Fig. 8.4.** First derivative of TGA curves of CS/GPTMS\_DSP, CS/GPTMS\_DSP\_AgNP5, CS/GPTMS\_DSP\_AgNP10 and CS/GPTMS\_DSP\_AgNP15 porous membranes.

**Table 8.1** Maximum water evaporation temperature ( $T_{we}$ ), maximum degradation rate temperature ( $T_d$ ) and corresponding and total weight loss for CS based samples.

Sample	$T_{we}$ (°C)	$T_{we}$ Weight loss (%)	$T_d$ (°C)	$T_d$ Weight loss (%)	Total weight loss (%)
CS/GPTMS_DSP	87.0	10.2	273	41.5	51.7
CS/GPTMS_DSP_AgNP5	137.8	6.0	291.8	35.6	41.6
CS/GPTMS_DSP_AgNP10	138.6	6.5	291.8	36.9	43.5
CS/GPTMS_DSP_AgNP15	138.9	5.8	292.0	37.0	42.8

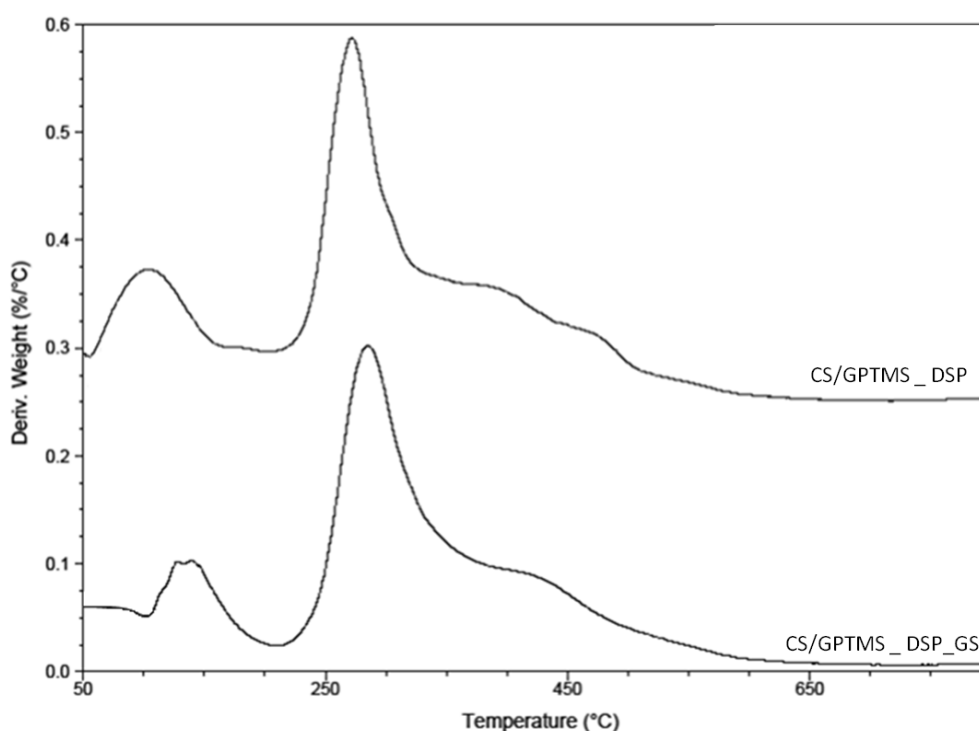


**Fig. 8.5.** First derivative of TGA curves of CS/GPTMS\_DSP and CS/GPTMS\_DSP\_GS porous membranes.

### 8.3.3 Mechanical properties

Tensile and compressive tests were performed on wet state samples to mimic the physiological environment. Moreover, for the *in vivo* implantations on Testudo Hermanni chelonians, membranes were soaked with 0.9 % NaCl solutions prior to implantation to have an increase in membranes flexibility resulting in a easy manipulation (see paragraph 8.2.3.8).

#### 8.3.3.1 Tensile test

Tensile tests were performed on CS/GPTMS\_DSP, CS/GPTMS\_AgNP5, CS/GPTMS\_AgNP10, CS/GPTMS\_AgNP15 and CS/GPTMS\_DSP\_GS porous membranes in wet conditions to determine the effect of the antibacterial agents on sample stiffness. All

samples had a uniform thickness of about 2 mm. CS based membranes samples showed an elasto-plastic behaviour; for all specimens, at low strains (lower than 10%) the stress increased linearly with an increase in the strain while for strains >10%, the stress increased slowly with increasing strain until failure occurred (data not shown).

Addition of AgNPs resulted in a stiffer material confirming the reinforcing effect of the nanoparticles in the polymeric matrix, which is consistent with previously reported results [36, 39]. As can be seen from Table 8.2, the elastic modulus of the samples containing Ag nanoparticles differed significantly from the control (\* $p < 0.05$  for CS/GPTMS\_DSP\_AgNP5 and CS/GPTMS\_DSP\_AgNP10; \*\* $p < 0.01$  for CS/GPTMS\_DSP\_AgNP15). With increasing content of AgNPs, the E increased to a value ranging from 0.400-0.460 MPa (for CS/GPTMS\_DSP\_AgNP5 and CS/GPTMS\_DSP\_AgNP10) to  $1.834 \pm 0.693$  MPa (CS/GPTMS\_DSP\_AgNP15). Moreover, E of membranes containing AgNPs 15 wt.% was significantly different from that of CS/GPTMS\_DSP\_AgNP5 and CS/GPTMS\_DSP\_AgNP10 (\* $p < 0.05$  and \*\* $p < 0.01$  respectively). The increase stiffness of CS/GPTMS\_DSP\_AgNP15 could be ascribed to the decrease of the degree of sample porosity and to the physical attraction between CS and AgNPs.

A significant increase of E value was also observed for CS/GPTMS\_DSP\_GS samples compared to control (\* $p < 0.05$ ) obtaining a value of  $1.180 \pm 0.560$  MPa. This tensile results suggested that the incorporation of GS into CS/GPTMS\_DSP could improve the tensile properties of CS based membrane and is probably associated to the morphological changes that occur following the second freeze-drying.

Materials used to fabricate wound dressing are expected to possess mechanical flexibility to favour their surgical application and the *in vivo* permanence on the wound site. Furthermore, a membrane able to mimic the behaviour of the natural skin tissue should possess a similar elastic modulus. In the literature, the Young's modulus of the skin, E, varies between 0.42 MPa and 0.85 MPa for torsion tests [40], 4.6 MPa and 20 MPa for tensile tests [41, 42] and between 0.05 MPa and 0.15 MPa for suction tests [43]. All the investigated samples had an E value in the range of 0.3-2.5 MPa comparable with the skin range value reported in the literature.

**Table 8.2.** Elastic modulus calculated from the corresponding stress-strain curves of wet CS/GPTMS\_DSP based samples (average value  $\pm$  standard deviation).

Sample	$E_{wet}$ (MPa)
CS/GPTMS_DSP	$0.085 \pm 0.010$
CS/GPTMS_DSP_AgNP5	$0.405 \pm 0.185$
CS/GPTMS_DSP_AgNP10	$0.397 \pm 4.14$
CS/GPTMS_DSP_AgNP15	$1.834 \pm 0.693$
CS/GPTMS_DSP_GS	$1.180 \pm 0.560$

### 8.3.3.2 Compressive test

Fig. 8.6 shows the compressive stress–strain curves for the AgNPs loaded CS/GPTMS\_DPS porous scaffolds. CS/GPTMS\_DSP containing Ag nanoparticles were characterized by a linear elastic regime at low deformations (elongation 0-10%) and a collapse regime at higher deformations (between 10- 20%). Samples did not reach final fracture and underwent densification. Data for wet CS/GPTMS\_DSP specimens were not reported since load value reached were too low to be acquired by the equipment used. The addition of different amount of AgNPs showed an increase of the E and E\* by obtaining values of about 0.030 MPa and 0.035 MPa for CS/GPTMS\_DSP\_AgNP5 and CS/GPTMS\_DSP\_AgNP10 to  $0.070\pm 0.012$  MPa and  $0.093\pm 0.007$  for CS/GPTMS\_DSP based membranes containing the highest amount of silver nanoparticles (15 % wt./wt.), respectively.

In addition, the stress and strain values of transition from linear to collapse regime ( $\sigma^*$  and  $\epsilon^*$ ) were observed for increased stress values ( $0.009\pm 0.001$  MPa for CS/GPTMS\_DSP\_AgNP5 to about 0.011 MPa for CS/GPTMS\_DSP\_AgNP10 and CS/GPTMS\_DSP\_AgNP15) and for increased elongations (from about 20 % for CS/GPTMS\_DSP\_AgNP5 and CS/GPTMS\_DSP\_AgNP10 to  $12.848\pm 2.640$  for CS/GPTMS\_DSP\_AgNP15) in the case of the highest amount of AgNPs (15 wt. %) incorporated into porous membranes compared to 5 wt.% and 10 wt. % Ag nanoparticles addition (Table 8.3). The increase of E and E\* values for CS/GPTMS\_DSP\_AgNP15 samples (statistical significant compared to CS/GPTMS\_DSP\_AgNP5 samples,  $*p<0.05$ ) was a consequence of the mechanical reinforcement associated with the addition of Ag nanoparticles and of the decrease of sample porosity with increasing the amount of AgNPs.

The characteristic stress-strain curve of soft and porous materials was also observed for CS/GPTMS\_DSP\_GS samples (data not shown). After the introduction of GS to CS/GPTMS\_DSP, E, E\*,  $\sigma^*$  and  $\epsilon^*$  were comparable to CS/GPTMS\_DSP\_AgNP15 obtaining values of  $0.088\pm 0.038$  MPa,  $0.093\pm 0.029$  MPa,  $0.010\pm 0.000$  MPa and  $12.848\pm 3.125$ , respectively (Table 8.3). The surface modification following the incorporation of GS into the CS based porous membranes seem to affect the mechanical properties of samples.

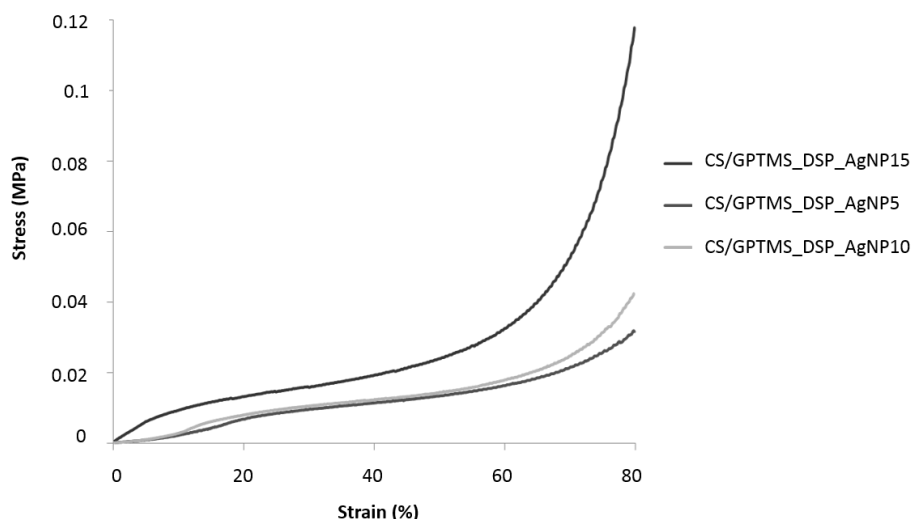


**Fig. 8.6.** Compression stress versus strain curves of CS/GPTMS\_DSP\_AgNP15, CS/GPTMS\_DSP\_AgNP10 and CS/GPTMS\_DSP\_AgNP5.

**Table 8.3** The elastic modulus (E), the collapse modulus (E\*) and the collapse stress and strain ( $\sigma^*$  and  $\epsilon^*$ , respectively) of CS and CS/GPTMS membranes.

Sample	E (MPa)	E* (MPa)	$\sigma^*$ (MPa)	$\epsilon^*$ (%)
CS/GPTMS_DSP_AgNP5	0.032±0.007	0.034±0.005	0.009±0.001	23.720±3.548
CS/GPTMS_DSP_AgNP10	0.030±0.023	0.040±0.021	0.011±0.001	19.300±9.957
CS/GPTMS_DSP_AgNP15	0.070±0.012	0.093±0.007	0.011±0.000	12.848±2.640
CS/GPTMS_DSP_GS	0.088±0.038	0.093±0.029	0.010±0.000	12.848±3.125

### 8.3.4 Water uptake and dissolution tests

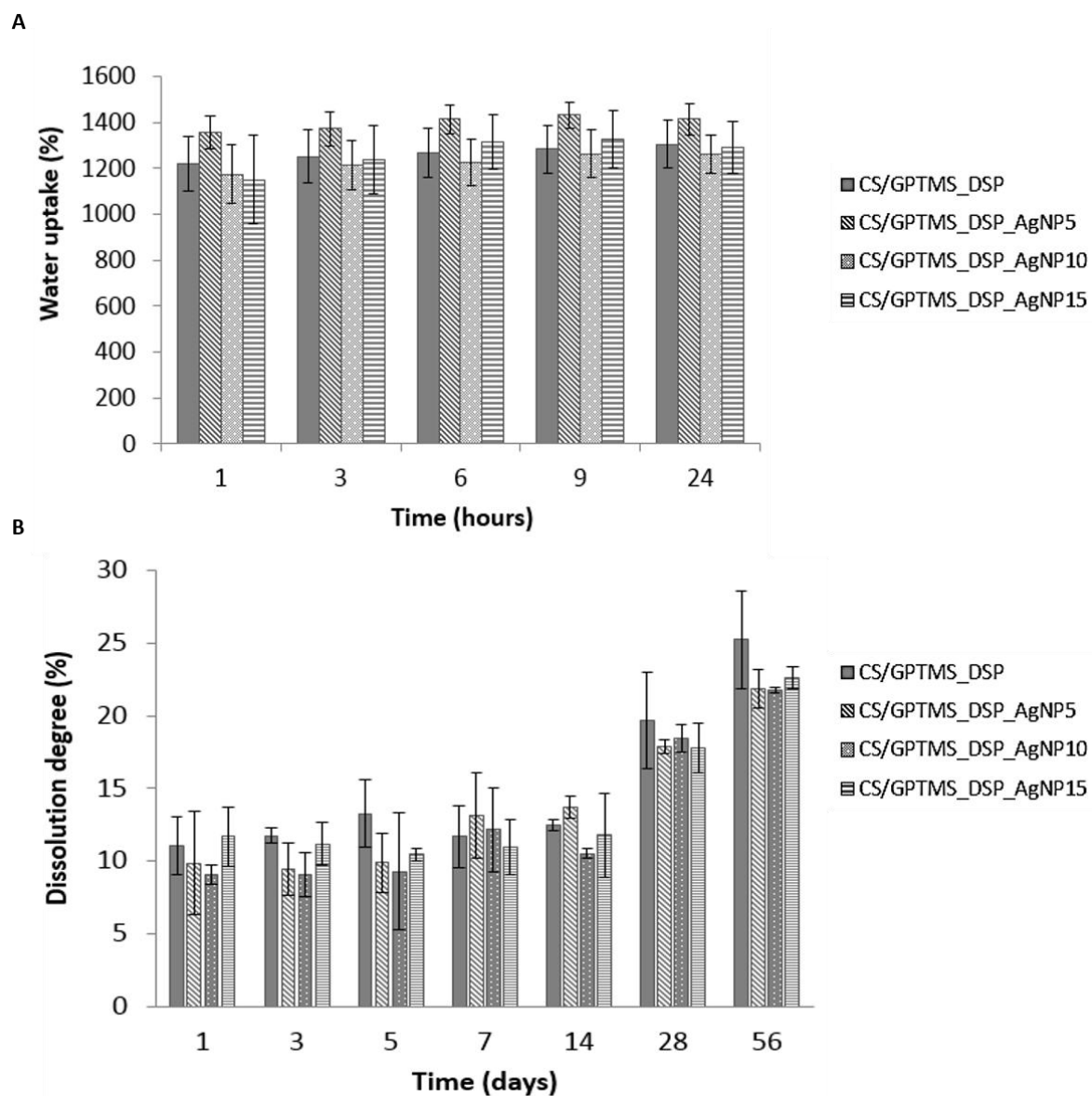
Water uptake and dissolution degree of CS/GPTMS\_DSP samples loaded with Ag nanoparticles and GS are shown in Fig 8.7 and Fig 8.8, respectively.

Fig 8.7A reports the water uptake of CS/GPTMS\_DSP, CS/GPTMS\_DSP\_AgNP5, CS/GPTMS\_DSP\_AgNP10 and CS/GPTMS\_DSP\_AgNP15. A comparison of the swelling percentage of AgNPs loaded samples to control revealed that the water uptake was similar for all samples at each time point. In addition, the incorporation of different amount of Ag nanoparticles into the porous membranes did not affect the water uptake behavior of samples. In detail, porous membranes increased considerably their weight immediately after 1 hour of immersion in PBS solution reaching values of water uptake of 1219±19%, 1356±9, 1174±126% and 1150±193%, for CS/GPTMS\_DSP, CS/GPTMS\_DSP\_AgNP5, CS/GPTMS\_DSP\_AgNP10 and CS/GPTMS\_DSP\_AgNP15 respectively. Then, the swelling values remained stable till the end of the experiment.

The dissolution profiles of AgNPs loaded CS based samples after 56 days of immersion in PBS are presented in Fig. 8.7B. CS/GPTMS\_DSP, the CS/GPTMS\_DSP\_AgNP5,

CS/GPTMS\_DSP\_AgNP10 and the CS/GPTMS\_DSP\_AgNP15 membranes decreased their weight of  $11.0 \pm 2.0$  %,  $9.9 \pm 3.5$  %,  $9.0 \pm 0.7$  % and  $11.6 \pm 2.0$  % after 1 day incubation in PBS, respectively. The initial high weight loss was associated to the release of salts into PBS solution, as described in paragraph 2.3.4. The weight loss values remained stable after 14 days, then a moderately increase was measured after 28-56 days. Final dissolution values of  $25.2 \pm 3.3$  % for CS/GPTMS\_DSP,  $21.8 \pm 1.3$  % for CS/GPTMS\_DSP\_AgNP5,  $21.7 \pm 0.2$  % for CS/GPTMS\_DSP\_AgNP10 and  $22.5 \pm 0.8$  % for CS/GPTMS\_DSP\_AgNP15 were reached after 56 days incubation in PBS. Compared to the control membranes, the addition of AgNPs slightly enhanced the stability in aqueous media of CS/GPTMS\_DSP for long incubation time period in PBS (28 and 56 days). No significant differences were observed between all samples at each time point.

The water uptake of porous membranes was measured to examine the changes of properties of CS/GPTMS\_DSP in the absence and presence of GS. As shown in Fig 8.8A, the water uptake of samples without GS was increased faster than that of the CS/GPTMS\_DSP\_GP. The swelling degree of GS loaded CS/GPTMS\_DSPS reached values of  $863 \pm 205$  % after 1 hours incubation in PBS and a slightly increase was observed till 24 hours of immersion in physiological solution ( $973 \pm 165$  %). Significant differences were observed between control and CS/GPTMS\_DSP\_GS at the first two time points of experiment ( $*p < 0.05$ ). The lower water absorption behavior of CS based samples containing GS could be associated to the microstructure remodelling of the surface that occurs after the loading of the antibiotic agent. Fig. 8.8B shows the percentage weight loss of the CS/GPTMS\_DSP and CS/GPTMS\_DSP\_GS membranes. The weight loss of membranes containing the antibiotic decreased of  $11.4 \pm 0.8$  % after 1 day in PBS and maintained stable till 5 days, showing comparable values to the control. After this time point, the dissolution degree increased from  $14.6 \pm 1.4$  % (7 days in PBS) to  $22.1 \pm 0.0$  % (28 days in PBS). Moreover, weight loss of membranes containing GS showed significant differences compared to CS/GPTMS\_DSP at days 14 ( $***p < 0.001$ ) and was attributed both to the degradation of CS and to the GS release from the polymer matrix. On the contrary, after 56 the sample containing GS was decreased to about 20% of its own weight, meanwhile, the control was decreased approximately to 25% ( $*p < 0.05$ ).



**Fig. 8.7** Water uptake (A) and dissolution degree (B) of CS/GPTMS\_DSP, CS/GPTMS\_DSP\_AgNP5, CS/GPTMS\_DSP\_AgNP10 and CS/GPTMS\_DSP\_AgNP15 porous membranes in PBS as a function of time. Column heights correspond to the mean values. Bars indicate standard deviations ( $n = 3$ ).

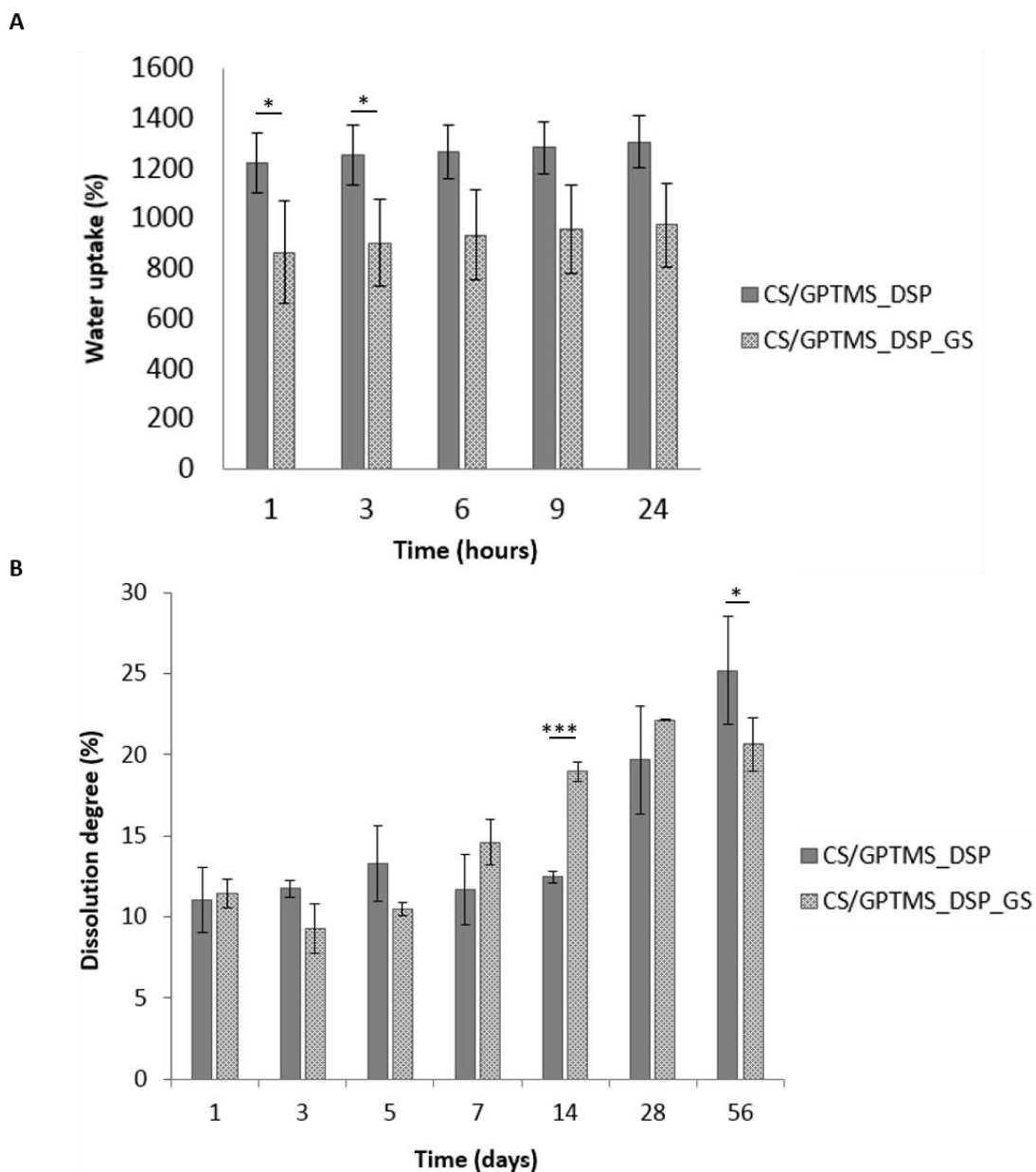


**Fig. 8.8** Water uptake (A) and dissolution degree (B) of CS/GPTMS\_DSP and CS/GPTMS\_DSP\_GS porous membranes in PBS as a function of time. Column heights correspond to the mean values. Bars indicate standard deviations (n = 3). \*p < 0.05, \*\*\*p < 0.001.

### 8.3.5 Drug release evaluation

The GS release from CS/GPTMS\_DSP porous membranes was evaluated *in vitro* quantifying the amount of GS in the collected medium. Figure 8.9 shows the cumulative release after 1, 3, 6 and 24 hours and at 2, 5, 7, 14, 28 and 56 days. An initial burst in release was observed at 24 hours (about 70% with respect to the GS loaded into the membranes) followed by a moderate release over the subsequent days (around 0.55% each day). During the first 24 hours the release could be mainly due to a diffusive mechanism and then, in the following days, the CS/GPTMS\_DSP\_GS degradation allowed the release of a constant and moderate amount of GS.

The delivery of antibiotics to local wound sites through the membranes may be a preferred option to systemic administration since (i) reduce the risk of systemic toxicity such as the cumulative cell and organ toxicity of the aminoglycosides in the ears and kidneys [44, 45], (ii) provide tissue compatibility and low occurrence of bacterial resistance [46] and (iii) overcome the problem of ineffective systemic antibiotic therapy resulting from poor blood circulation. In this specific field for the treatment of chelonian shell traumas, the high initial GS release could enhance the antimicrobial effect, reducing the bacterial population on the wound site since from the first day after implantation.

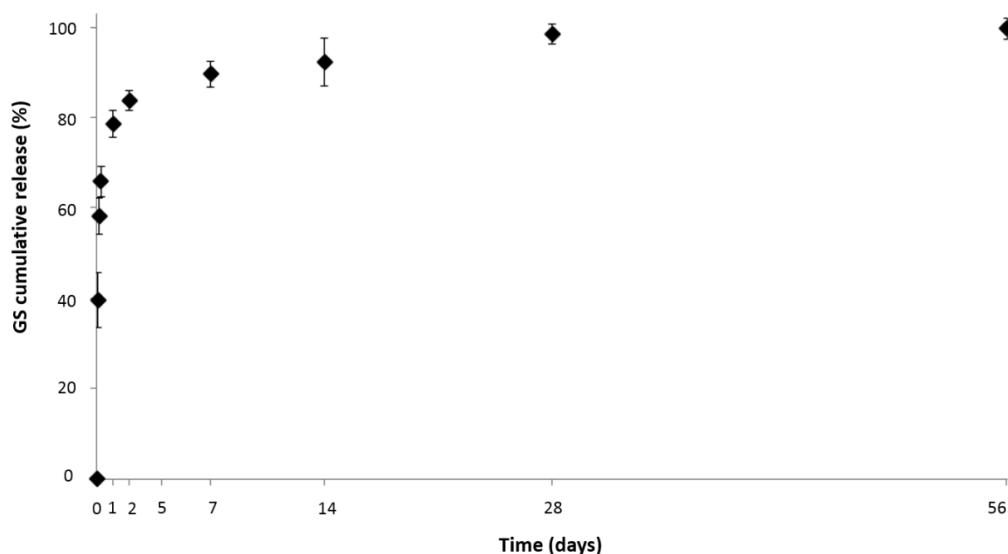


**Fig. 8.9.** GS release after 1, 3, 6, 24 hours and 2, 5, 7, 14, 28 and 56 days. The curve reports the percentage cumulative release values normalized respect to the initial amount of the GS incorporated within the CS/GPTMS\_DSP\_GS porous membranes. Markers correspond to the mean values. Bars indicate standard deviations (n = 3)

### 8.3.6 Antibacterial tests

In order to convict the effect of GS and AgNPs on both Gram<sup>-</sup> (*S. Aureus*, *P. aeruginosa* and *P. mirabilis*) and Gram<sup>+</sup> (*E. Coli*, *E. faecalis*) bacteria, time-killing assay was performed on CS/GPTMS\_DSP, CS/GPTMS\_DSP\_GS and CS/GPTMS\_DSP\_AgNP10 by measuring the reduction of the number of CFU recovered at 18 hours. CS/GPTMS\_DSP\_AgNP10 samples was selected as optimized scaffolds. Fig 8.10 shows the qualitative antibacterial efficacy exerted by the three membranes on *S. Aureus*. The results of the antibacterial screening of the tested scaffolds are presented in Fig. 8.11. The AgNPs impregnated CS membranes showed a bactericidal effect on all bacteria: growth of *S. Aureus*, *E. Coli*, *E. Fecalis*, *P. aeruginosa* and *P. mirabilis* was reduced by logarithmic orders of 3.4, 1.5, 1.8, 2.3 and 1.6, respectively relative to the control. GS loaded CS/GPTMS\_DSP membranes revealed total bactericidal activity against *E. coli*, *S. aureus* and *E. fecalis* but they were unable to inhibit bacterial propagation in case of *P. aeruginosa* strain as compared to CS/GPTMS\_DSP. *P. mirabilis* was reduced by logarithmic orders 1.27 respect to the control, showing results comparable to that obtained by CS/GPTMS\_DSP\_AgNP10. The most effective sample

against *E. coli*, *S. aureus* and *E. fecalis* strains was the one impregnated with GS, while the highest antibacterial activity against *P. aeruginosa* was found for membranes containing Ag nanoparticles. The simultaneous loading of two agents (GS and AgNPs) on CS membranes shows to improve the antibacterial effect against a broad spectrum of strains reducing the risk of infections that can consequently compromise the healing process.

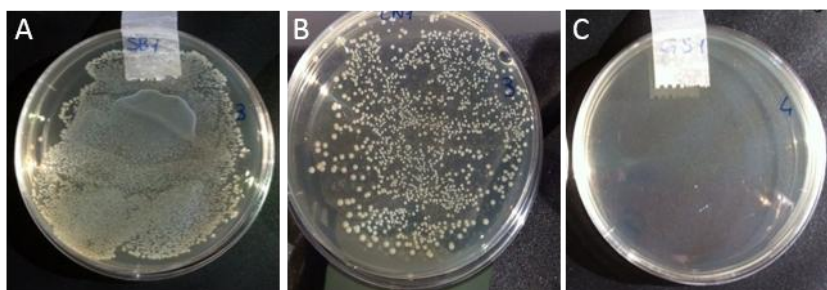


**Fig. 8.10.** *S. Aureus* growth in contact with control (A), CS/GPTMS\_DSP\_GS (B) and CS/GPTMS\_DSP\_AgNP10 (C) membranes without MHB dilutions.

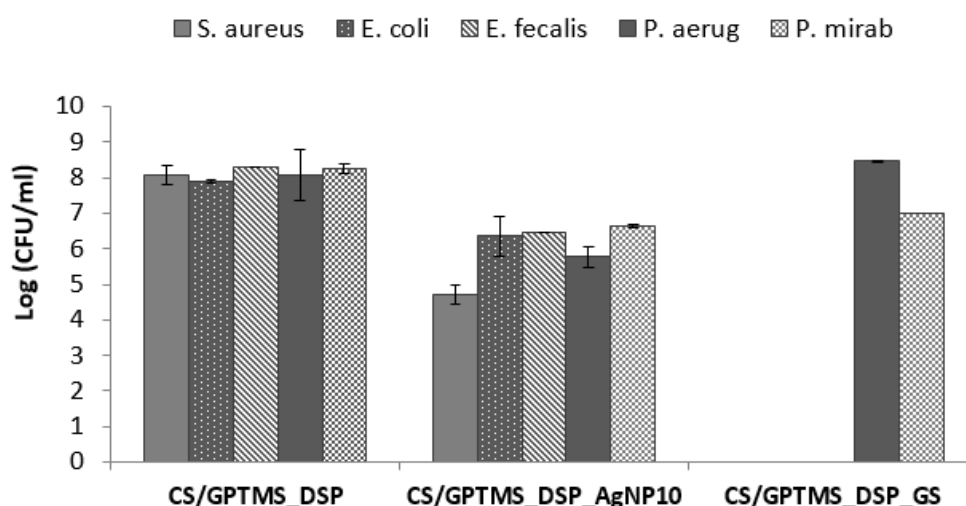


**Fig. 8.11** Kinetics of growth inhibition of *S. Aureus*, *E. Coli*, *E. Fecalis*, *P. aeruginosa* and *P. mirabilis* in presence CS/GPTMS\_DSP, CS/GPTMS\_DSP\_GS and CS/GPTMS\_DSP\_AgNP10.

### 8.3.7 Preliminary *in vivo* tests

To estimate the wound healing effect of the CS/GPTMS\_DSP\_GS for the treatment of carapace injuries in chelonians, GS loaded porous membranes and wet-to-dry gauzes (conventional treatment) were implanted in shell traumatized *Testudo Hermannii* after swab collection, wound lavage, debridement, and disinfection of the injury site. Each wound was observed for a period of 21 days post-operation. On day 21, 33% of the total wounds treated with the CS/GPTMS\_DSP\_GS was healed, whereas, 22% and 45% evidenced the implant failure and chelonian death, respectively. In addition, all chelonians treated with gauze dressing died, showing the potential use of the developed antimicrobial membranes as an alternative to wet-to-dry conventional treatments.

## 8.4 Conclusion

In this chapter, biodegradable wound dressings based on CS porous membranes with improved antimicrobial activities were developed to treat chelonian shell injuries. CS membranes containing different ratios of AgNPs (5, 10 and 15% wt./wt.) or GS were obtained by freeze-drying technique. Mechanical characterization was performed on samples showing that the incorporation of AgNPs or GS enhanced the stiffness of CS/GPTMS\_DSP samples. Moreover, a strict correlation was observed between the Young modulus and the amount of AgNPs incorporated into the membranes: E increased as the AgNPs concentration shifted from 5% wt. to 15 wt.%. The high swelling degree, which is one of the important factor for reducing the risk of wound dehydration, was observed for all antimicrobial agent loaded samples reaching final values of about 1200-1300% and 950% for AgNPs and GS loaded membranes after 24 hours of incubation in physiological solution, respectively. However, the incorporation of the antimicrobial agents into CS/GPTMS\_DSP affected the surface morphologies of porous membranes: i) pore occlusion on the surface of CS based membranes containing AgNPs was detected increasing the amount of AgNPs. For this reason, CS/GPTMS\_DSP\_AgNP10 was selected as ideal candidate for this application field; ii) new pores with higher size and formation of sheets on the surface (reducing the interconnectivity) were formed following rehydration and re-lyophilization processes used for the GS loading treatment. GS release profile from CS/GPTMS\_DSP\_GS demonstrated high burst release of the antibiotics in the first 24 hours (about 70% with respect to the GS loaded into the membranes), followed by gradual release at a decreasing rate over time.

Finally, the investigation focused on the GS and AgNPs (10% wt./wt.) effect on bacterial inhibition, shows that the presence of either AgNPs or GS improved the antimicrobial activity of CS based porous membranes. GS loaded samples were highly efficient against *E. coli*, *S. aureus* and *E. fecalis* strains while CS/GPTMS\_DSP\_AgNP10 increased the inhibitory effect against *P. aeruginosa* and *P. mirabilis* bacteria compared to control and GS loaded samples. From preliminary *in vivo* results, 33% of *Testudo Hermanni* treated with of CS/GPTMS\_DSP\_GS healed confirming the potential use of GS loaded membranes for the treatment in chelonian shell injuries. Future works will be addressed to develop composite membranes based on CS impregnated with both AgNPs and antibiotics GS with the aim to improve the antibacterial activity against a broad spectrum of strains.

## References

1. Fleming, G., Clinical technique: chelonian shell repair. *Journal of Exotic Pet Medicine*, 2008. **17**(4): p. 246-258.
2. Alibardi, L., Ultrastructural and immunohistochemical observations on the process of horny growth in chelonian shells. *Acta Histochem*, 2006. **108**(2): p. 149-62.
3. Jackson, O.F., Tortoise shell repair over two years. *Vet Rec*, 1978. **102**(13): p. 284-5.
4. Frye, F.L., Clinical evaluation of a rapid polymerizing epoxy resin for repair of shell defects in tortoises. *Vet Med Small Anim Clin*, 1973. **68**(1): p. 51-3.
5. Zeman, W.V., F.G. Falco, and J.J. Falco, Repair of the carapace of a box turtle using a polyester resin. *Lab Anim Care*, 1967. **17**(4): p. 424-5.
6. Holt, P.E., Healing of a surgically induced shell wound in a tortoise. *Vet Rec*, 1981. **108**(5): p. 102.
7. Mader, D., Bennet, RA., Funk RS., *Reptile Medicine and Surgery* ed. M. DR. 2006, St Louis: Saunders/Elsevier. 581-630.
8. Mayer, J. and T. Donnelly, *Clinical Veterinary Advisor, Birds and Exotic Pets*, ed. M.J.a.D. TM. 2013: Elsevier Health Sciences.
9. Lafortune, M., et al., Vacuum-assisted closure (Turtle VAC) in the management of traumatic shell defects in chelonians. *Journal of Herpetological Medicine and Surgery*, 2005. **15**: p. 4-8.
10. Mitchell, M.A. and T.N. Tully, *Manual of Exotic Pet Practice*. 2009: Elsevier Health Sciences.
11. Amable, P.R., et al., Platelet-rich plasma preparation for regenerative medicine: optimization and quantification of cytokines and growth factors. *Stem Cell Res Ther*, 2013. **4**(3): p. 67.
12. Pelizzone, I., et al. Shell fracture repair a comparison of different methods and the use of PRP (Platelet-rich-plasma). in *International Conference on Reptile and amphibian Medicine*. 2012. Cremona, Italy.
13. Mathews, K.A. and A.G. Binning, Wound management using honey. *Compend. Con. Edu*, 2002. **24**(1): p. 53-59.
14. Norton, T., et al. Medical and surgical management of automobile and boat strike trauma in Diamondback Terrapins and marine turtles. 2010.
15. Mitchell, M.A. and O. Diaz-Figueroa, Wound management in reptiles. *Vet Clin North Am Exot Anim Pract*, 2004. **7**(1): p. 123-40.
16. Richards, J., Metal bridges-a new technique of turtle shell repair. *J Herp Med Surg*, 2001. **11**(4): p. 31-34.
17. Fowler, A. and N. Magelakis, Shell fracture repair using glass ionomer cement in the long-neck tortoise (*Chelodina longicollis*), in *Wildlife Disease Association-Australian section*. 2003: Healesville, Victoria.
18. Kishimori, C. and G. Lewbart, Chelonian shell fracture repair techniques. *Exotic DVM*, 2001. **3**(5): p. 35-41.
19. Vella, D., Reports on effective modern shell repair techniques for turtles, in *The Veterinarian S.M.P.P. Ltd*, Editor. 2006: Sidney.
20. Tobias, K. Wound management. in *SCIVAC*. 2014. Rimini, Italy.
21. Argenta, L.C. and M.J. Morykwas, Vacuum-assisted closure: a new method for wound control and treatment: clinical experience. *Ann Plast Surg*, 1997. **38**(6): p. 563-76; discussion 577.
22. Gabriel, A., et al., A clinical review of infected wound treatment with Vacuum Assisted Closure (V.A.C.) therapy: experience and case series. *Int Wound J*, 2009. **6 Suppl 2**: p. 1-25.

23. Eppley, B.L., J.E. Woodell, and J. Higgins, Platelet quantification and growth factor analysis from platelet-rich plasma: implications for wound healing. *Plastic and Reconstructive Surgery*, 2004. **114**(6): p. 1502-8.
24. Coke, R.L. and P.A. Reyes-Fore. Treatment of a Radiated tortoise (*Geochelone Radiata*) with Komodo dragon (*Varanus Komodoensis*) bite wounds. 2004.
25. Me, N., et al., Antibacterial activity of chitosan coated Ag-loaded nano-SiO<sub>2</sub> composites *Carbohydrate Polymers*, 2009. **78**(1): p. 54-59.
26. Sanpui, P., et al., The antibacterial properties of a novel chitosan-Ag-nanoparticle composite. *International Journal of Food Microbiology*, 2008. **124**(2): p. 142-6.
27. Kim, S., et al., Oxidative stress-dependent toxicity of silver nanoparticles in human hepatoma cells. *Toxicology in Vitro*, 2009. **23**(6): p. 1076-84.
28. Kwakman, P.H., et al., Medical-grade honey enriched with antimicrobial peptides has enhanced activity against antibiotic-resistant pathogens. *Eur J Clin Microbiol Infect Dis*, 2011. **30**(2): p. 251-7.
29. Kwakman, P.H., et al., How honey kills bacteria. *Faseb Journal*, 2010. **24**(7): p. 2576-82.
30. Rudin, A., et al., Antibacterial activity of gentamicin sulfate in tissue culture. *Appl Microbiol*, 1970. **20**(6): p. 989-90.
31. Falco, F.G., H.M. Smith, and G.M. Arcieri, Nephrotoxicity of aminoglycosides and gentamicin. *J Infect Dis*, 1969. **119**(4): p. 406-9.
32. O'Shea, R. and R.L. Ball. Use of bovine tendon collagen for wound repair in *Varanus komodoensis*. 2010.
33. Abdelrahman, T. and H. Newton, Wound dressings: principles and practice. *Surgery (Oxford)*, 2011. **29**(10): p. 491-495.
34. Boateng, J.S., et al., Wound healing dressings and drug delivery systems: a review. *J Pharm Sci*, 2008. **97**(8): p. 2892-923.
35. Lee, J.J., et al., Investigation on biodegradable PLGA scaffold with various pore size structure for skin tissue engineering. *Current Applied Physics*, 2007. **7**(1): p. 37-40.
36. Rhim, J.W., et al., Preparation and characterization of bio-nanocomposite films of agar and silver nanoparticles: laser ablation method. *Carbohydr Polym*, 2014. **103**: p. 456-65.
37. Bumgardner, J.D., et al., Contact angle, protein adsorption and osteoblast precursor cell attachment to chitosan coatings bonded to titanium. *J Biomater Sci Polym Ed*, 2003. **14**(12): p. 1401-9.
38. Vasile, B.S., et al., Synthesis and characterization of a novel controlled release zinc oxide/gentamicin-chitosan composite with potential applications in wounds care. *International Journal of Pharmaceutics*, 2014. **463**(2): p. 161-9.
39. Chang, P.R., et al., Fabrication and characterisation of chitosan nanoparticles/plasticised-starch composites. *Food Chemistry*, 2010. **120**(3): p. 736-740.
40. Agache, P.G., et al., Mechanical properties and Young's modulus of human skin in vivo. *Arch Dermatol Res*, 1980. **269**(3): p. 221-32.
41. Manschot, J.F. and A.J. Brakkee, The measurement and modelling of the mechanical properties of human skin in vivo--II. The model. *J Biomech*, 1986. **19**(7): p. 517-21.
42. Manschot, J.F. and A.J. Brakkee, The measurement and modelling of the mechanical properties of human skin in vivo--I. The measurement. *J Biomech*, 1986. **19**(7): p. 511-5.
43. Diridollou, S., et al., In vivo model of the mechanical properties of the human skin under suction. *Skin Res Technol*, 2000. **6**(4): p. 214-221.
44. Garric, X., M. Vert, and J.P. Moles, [Development of new skin substitutes based on bioresorbable polymer for treatment of severe skin defects]. *Ann Pharm Fr*, 2008. **66**(5-6): p. 313-8.
45. Stashak T. S. , F.E., Othic A., Update on Wound Dressings: Indications and Best Use, C.T.E. Pract, Editor. 2004. p. 148-163.

46. Kim, H.L., et al., Evaluation of electrospun (1,3)-(1,6)-beta-D-glucans/biodegradable polymer as artificial skin for full-thickness wound healing. *Tissue Eng Part A*, 2012. **18**(21-22): p. 2315-22.

# **Section V**

## **Conclusions**



# Chapter 9

## Final discussion and conclusions

### 9.1 General discussion

Tissue engineering (TE) is defined by Laurencin *et al.* as the application of biological, chemical, and engineering principles to the repair, restoration, or regeneration of living tissues by using biomaterials, cells, and factors alone or in combination [1]. It involves the fundamental understanding of structure–function relationships in normal and pathological tissues and the development of biological substitutes that promote tissue repair and/or functional restoration. In this therapeutic approach, biomaterials, usually in the form of 3 dimensional frameworks, play multiple significant roles to provide structural maintenance of the defect shape and serve as temporary extracellular matrix (ECM) for cell adhesion, proliferation, differentiation, and maturation. After some advances and relatively successful clinical applications for hard tissues over the past decade [2], much of the effort is now being directed at soft tissue reconstruction. Engineering two-dimensional (2D) soft tissues (e.g. cornea [3] and skin [4, 5]), and complex three-dimensional (3D) tissues (e.g. cardiac [6] and neural [7]) is a far more challenging task.

Among the various biomaterials, polysaccharides have recently gained interest as materials for scaffold fabrication, since their carbohydrate moieties interact with or are integral component of several matrix glycoproteins and cell adhesion molecules [8]. Chitosan (CS), a copolymer of glucosamine and N-acetyl-glucosamine, is obtained by alkaline deacetylation of chitin, which is the main component of the exoskeleton of crustaceans, such as shrimps [9]. CS has been widely investigated in TE because it exhibits unique and appealing biological properties in terms of biocompatibility, biodegradability, non-toxicity, antimicrobial, haemostatic, antitumoral and anticholesteremic activities [10-15]. Moreover, due to the cationic nature of CS molecules and the abundant functional amine and hydroxyl groups on its backbone, CS can be easily processed into various forms (gels, sponges, membranes, beads and scaffolds) [16-19] and physically or chemically modified for the delivery of bioactive molecules and drugs [20]. These properties, find several biomedical applications in soft tissue engineering (i.e. cartilage [21, 22], liver [23, 24] and nerve [25, 26]), wound healing [4, 5, 27] and as excipients for drug delivery [16-18, 28, 29]. For most medical application, CS has been crosslinked in order to improve its

mechanical strength and maintain a predefined shape of the implant under physiological conditions. Commonly used chemical crosslinkers in literature include epoxy compounds [30], aldehydes (formaldehyde, glyceraldehyde and glutaraldehyde) [31, 32] and carbodiimides [33]. They all exhibit a certain degree of cytotoxicity and may therefore impair biocompatibility of CS scaffolds. For this reason, increasing interest has been recently gained by less cytotoxic crosslinking agents such as enzymes [34] or naturally derived crosslinking agents, having a lower toxicity [35-38]. The effect of crosslinking strongly influences the *in vivo* performance of the scaffolds in terms of mechanical properties, degradation, water stability and cellular response and can be optimized to obtain the desired properties required in different biomedical applications. A detailed investigation of the influence of different crosslinkers on the features of the final CS membrane is fundamental to select the proper methods to crosslink CS to satisfy specific biological and surgical requirements.

In this work **CS based compact films** were **crosslinked using different compounds** with the aim to provide the basis for the selection of a crosslinking strategy able to impart the required properties to CS membranes in the design of biomaterial constructs for human and veterinary application in soft TE (Chapter 2). Three non cytotoxic and widely used compounds were selected: genipin (GP),  $\gamma$ -glycidoxypropyltrimethoxysilane (GPTMS), dibasic sodium phosphate (DSP) and a combination of GPTMS and DSP (GPTMS\_DSP). CS crosslinked flat membranes were prepared via solvent casting following the addition of the different crosslinking agents. From the preliminary characterization, it was found that CS samples crosslinked with chemical compounds (CS/GP, CS/GPTMS, CS/GPTMS\_DSP) contributed to improve mechanical strength and stability in physiological conditions compared to uncrosslinked and ionic crosslinked CS (CS/DSP). On the other hand, DSP addition increased the hydrophilicity, the water uptake and the flexibility of CS samples. By combining GPTMS with DSP allowed intermediate physic-chemical, mechanical and swelling behaviour were observed with respect to the single use of chemical or ionic compounds.

The obtained results provided the basis for choosing the proper crosslinking method for the development of different typologies of CS scaffolds in i) human peripheral nerve regeneration and ii) animal wound healing applications.

#### **i) Peripheral nerve regeneration in human**

Peripheral nerve regeneration is a challenging task in neurosurgery with relevant clinical and socioeconomic implications since nerve injuries may lead to a lifelong function impairment and pain that may seriously compromise the quality of life [39]. The repair of peripheral nerve lesions has been attempted in many different ways, which have in common the goal of directing the regenerating nerve fibres into the proper distal endoneurial tubes. Coaptation of the two nerve ends is commonly used to repair short nerve defects [40]. When larger nerve gaps exist (20 mm or longer in humans), the

current clinical gold standard for repairing larger nerve deficits involves using nerve autografts. However, autografts are plagued by issues such as a shortage of donor nerves, a mismatch of donor nerve size with the recipient site, and occurrences of neuroma formation; and even in the best-case scenarios, complete recovery of function is rare [41, 42]. Thus, bioengineering strategies are currently focused on developing devices (nerve guide channels, NGCs) that provide an appropriate microenvironment to support and enhance the regeneration process. Advances in engineered NGCs are directed to the mimicking of the properties of natural tissues using multifunctional materials and/or conduits that can solve the limitations associated with traditional surgical approaches (short gap length, lay regeneration time, possible neuroma formation). Among the various biomaterials investigated, CS potential use in peripheral nerve regeneration has been demonstrated both *in vitro* and *in vivo* [43, 44]. Moreover, amino groups of CS chains have been found to regulate the adhesion and proliferation of glial cells and the differentiation of neural stem cells (NSCs) [45].

In this thesis work, **biocompatible and degradable CS membranes** were prepared through different fabrication techniques and parameters were optimized to promote peripheral nerve regeneration. On the basis of the results of the previous part, two crosslinkers were selected (DSP and GPTMS). **Two alternative for CS based hollow NGCs** and a **nanostructured internal filler** were developed.

The two NGC developed are characterized by innovative features in terms of possibility to wrap the membranes during surgery allowing to adapt the NGC dimensions to the patient and to reduce the adhesion of fibrotic tissue to the external part of the conduit that can compromise the nerve regeneration process.

- i. **CS flat membranes** were developed with the aim to obtain a final device that can be easily manipulated and rolled up to obtain flexible NGCs adaptable to the size of the trunked nerves. CS flat scaffolds were crosslinked using DSP alone (CS/DSP) or combined with GPTMS (CS/GPTMS\_DSP) (Chapter 4). The constituent ratio of crosslinking agents and CS was selected in the first part of the thesis to obtain a composite material having both proper mechanical properties and good biocompatibility. CS/DSP and CS/GPTMS\_DSP flat membranes were obtained by solvent casting and they could be easily wrapped to form a NGC. The developed membranes showed a good permeability to small molecules, such as glucose and salts, guaranteeing the exchange of nutrients across the tube wall. *In vitro* characterization performed on model membranes showed that CS/DSP and CS/GPTMS\_DSP material extracts did not exert any cytotoxic effects on Schwann-like cells (RT4\_D6P2T). Cell adhesion, proliferation, and function were evaluated and confirmed on CS/GPTMS\_DSP samples because they showed higher mechanical stability under physiological conditions and they were considered as “the worst case” (biomaterials employed for CS/GPTMS\_DSP fabrication were the same of CS/DSP supplemented with GPTM). Moreover, CS/GPTMS\_DSP showed to direct

RT4-D6P2T attachment resulting in characteristic cell morphology typical of SCs and to support the neurite outgrowth of dorsal root ganglia (DRG) cultured on this substrate. Finally, *in vivo* tests were carried out on both the two types of nerve scaffolds due to their biocompatibility, easy manipulation and suturability. Membranes were used for bridge implantation across 10-mm long median nerve defects in rats, and the outcomes of peripheral nerve repair were evaluated. During *in vivo* tests CS/GPTMS\_DSP tubes were detached from the distal suturing site and functional recovery did not occurred at 12 weeks post-operative as also confirmed by histological investigation. On the contrary, crushed nerve encircled with CS/DSP membranes, allowed nerve fibre regeneration and functional recovery, with effects approaching those elicited by autografts which are considered as the “gold standard” for treating large peripheral nerve defects (20 mm in humans). CS/DSP\_GPTMS conduits revealed a low adhesion of fibrous tissue on the external part compared to CS/DSP.

- ii. **Bi-layer CS membranes** were developed by combining two kinds of CS flat membranes crosslinked with different compounds (optimized in Chapter 4) to produce scaffolds with high capability to promote nerve regeneration (inner layer) and to reduce the risk of collapse under compression during axonal outgrowth on the (outer layer) (Chapter 5). Bi-layer membranes were fabricated by a two-step coating technique and were composed of a CS/DSP inner layer and a CS/GPTMS\_DSP outer layer. For the development of the external side, the amount of GPTMS was decreased from 50% to 25% wt./wt. compared to flat membranes previously prepared (Chapter 4) in order to limit compositional differences between the inner and outer layer and to achieve a tight connection of the final device. The bi-layer samples showed an adequate mechanical behaviour both in terms of elongation at break and resistance, properties imparted by the CS/DSP internal side and CS/GPTMS25\_DSP external side , respectively. The bi-layer device was easily manipulated and wrapped to form a cylindrical conduit under physiological condition after immersion in aqueous solutions for 2-3 minutes . Gradual and controlled permeation to small molecules was observed. Finally, preliminary *in vivo* tests were carried out on the bi-layers flat membranes for bridge implantation across 10-mm long median nerve defects in rats. After 12 weeks post-operative, nerves treated with bi-layer tubes displayed regenerated and aligned fibers at the injury site with no fibrous capsule formation at the external site.
- iii. **An internal filler based on CS electrospun nanofibres** were prepared from 0.5 M acetic acid solutions in the form of non-woven nanofibrous matrices with high specific surface areas and relatively small pores. The electrospun matrices formed a three-dimensional microenvironment for cell attachment and growth mimicking the ECM structure. In peripheral nerve TE, nanofibres with average diameter around 100-200 nm have been reported to be advantageous for glial cell adhesion and

proliferation as compared to fibres characterized by a diameter of 700 nm [46, 47]. Polyethylene oxide (PEO) and dimethylsulphoxide (DMSO) were added to the CS solution to allow CS solution spinnability at high polymer concentration (5% wt./vol.). Optimization of the process and solution parameters allowed to obtain CS nanofibres with size of  $128\pm 17$  nm. Crosslinked nanofibres with improved mechanical and physiological stability were obtained for the first time. DSP was selected as nanofibres crosslinker and it was added to the CS optimized solution before fibre spinning. As observed by morphological analysis, DSP crosslinking did not modify the fibre structure as compared to the uncrosslinked CS nanofibres and **DSP crosslinked CS nanofibres** showed a slightly decrease in fibre dimension ( $109\pm 17$  nm). Moreover, DSP enhanced the mechanical strength (E, from  $63\pm 10$  MPa to  $113\pm 8$  MPa) and the structural integrity under physiological condition of CS nanofibres.

## ii) Wound healing in veterinary application

Recently, much attention has been given to CS in veterinary applications, as a wound healing agent, antimicrobial agent, bandage material, skin grafting template, hemostatic agent and drug delivery vehicle. In this thesis work, due to the similarity of animal wound healing process with humans, CS was selected to obtain **porous membranes with improved antimicrobial activity for the treatment of chelonian shell injuries** (Chapter 8). The bioengineered membrane has the function of protecting the wound site from contamination and it may be produced in order to stimulate the rapid complete regeneration of the injured tissue and healing of the wound. Moreover, bioengineered membranes should be able to : ii) absorb exudates and toxic components from the wound surface; ii) maintain a high humidity at the wound/dressing interface in order to avoid desiccation and to promote re-epithelialization and cellular migration, iii) be biodegradable, avoiding to periodically remove the device causing trauma to the wound and iv) allow the local drug delivery of bioactive molecules or antibiotics. Among the natural polymers, CS (alone or coupled with antimicrobial or antibiotic agents) has been widely used in wound management both in humans and animals [48]. CS have been found to enhance the function of antinflammatory cells such as polymorphonuclear leukocytes (PMN) and macrophages and to promote the formation of granulation tissue [49].

According to the recent literature, the development of skin dressings based on CS for the treatment of chelonian shell injuries seem to be the ideal substitute to conventional veterinary approaches (i.e. epoxy resins [50-55], wet-to-dry bandages [50, 56], vacuum assisted closure (VAC) [57, 58], platelet-rich-plasma (PRP) treatment [59, 60] or ointments [61, 62]) which have all several associated drawbacks.

For this purpose, CS porous membranes with improved antimicrobial properties were prepared by the freeze-drying technique to promote the wound healing process and to reduce the bacterial proliferation in chelonian shell injury. To increase CS mechanical properties and its biocompatibility, GPTMS and DSP crosslinkers were added to the CS

solution (CS/GPTMS\_DSP). The constituent ratio of crosslinking agents and CS was selected in the first part of the thesis (Chapter 2). Moreover, to impart the desired antibacterial properties to the developed membranes, different ratios of silver nanoparticles (AgNPs, 5%, 10% and 15% wt./wt. respect to the total amount of CS) and gentamicin sulphate (GS, 3.5 mg/ml dosage selected according to the conventional veterinary treatment for chelonian carapace healing) were incorporated into the CS matrices. The application of dressing materials based on natural products with antimicrobial properties limits the systemic use of antibiotics whose side-effects often result in wrong action or even damage to the patient's kidney and liver, and also decreasing the bacterial proliferation at the wound site [63, 64]. Mechanical characterization performed on samples showed that the incorporation of AgNPs or GS enhanced the stiffness of CS/GPTMS\_DSP samples. High swelling degree, which is one of the important factor for reducing the risk of wound dehydration, was observed for all antimicrobial agent loaded samples. From the morphological characterization AgNP optimal concentration was selected (10% wt./wt.): total pore occlusion on the surface of CS based membranes containing the maximum amount of AgNP incorporated. GS release was successfully released from CS/GPTMS\_DSP loaded with the antibiotics. Finally, the investigation focused on the GS and AgNPs (10 % wt.wt, optimized concentration) effects on bacterial inhibition: the presence of either AgNPs or GS improved the antimicrobial activity of CS based porous membranes against *Gram*<sup>+</sup> and *Gram*<sup>-</sup> bacteria. From preliminary *in vivo* tests, it was found that GS loaded membranes contributed to enhance wound healing in chelonians compared to wet-to-dry bandages.

## 9.2 Conclusion and future developments

In conclusion, CS based bioartificial constructs showing promising chemico-physical, mechanical and biological properties were developed for soft TE engineering both in human and veterinary applications. The easy processability of CS allowed to obtain different structures by selecting the proper crosslinking and fabrication methods.

Innovative CS based biomedical devices for peripheral nerve repair developed and characterized for their *in vitro* and *in vivo* response showing promising results in terms of biocompatibility and functional recovery. The dip-coating rotating mandrel technique has been preliminary investigated for the obtainment of pre-shaped guides with a diameter depending on the mandrel size. The use of pre-shaped devices could reduce the time of surgery and the risks of surgical mistakes compared to nerve guide membranes, however, adaptability of the device to the nerve size is often required (Fig. 9.1).

Concerning the CS based internal filler, encouraging preliminary *in vitro* results were obtained in collaboration with the Neuroscience University Cavaliere Ottolenghi (Torino, Italy) confirming the ability of cells to adhere and proliferate on CS nanofibrous matrices (Fig. 9.2).

The developed NGCs (CS/DSP or bi-layer samples) and the prepared internal filler (CS nanofibrous matrix) will be finally combined to solve the limitations associated with the use of hollow conduits (short gap length, long regeneration time, neuroma formation). The incorporation of aligned nanofibres into NGCs has been found to induce Schwann cell alignment resulting in oriented axonal growth while preventing neuroma formation in the peripheral nerve injury [65]. Further *in vivo* analysis using rats will be fundamental to analyze the influence of different strategies (materials, structure, topological features, haptotactic cues and chemotactic stimuli) for the regeneration process.

CS porous membranes with improved antimicrobial properties showed inhibitory effects against five different bacterial strains. GS loaded samples were found to totally exert their antibacterial activity against *E. coli*, *S. aureus* and *E. fecalis* bacteria, while AgNP loaded membranes showed slight inhibitory effect against all Gram<sup>+</sup> and Gram<sup>-</sup> strains. By the obtained results, the combined incorporation of both GS and AgNPs into the developed porous membranes could improve the antimicrobial activity against a broad spectrum of strains and, as a consequence, it could reduce bacterial proliferation during wound healing in chelonians. After a preliminary *in vitro* characterization samples, GS and AgNPs samples will be tests for their antibacterial activity .

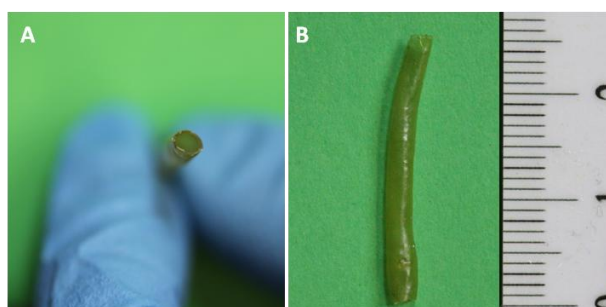


**Fig. 9.1.** Qualitative image of CS/DSP cylindrical conduits prepared by the dip-coating rotating mandrel technique.

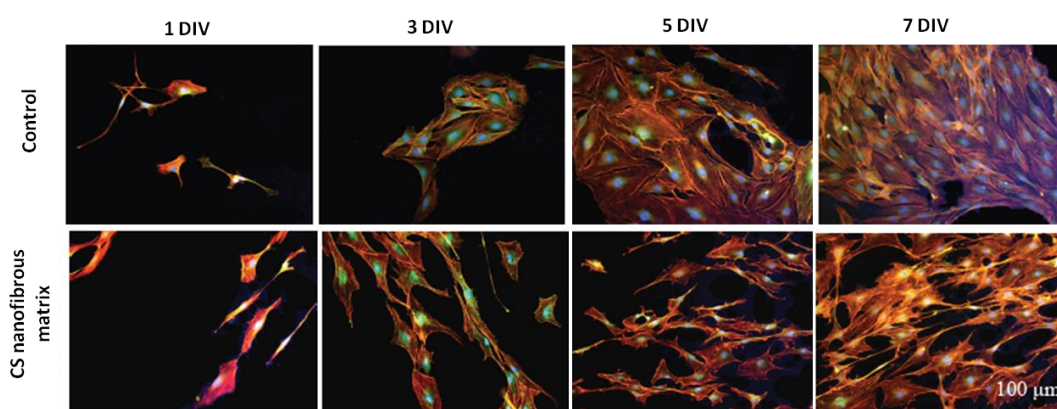


**Fig. 9.2.** Fluorescent imaging of RT4-D6P2T on control and CS nanofibrous matrices after 1,3, 5 and 7 days *in vitro* (DIV). 4'-6-Diamidino-2-phenylindole (DAPI),  $\alpha$ - vinculin and  $\alpha$ -actin staining of proliferating cells on CS nanofibrous matrix and on positive control.

## References

1. Laurencin, C.T., et al., Tissue engineering: Orthopedic applications. *Annual Review of Biomedical Engineering*, 1999. **1**: p. 19-46.
2. Amini, A.R., C.T. Laurencin, and S.P. Nukavarapu, Bone tissue engineering: recent advances and challenges. *Crit Rev Biomed Eng*, 2012. **40**(5): p. 363-408.
3. Nishida, K., et al., Corneal reconstruction with tissue-engineered cell sheets composed of autologous oral mucosal epithelium. *New England Journal of Medicine*, 2004. **351**(12): p. 1187-1196.
4. Mi, F.L., et al., Control of wound infections using a bilayer chitosan wound dressing with sustainable antibiotic delivery. *Journal of Biomedical Materials Research*, 2002. **59**(3): p. 438-449.
5. Dai, M., et al., Chitosan-Alginate Sponge: Preparation and Application in Curcumin Delivery for Dermal Wound Healing in Rat. *Journal of Biomedicine and Biotechnology*, 2009.
6. Lu, W.N., et al., Functional improvement of infarcted heart by co-injection of embryonic stem cells with temperature-responsive chitosan hydrogel. *Tissue Eng Part A*, 2009. **15**(6): p. 1437-47.
7. Valmikinathan, C.M., et al., Photocrosslinkable chitosan based hydrogels for neural tissue engineering. *Soft Matter*, 2012. **8**(6): p. 1964-1976.
8. Minuth, W.W., M. Sittinger, and S. Kloth, Tissue engineering: generation of differentiated artificial tissues for biomedical applications. *Cell and Tissue Research*, 1998. **291**(1): p. 1-11.
9. Dash, M., et al., Chitosan-A versatile semi-synthetic polymer in biomedical applications. *Progress in Polymer Science*, 2011. **36**(8): p. 981-1014.
10. Solov'eva, T., et al., Marine Compounds with Therapeutic Potential in Gram-Negative Sepsis. *Marine Drugs*, 2013. **11**(6): p. 2216-2229.
11. Illum, L., Chitosan and its use as a pharmaceutical excipient. *Pharmaceutical Research*, 1998. **15**(9): p. 1326-1331.
12. Thomas, V., M. Bajpai, and S.K. Bajpai, In Situ Formation of Silver Nanoparticles within Chitosan-attached Cotton Fabric for Antibacterial Property. *Journal of Industrial Textiles*, 2011. **40**(3): p. 229-245.
13. Kim, K.W., et al., Antimicrobial activity of native chitosan, degraded chitosan, and O-carboxymethylated chitosan. *Journal of Food Protection*, 2003. **66**(8): p. 1495-1498.
14. Busilacchi, A., et al., Chitosan stabilizes platelet growth factors and modulates stem cell differentiation toward tissue regeneration. *Carbohydrate Polymers*, 2013. **98**(1): p. 665-676.
15. Seo, W.G., et al., Synergistic cooperation between water-soluble chitosan oligomers and interferon-gamma for induction of nitric oxide synthesis and tumoricidal activity in murine peritoneal macrophages. *Cancer Letters*, 2000. **159**(2): p. 189-195.
16. Unsoy, G., et al., Synthesis of Doxorubicin loaded magnetic chitosan nanoparticles for pH responsive targeted drug delivery. *European Journal of Pharmaceutical Sciences*, 2014. **62**: p. 243-250.
17. Bhattarai, N., J. Gunn, and M.Q. Zhang, Chitosan-based hydrogels for controlled, localized drug delivery. *Advanced Drug Delivery Reviews*, 2010. **62**(1): p. 83-99.
18. Lai, H.L., A. Abu'Khalil, and D.Q.M. Craig, The preparation and characterisation of drug-loaded alginate and chitosan sponges. *International Journal of Pharmaceutics*, 2003. **251**(1-2): p. 175-181.
19. Aziz, M.A., et al., Antimicrobial Properties of a Chitosan Dextran-Based Hydrogel for Surgical Use. *Antimicrobial Agents and Chemotherapy*, 2012. **56**(1): p. 280-287.

20. Agnihotri, S.A., N.N. Mallikarjuna, and T.M. Aminabhavi, Recent advances on chitosan-based micro- and nanoparticles in drug delivery. *Journal of Controlled Release*, 2004. **100**(1): p. 5-28.
21. Becker, E.B.E. and A. Bonni, Cell cycle regulation of neuronal apoptosis in development and disease. *Progress in Neurobiology*, 2004. **72**(1): p. 1-25.
22. Zhang, K.X., et al., Repair of an articular cartilage defect using adipose-derived stem cells loaded on a polyelectrolyte complex scaffold based on poly(L-glutamic acid) and chitosan. *Acta Biomaterialia*, 2013. **9**(7): p. 7276-7288.
23. Verma, P., et al., Formation and characterization of three dimensional human hepatocyte cell line spheroids on chitosan matrix for in vitro tissue engineering applications. *In Vitro Cellular & Developmental Biology-Animal*, 2007. **43**(10): p. 328-337.
24. Li, J.L., et al., Culture of primary rat hepatocytes within porous chitosan scaffolds. *Journal of Biomedical Materials Research Part A*, 2003. **67A**(3): p. 938-943.
25. Freier, T., et al., Controlling cell adhesion and degradation of chitosan films by N-acetylation. *Biomaterials*, 2005. **26**(29): p. 5872-5878.
26. Yuan, Y., et al., The interaction of Schwann cells with chitosan membranes and fibers in vitro. *Biomaterials*, 2004. **25**(18): p. 4273-4278.
27. Madhumathi, K., et al., Development of novel chitin/nanosilver composite scaffolds for wound dressing applications. *Journal of Materials Science-Materials in Medicine*, 2010. **21**(2): p. 807-813.
28. Jayakumar, R., R.L. Reis, and J.F. Mano, Synthesis and characterization of pH-sensitive thiol-containing chitosan beads for controlled drug delivery applications. *Drug Delivery*, 2007. **14**(1): p. 9-17.
29. Li, W., et al., Preparation, Characterization, and Property of Chitosan/Polyethylene Oxide Electrospun Nanofibrous Membrane for Controlled Drug Release. *Integrated Ferroelectrics*, 2014. **151**(1): p. 164-178.
30. Kawamura, Y., et al., Adsorption of Metal-Ions on Polyaminated Highly Porous Chitosan Chelating Resin. *Industrial & Engineering Chemistry Research*, 1993. **32**(2): p. 386-391.
31. Singh, A., et al., External stimuli response on a novel chitosan hydrogel crosslinked with formaldehyde. *Bulletin of Materials Science*, 2006. **29**(3): p. 233-238.
32. Beppu, M.M., et al., Crosslinking of chitosan membranes using glutaraldehyde: Effect on ion permeability and water absorption. *Journal of Membrane Science*, 2007. **301**(1-2): p. 126-130.
33. Deng, Y., et al., Preparation and characterization of hyaluronan/chitosan scaffold crosslinked by 1-ethyl-3-(3-dimethylaminopropyl) carbodiimide. *Polymer International*, 2007. **56**(6): p. 738-745.
34. Kuboe, Y., et al., Quinone cross-linked polysaccharide hybrid fiber. *Biomacromolecules*, 2004. **5**(2): p. 348-357.
35. Chiono, V., et al., Genipin-crosslinked chitosan/gelatin blends for biomedical applications. *Journal of Materials Science-Materials in Medicine*, 2008. **19**(2): p. 889-898.
36. Muzzarelli, R.A.A., Genipin-crosslinked chitosan hydrogels as biomedical and pharmaceutical aids. *Carbohydrate Polymers*, 2009. **77**(1): p. 1-9.
37. Mi, F.L., et al., In vitro evaluation of a chitosan membrane cross-linked with genipin. *Journal of Biomaterials Science-Polymer Edition*, 2001. **12**(8): p. 835-850.
38. Tonda-Turo, C., et al., Comparative analysis of gelatin scaffolds crosslinked by genipin and silane coupling agent. *International Journal of Biological Macromolecules*, 2011. **49**(4): p. 700-6.
39. Nicholson, B. and S. Verma, Comorbidities in chronic neuropathic pain. *Pain Med*, 2004. **5 Suppl 1**: p. S9-S27.

40. Bellamkonda, R.V., Peripheral nerve regeneration: an opinion on channels, scaffolds and anisotropy. *Biomaterials*, 2006. **27**(19): p. 3515-8.
41. Liu, Y., et al., Reconstruction of a tissue-engineered skin containing melanocytes. *Cell Biol Int*, 2007. **31**(9): p. 985-90.
42. Jkema-Paassen, J., et al., Transection of peripheral nerves, bridging strategies and effect evaluation. *Biomaterials*, 2004. **25**(9): p. 1583-92.
43. Muzzarelli, R.A.A., Chitins and chitosans for the repair of wounded skin, nerve, cartilage and bone. *Carbohydrate Polymers*, 2009. **76**(2): p. 167-182.
44. Freier, T., et al., Chitin-based tubes for tissue engineering in the nervous system. *Biomaterials*, 2005. **26**(22): p. 4624-32.
45. Ren, Y.J., et al., In vitro behavior of neural stem cells in response to different chemical functional groups. *Biomaterials*, 2009. **30**(6): p. 1036-44.
46. Bhattarai, N., et al., Electrospun chitosan-based nanofibers and their cellular compatibility. *Biomaterials*, 2005. **26**(31): p. 6176-84.
47. Christopherson, G.T., H. Song, and H.Q. Mao, The influence of fiber diameter of electrospun substrates on neural stem cell differentiation and proliferation. *Biomaterials*, 2009. **30**(4): p. 556-64.
48. Minami, S., et al., Veterinary practice with chitin and chitosan. *EXS*, 1999. **87**: p. 265-77.
49. Rickard, K.A., et al., Role of nutrition support in the management of children with cancer. *Prog Clin Biol Res*, 1983. **132D**: p. 179-92.
50. Fleming, G., Clinical technique: chelonian shell repair. *Journal of Exotic Pet Medicine*, 2008. **17**(4): p. 246-258.
51. Jackson, O.F., Tortoise shell repair over two years. *Vet Rec*, 1978. **102**(13): p. 284-5.
52. Frye, F.L., Clinical evaluation of a rapid polymerizing epoxy resin for repair of shell defects in tortoises. *Vet Med Small Anim Clin*, 1973. **68**(1): p. 51-3.
53. Zeman, W.V., F.G. Falco, and J.J. Falco, Repair of the carapace of a box turtle using a polyester resin. *Lab Anim Care*, 1967. **17**(4): p. 424-5.
54. Holt, P.E., Healing of a surgically induced shell wound in a tortoise. *Vet Rec*, 1981. **108**(5): p. 102.
55. Mader, D., Bennet, RA., Funk RS., *Reptile Medicine and Surgery* ed. M. DR. 2006, St Louis: Saunders/Elsevier. 581-630.
56. Mayer, J. and T. Donnelly, *Clinical Veterinary Advisor, Birds and Exotic Pets*, ed. M.J.a.D. TM. 2013: Elsevier Health Sciences.
57. Lafortune, M., et al., Vacuum-assisted closure (Turtle VAC) in the management of traumatic shell defects in chelonians. *Journal of Herpetological Medicine and Surgery*, 2005. **15**: p. 4-8.
58. Mitchell, M.A. and T.N. Tully, *Manual of Exotic Pet Practice*. 2009: Elsevier Health Sciences.
59. Amable, P.R., et al., Platelet-rich plasma preparation for regenerative medicine: optimization and quantification of cytokines and growth factors. *Stem Cell Res Ther*, 2013. **4**(3): p. 67.
60. Pelizzone, I., et al. Shell fracture repair a comparison of different methods and the use of PRP (Platelet-rich-plasma). in *International Conference on Reptile and amphibian Medicine*. 2012. Cremona, Italy.
61. Mathews, K.A. and A.G. Binning, Wound management using honey. *Compend. Con. Edu*, 2002. **24**(1): p. 53-59.
62. Norton, T., et al. Medical and surgical management of automobile and boat strike trauma in Diamondback Terrapins and marine turtles. 2010.
63. Chu, H.Q., et al., Aminoglycoside ototoxicity in three murine strains and effects on NKCC1 of stria vascularis. *Chin Med J (Engl)*, 2006. **119**(12): p. 980-5.

64. Patrick, B.N., M.P. Rivey, and D.R. Allington, Acute renal failure associated with vancomycin- and tobramycin-laden cement in total hip arthroplasty. *Ann Pharmacother*, 2006. **40**(11): p. 2037-42.
65. Wang, W., et al., Effects of Schwann cell alignment along the oriented electrospun chitosan nanofibers on nerve regeneration. *Journal of Biomedical Materials Research Part A*, 2009. **91A**(4): p. 994-1005.